RECOVERY OF LITHIUM AND COBALT FROM SPENT LITHIUM-ION BATTERY THROUGH BIO-HYDROMETALLURGICAL PROCESS

THANAPON CHANDAKHIAW

A Thesis Submitted in Partial Fulfillment of the Requirements for the Degree of
Doctor of Philosophy in Materials Engineering
Suranaree University of Technology
Academic Year 2024

การกู้คืนลิเทียมและโคบอลต์จากแบตเตอรี่ชนิดลิเทียมไอออนใช้งานแล้ว
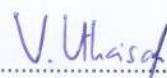# ด้วยกระบวนการชะละลายทางชีวภาพและโลหวิทยาสารละลาย

นายธนพล จันดาเขียว

วิทยานิพนธ์นี้เป็นส่วนหนึ่งของการศึกษาตามหลักสูตรปริญญาวิศวกรรมศาสตรดุษฎีบัณฑิต
สาขาวิชาวิศวกรรมวัสดุ
มหาวิทยาลัยเทคโนโลยีสุรนารี
ปีการศึกษา 2567

RECOVERY OF LITHIUM AND COBALT FROM SPENT LITHIUM-ION BATTERY THROUGH BIO-HYDROMETALLURGICAL PROCESS

Suranaree University of Technology has approved this thesis submitted in partial fulfillment of the requirements for the Degree of Doctor of Philosophy.
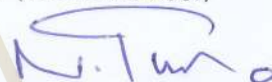
Thesis Examining Committee

_____

(Assoc. Prof. Dr. Vitoon Uthaisangsuk)

Chairperson

_____

(Asst. Prof. Dr. Sakhob Khumkoa)

Member (Thesis Advisor)

_____

(Prof. Dr. Neung Teaumroong)

Member

_____

(Asst. Prof. Dr. Tapany Patcharawit)

Member

_____

(Asst. Prof. Dr. Usanee Kitkamthorn)

Member

_____

(Assoc. Prof. Dr. Yupaporn Ruksakulpiwat)

Vice Rector for Academic Affairs

and Quality Assurance

_____

(Assoc. Prof. Dr. Pornsiri Jongkol)

Dean of Institute of Engineering

ธนพล จันดาเขียว : การกู้คืนลิเทียมและโคบอลต์จากแบตเตอรี่ชนิดลิเทียมไอออนใช้งานแล้ว
ด้วยกระบวนการชะละลายทางชีวภาพและโลหวิทยาสารละลาย (RECOVERY OF LITHIUM
AND COBALT FROM SPENT LITHIUM-ION BATTERY THROUGH BIO-
HYDROMETALLURGICAL PROCESS) อาจารย์ที่ปรึกษา : ผู้ช่วยศาสตราจารย์ ดร. สงบ คำค้อ,
166 หน้า.

คำสำคัญ : แบตเตอรี่ลิเทียมไอออน/การชะละลายทางชีวภาพ/*Aspergillus*/*Penicillium*/การกู้คืน
โลหะในขั้นตอนเดียว

วิทยานิพนธ์นี้นำเสนอกระบวนการสกัดโคบอลต์และลิเทียมจากแบตเตอรี่ลิเทียมไอออนที่ใช้
แล้วโดยใช้กระบวนการชะละลายทางชีวภาพและโลหวิทยาสารละลาย มีวัตถุประสงค์เพื่อพัฒนา
วิธีการสกัดและกู้คืนโลหะมีค่าจากแบตเตอรี่ลิเทียมไอออนที่เสื่อมสภาพโดยการผลิตเป็นวัตถุดิบ
ทดแทนเพื่อนำมาใช้ใหม่ ในการทดลองได้ใช้ผงแคโทดของแบตเตอรี่ชนิดลิเทียมโคบอลต์ออกไซด์
($LiCoO_2$) จากแบตเตอรี่สมาร์ทโฟนที่เสื่อมสภาพเป็นวัตถุดิบ และได้ทำการคัดเลือกสายพันธุ์เชื้อรา
จากดินปนเปื้อนโลหะ เชื้อราที่สามารถเจริญเติบโตได้ดีในสภาวะที่มีลิเทียมและโคบอลต์สูงถูกเลือก
นำมาใช้ในกระบวนการชะละลายทางชีวภาพ ในการทดลองได้ศึกษาอิทธิพลของการใช้อาหารเลี้ยง
เชื้อชนิด PDB (potato dextrose broth) และ น้ำตาลซูโครส (sucrose medium) ร่วมกับการปรับ
ค่า pH เริ่มต้นของอาหารเลี้ยงเชื้อ องค์ประกอบของอาหารเลี้ยงเชื้อ และความหนาแน่นของของแข็ง
ต่อของเหลว (pulp density) ที่ส่งผลต่อการสกัดโคบอลต์และลิเทียมของเชื้อรา นอกจากนี้ ยังได้
ศึกษาการตกตะกอนของโคบอลต์ในรูปของโคบอลต์ (II,III) ออกไซด์ (Co_3O_4) และลิเทียมในรูปของ
สารประกอบฟอสเฟตจากสารละลายที่ได้จากการชะละลายทางชีวภาพ จากการวิจัยพบว่าเชื้อราสาย
พันธุ์ *Aspergillus* sp. JMET 15 และ *Penicillium* sp. JMET 24 สามารถเติบโตได้ดีใน
สภาพแวดล้อมที่มีลิเทียมและโคบอลต์เข้มข้น นอกจากนี้ ยังพบว่าน้ำตาลซูโครสช่วยเพิ่มประสิทธิภาพ
การสกัดโลหะได้ดีกว่า PDB ค่า pH เริ่มต้นและองค์ประกอบของอาหารเลี้ยงเชื้อได้ส่งผลทำให้
ประสิทธิภาพการสกัดโลหะสูงขึ้นอย่างมีนัยสำคัญ การกู้คืนโคบอลต์ให้อยู่ในรูปโคบอลต์ออกไซด์และ
ลิเทียมให้อยู่ในรูปลิเทียมฟอสเฟตจากสารละลายที่ได้จากการชะละลายทางชีวภาพสามารถทำได้โดย
การตกตะกอนแบบเลือก (selective precipitation) โดยสามารถกู้คืนโคบอลต์และลิเทียมได้มากกว่า
98% และ 95% ตามลำดับ

สาขาวิชา วิศวกรรมโลหการ   ลายมือชื่อนักศึกษา _ธนพล จันดาเขียว_

ปีการศึกษา 2567   ลายมือชื่ออาจารย์ที่ปรึกษา _สงบ คำค้อ_

THANAPON CHANDAKHIAW : RECOVERY OF LITHIUM AND COBALT FROM SPENT LITHIUM-ION BATTERY THROUGH BIO-HYDROMETALLURGICAL PROCESS. THESIS ADVISOR : ASST. PROF. SAKHOB KHUMKOA, Ph.D., 166 PP.

Keyword: Lithium-ion battery/Bioleaching/*Aspergillus*/*Penicillium*/One-step recovery of metal

This thesis presents a methodology for extracting cobalt and lithium from spent lithium-ion batteries utilizing a bio-hydrometallurgical approach. The objective was to develop methods for extracting and recovering valuable metals from lithium-ion battery waste by producing alternative raw materials for reuse. The experimental work utilized cathode powder from lithium cobalt oxide ($LiCoO_2$) batteries, sourced from deteriorated smartphones as the experimental raw material, and fungal strains were isolate from metal-contaminated soil. Fungi capable of thriving in environments with high concentrations of lithium and cobalt were selected for the bioleaching process. The research investigated the influence of potato dextrose broth (PDB) and sucrose medium, along with adjusting the initial pH, media composition, and pulp density (solid-to-liquid ratio) on the fungal extraction efficiency of cobalt and lithium. Furthermore, the study examined the precipitation of cobalt as cobalt (II, III) oxide (Co_3O_4) and lithium as phosphate compounds from the bioleaching solution. The findings demonstrated that the fungal strains *Aspergillus* sp. JMET 15 and *Penicillium* sp. JMET 24 exhibited robust growth in environments with high concentrations of lithium and cobalt. Additionally, sucrose medium enhanced metal extraction efficiency compared to PDB. Initial pH values and media composition significantly improved metal extraction efficiency. The recovery of cobalt as cobalt oxide and lithium as lithium phosphate from the bioleaching solution could be achieved through selective precipitation, with recovery rates exceeding 98% and 95%, respectively.

School of Metallurgical Engineering
Academic Year 2024

Student's Signature Thanapon Chandakhiaw
Advisor's Signature S. Khumkoa

ACKNOWLEDGEMENTS

Thanapon Chandakhiaw

TABLE OF CONTENTS

TABLE OF CONTENTS (Continued)

TABLE OF CONTENTS (Continued)

TABLE OF CONTENTS (Continued)

TABLE OF CONTENTS (Continued)

Page

LIST OF TABLES

LIST OF FIGURES

LIST OF FIGURES (Continued)

LIST OF FIGURES (Continued)

LIST OF FIGURES (Continued)

Figure   **Page**

LIST OF FIGURES (Continued)

LIST OF FIGURES (Continued)

SYMBOLS AND ABBREVIATIONS

%	percentage sign
°C	degree celcius
μL	microliter
μm	micrometer
Å	angstrom
AR	analytical reagent
bp	base pairs
$C_{initial}$	initial concentration
C_{final}	final concentration
CM	composite medium
CN	non-cathode (fungal in the medium without cathode powder)
CNTs	carbon nanotubes
CS	cathode sterile (only cathode powder in the medium)
D	day
DEC	diethyl carbonate
deg	degree
DMC	dimethyl carbonate
DNA	deoxyribonucleic acid
E_0	absorption edge energy
EAF	electric arc furnace
EC	ethylene carbonate
EDTA	ethylenediaminetetraacetic acid

SYMBOLS AND ABBREVIATIONS (Continued)

EMC	methyl ethyl carbonate
eV	electron volt
EXAFS	extended X-ray absorption fine structure
FESEM	field emission scanning electron microscopy
FT	Fourier-transformed
G	Graphite
g	gram
HPLC	high performance liquid chromatography
hr	hour
ICP-OES	inductively coupled plasma optical emission spectrometry
IEA	The International Energy Agency
IOB	iron oxidizing bacteria
k	photoelectron wave vector
keV	kiloelectron volt
L	liter
LCO	lithium cobalt oxide
LFP	lithium iron phosphate
LIB	Lithium-ion batteries
LMO	lithium manganese oxide
LNO	lithium nickel oxide
LTO	lithium titanite oxide
M	molar
mL	mililiter
mm	millimeter

SYMBOLS AND ABBREVIATIONS (Continued)

mM	Millimolar
min.	minute
NCA	lithium nickel cobalt aluminium oxide
NCBI	National Center for Biotechnology Information
NCO	lithium nickel cobalt oxide
NMC	nickel manganese cobalt oxide
PC	propylene carbonate
PCR	polymerase chain reaction
PDA	potato dextrose agar
PDB	potato dextrose brot
PE	polyethylene
PET	polyethylene terephthalate
PP	polypropylene
ppm	part per million
PVDF	polyvinylidene fluoride
RNA	ribonucleic acid
rpm	rounds per minute
s	second
s/l ratio	solid to liquid ratio
SDS	sodium dodecyl sulfate
SEM	scaning electron microscopy
SLRI	Synchrotron Light Research Institute
SM	sucrose medium
SOB	sulfur oxidizing bacteria

SYMBOLS AND ABBREVIATIONS (Continued)

SUT	Suranaree University of Technology
T	test sample (fungal and cathode powder in the medium)
TE	Tris-EDTA
Tris	tris(hydroxymethyl)aminomethane
UV	ultraviolet
w/v	weight by volume
wt	weight
WT	wavelet transform
XANES	X-ray absorption near edge structure
XAS	X-ray absorption spectroscopy
XRD	X-ray diffraction
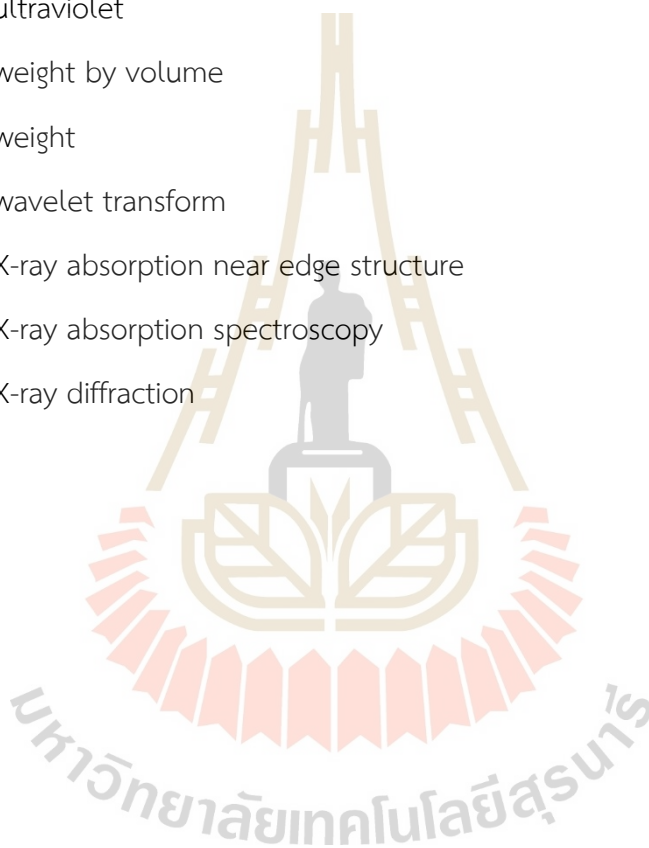
CHAPTER I

INTRODUCTION

1.1   Significance of Study

In the era of globalization, rapid advancements in science and technology have significantly enhanced the quality of human life. Various forms of wireless electronic devices have been developed, including communication tools, tablets, watches, medical devices, military equipment, and electric vehicles. Notably, in 2020, the COVID-19 pandemic profoundly impacted all aspects of human life, necessitating remote work and learning to prevent further spread of the virus. Consequently, the demand for essential electronic devices in daily routines increased. Behind the operation of these devices lies a crucial component: the battery. Among the widely used types is the lithium-ion battery, known for its stability, high energy density, long-life cycle, low self-discharge rate, and lightweight nature (Chen et al., 2018, 2019; Freitas & Garcia, 2007; Garcia et al., 2008; Georgi-Maschler et al., 2012; L. Li et al., 2010, 2012; Niu et al., 2014; Wang et al., 2012; B. Xin et al., 2009; Y. Xin et al., 2016). These characteristics allow electronic devices using lithium-ion batteries to be lighter and/or smaller while providing the same electrical output as other battery types. According to statistical data by Melania Scerra (2021), the total market value of lithium-ion batteries in 2020 was USD 40.5 billion, and it is projected to increase by approximately 50%, reaching USD 91.9 billion by 2026, as shown in Figure 1.1.

The International Energy Agency (IEA) reported that lithium-ion battery manufacturing capacity is expected to increase from 1.57 TWh in 2022 to 6.79 TWh in 2030 (IEA, 2023). Life cycle of lithium-ion battery was estimated to 500-30,000 cycles up to electrode materials (500-1500 cycles for lithium cobalt oxide cathode with graphite anode (LCO-C) (Swain, 2017; P. K. S. Zhang Chao-Yang Wang, San Ping Jiang, Xueliang Sun, Jiujun, 2017), 1,000-7,000 cycles for nickel manganese cobalt oxide cathode with graphite anode (NMC-C) and 30,000 cycles for lithium nickel cobalt oxide cathode with lithium titanite oxide anode (NCO-LTO) (Arshad et al., 2022)).

According to lifetime estimations, portable devices had a lifespan of approximately 2-3 years and electric vehicles around 10 years before becoming waste (Alipanah et al., 2021; Biswal & Balasubramanian, 2023; Chen et al., 2018; Park et al., 2017).

Projected size of the global lithium-ion battery market from 2020 to 2026 (in billion U.S. dollars)
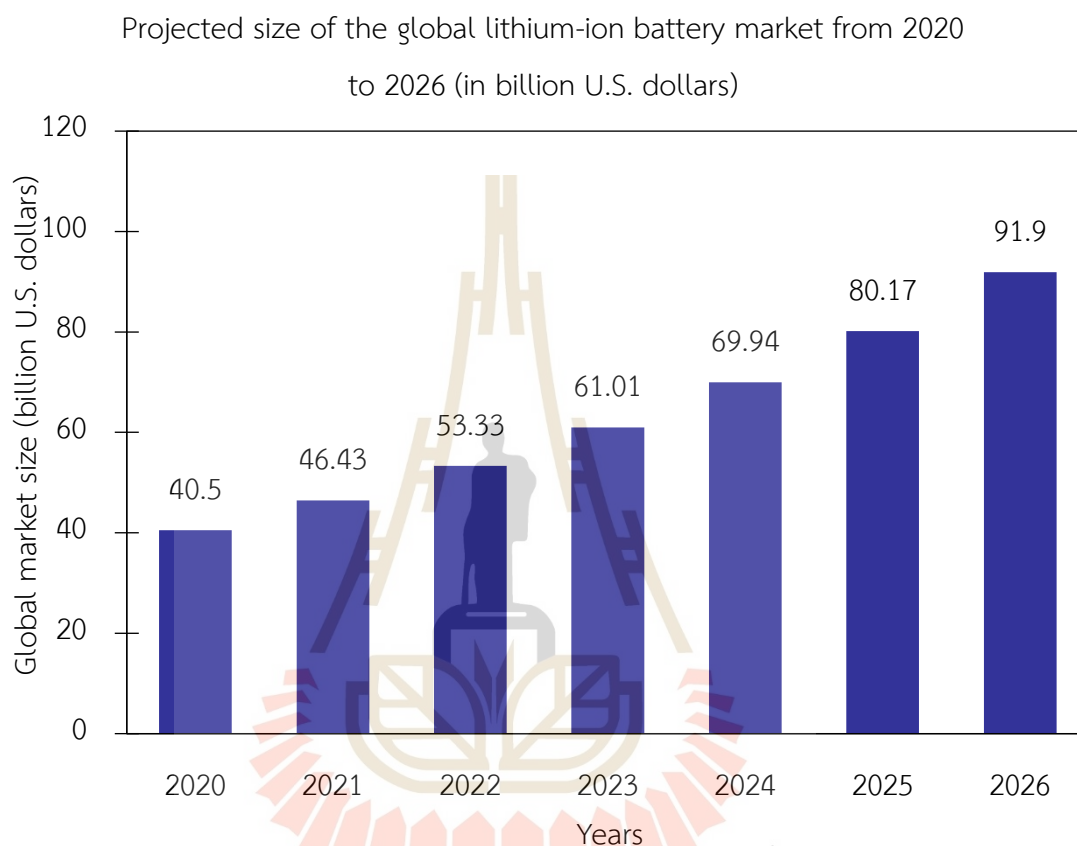
Figure 1.1   Projected Growth of the Lithium-Ion Battery Market from 2020 to 2026 (in Billion USD) (Scerra, 2021)

Improper management of battery waste can have severe environmental and health impacts due to the leakage of heavy metals and organic compounds. (Asadi Dalini et al., 2021). However, battery waste is also considered a renewable resource, rich in valuable metals compared to natural sources. For instance, lithium-ion batteries typically contain 30.8-42.9% cobalt (Co), 13% copper (Cu), 6.5-10% aluminum (Al), and 2.45-8.88% lithium (Li) based on LCO cathode composition. (Mantuano et al., 2006). In contrast, copper-cobalt oxide ore from the Democratic

Republic of Congo, the world's largest cobalt producer, contains only 11.58% Co. (Crundwell et al., 2020; M. Zhang et al., 2012), and high-grade spodumene, a lithium-rich mineral, contains 3.72% Li (Moon & Fuerstenau, 2003). Therefore, the effective recycling of lithium-ion batteries not only mitigates environmental issues but also helps address concerns about the scarcity of raw materials.

Cobalt can be utilized in various applications, including as a component of cathodes in lithium-ion batteries, in superalloys that maintain high strength at elevated temperatures, in the production of high-hardness cutting tools, and as pigments in ceramics. As illustrated in Figure 1.2, the proportion of cobalt used in batteries has increased from 51% in 2016 to an estimated 62% in 2020. Similarly, the use of lithium in batteries has also risen, as shown in Figure 1.3. Other applications of lithium include the production of ceramics and glass, lubricants, flux in continuous casting, air treatment systems, oxygen production in spacecraft, polymer manufacturing processes, the aluminum production industry, and as an alloy in aerospace-grade aluminum. In the medical field, lithium is used in dental prosthetics, coatings, and psychiatric medications.
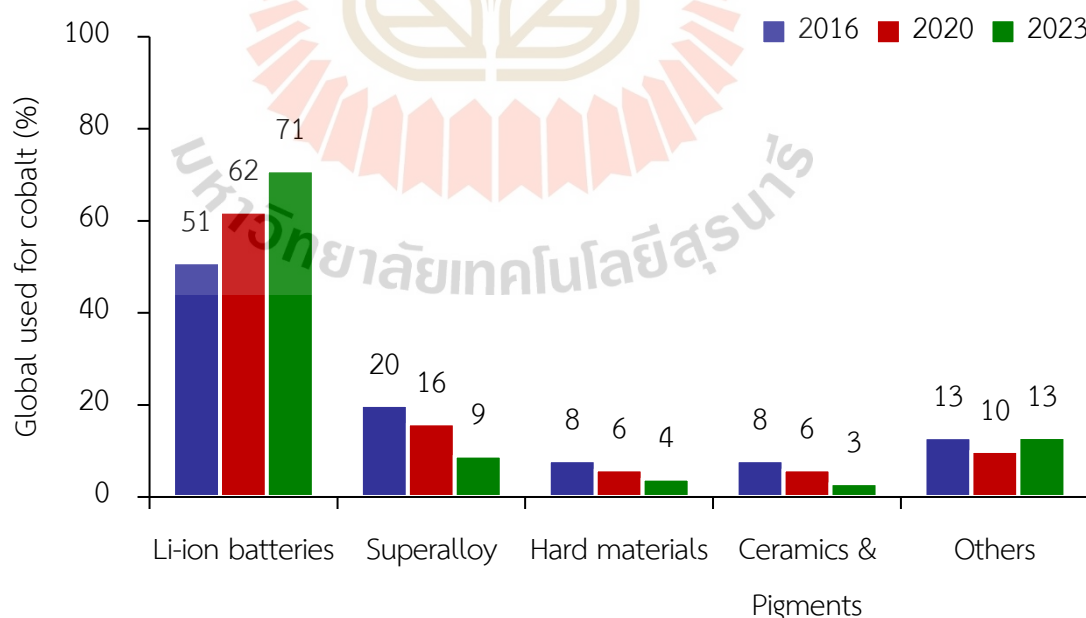
Figure 1.2   The proportion of cobalt usage in 2016, 2020, and 2023 (Cobalt Institute, 2024)
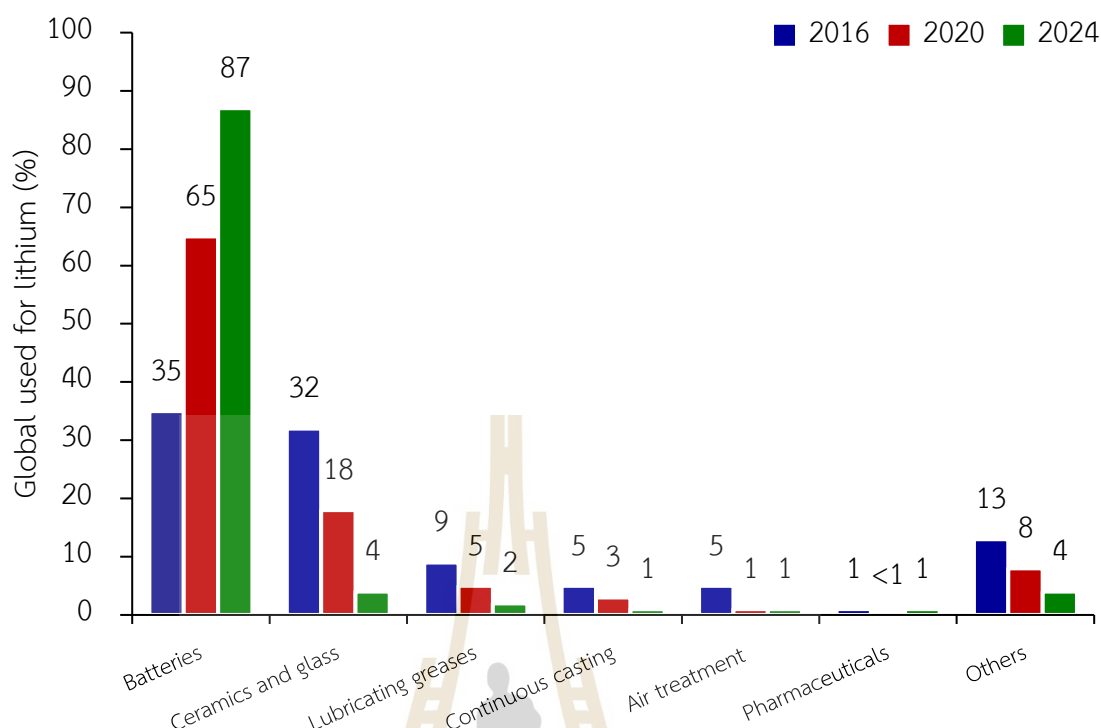
Figure 1.3 The proportion of lithium usage in 2015, 2020, and 2024 (U. S. Geological
Survey, 2024).

Based on the survey of metal prices, it was observed that the price of cobalt
has fluctuated over different periods, ranging from $21,750 per ton (746,949.36 Baht
per ton) to a peak of $95,250 per ton (3,271,123.04 Baht per ton) in 2018. As of
November 2024, the current price of cobalt is 834.523 Baht per kilogram (Trading
Economics, 2024). In comparison, the current price of lithium is 346.7 Baht per
kilogram (November 2024) (Daily Metal Price, 2024). When compared to other
commonly used industrial metals, cobalt and lithium are relatively more expensive.
For instance, the prices of iron and copper are 15-20 Baht per kilogram and 319.83
Baht per kilogram, respectively (November 2024) (Daily Metal Price, 2024; Trading
Economics, 2024).

Thailand lacks the technology to manage and recycle end-of-life lithium-ion
batteries efficiently. Additionally, the transportation of these battery wastes is
regulated by the government and the Basel Convention, which prevents the

collection and cross-border recycling of battery waste in countries lacking the necessary capabilities. Therefore, research and development in managing and recycling end-of-life lithium-ion batteries should be prioritized urgently. Currently, technology and expertise for managing end-of-life batteries at an industrial level are being developed worldwide, as shown in Table 1.1. The recycling processes used include pyrometallurgy and hydrometallurgy.

Table 1.1 Example of worldwide industrial level of battery recycling processes (Swain, 2017).

Company	Battery types	Process	Location
Toxco	Ni, Li-based	Cyromilling (Li) pyrometallurgy (Ni)	Trail, BC, Canada Baltimore, OH, USA
Salesco Systems	All type battery	Pyrometallurgy	Phoenix, AZ, USA
OnTo Technology	Li-based	Liquid-liquid extraction	Bend, OR, USA
AERC	All type battery	Pyrometallurgy	Allentown, PA, USA Hayward, CA, USA West Melbourne, FL, USA
Dowa	All type battery	Pyrometallurgy	Japan
Japan Recycle	All type battery	Pyrometallurgy	Osaka, Japan
Sony Corp. & Sumitomo Metals and Mining Co.	All type battery	Pyrometallurgy	Japan
XStrata	All type battery	Pyrometallurgy + electrowinning	Horne Que, Nikkelverk Nor, Sudbury Ont, Canada
Accurec	All type battery	Pyrometallurgy	Mulhiem Grenada
DK	All type battery	Pyrometallurgy	Duisburg, Greece
AEA Technology	Li-based		Sutherland, Scotland
Batrec AG	Li-based, Hg	Pyrometallurgy	Wimmis, CH, Switzerland
AFE Group (Valdi)	All type battery	Pyrometallurgy	Zurich CH, Switzerland Rogerville, France

Table 1.1   Example of worldwide industrial level of battery recycling processes
(Swain, 2017) (continued).

Company	Battery types	Process	Location
Citron	All type battery	Pyrometallurgy	Zurich CH, Switzerland Rogerville, France
Euro Dieuze/SARP	All type battery	Hydrometallurgy	Lorraine, France
SNAM	Cd, Ni, MH, Li	Pyrometallurgy	Saint Quentin Fallavier, France
IPGNA Ent. (Recupyl)	All type battery	Hydrometallurgy	Grenoble, France
Umicore	All type battery	Pyrometallurgy + electrowinning	Hooboken, Belgium

The recycling process of lithium-ion batteries in the industrial sector primarily employs pyrometallurgical and hydrometallurgical methods. However, in metal extraction, biometallurgy is also utilized, which involves the application of biotechnological knowledge, particularly the interaction of microorganisms with metals. Examples include bioleaching, where metals are dissolved by acids produced by microorganisms, and bioaccumulation, where metals are absorbed and accumulated within the cells or cell membranes of microorganisms (Adetunji et al., 2023; Deng et al., 2013; J. Li et al., 2023; Roy et al., 2021; Watling, 2016).

Each of these processes has distinct advantages and limitations, as shown in Table 1.2. Pyrometallurgical processes cannot directly recover lithium due to its low boiling point of 1330°C, which is exceeded by the high temperatures required in smelting furnaces. Consequently, lithium is lost in the exhaust gases, making the process energy-intensive and costly. To be economically viable, large quantities of raw materials must be processed simultaneously, posing a challenge in collecting sufficient quantities of these materials. Hydrometallurgical processes, on the other hand, can produce higher purity products and recover more metals with lower energy consumption compared to pyrometallurgical methods. However, they generate significant amounts of liquid waste and involve more complex separation steps. Biometallurgical processes, unlike hydrometallurgical methods, do not generate large

quantities of strong acids. However, they are time-consuming and less efficient in the presence of high metal concentrations, as metals can inhibit microbial growth. Nevertheless, global awareness of environmental and sustainability management has highlighted the importance of these processes. Consequently, biometallurgical methods have been selected for further development and in-depth study to enhance their efficiency and potential for commercial metal recycling.

Numerous bioleaching microorganisms, including chemolithoautotrophic acidophilic sulfur and/or iron-oxidizing bacteria or archaea, as well as filamentous fungi, have been reported (Burgstaller & Schinner, 1993; Dusengemungu et al., 2021; Schippers, 2007). However, fungi offer several advantages over bacteria. Filamentous fungi exhibit strong adaptability, can thrive in environments with high metal concentrations ranging from acidic to basic conditions, and have a short lag phase (Dusengemungu et al., 2021; Horeh et al., 2016; Yao et al., 2018). They are capable of leaching alkali substrates such as metal oxide compound waste. *Aspergillus* and *Penicillium* are two significant genera of filamentous fungi in biotechnology and medicine (Houbraken et al., 2014; Tsang et al., 2018). Biswal et al. (2018) reported that the leaching efficiency of *A. niger* was higher than that of bacteria (*Acidithiobacillus thiooxidans*) and acid leaching. The fungal bioleaching of LIB waste has primarily focused on the leaching efficiency and recovery of Co and Li from leached solutions using *A. niger* (Bahaloo-Horeh et al., 2018; Bahaloo-Horeh & Mousavi, 2017; Biswal et al., 2018; Horeh et al., 2016), while *Penicillium* is another frequently used fungus, primarily utilized to leach waste such as electronic waste, spent catalysts, contaminated soil, slag, mine tailings, and low-grade ores (Deng et al., 2013; Dusengemungu et al., 2021; Rezza et al., 1997, 2001). The bioleaching of battery waste using *Penicillium* has not been extensively explored.

Table 1.2   Evaluating the advantages and limitations of different methods for
recycling lithium-ion batteries (LIBs) (Asadi Dalini et al., 2021).

Process	Advantages	Limitations
Pyrometallurgy	- Simple operation - High capacity - Can charge a mixed type of battery	- Lithium loss - High energy consumption - High gas emission
Biometallurgy	- Simple operation - Low energy consumption - Eco-friendly - Economical	- Slow kinetics - Low efficiency in high pulp density
Hydrometallurgy	- High recovery and high purity products - Low energy consumption - Low gas emissions - High Selectivity	- Wastewater production - Long and complex process

1.2   Research objective

The primary objective of this dissertation is to develop a novel and effective
method for the bioleaching of lithium-ion batteries using fungi, to recover valuable
metals from battery waste, and convert them into new raw materials. The specific
objectives of this research are as follows:

1.2.1   To identify an effective fungal strain for the recycling of degraded
lithium-ion battery waste through bioleaching methods.

1.2.2   To optimize the nutrient broth composition to enhance fungal growth
in environments with high concentrations of lithium and cobalt.

1.2.3   To investigate the precipitation of cobalt as cobalt (II, III) oxide (Co_3O_4)
from the bioleaching process.

1.2.4   To examine the precipitation of lithium in the form of phosphate
compounds from solutions obtained through bioleaching.

1.3   Scope and limitations of the research

This research aimed to develop a recycling process for lithium-ion batteries using bio-hydrometallurgy. The deteriorated cathode powder raw material used in this work was lithium cobalt oxide ($LiCoO_2$), also known as the LCO type, which was manually dismantled from smartphone batteries collected from mobile repair shops in Thailand. The research was divided into three main parts, as follows.

1.3.1   Screening of fungus and preliminary study of bioleaching

The effective fungal strains were selected by collecting and screening various metal-contaminated soils from the yard industry in Thailand. The adaptable fungi in lithium-cobalt-contaminated potato dextrose agar (PDA) at concentrations of 0.1 – 1 wt.% were preliminarily studied for bioleaching in potato dextrose broth (PDB) and sucrose medium (SM) with 1% w/v deteriorated cathode powder for 30 days. Then, the selected broth and strain (chosen based on the highest concentrations of lithium and cobalt in the leached solution and the purity of the precipitated cobalt oxide) were used to develop leaching efficiency at higher pulp density further.

1.3.2   Optimization of bioleaching process

The highest concentrations of lithium and cobalt in the leached solution, as well as the purity of the precipitated cobalt oxide from the previous section, were optimized to achieve industrial productivity that is competitive with other recycling methods, such as pyro- and hydrometallurgical processes. Higher pulp density and shorter processing times were identified as key factors for enhancing the competitiveness of bioleaching compared to conventional leaching methods. This study examined the parameters of the initial broth's pH and composition concentration of the medium to increase the pulp density.

1.3.3   The recovery of cobalt and lithium from bioleached solution

The bioleached solution containing cobalt and lithium underwent selective precipitation. Cobalt was recovered as cobalt oxide (Co_3O_4) mesoporous nanoparticles by adding oxalic acid as the precipitant. For lithium, lithium phosphate (Li_3PO_4) was precipitated by adding disodium hydrogen phosphate (Na_2HPO_4) at a pH of 12, with NaOH added to adjust the pH prior to lithium precipitation.

1.4   Expected results

1.4.1.   The exploration of high-performance fungi in the bioleaching system for lithium-ion batteries will be conducted.

1.4.2.   The effect of different carbon sources (glucose from potato dextrose broth and sucrose from sucrose medium) on the leaching efficiency of deteriorated cathode powder will be determined.

1.4.3.   The bioleaching process for deteriorated LCO-type cathode powder using a fungal system will be developed to achieve higher leaching efficiency at increased pulp density (>1% w/v).

1.4.4.   Methods for recovering cobalt and lithium from the bioleaching solution as new raw materials for lithium-ion batteries or other suitable applications will be discovered.

1.5   References

Adetunji, A. I., Oberholster, P. J., & Erasmus, M. (2023). Bioleaching of Metals from E-Waste Using Microorganisms: A Review. *Minerals*, *13*(6), Article 6. https://doi.org/10.3390/min13060828

Alipanah, M., Saha, A. K., Vahidi, E., Jin, H., Alipanah, M., Saha, A. K., Vahidi, E., & Jin, H. (2021). Value recovery from spent lithium-ion batteries: A review on technologies, environmental impacts, economics, and supply chain. *Clean Technologies and Recycling*, *1*(2), Article ctr-01-02-008. https://doi.org/10.3934/ctr.2021008

Arshad, F., Lin, J., Manurkar, N., Fan, E., Ahmad, A., Tariq, M.-N., Wu, F., Chen, R., & Li, L. (2022). Life Cycle Assessment of Lithium-ion Batteries: A Critical Review. *Resources, Conservation and Recycling*, *180*, 106164. https://doi.org/10.1016/j.resconrec.2022.106164

Asadi Dalini, E., Karimi, Gh., Zandevakili, S., & Goodarzi, M. (2021). A Review on Environmental, Economic and Hydrometallurgical Processes of Recycling Spent Lithium-ion Batteries. *Mineral Processing and Extractive Metallurgy Review*, *42*(7), 451–472. https://doi.org/10.1080/08827508.2020.1781628

Bahaloo-Horeh, N., & Mousavi, S. M. (2017). Enhanced recovery of valuable metals from spent lithium-ion batteries through optimization of organic acids produced by *Aspergillus niger*. *Waste Management*, *60*, 666–679. https://doi.org/10.1016/j.wasman.2016.10.034

Bahaloo-Horeh, N., Mousavi, S. M., & Baniasadi, M. (2018). Use of adapted metal tolerant *Aspergillus niger* to enhance bioleaching efficiency of valuable metals from spent lithium-ion mobile phone batteries. *Journal of Cleaner Production*, *197*, 1546–1557. https://doi.org/10.1016/j.jclepro.2018.06.299

Biswal, B. K., & Balasubramanian, R. (2023). Recovery of valuable metals from spent lithium-ion batteries using microbial agents for bioleaching: A review. *Frontiers in Microbiology*, *14*. https://www.frontiersin.org/articles/10.3389/fmicb.2023.1197081

Biswal, B. K., Jadhav, U. U., Madhaiyan, M., Ji, L., Yang, E.-H., & Cao, B. (2018). Biological Leaching and Chemical Precipitation Methods for Recovery of Co and Li from Spent Lithium-Ion Batteries. *ACS Sustainable Chemistry & Engineering*, *6*(9), 12343–12352. https://doi.org/10.1021/acssuschemeng.8b02810

Burgstaller, W., & Schinner, F. (1993). Leaching of metals with fungi. *Journal of Biotechnology*, *27*(2), 91–116. https://doi.org/10.1016/0168-1656(93)90101-R

Chen, X., Cao, L., Kang, D., Li, J., Zhou, T., & Ma, H. (2018). Recovery of valuable metals from mixed types of spent lithium ion batteries. Part II: Selective extraction of lithium. *Waste Management*, *80*, 198–210. https://doi.org/10.1016/j.wasman.2018.09.013

Chen, X., Kang, D., Cao, L., Li, J., Zhou, T., & Ma, H. (2019). Separation and recovery of valuable metals from spent lithium ion batteries: Simultaneous recovery of Li and Co in a single step. *Separation and Purification Technology*, *210*, 690–697. https://doi.org/10.1016/j.seppur.2018.08.072

Cobalt Institute. (2024). *Cobalt Market Report 2023—Cobalt Institute*.
https://www.cobaltinstitute.org/resource/cobalt-market-report-2023/

Crundwell, F. K., du Preez, N. B., & Knights, B. D. H. (2020). Production of cobalt from copper-cobalt ores on the African Copperbelt – An overview. *Minerals Engineering*, *156*, 106450. https://doi.org/10.1016/j.mineng.2020.106450

Daily Metal Price. (2024). *Daily Metal Price: Lithium Price (USD / Kilogram) Chart for the Last 10 Years*.
https://www.dailymetalprice.com/metalpricecharts.php?c=li&u=kg&d=0

Deng, X., Chai, L., Yang, Z., Tang, C., Wang, Y., & Shi, Y. (2013). Bioleaching mechanism of heavy metals in the mixture of contaminated soil and slag by using indigenous *Penicillium chrysogenum* strain F1. *Journal of Hazardous Materials*, *248–249*, 107–114. https://doi.org/10.1016/j.jhazmat.2012.12.051

Dusengemungu, L., Kasali, G., Gwanama, C., & Mubemba, B. (2021). Overview of fungal bioleaching of metals. *Environmental Advances*, *5*, 100083.
https://doi.org/10.1016/j.envadv.2021.100083

Freitas, M. B. J. G., & Garcia, E. M. (2007). Electrochemical recycling of cobalt from cathodes of spent lithium-ion batteries. *Journal of Power Sources*, *171*(2), 953–959. https://doi.org/10.1016/j.jpowsour.2007.07.002

Garcia, E. M., Santos, J. S., Pereira, E. C., & Freitas, M. B. J. G. (2008). Electrodeposition of cobalt from spent Li-ion battery cathodes by the electrochemistry quartz crystal microbalance technique. *Journal of Power Sources*, *185*(1), 549–553.
https://doi.org/10.1016/j.jpowsour.2008.07.011

Georgi-Maschler, T., Friedrich, B., Weyhe, R., Heegn, H., & Rutz, M. (2012). Development of a recycling process for Li-ion batteries. *Journal of Power Sources*, *207*, 173–182. https://doi.org/10.1016/j.jpowsour.2012.01.152

Horeh, N. B., Mousavi, S. M., & Shojaosadati, S. A. (2016). Bioleaching of valuable metals from spent lithium-ion mobile phone batteries using Aspergillus niger. *Journal of Power Sources*, *320*, 257–266. https://doi.org/10.1016/j.jpowsour.2016.04.104

Houbraken, J., de Vries, R. P., & Samson, R. A. (2014). Modern Taxonomy of Biotechnologically Important *Aspergillus* and *Penicillium* Species. In S. Sariaslani & G. M. Gadd (Eds.), *Advances in Applied Microbiology* (Vol. 86, pp. 199–249). Academic Press. https://doi.org/10.1016/B978-0-12-800262-9.00004-4

IEA. (2023, May 22). *Lithium-ion battery manufacturing capacity, 2022-2030 – Charts – Data & Statistics*. IEA. https://www.iea.org/data-and-statistics/charts/lithium-ion-battery-manufacturing-capacity-2022-2030

Li, J., Zhang, H., Wang, H., & Zhang, B. (2023). Research progress on bioleaching recovery technology of spent lithium-ion batteries. *Environmental Research*, *238*, 117145. https://doi.org/10.1016/j.envres.2023.117145

Li, L., Ge, J., Wu, F., Chen, R., Chen, S., & Wu, B. (2010). Recovery of cobalt and lithium from spent lithium ion batteries using organic citric acid as leachant. *Journal of Hazardous Materials*, *176*(1), 288–293. https://doi.org/10.1016/j.jhazmat.2009.11.026

Li, L., Lu, J., Ren, Y., Zhang, X. X., Chen, R. J., Wu, F., & Amine, K. (2012). Ascorbic-acid-assisted recovery of cobalt and lithium from spent Li-ion batteries. *Journal of Power Sources*, *218*, 21–27. https://doi.org/10.1016/j.jpowsour.2012.06.068

Mantuano, D. P., Dorella, G., Elias, R. C. A., & Mansur, M. B. (2006). Analysis of a hydrometallurgical route to recover base metals from spent rechargeable batteries by liquid–liquid extraction with Cyanex 272. *Journal of Power Sources*, *159*(2), 1510–1518. https://doi.org/10.1016/j.jpowsour.2005.12.056

Moon, K. S., & Fuerstenau, D. W. (2003). Surface crystal chemistry in selective flotation of spodumene (LiAl[SiO$_3$]$_2$) from other aluminosilicates. *International Journal of Mineral Processing*, *72*(1), 11–24. https://doi.org/10.1016/S0301-7516(03)00084-X

Niu, Z., Zou, Y., Xin, B., Chen, S., Liu, C., & Li, Y. (2014). Process controls for improving bioleaching performance of both Li and Co from spent lithium ion batteries at high pulp density and its thermodynamics and kinetics exploration. *Chemosphere*, *109*, 92–98. https://doi.org/10.1016/j.chemosphere.2014.02.059

Park, Y. M., Lim, H., Moon, J.-H., Lee, H.-N., Son, S. H., Kim, H., & Kim, H.-J. (2017). High-Yield One-Pot Recovery and Characterization of Nanostructured Cobalt Oxalate from Spent Lithium-Ion Batteries and Successive Re-Synthesis of LiCoO2. *Metals*, *7*(8), Article 8. https://doi.org/10.3390/met7080303

Rezza, I., Salinas, E., Calvente, V., Benuzzi, D., & Tosetti, M. I. S. de. (1997). Extraction of lithium from spodumene by bioleaching. *Letters in Applied Microbiology*, *25*(3), 172–176. https://doi.org/10.1046/j.1472-765X.1997.00199.x

Rezza, I., Salinas, E., Elorza, M., Sanz de Tosetti, M., & Donati, E. (2001). Mechanisms involved in bioleaching of an aluminosilicate by heterotrophic microorganisms. *Process Biochemistry*, *36*(6), 495–500. https://doi.org/10.1016/S0032-9592(00)00164-3

Roy, J. J., Cao, B., & Madhavi, S. (2021). A review on the recycling of spent lithium-ion batteries (LIBs) by the bioleaching approach. *Chemosphere*, *282*, 130944. https://doi.org/10.1016/j.chemosphere.2021.130944

Scerra, M. (2021). *Projected lithium-ion battery market size worldwide*. Statista. https://www.statista.com/statistics/1011187/projected-global-lithium-ion-battery-market-size/

Schippers, A. (2007). Microorganisms Involved in Bioleaching and Nucleic Acid-Based Molecular Methods for Their Identification and Quantification. In E. R. Donati & W. Sand (Eds.), *Microbial Processing of Metal Sulfides* (pp. 3–33). Springer Netherlands. https://doi.org/10.1007/1-4020-5589-7_1

Swain, B. (2017). Recovery and recycling of lithium: A review. *Separation and Purification Technology*, *172*, 388–403. https://doi.org/10.1016/j.seppur.2016.08.031

Trading Economics. (2024). *TRADING ECONOMICS | 20 million INDICATORS FROM 196 COUNTRIES*. https://tradingeconomics.com/

Tsang, C.-C., Tang, J. Y. M., Lau, S. K. P., & Woo, P. C. Y. (2018). Taxonomy and evolution of *Aspergillus*, *Penicillium*, and Talaromyces in the omics era – Past, present, and future. *Computational and Structural Biotechnology Journal*, *16*, 197–210. https://doi.org/10.1016/j.csbj.2018.05.003

U. S. Geological Survey. (2024). Mineral commodity summaries 2024. In *Mineral Commodity Summaries* (2024). U.S. Geological Survey. https://doi.org/10.3133/mcs2024

Wang, J., Chen, M., Chen, H., Luo, T., & Xu, Z. (2012). Leaching Study of Spent Li-ion Batteries. *Procedia Environmental Sciences*, *16*, 443–450. https://doi.org/10.1016/j.proenv.2012.10.061

Watling, H. (2016). Microbiological Advances in Biohydrometallurgy. *Minerals*, *6*(2), Article 2. https://doi.org/10.3390/min6020049

Xin, B., Zhang, D., Zhang, X., Xia, Y., Wu, F., Chen, S., & Li, L. (2009). Bioleaching mechanism of Co and Li from spent lithium-ion battery by the mixed culture of acidophilic sulfur-oxidizing and iron-oxidizing bacteria. *Bioresource Technology*, *100*(24), 6163–6169. https://doi.org/10.1016/j.biortech.2009.06.086

Xin, Y., Guo, X., Chen, S., Wang, J., Wu, F., & Xin, B. (2016). Bioleaching of valuable metals Li, Co, Ni and Mn from spent electric vehicle Li-ion batteries for recovery. *Journal of Cleaner Production*, *116*, 249–258. https://doi.org/10.1016/j.jclepro.2016.01.001

Yao, Y., Zhu, M., Zhao, Z., Tong, B., Fan, Y., & Hua, Z. (2018). Hydrometallurgical Processes for Recycling Spent Lithium-Ion Batteries: A Critical Review. *ACS Sustainable Chemistry & Engineering*, *6*(11), 13611–13627. https://doi.org/10.1021/acssuschemeng.8b03545

Zhang, M., Zhu, G., Zhao, Y., & Feng, X. (2012). A study of recovery of copper and cobalt from copper–cobalt oxide ores by ammonium salt roasting. *Hydrometallurgy*, *129–130*, 140–144. https://doi.org/10.1016/j.hydromet.2012.06.014

Zhang, P. K. S., Chao-Yang Wang, San Ping Jiang, Xueliang Sun, Jiujun (Ed.). (2017). *Electrochemical Energy: Advanced Materials and Technologies*. CRC Press. https://doi.org/10.1201/9781351228756

CHAPTER II
LITERATURE REVIEWS

This chapter provides a comprehensive review of the existing literature relevant to the study of lithium-ion batteries and their recycling. The chapter is structured to cover the fundamental principles of lithium-ion batteries, the role of microorganisms in metal extraction, and the latest advancements in recycling technologies for lithium-ion batteries.

2.1. Lithium-ion battery and principles

2.1.1 Principle of lithium-ion battery

Lithium-ion batteries (LIB) are a type of rechargeable battery that have become integral to modern technology due to their high energy density, lightweight nature, and ability to recharge. The fundamental principle behind LIB involves the movement of lithium ions between the anode and cathode through an electrolyte, a process that converts chemical energy into electrical energy. LIB consists of five main components: the cathode, the anode, the electrolyte solution, the separator that isolates the anode from the cathode, and the casing material. Each component is made from varied materials and construction as follows:

Cathode: The cathode, which is the positive electrode, is made from lithium-containing metal oxide compounds such as $LiCoO_2$, $LiNiO_2$, $LiMn_2O_4$, $LiFePO_4$, and $LiNi_xCo_yMn_zO_2$. $LiCoO_2$ is the most used type due to its high current density and ease of production. Commercially available LIB cathodes typically consist of 90% $LiCoO_2$, 6-8% conductive material, and 4% polyvinylidene fluoride (PVDF) as a binder to adhere the $LiCoO_2$ powder to the aluminum foil electrode.

Anode: The anode, which serves as the negative electrode, primarily utilizes carbon-based materials, including graphite, petroleum coke, and carbon fiber. The anode structure also uses PVDF as a binder to adhere the electrode powder to copper.

Electrolyte: The electrolyte acts as a medium for the movement of lithium ions between the anode and cathode to deliver charge. Liquid electrolytes are the most used today, consisting mainly of organic solvents and lithium salts. Organic solvents include propylene carbonate (PC), ethylene carbonate (EC), dimethyl carbonate (DMC), diethyl carbonate (DEC), and ethyl methyl carbonate (EMC). Lithium salts used in electrolytes include $LiPF_6$, $LiBF_4$, $LiCF_3SO_3$, and $Li(SO_2CF_3)_2$. The most used liquid electrolytes are mixtures of two to three carbonate solvents, such as DMC or EMC, combined with the lithium salt $LiPF_6$.

Separator: The separator is a porous polymer that allows lithium ions to pass through while preventing short circuits between the electrodes. It is mainly made of polyethylene (PE) or polypropylene (PP).

Shell: The shell is typically made of stainless steel, nickel-plated steel, or plastic such as polyethylene terephthalate (PET) or polypropylene (PP) (Zhao et al., 2019).

All of these components are arranged in layers and can be folded or rolled into various shapes, as illustrated in Figure 2.1.

Working Principle of Lithium-Ion Batteries: A fully charged lithium-ion battery (LIB) can supply electrical current to electronic devices through the movement of lithium ions from the anode, via the electrolyte solution, to the cathode. At the anode, a redox reaction occurs where lithium undergoes oxidation, becoming lithium ions and releasing electrons. These electrons travel from the anode (the negative electrode) to the cathode (the positive electrode). This electron movement generates an electric current that flows in the opposite direction to the movement of electrons. As the lithium at the anode undergoes oxidation and depletes, the battery's ability to supply current diminishes, necessitating recharging by connecting to an external power source. During recharging, the reactions mentioned earlier reverse: lithium at the cathode is oxidized by the external potential, becoming ions that move through the electrolyte solution to receive electrons at the anode, where they embed in the graphite structure, as shown in Figure 2.2.
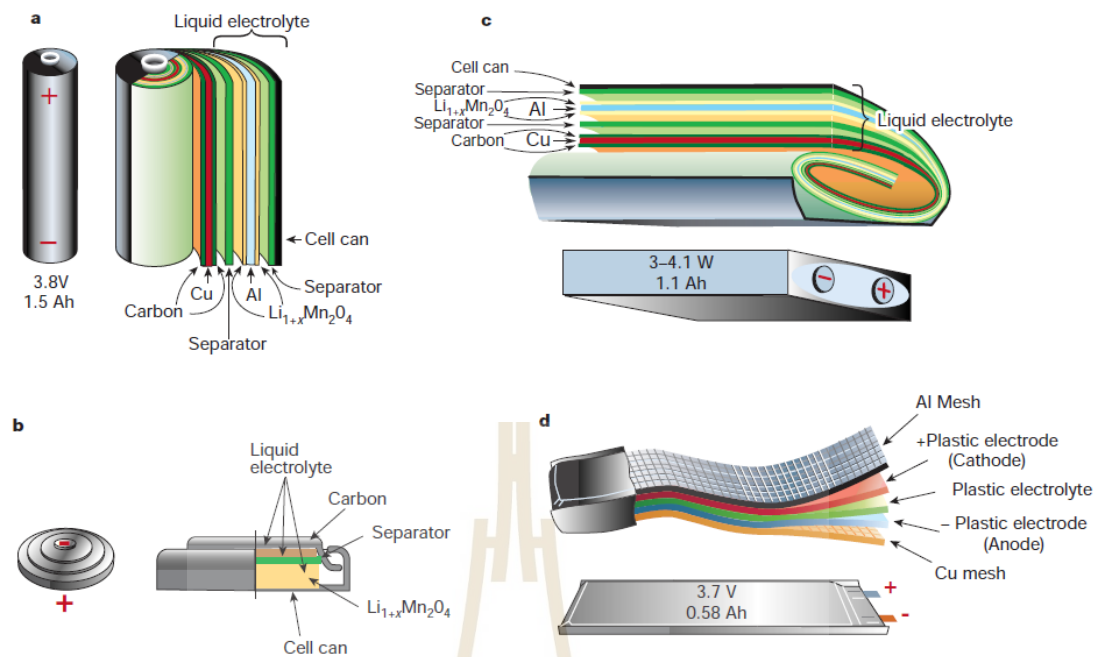
Figure 2.1   Characteristics and components of various types of lithium-ion batteries: (a) cylindrical, (b) coin or button, (c) prismatic, (d) thin film (Tarascon & Armand, 2001).
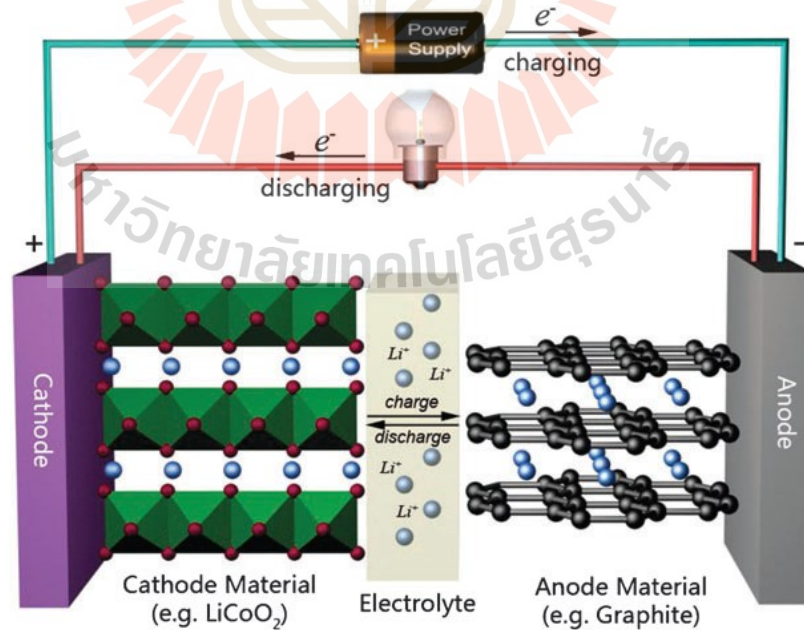
Figure 2.2   Movement of lithium ions during charging and discharging in a LIB (Liu et al., 2011).

The reactions occurring during the charging and discharging of the anode, cathode, and the overall reaction of a LIB ($LiCoO_2$/graphite electrode) can be written as follows:

Cathode: $LiCoO_2$ $\xrightleftharpoons[\text{discharge}]{\text{charge}}$ $Li_{1-x} + CoO_2 + xLi^+ + xe^-$ (2.1)

Anode: $C_6 + xLi^+ + xe^-$ $\xrightleftharpoons[\text{discharge}]{\text{charge}}$ Li_xC_6 (2.2)

Net reaction: $LiCoO_2 + C_6$ $\xrightleftharpoons[\text{discharge}]{\text{charge}}$ $Li_{1-x} + CoO_2 + Li_x C_6$ (2.3)
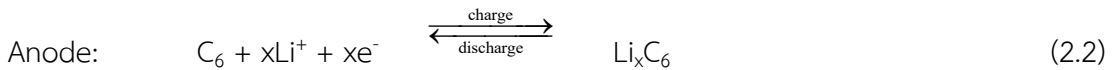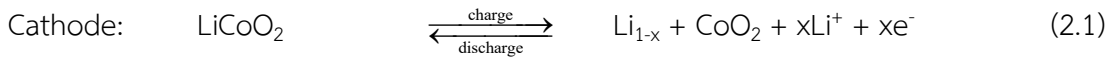
2.1.2 Classification of lithium-ion battery

LIBs have fundamentally transformed the power supply landscape for a wide range of devices, including smartphones and electric vehicles. These batteries are distinguished by their high energy density, extended cycle life, and lightweight characteristics. Nevertheless, it is essential to recognize that there is significant variability among LIBs. Li-ion batteries can be classified by the types of cathodes and anodes according to the changeable crystal structure during the reversible electrochemical reaction, as intercalation-type and conversion-type.

Intercalation-typed electrode materials are a solid host structure, into which Li^+ (guest ion) can be inserted and removed from the host reversibly without intrinsic structure transformation or notable volumetric change (Nitta et al., 2015; G. Wang et al., 2024). The reaction that Li^+ undergoes is an intercalation and de-intercalation process, which can be written as equation (2.4)

$$M + yLi^+ + ye^- \leftrightarrow Li_yM \qquad (2.4)$$

Where M represents a random intercalation-typed material (G. Wang et al., 2024).

Conversion-typed electrode materials undergo a solid-state redox reaction during charge and discharge, resulting in changes to the crystalline structure. The breaking and recombination of chemical bonds accompany this process. The

chemical reaction can proceed via two mechanisms, depending on the electrode materials. Firstly, when Li^+ is lithiated into electrode compounds, also known as 'conversion-type compounds,' a single replacement reaction occurs, as described by Equation (2.5). In the case of pure element electrodes, Li^+ reacts with these materials to form lithium-based alloys, as shown in equation (2.6). 'Alloying materials' are the materials that undergo the latter mechanism.

$$M_xA_y + 2yLi^+ + 2ye^- \longleftrightarrow yLi_2A + xM \qquad (2.5)$$
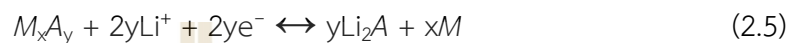
Where M is a metal element, and A is a non-metal element.

$$M + yLi^+ + ye^- \longleftrightarrow Li_yM \qquad (2.6)$$

Where M is a metal element or metalloid, including Se and I

From the reaction mechanism, conversion-type electrodes exhibit significantly higher specific capacities but undergo more significant volume expansion during the redox reaction compared to intercalation-type materials. Nevertheless, the conversion-type electrode undergoes continuous phase transitions during cycling, leading to irreversible structural damage and significant volume expansion (approximately 10-100% for the cathode and 200% for the anode). This results in poor rate performance and noticeable capacity degradation (G. Wang et al., 2024).

2.1.2.1 Intercalation-type cathode electrode

Intercalation-typed cathode materials are typically divided into two groups: transition metal oxide-typed and polyanion-typed.

(1) Transition metal oxide type: It can be sorted as a layered structure and a spinel structure. Layered structure (Figure 2.3 (a)) with the formula $LiMO_2$ (M=transition metal: Co, Mn, Ni). $LiCoO_2$ (LCO) has been a conventional commercial material for layered structures in LIBs for more than thirty years, since its introduction by Sony in 1991. It was being used as the most active cathode material (Kotal et al., 2022). Other compounds which are a layered structure, such as $LiNiO_2$

(LNO), LiMnO$_2$ (LMO), LiNi$_{0.5}$Mn$_{0.5}$O$_2$ (NMO), LiNi$_x$Co$_y$Mn$_{1-x-y}$O$_2$ (NCM or NMC), LiNi$_{0.8}$Co$_{0.15}$Al$_{0.05}$O$_2$ (NCA), lithium-rich materials (Li$_2$MnO$_3$, xLi$_2$MnO$_3$·(1-x)LiMO$_2$: M=Ni, Co, Mn), etc. Spinel structure (Figure 2.3 (b)) with the formula LiM$_2$O$_4$ (M=transition metal: Co, Mn, Ni). LiMn$_2$O$_4$ is the most familiar compound of this type.
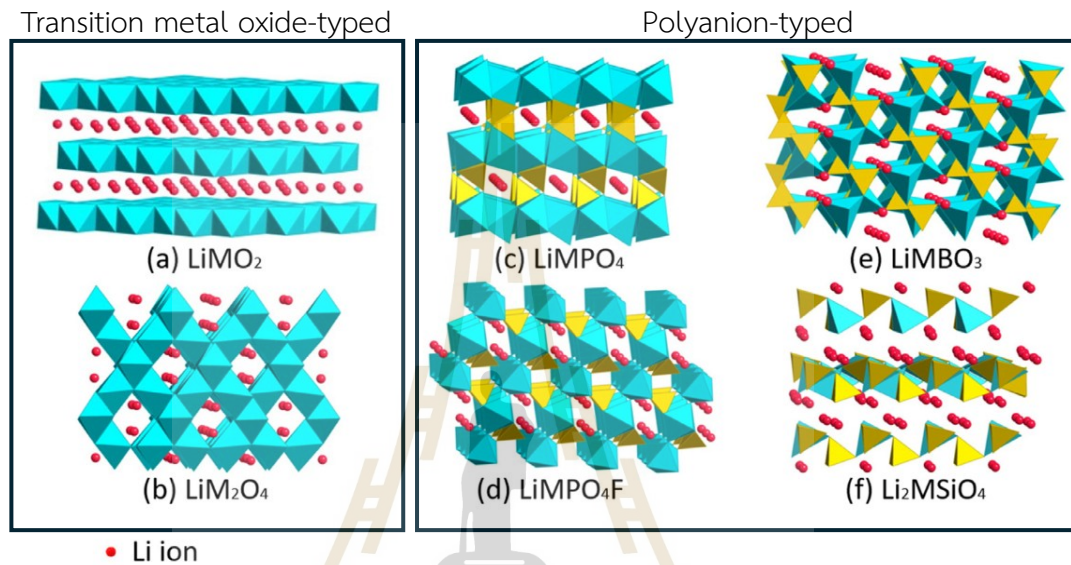
Figure 2.3   Crystal structure of intercalation-typed cathode materials (a) layered LiMO$_2$, (b) Spinel-structured LiM$_2$O$_4$, and polyanionic (c) LiMPO$_4$, (d) LiMPO$_4$F, (e) LiMBO$_3$, (F) Li$_2$MSiO$_4$ (M refer to transition metals; blue: transition metal oxide; yellow: phosphate or fluorophosphate or borate or silicate; red Li ions) (B. Xu et al., 2012).

(2) Polyanion Type: Researchers have developed a new class of compounds known as polyanions. These large polyanions, primarily $(XO_4)^{3-}$ (where X = S, P, Si, As, Mo, W), occupy lattice positions, thereby increasing the redox potential in the cathode and stabilizing its structure. In commercial LIBs, LiFePO$_4$ (LFP) is the representative compound for this type due to its thermal stability and high-power capability within the phosphate polyanion structure, which is phosphate-based (LiMPO$_4$ or olivine structure). The crystal structure of phosphate-based or olivine structure is shown in Figure 2.3 (c). Other polyanion-type structures, such as borate-

based (LiMBO$_3$), silicate-based (LiMSO$_4$), and fluorophosphate-based (tavorite structure) (LiMPO$_4$F), are shown in Figure 2.3 (e), (f), and (d), respectively.

2.1.2.2 Intercalation-type anode electrode

Carbon-based materials are commonly used as intercalation-type anode materials in commercial lithium-ion batteries (LIBs), offering balanced electrochemical performance at an acceptable cost. In addition to the widely used graphite, other carbon materials with various microstructures and morphologies have been explored, including graphene, hard carbon, carbon nanofibers, and carbon nanotubes (CNTs). Li$_4$Ti$_5$O$_{12}$ (LTO) has been developed for low-temperature environments (down to -30°C). It exhibits minimal volumetric change during charge and discharge cycles (approximately 0.2%), compared to graphite, which undergoes a volumetric change of about 10% (Nitta et al., 2015; G. Wang et al., 2024). Several examples of intercalation-type anode materials crystal structure are depicted in Figure 2.4.
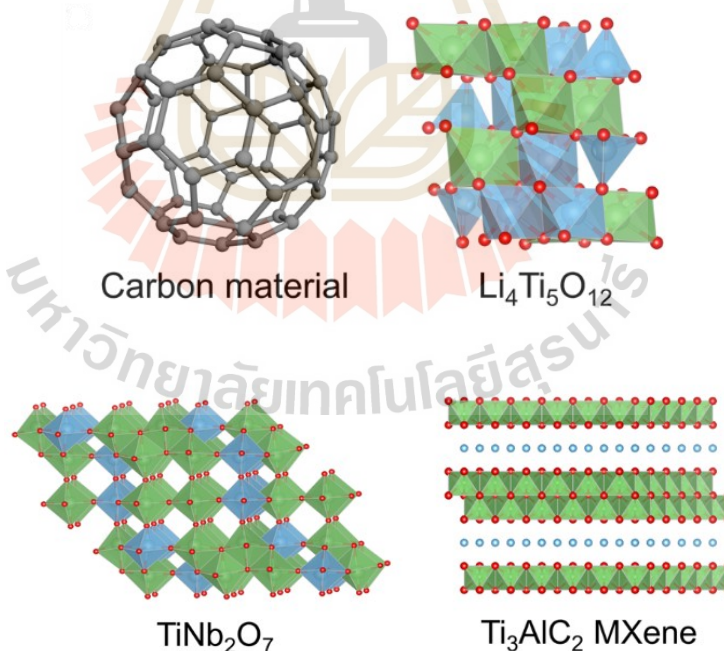
Figure 2.4 Crystal structure of intercalation-type anode materials (G. Wang et al., 2024).

2.1.2.3 Conversion-typed cathode electrode

Conversion-type cathode materials include metal halides (chlorides and fluorides) and metal chalcogenides (sulfides and selenides), which undergo redox reactions as described in equation (2.5). Additionally, elemental electrodes such as sulfur, selenium, tellurium, and iodine exhibit reversible redox reactions as shown in equation (2.6). The volume expansion of the crystal structure of the conversion-type cathode compound according to equation (2.5) as illustrated in Figure 2.5.
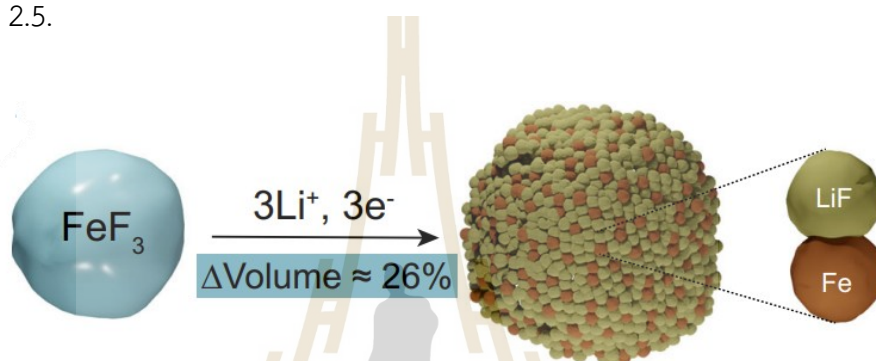
Figure 2.5   Schematics of the volume expansion of the metal halide electrode (FeF_3) upon its lithiation (Baumgärtner et al., 2022).

2.1.2.4 Conversion-type anode electrode

Examples of conversion-type anodes are shown in Figures 2.6 and 2.7. Various conversion-type anode compounds have been developed, including transition metal oxides (MnO, Co_3O_4, Fe_2O_3, etc.) and transition metal sulfides (MoS_2, FeS, WS_2, etc.). Instead of conversion-type alloying materials, metals and metalloids such as Sb, Ga, Si, Zn, Ge, and Sn were selected.
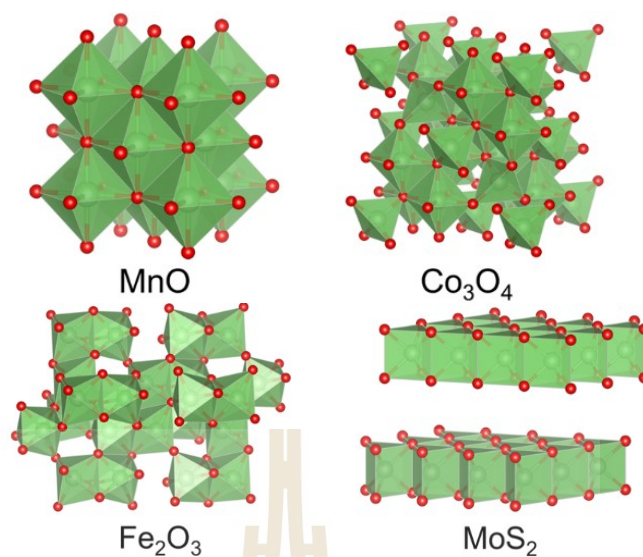
Figure 2.6   Crystal structure of conversion-type compounds anode materials (G. Wang et al., 2024).
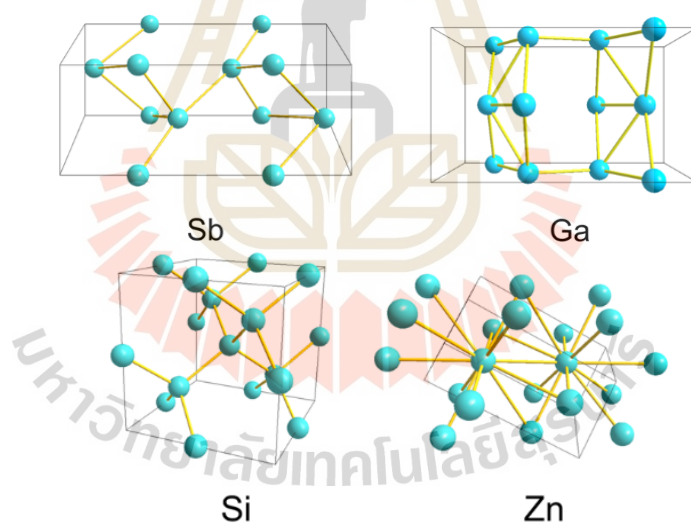
Figure 2.7   Crystal structure of alloying anode materials (G. Wang et al., 2024).

During the lithiation–delithiation process, lithium ions (Li$^+$, represented as green dots in Figure 2.8) are inserted into the host sites of the electrode materials. As illustrated in Figures 2.8(a) and 2.8(b), this intercalation mechanism occurs in graphite and lithium titanate, which possess intercalation-type crystal structures, as described by equation (2.4). These materials exhibit minimal changes in their crystal structures during cycling.

In contrast, conversion-type alloying materials, such as silicon (Figure 2.8(c)), undergo significant structural transformations due to alloying and/or the formation of intermetallic compounds between lithium atoms and the anode material. This reaction results in substantial volume expansion—up to 270%—upon full lithiation of silicon, as depicted in Figure 2.8(c).
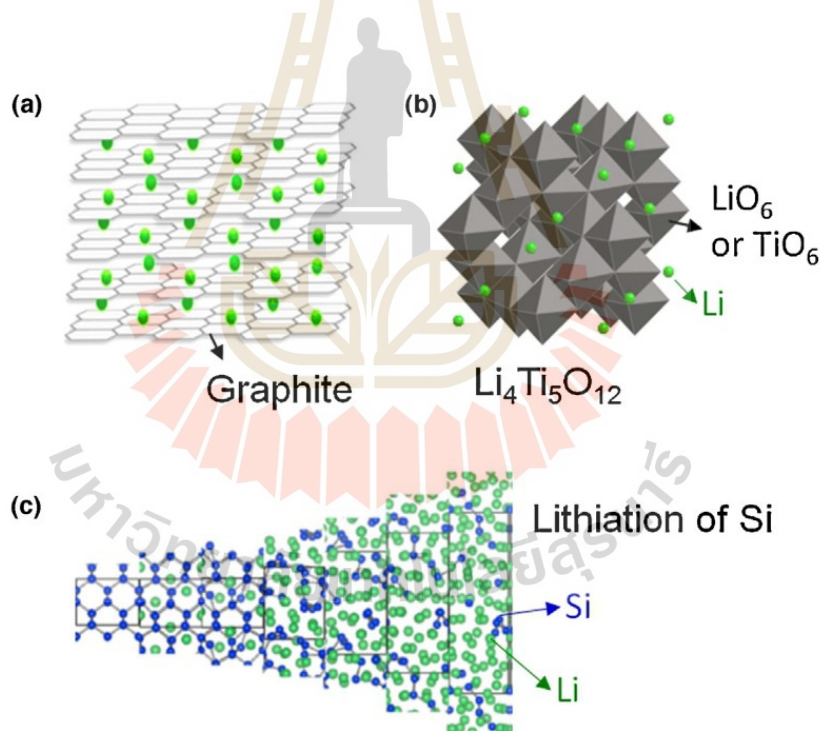
Figure 2.8   Crystal structures of (a) lithiated graphite, (b) lithium titanate (LTO), and (c) silicon during lithiation, which shows the expansion of volume (270% volume change when fully lithiated) (Nitta et al., 2015).

A variety of electrode materials have been developed over the past few decades. Figure 2.9 and Figure 2.10 illustrate the classification details of electrode materials for LIBs, respectively, for the cathode and anode. The most commercialized couple of cathode and anode materials were intercalation-type materials, such as LCO/Graphite (G), NMC/G, NCA/G, and LFP/G.
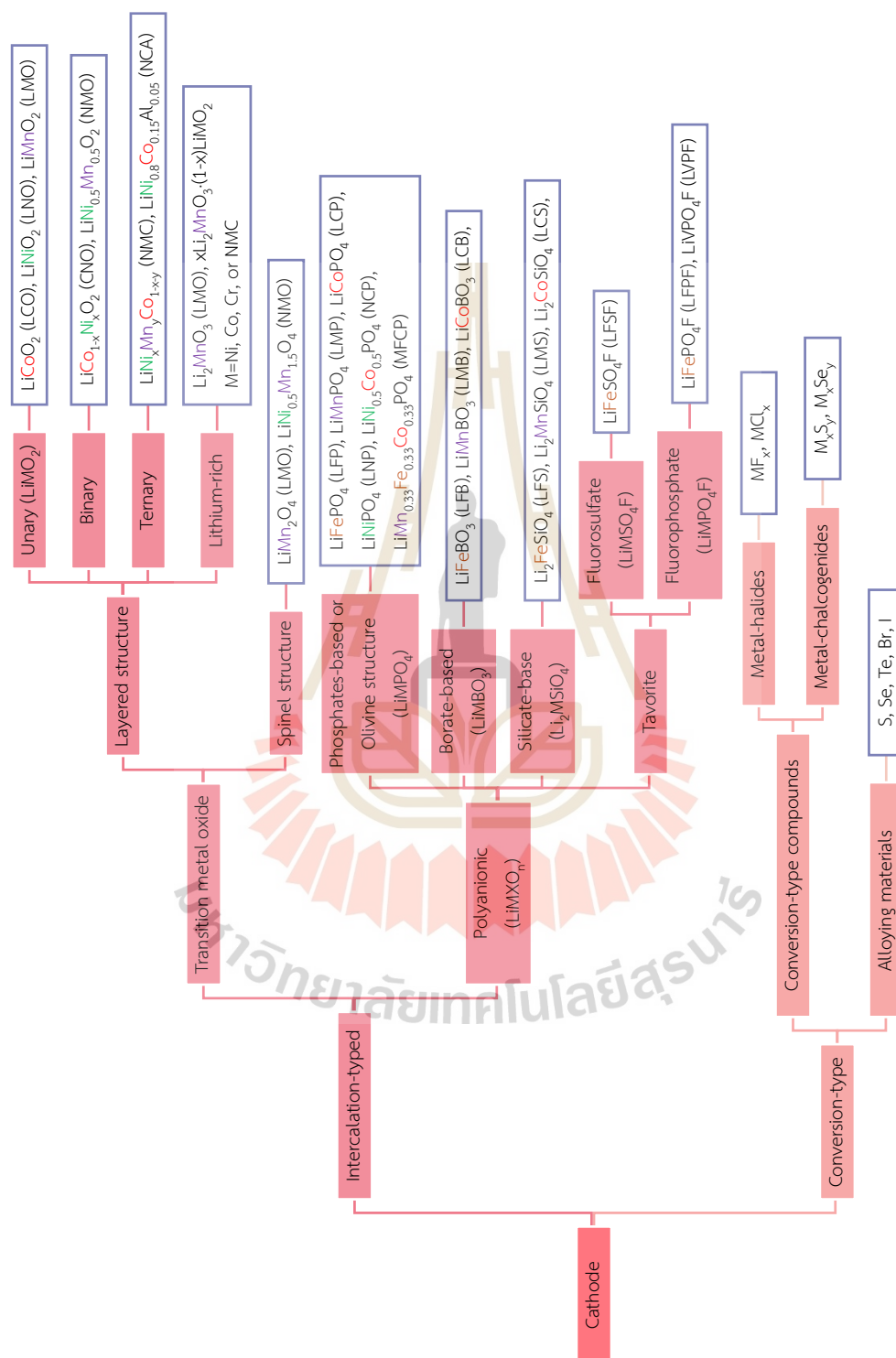
Figure 2.9   Classifications of cathode materials for LIBs.
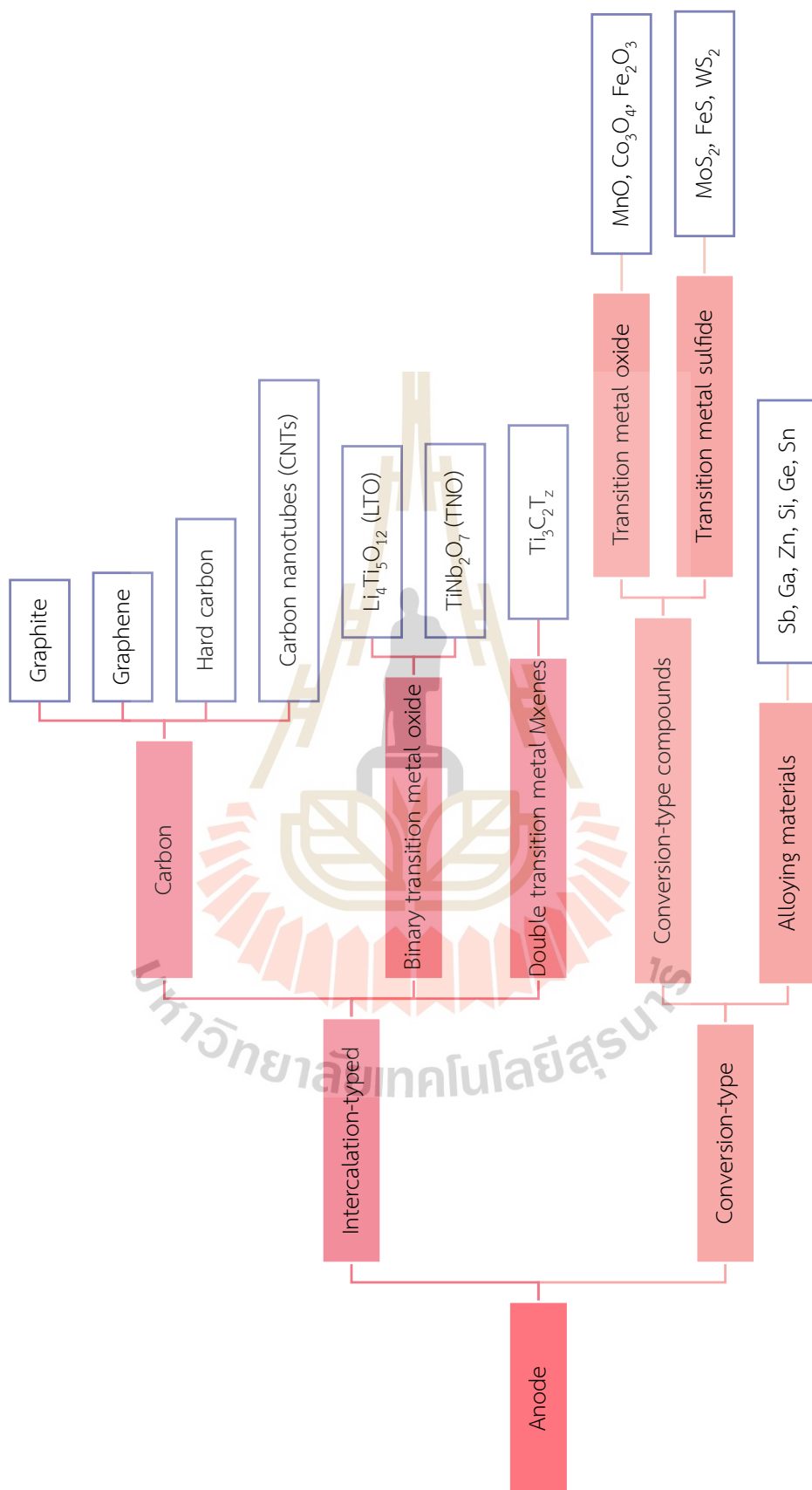
Figure 2.10   Classifications of anode materials for LIBs.

Qualifications of each commercialized type of LIBs are shown in the radar maps in Figure 2.11. LCO/G was the first and the most commercially successful form of layered transition metal oxide cathodes, known for its high-rate capability. However, it is the most expensive due to the limited availability of cobalt resources. This material is still used in the majority of commercial Li-ion batteries (Nitta et al., 2015). NCA/G offers the highest energy density but has the lowest safety. Both spinel LMO/G and NMO/G have a low life cycle but are cost-effective and safe. NMO/G has a high energy density, whereas LMO/G has a low energy density. Although LFP/G has moderate energy density, it excels in safety, life cycle, sustainability, and cost-effectiveness. LFP/G is often selected as the power source in electric vehicles. NMC/G is widely used in various applications, including electric vehicles and portable electronics, due to its balanced performance characteristics.
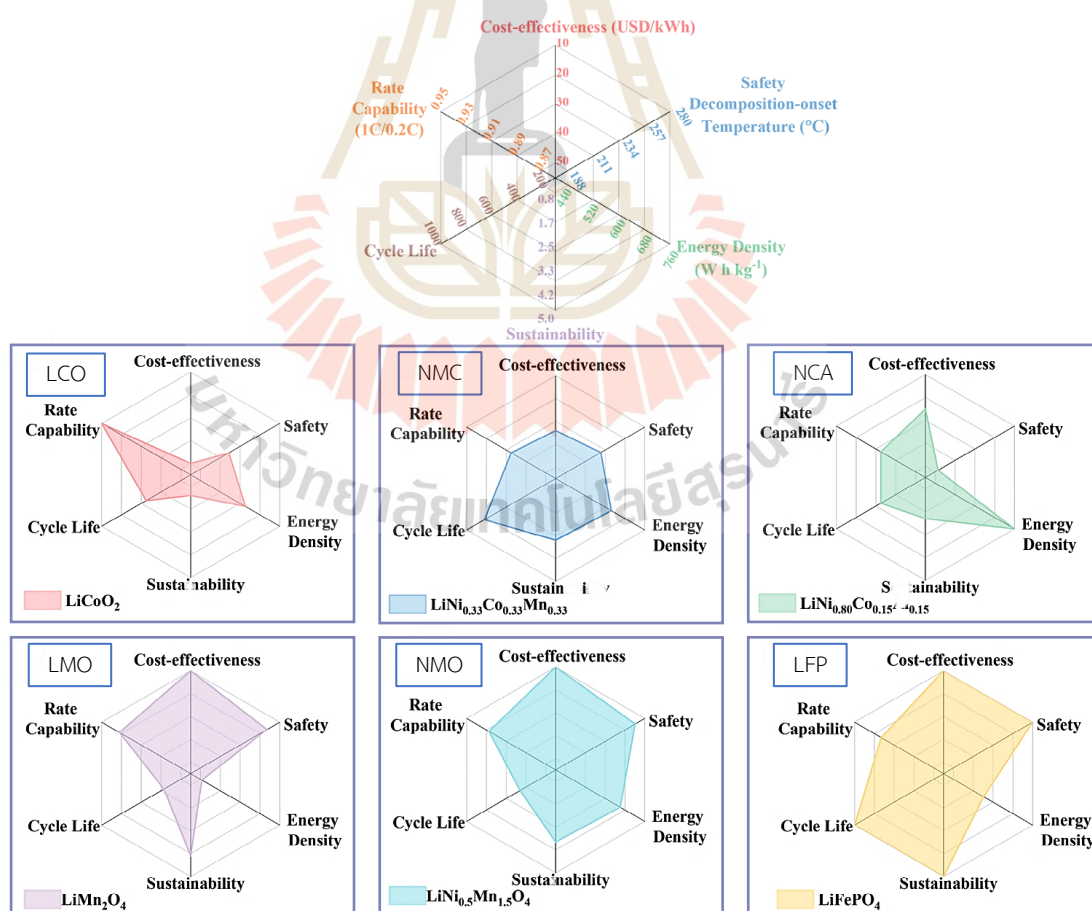
Figure 2.11 Radar maps of qualifications for each commercialized LIB (Ma et al., 2024).

2.2. Microorganism and metal extraction (biometallurgy)

2.2.1 Microorganism and metal extraction

Generally, metallurgical processes for metal extraction can be divided into three categories:

Pyrometallurgy involves the use of heat to extract metals, such as in the smelting process.

Hydrometallurgy: This process uses acidic or alkaline solutions to dissolve metals (leaching) from solids into ions that are soluble in the solution or precipitate as metal compounds.

Electrometallurgy: This is commonly used to extract metals with high purity (electrorefining) or to extract metals from solutions in their pure metal form (electrowinning).

However, around 1960, it was discovered that the bacterium *Acidithiobacillus ferrooxidans* (formerly known as *Thiobacillus*) can grow by oxidizing ferrous ions (Fe^{2+}) and sulfur, thereby increasing the acidity of the environment. Despite the lower pH caused by sulfuric acid produced from the bacterium's cellular activities, the bacteria can still survive. They can also thrive in environments with high levels of metal contamination. Kennecott Mining Company began using *A. ferrooxidans* for bioleaching copper from low-grade copper ore at the Bingham Canyon Mine in Utah, USA (Brierley, 2008; Johnson, 2014). Subsequently, studies on the mechanisms of metal extraction by microorganisms identified three main groups capable of metal extraction: bacteria, archaea, and fungi. These microorganisms can produce acids that dissolve metals, similar to hydrometallurgical processes, but the mechanisms and types of acids produced differ. Bacteria and archaea typically produce sulfuric acid, while fungi produce organic acids. When these microbial-produced acids react with metals, they transform the metals into ions or water-soluble compounds (bioleaching) (Donati & Sand, 2007). These can then be further processed to obtain the desired products using hydrometallurgical or electrometallurgical methods, as illustrated in Figure 2.12.
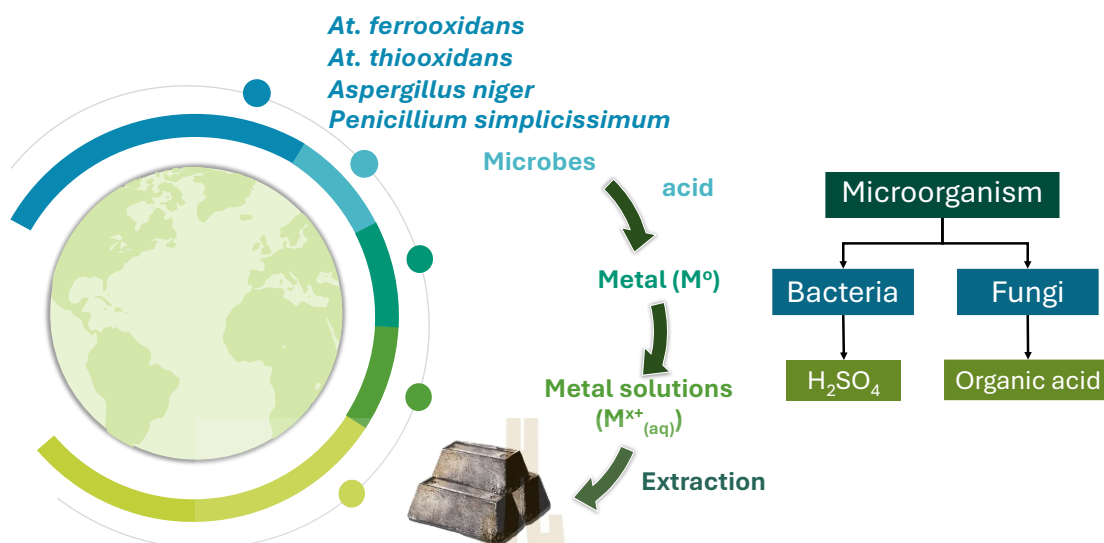
Figure 2.12 Overview of microbial metal extraction.

2.2.2 Bioleaching mechanism

The mechanisms of bioleaching primarily occur in two forms, depending on the type of microbes used. Firstly, in bacterial leaching (including archaea), sulfuric acid is the primary agent that corrodes and leaches metals from raw materials. Secondly, in fungal leaching, metal species are either leached or precipitated as organic compounds due to the various types of organic acids secreted by fungi.

2.2.2.1 Bacterial leaching

Bacteria that can be utilized for bioleaching must belong to the group of acidophiles, which can thrive in acidic environments. These bacteria obtain energy through the oxidation of inorganic substances, such as H_2S, NH^{4+}, or Fe^{2+}, and utilize inorganic compounds as electron donors. This group of bacteria is referred to as chemolithotrophic. Additionally, they must be able to survive in environments with high levels of metal contamination. During their cellular activities, these bacteria oxidize ferrous ions (Fe^{2+}) to ferric ions (Fe^{3+}). The Fe^{3+} then reduces insoluble metal sulfides to soluble metal ions, while the sulfur from the metal sulfides is oxidized to produce sulfuric acid (H_2SO_4). In cases where the metal sulfide substrate does not react with protons, this process is known as the thiosulfate pathway, as illustrated in

Figure 2.13 (a). Conversely, when the metal sulfide substrate reacts with protons, such as FeS_2, MoS_2, and WS_2, hydrogen ions are consumed, resulting in the formation of elemental sulfur (S_8), as shown in Figure 2.13 (b), which is referred to as the polysulfide pathway.
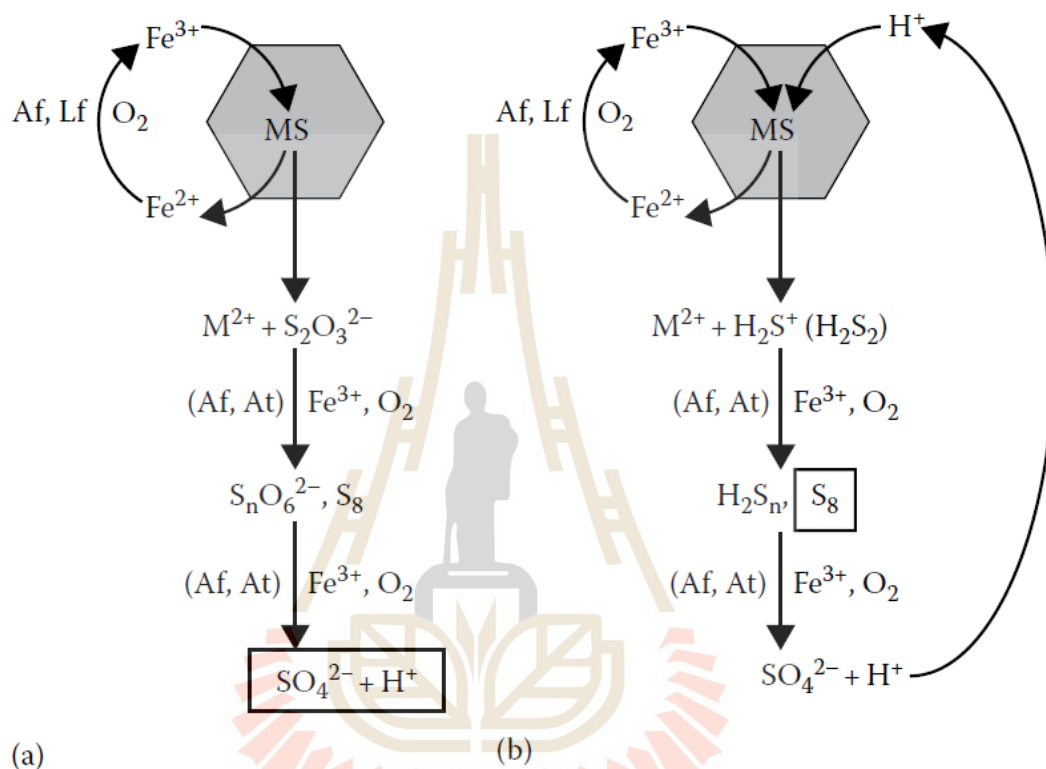
Figure 2.13 Comparative diagram of the thiosulfate pathway (a) and the polysulfide pathway (b) (Donati & Sand, 2007).

Examples of bacteria (and archaea) capable of thriving in acidic environments (acidophiles) and oxidizing metal sulfides, ferrous ions, and sulfur are presented in Table 2.1

Table 2.1   Physiological properties of acidophilic and metal sulfide oxidizing bacteria and archaea (Donati & Sand, 2007).

Species	Oxidation of				Growth
	Pyrite	Other MS	Fe(II)ions	Sulfur	
Mesophilic and moderately thermophilic Bacteria					
Acidimicrobium ferrooxidans	+	na	+	-	F
Acidithiobacillus albertensis	-	+	-	+	A
Acidithiobacillus caldus	-	+	-	+	F
Acidithiobacillus ferrooxidans	+	+	+	+	A
Acidithiobacillus thiooxidans	-	+	-	+	A
Alicyclobacillus disulfidooxidans	+	na	+	+	F
Alicyclobacillus tolerans	+	+	+	+	F
"Caldibacillus ferrivorus"	+	na	+	+	F
"Ferrimicrobium acidiphilum"	+	na	+	-	H
Leptospirillum ferriphilum	+	+	+	-	A
"Leptospirillum ferrodiazotrophum"	na	na	+	na	A
Leptospirillum ferrooxidans	+	+	+	-	A
Sulfobacillus acidophilus	+	+	+	+	F
"Sulfobacillus montserratensis"	+	na	+	+	F
Sulfobacillus sibiricus	+	+	+	+	F
Sulfobacillus thermosulfidooxidans	+	+	+	+	F
Sulfobacillus thermotolerans	+	+	+	+	F
"Thiobacillus plumbophilus"	-	+	-	+	A
"Thiobacillus prosperus"	+	+	+	+	A
Thiomonas cuprina	-	+	-	+	F
Mesophilic and moderately thermophilic Archaea					
"Ferroplasma acidarmanus"	+	na	+	-	F
Ferroplasma acidiphilum	+	na	+	-	F
"Ferroplasma cupricumulans"	na	+	+	+	F
Extremely thermophilic Archaea					
Acidianus brierleyi	+	+	+	+	F
Acidianus infernus	+	+	+	+	A
Metallosphaera hakonensis	na	+	na	+	F
Metallosphaera prunae	+	+	+	+	F
Metallosphaera sedula	+	+	+	+	F
Sulfolobus metallicus	+	+	+	+	A
Sulfolobus yangmingensis	na	+	na	+	F
Sulfurococcus mirabilis	+	+	+	+	F
Sulfurococcus yellowstonensis	+	+	+	+	F

MS = Metal sulfides other than pyrite; A = autotroph; F = facultative autotroph and/or mixotroph; H = heterotroph; na = data not available; species without standing in nomenclature (http://www.bacterio.cict.fr/) are given in quotation marks

2.2.2.2 Fungal leaching

In addition to the bacteria and archaea mentioned in section 2.2.2.1, another group of microorganisms that can be utilized for bioleaching is fungi. Fungi, which are more evolutionarily advanced than bacteria, can produce acids through the metabolism of carbohydrates (polysaccharides), amino acids, and proteins to obtain energy for survival. The acids produced by fungi differ from the sulfuric acid produced by bacteria and vary depending on the type of fungi and the substrates used for decomposition, resulting in various organic acids with more complex molecular structures than inorganic acids, such as sulfuric acid.

Moreover, fungi can grow in a broader range of pH environments compared to bacteria, making them more effective for recycling or extracting metals from waste, as metals often exist in compounds that can be either acidic or basic in nature. Additionally, fungi can produce larger quantities of acid than bacteria. Metal bioleaching by fungi involves three main mechanisms: acidolysis, complexolysis, and redoxolysis (Hong, 2017).

Acidolysis: This mechanism involves converting metals from insoluble compounds, such as metal oxides, into ions that are more soluble in solutions. The acids produced by fungi provide protons that react with oxygen on the surface of metal oxide compounds, forming water and releasing metal ions into the solution. An example is the conversion of nickel oxide as shown in equation (2.7):

$$NiO + 2H^+ \longrightarrow Ni^{2+} + H_2O \tag{2.7}$$

Complexolysis: This mechanism allows metal ions to remain dissolved in solutions by forming complex compounds. Examples include oxalic acid complexes with aluminum, iron, and magnesium; citric acid complexes with magnesium and calcium; and tartaric acid complexes with iron, calcium, silicon, magnesium, and aluminum. An example is the formation of nickel citrate from nickel ions and citric acid, as shown in equation (2.8), which also regenerates protons for further acidolysis reactions. Metals dissolved through acidolysis become more stable

in solution due to complexolysis, as the ions form coordinate covalent bonds with ligands, preventing them from reacting with other elements to form new compounds:

$$Ni^{2+} + C_6H_8O_7 \longrightarrow Ni(C_6H_5O_7)^- + 3H^+ \qquad (2.8)$$
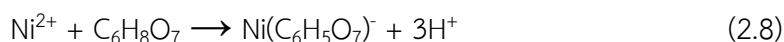
Redoxolysis: This mechanism involves oxidation-reduction (redox) reactions, such as the conversion of insoluble manganese (IV) oxide to manganese (II) ions, as shown in equation (2.9):

$$MnO_2 + 2e^- + 4H^+ \longrightarrow Mn^{2+} + 2H_2O \qquad (2.9)$$
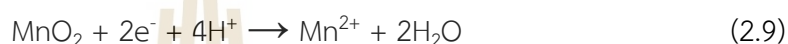
2.3. Recent recycling technology for lithium-ion batteries

Based on a review of research related to lithium-ion battery recycling, the processes can be categorized into four groups: pyrometallurgy (high-temperature processing), hydrometallurgy (chemical leaching and precipitations), direct recycling (reusing components), and biometallurgy (using biological agents). Each process has distinct advantages and limitations, which are discussed in the following sections.

2.3.1 Battery recycling via pyrometallurgy

Pyrometallurgy is a process that involves the application of heat, including calcination to decompose raw materials, roasting to induce chemical reactions at elevated temperatures, and smelting to produce alloys by adding reducing agents and fluxes. Pyrometallurgy is a relatively straightforward process that can be conducted on a large scale. Consequently, the recycling of lithium-ion batteries using pyrometallurgy is easily applicable in industrial settings.

Georgi-Maschler et al. (2012) experimented on the recycling of lithium-ion batteries using smelting reduction in an electric arc furnace (EAF) with an internal temperature of 1,700 - 1,750°C. The process yielded a cobalt-based alloy as the primary product. In addition to the metal, the method also produced slag and dust, which were emitted along with the exhaust gases, as shown in Figure 2.14. Chemical composition analysis using ICP-OES revealed that the slag and dust collected in the

gas capture equipment contained lithium at concentrations of 1.4% and 20.1%, respectively. The composition of other elements is presented in Table 2.2.

Metal (Co-Base alloy)   Slag   Flue dust

Figure 2.14 Products from battery smelting in an EAF furnace (left) metal, (center) slag, and (right) dust (Georgi-Maschler et al., 2012).

Table 2.2   Chemical composition (mass%) of metal, slag, and dust obtained from smelting (Georgi-Maschler et al., 2012).

	Al	Ca	Co	Cr	Cu	Fe	Li	Mn	Ni	Si	C	P
Metal	0.4	n.v.	55.3	0.4	1.1	22.9	n.v.	1.4	2.1	15.7	n.v.	0.6
Slag	n.d.	38.3	1.1	n.d.	n.v.	1.3	1.4	n.v.	n.v.	15.6	7.3	0.1
Flue dust	-	22.3	19.4	-	0.7	-	20.1	-	-	-	13.2	-

To recover lithium lost in the slag and dust generated during smelting, the slag and dust are further processed using hydrometallurgical techniques. This involves leaching the slag and dust with sulfuric acid, followed by the addition of sodium carbonate to precipitate lithium as lithium carbonate with a purity exceeding 99%. This high-purity lithium carbonate can be used as a raw material to produce specialty glass.

Since lithium has a boiling point of only 1,330°C, it can be lost in significant amounts, such as dust and gas. Therefore, combining pyrometallurgy and hydrometallurgy can be more effective for extracting and recovering metals than using pyrometallurgy alone.

2.3.2 Battery recycling via hydrometallurgy

Research in hydrometallurgy for extracting lithium and cobalt from lithium-ion batteries primarily involves leaching using acid solutions. Each study varies in the type of acid and additional substances used to enhance leaching efficiency. Based on the type of acid used, leaching can be categorized into two main groups: inorganic acid leaching and organic acid leaching, as summarized in Table 2.3

Table 2.3 Recycling of lithium-ion batteries using different types of acid leaching methods

Type of acid (conc.) (ref.)	Additional	Optimum condition	Products	%recovery
H_2SO_4 (2M) (Shin et al., 2005)	H_2O_2 15 vol% (as reducing agent)	s/l ratio = 50 g/L, duration 10 min., 75°C, agitation 300 rpm	Leached solution	~100% Co ~100% Li
H_2SO_4 (0.75M) (Ferreira et al., 2009)	H_2O_2 1 vol% (as reducing agent) NaOH 15% w/w (separated Al)	s/l ratio = 33.33 g/L, duration 60 min., 40°C, agitation 300 rpm	Leached solution $CoSO_4(H_2O)$	97% Co 100% Li
H_2SO_4 (3M) (J. Wang et al., 2012)	$Na_2S_2O_3$ 0.25M (as reducing agent)	s/l ratio = 66.67 g/L, duration 180 min., 90°C	Leached solution	99.95% Co 99.71% Li
H_2SO_4 (2M) (Nayl et al., 2017)	H_2O_2 4 vol% (as reducing agent) NH_4OH 4M (separated Cu and Al) NaOH 2M (precipitant) Saturated solution of Na_2CO_3 (precipitant)	s/l ratio = 100 g/L, duration 120 min., 70°C, agitation 250 rpm	$Co(OH)_2$ (95%recovery) Li_2CO_3 (90%recovery) $NiCO_3$ (91%recovery) $MnCO_3$ (94%recovery)	99.6% Co 98.8% Li 99.4% Ni 97.8% Mn
H_2SO_4 (1M) (Meshram et al., 2015)	$NaHSO_3$ 0.075M (as reducing agent) Oxalic acid, NaOH, and a saturated solution of Na_2CO_3 (precipitant)	s/l ratio = 20 g/L, duration 240 min., 95°C, agitation 500 rpm	Cobalt oxalate (96% purity) Li_2CO_3 $NiCO_3$ $MnCO_3$	91.6% Co ~96.7% Li 96.4% Ni 87.9%Mn
H_2SO_4 (2M) (Peng et al., 2018)	Ascorbic acid 0.11M (as reducing agent)	s/l ratio = 200 g/L, duration 90 min., 80°C, agitation 200 rpm	Leached solution	93.8% Co 95.7% Li

Table 2.3 Recycling of lithium-ion batteries using different types of acid leaching
methods (continued)

Type of acid (conc.) (ref.)	Additional	Optimum condition	Products	%recovery
HCl (3M) (Freitas & Garcia, 2007)	H_2O_2 30% v/v (as reducing agent)	s/l ratio = 18.3 g/L, duration 120 min., 80°C	Cobalt electrodeposit	96.9% charge efficiency of Co
HCl (4M) (J. Li et al., 2009)	NaOH (remove impurities)	duration 120 min., 80°C	Leached solution	99% Co 97% Li
H_3PO_4 (0.8M) (Chen et al., 2018)	H_2O_2 4 vol% (as reducing agent)	s/l ratio = 33.33 g/L, duration 20 min., 40°C	Li_3PO_4 (98.4% purity) Co residual	100% Li
Oxalic acid (3M) (Sohn et al., 2006)	-	s/l ratio = 50 g/L, duration 90 min., 80°C, agitation 300 rpm	Leached solution	<1% Co >99% Li
Citric acid (1.25M) (L. Li et al., 2010)	H_2O_2 1 vol% (as reducing agent)	s/l ratio = 20 g/L, duration 30 min., 90°C, agitation 300 rpm	Leached solution	>90% Co ~100% Li
Ascorbic acid (1.25M) (L. Li et al., 2012)	-	s/l ratio = 25 g/L, duration 20 min., 70°C, agitation 300 rpm	Leached solution	94.8% Co 98.5% Li
Tartaric acid (0.6M) (Chen et al., 2019)	H_2O_2 3 vol% % (as reducing agent)	s/l ratio = 33.33 g/L, duration 30 min., 80°C, agitation 300 rpm	Li^+ enriched solution Cobalt tartrate	98% Co 97% Li

Utilization of inorganic acids for leaching lithium-ion batteries has
demonstrated significant recovery of metals. A notable aspect of these studies is the
use of reducing agents in the leaching process. This is because cobalt in the feed
material exists as Co^{3+}, which is insoluble in solution. Adding reducing agents converts
Co^{3+} to the more soluble Co^{2+}. Commonly used reducing agents include hydrogen
peroxide (H_2O_2), with some studies also employing sodium thiosulfate ($Na_2S_2O_3$),
sodium bisulfite ($NaHSO_3$), or ascorbic acid, all of which achieve high metal recovery
rates.

In the study by Meshram et al. (2015), sodium bisulfite was used to reduce cobalt ions in 1M sulfuric acid, followed by the addition of oxalic acid after leaching. The pH was adjusted to 1.5, and the temperature was set to 50°C to precipitate the dissolved cobalt as cobalt oxalate ($CoC_2O_4 \cdot 2H_2O$), as confirmed by the X-ray diffraction patterns of the precipitate shown in Figure 2.15. Subsequently, other metals were sequentially precipitated. Manganese was precipitated by adjusting the pH to 7.5 with 5 M sodium hydroxide and adding a saturated sodium carbonate solution to form manganese carbonate. The pH was then adjusted to 9 with sodium hydroxide and saturated sodium carbonate solution to precipitate nickel carbonate. Finally, lithium carbonate was precipitated by adjusting the pH to 14 and adding sodium carbonate again, with heating to reduce the solution volume by 50%. The overall procedure and metal precipitation steps are illustrated in Figure 2.16.
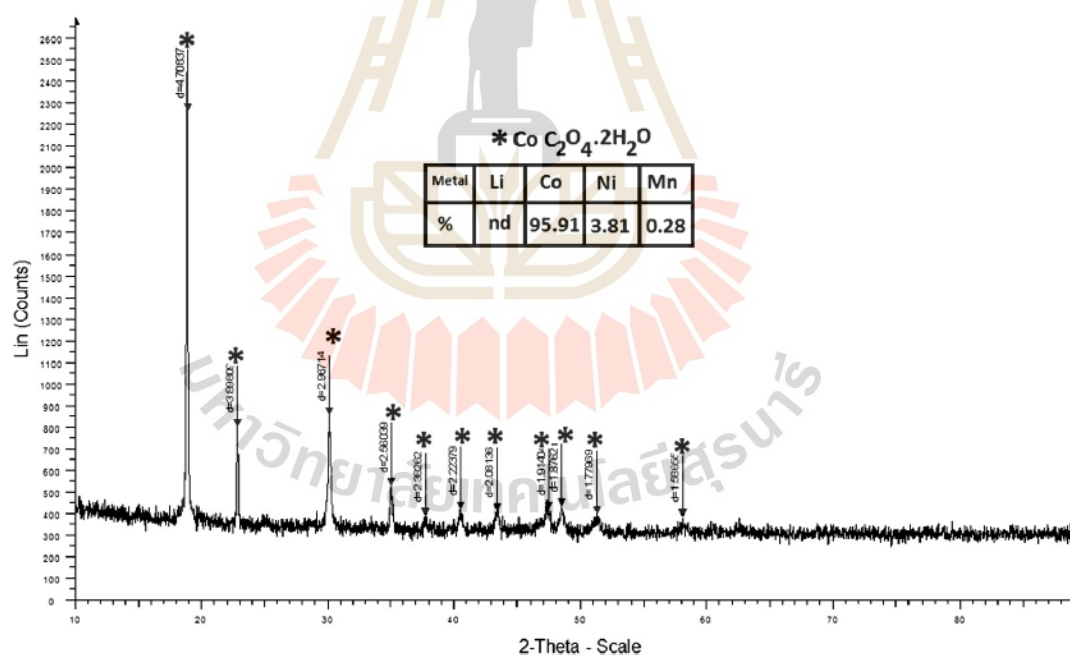
Figure 2.15 X-ray diffraction (XRD) pattern of precipitated cobalt oxalate (Meshram et al., 2015).
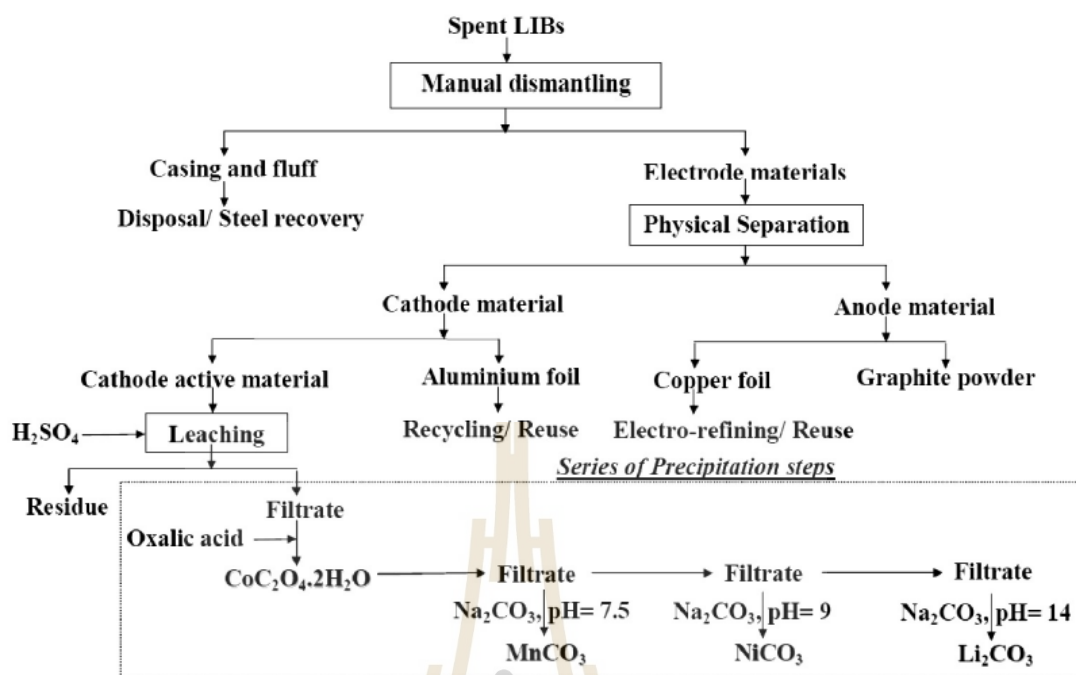
Figure 2.16 Overview of the process of lithium, manganese, nickel, and cobalt precipitation from sulfuric acid leaching of lithium-ion batteries (Meshram et al., 2015)

Additionally, the research by Kang et al. (2010) utilized oxalic acid to precipitate cobalt from a solution leached with 2M sulfuric acid, using 6% (by volume) hydrogen peroxide as a reducing agent. The cobalt was precipitated as cobalt oxalate, which was then calcined at temperatures above 300°C to form cobalt oxide. The research procedure by Kang et al. is illustrated in Figure 2.17, and the XRD analysis of the product before and after calcination is shown in Figure 2.18.
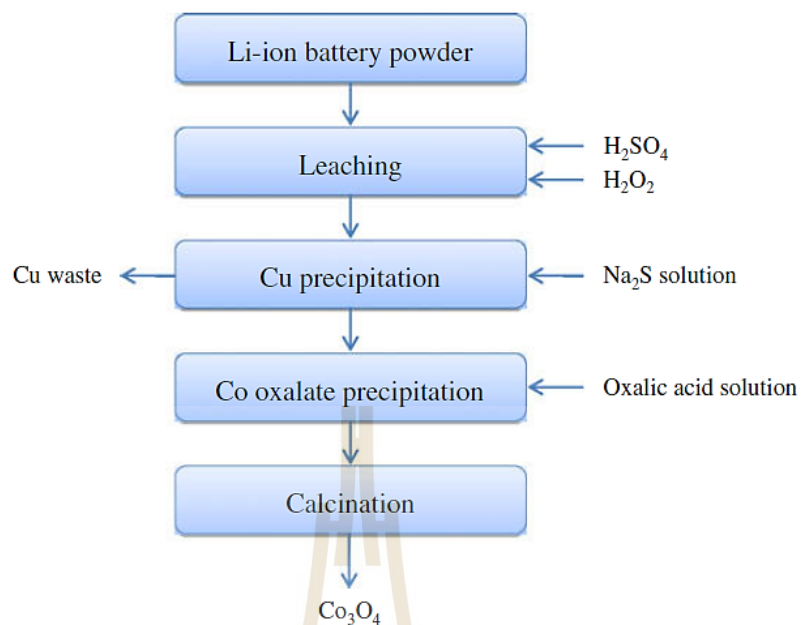
Figure 2.17 Cobalt oxide production process from lithium-ion battery leaching (Kang et al., 2010)
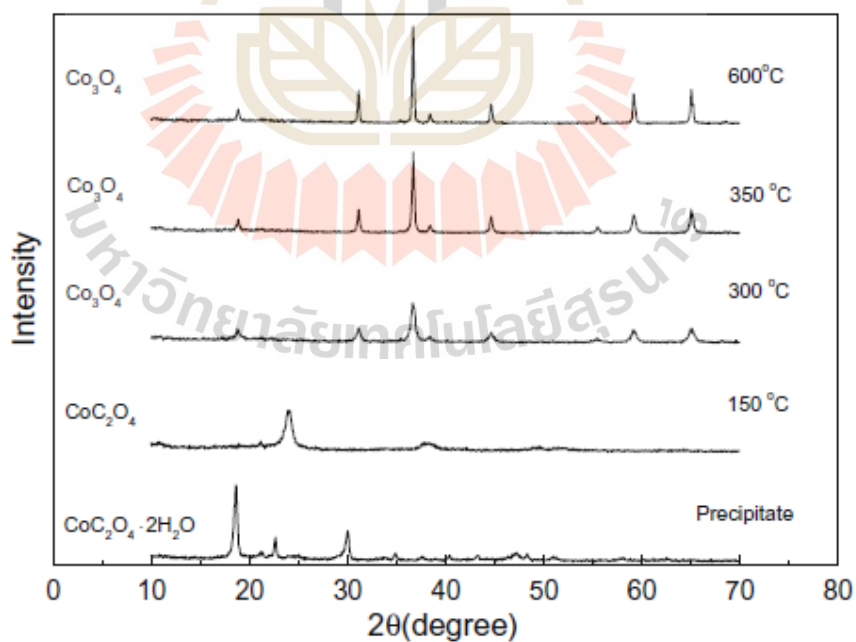
Figure 2.18 The crystal structure sequence of cobalt oxalate upon calcination to form cobalt oxide (Kang et al., 2010).

The study by Sohn et al. (2006) utilized 3M oxalic acid for leaching, achieving a lithium recovery rate of over 99%. However, cobalt recovery was less than 1% because cobalt precipitated as cobalt oxalate, as confirmed by the X-ray diffraction patterns shown in Figure 2.19
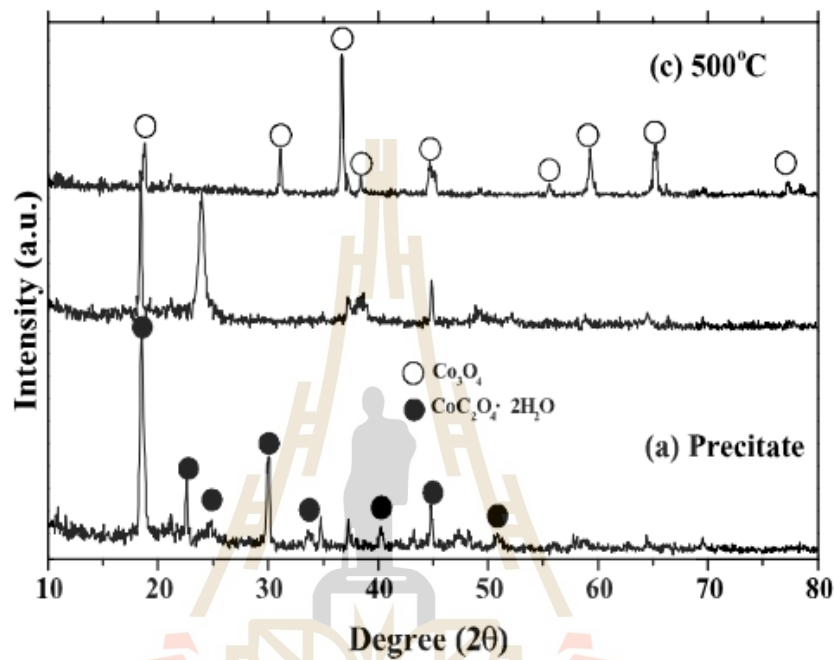
Figure 2.19 Diffraction pattern of residues from oxalic acid battery leaching (Sohn et al., 2006)

The hydrometallurgical process achieves very high recovery rates and specific reactions due to the different chemical reactivities of each element and reagent. However, raw materials undergo numerous complex steps to separate and recover each product with high purity. Although this process does not consume heat energy like pyrometallurgy, it requires numerous chemical reagents, including corrosive acids and some organic compounds, which can emit volatile or toxic gases (e.g., SO_2, NO_x).

2.3.3 Battery recycling via direct recycling

Direct recycling involves restoring the structure of degraded lithium-ion battery cathode powder to achieve electrochemical properties comparable to newly synthesized cathode powder. Degraded cathode powder typically has a lithium content in its crystal structure that is less than the molar ratio of lithium to transition metal compounds (Li/transition metal compounds < 1), or the transition metal compounds undergo structural or chemical changes with the electrolyte due to lithium loss. The process of adding lithium back into the crystal structure of degraded cathode powder is known as relithiation. The lithium used for relithiation can be sourced from lithium compounds such as lithium carbonate, lithium hydroxide, lithium phosphate, and lithium sulfate, which are selected based on the method and type of cathode powder. The mechanism of the LCO relithiation process is shown in Figure 2.20.
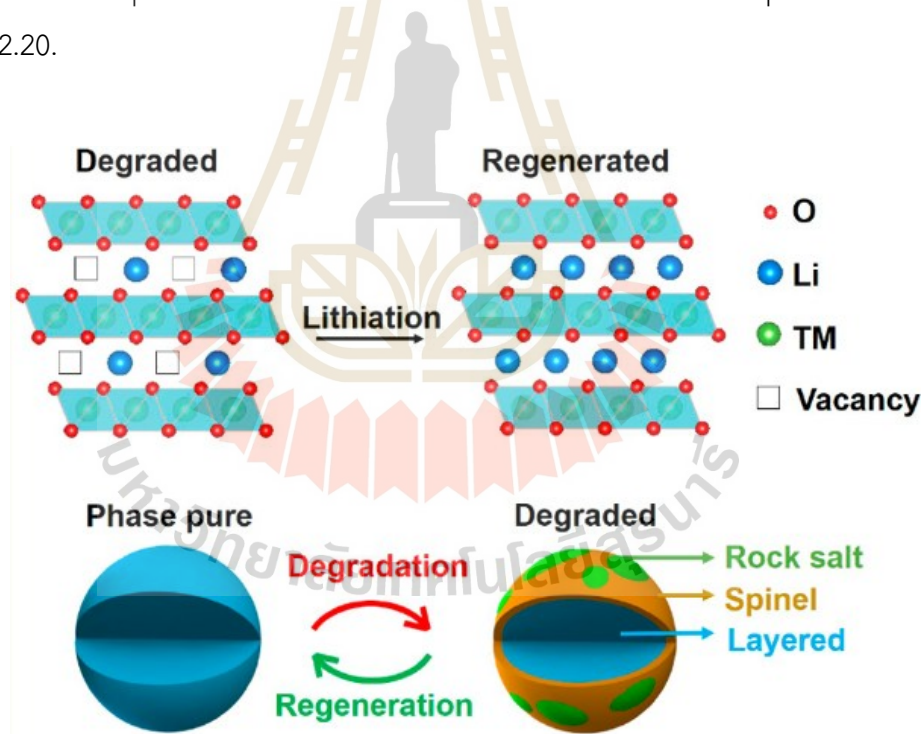
Figure 2.20 The mechanism of the LCO relithiation process (Shi et al., 2018)

Relithiation can be categorized based on the synthesis method as follows: solid-state sintering, electrochemical relithiation, ionothermal relithiation (also known as ionic liquids relithiation), solution relithiation, and eutectic relithiation. Among these, solution relithiation is a cost-effective method that can be applied to a wide variety of cathode powders, considering both chemical composition and crystal structure degradation. Lithium hydroxide is commonly used as the primary compound for lithium addition in the relithiation process. (Lan et al., 2024; P. Xu et al., 2023).

Direct recycling represents the most efficient process for converting end-of-life cathode materials into new ones. It is characterized by the lowest energy consumption, cost, and toxic gas emissions when compared to pyrometallurgy and hydrometallurgy. However, this method faces certain limitations when scaled up to pilot or industrial levels. Specifically, if the raw materials vary significantly in terms of battery waste type (i.e., different structures) or degree of deterioration, simultaneous relithiation becomes infeasible. Additionally, impurities in the raw powder can adversely affect the completeness and chemical composition of the final product (Pražanová et al., 2024).

2.3.4 Battery recycling via biometallurgy

This process involves the production of acids by microorganisms, which subsequently dissolve the metals in the batteries, a method similar to hydrometallurgical leaching. The research categorizes bioleaching into two groups: bacterial and fungal leachings, as summarized in Table 2.4. Bioleaching research predominantly utilizes bacteria capable of oxidizing iron and sulfur, while studies employing fungi are still relatively scarce. The bioleaching experiments are divided into three methods: one-step leaching, two-step leaching, and spent medium leaching.

Table 2.4 Recycling of lithium-ion batteries using bioleaching.

Microbes (ref.)	Methods and medium	Optimum condition	Product	%recovery
Acidithiobacillus ferrooxidans (Mishra et al., 2008)	One-step bioleaching 9K medium	pH = 2.5, s/l ratio = 5 g/L, duration 15 days., 30°C, agitation 200 rpm, S 10 g/L and Fe^{2+} 3 g/L (energy source)	Leached solution	65% Co 10% Li
Acidithiobacillus sp. (mixed IOB and SOB) (B. Xin et al., 2009)	Two-step bioleaching Basic medium	pH = 1.5, s/l ratio = 10 g/L, duration 12+10 days., 30°C, agitation 120 rpm, S 2 g/L and FeS_2 2 g/L (energy source)	Leached solution	- (mechanism study)
Acidithiobacillus ferrooxidans (L. Li et al., 2013)	Two-step bioleaching 9K medium	pH = 1.5, s/l ratio = 10 g/L, duration 2+7 days., 35°C, agitation 160 rpm, Fe^{2+} 35 g/L ($FeSO_4$) (energy source)	Leached solution	48.2% Co
Acidithiobacillus ferrooxidans (Zeng et al., 2012)	Two-step bioleaching 9K medium Cu^{2+} 0.75 g/L ($CuSO_4 5(H_2O)$) (catalyst)	pH = 1.5, s/l ratio = 10 g/L, duration 2+6 days., 35°C, agitation 160 rpm, Fe^{2+} 35 g/L ($FeSO_4$) (energy source)	Leached solution	99.9% Co
Acidithiobacillus ferrooxidans (Zeng et al., 2013)	Two-step bioleaching 9K medium Ag^+ 0.02 g/L ($AgNO_3$) (catalyst)	pH = 1.5, s/l ratio = 10 g/L, duration 2+7 days., 35°C, agitation 160 rpm, Fe^{2+} 35 g/L ($FeSO_4$) (energy source)	Leached solution	98.4% Co
Alicyclobacillus sp. (SOB) and Sulfobacillus sp. (IOB) (Niu et al., 2014)	Two-step bioleaching	pH = 2, s/l ratio = 20 g/L, duration X+11 days., 35°C, S + FeS_2 = 4 g/L (energy source)	Leached solution	72% Co 89% Li

Table 2.4   Recycling of lithium-ion batteries using bioleaching. (continued)

Microbes (ref.)	Methods and medium	Optimum condition	Product	%recovery
Acidithiobacillus ferrooxidans and *Leptospirillum ferriphilum* (IOB) (Y. Xin et al., 2016)	Two-step bioleaching Basic medium	pH = 1, s/l ratio = 10 g/L, duration X+9 days., 30°C, agitation 120 rpm, S 16 g/L and FeS_2 16 g/L (energy source)	Leached solution	89% Li (from $LiFePO_4$) 95% Li 96% Mn (from $LiMn_2O_4$) >90% Li, Mn 40% Co, Ni (from $LiNi_xCo_yMn_{1-x-y}O_2$)
Leptospirillum ferriphilum (IOB) (consortium) (Khatri et al., 2019)	Two-step bioleaching 9K medium	pH = 2, s/l ratio = 10 g/L, duration 2+6 days., 31°C, agitation 150 rpm, Fe^{2+} 9 g/L (energy source)	Leached solution	92±7% Cu-Zn-Ni-Co 37.74% Li
Aspergillus niger (Horeh et al., 2016)	Spent medium bioleaching Sucrose medium	pH = 2, s/l ratio = 10 g/L, duration 14+16 days., 30°C, agitation 130 rpm	Leached solution	45% Co 95% Li 100% Cu 70% Mn 65% Al 38% Ni

In one-step leaching, microorganisms are cultured simultaneously with the addition of metal-containing substrates on the first day of cultivation. The microorganisms are then allowed to grow for the specified duration. This method may affect the initial growth rate of microorganisms if the environment has excessively high metal concentration, resulting in lower acid production. However, certain microorganisms, such as fungi that can tolerate or prefer metal environments, may produce different amounts of acid compared to metal-free conditions.

Two-step leaching involves culturing microorganisms in a standard growth medium until they reach the log phase, after which the metal-containing substrates are added. This method enhances the survival rate of fully grown microorganisms and ensures a consistent level of acid production, thereby increasing the metal dissolution rate compared to one-step leaching.

Spent medium leaching involves culturing microorganisms in a metal-free growth medium until they reach the dead phase, where they can no longer grow due to insufficient nutrients. The dead microorganisms are then filtered out, and the remaining solution, containing acids produced by the microorganisms, is used for metal extraction, similar to the hydrometallurgical method.

In studies conducted by Li et al. (2013) and Zeng et al. (2012, 2013), it was found that the addition of certain metals as catalysts in the bioleaching process significantly increased the percentage of cobalt dissolution. Specifically, the cobalt dissolution increased from 48.2% to 99.9% with the addition of 0.75 g/L copper ions and to 98.4% with the addition of 0.02 g/L silver ions.

Numerous bioleaching bacteria (chemolithoautotrophic acidophilic sulfur and/or iron-oxidizing bacteria or archaea) (Schippers, 2007) and fungi (filamentous fungi) have been reported (Burgstaller & Schinner, 1993; Dusengemungu et al., 2021). However, fungi have several advantages over bacteria. Filamentous fungi have strong adaptability, grow in an environment with high metal concentrations, ranging from acidic to basic conditions, and have a short lag phase (Dusengemungu et al., 2021; Horeh et al., 2016; Yao et al., 2018). They can leach alkali substrates such as metal oxide compound waste. *Aspergillus* and *Penicillium* are two important genera of filamentous fungi in biotechnology and medicine (Houbraken et al., 2014; Tsang et al., 2018). Biswal et al. (2018) reported that the leaching efficiency *Aspergillus niger* (A. niger) was higher than that of bacteria (*Acidithiobacillus thiooxidans*) and acid leaching (Biswal et al., 2018).

The study by Horeh et al. (2016, 2017, 2018) on the extraction of valuable metals from lithium-ion batteries using bioleaching with the fungus *A. niger* found that different bioleaching methods resulted in the production of different organic acids by the fungus, as shown in Table 2.5. It was observed that oxalic acid

was produced in the highest amount during one-step leaching. However, when the bioleaching solution was analyzed for the dissolved metal components, as shown in Figure 2.21, one-step leaching resulted in the lowest cobalt extraction, while lithium dissolution remained high. This finding is consistent with the research by Sohn et al. (2006), which used oxalic acid for metal leaching in the hydrometallurgical process.

Table 2.5 Organic acid concentration in different bioleaching methods (Horeh et al., 2016).

Organic acid (mg/L)	1% (w/v) pulp density		
	One-step	Two-step	Spent medium
Citric	0	133	8,078
Oxalic	9,948	3,372	1,170
Malic	0	0	1,251
Gluconic	0	102	2,126
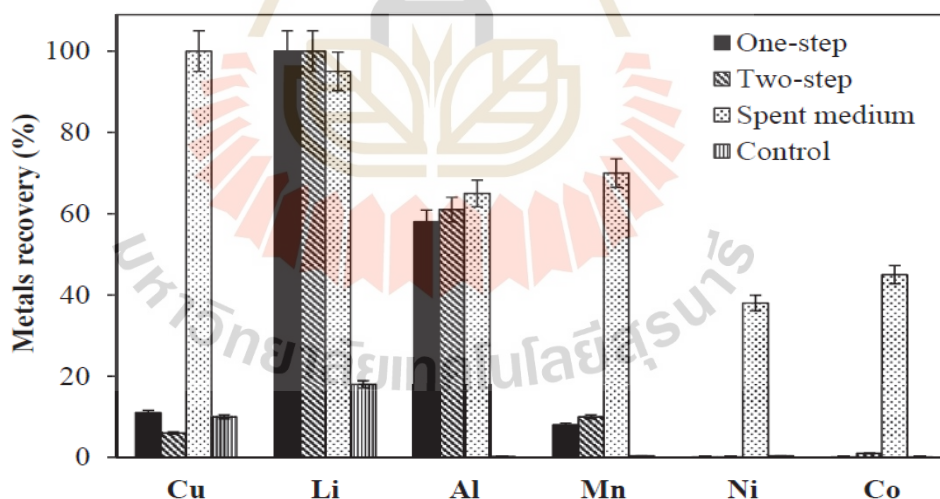
Figure 2.21 Recovery percentage of different metals in different bioleaching methods (Horeh et al., 2016).

In experiments using *A. niger* adapted to metals by culturing in metal-contaminated media, compared to non-adapted strains, it was found that the acids

produced during one-step leaching differed. The non-adapted strain produced only oxalic acid, whereas the adapted strain produced a variety of acids, including oxalic acid, malic acid, citric acid, and gluconic acid, as shown in Figure 2.22. Additionally, the amount of metal extracted in the non-adapted case could not dissolve cobalt, while the adapted strain could dissolve a broader range of metals, as illustrated in Figure 2.23.
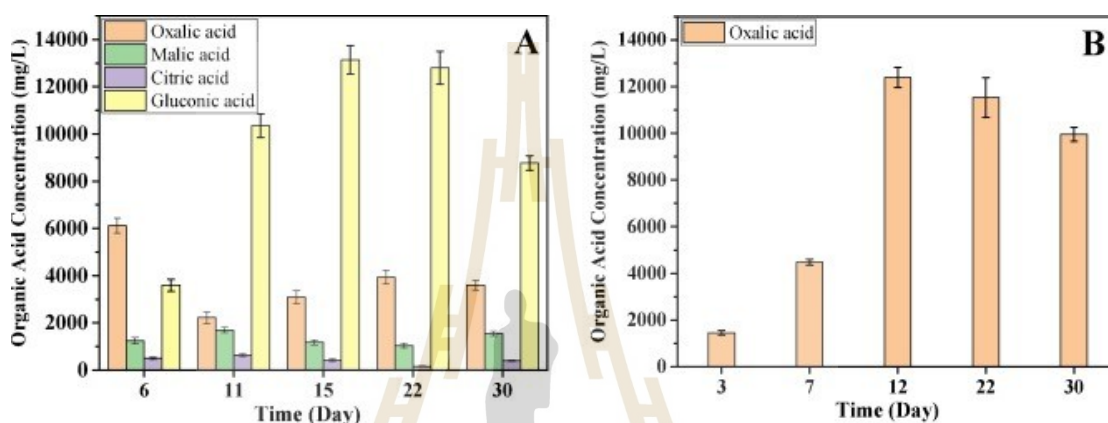
Figure 2.22 Types and amounts of organic acids produced by bioleaching of adapted (A) and unadapted (B) *Aspergillus niger* (Bahaloo-Horeh et al., 2018).
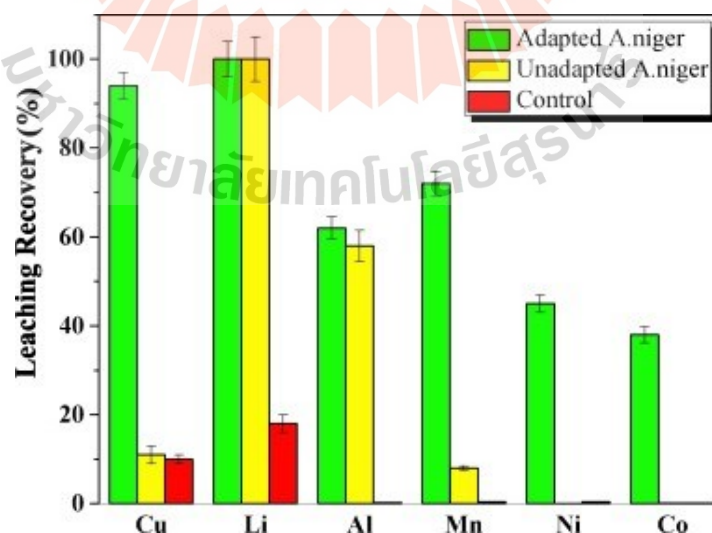
Figure 2.23 Percentage recovery of different metals in adapted and unadapted organisms (Bahaloo-Horeh et al., 2018).

Additionally, a comparative experiment was conducted to evaluate the leaching efficiency between acids produced by *A. niger* and chemically synthesized acids with the same concentration and type as those produced by the fungus. It was found that the acids produced by the fungus resulted in higher metal recovery. The researchers explained that, although the synthetic acids were mixed to match the proportions and composition of the fungal acids, the acids produced by *A. niger* contained other various organic acids in trace amounts that HPLC could not detect. The experimental results are shown in Figure 2.24.
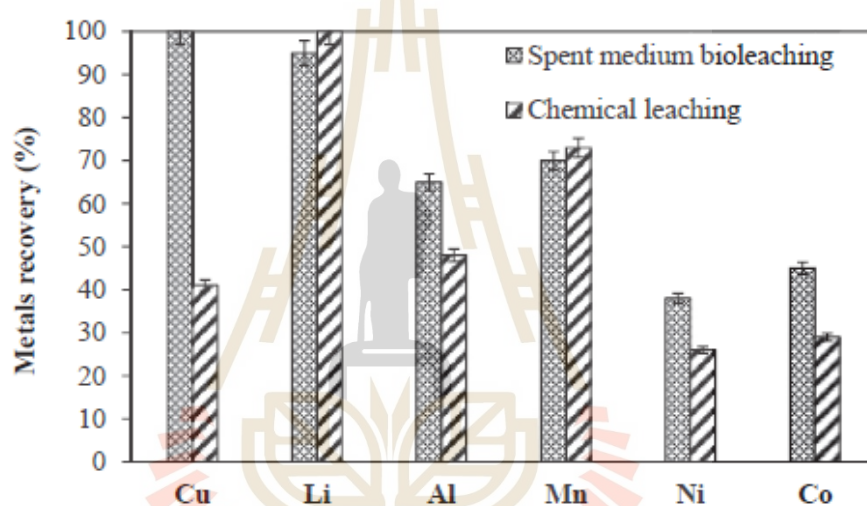
Figure 2.24 Percentage recovery of different metals in leaching with acid produced by *Aspergillus niger* compared with commercially available acids (Horeh et al., 2016).

2.4. Conclusion

This chapter provides an in-depth examination of lithium-ion batteries, encompassing their fundamental principles, classifications, and recycling technologies. The foundational principles of lithium-ion batteries, particularly those involving intercalation and conversion-type electrodes, are crucial for understanding their functionality and efficiency.

Recent advancements in recycling technologies, including pyrometallurgy, hydrometallurgy, direct recycling, and biometallurgy, have highlighted significant progress in the efficient recovery of valuable materials from spent batteries. Each method offers distinct advantages and challenges, contributing to the overarching goal of reducing waste and promoting a circular economy.

The role of biometallurgy, primarily using microorganisms and bioleaching mechanisms, offers a promising and sustainable approach to metal extraction and recycling. This approach not only supports environmental conservation but also enhances the sustainability of battery recycling processes. The continuous development and optimization of these technologies are crucial for meeting the growing demand for lithium-ion batteries while minimizing their environmental footprint. Notably, fungal bioleaching emerges as a particularly intriguing area for future research. Its potential to revolutionize metal extraction processes warrants further exploration and could lead to more efficient and eco-friendly recycling methods.

2.5. References

Bahaloo-Horeh, N., Mousavi, S. M., & Baniasadi, M. (2018). Use of adapted metal tolerant *Aspergillus niger* to enhance bioleaching efficiency of valuable metals from spent lithium-ion mobile phone batteries. *Journal of Cleaner Production*, *197*, 1546–1557. https://doi.org/10.1016/j.jclepro.2018.06.299

Baumgärtner, J. F., Krumeich, F., Wörle, M., Kravchyk, K. V., & Kovalenko, M. V. (2022). Thermal synthesis of conversion-type bismuth fluoride cathodes for high-energy-density Li-ion batteries. *Communications Chemistry*, *5*(1), 1–8. https://doi.org/10.1038/s42004-021-00622-y

Biswal, B. K., Jadhav, U. U., Madhaiyan, M., Ji, L., Yang, E.-H., & Cao, B. (2018). Biological Leaching and Chemical Precipitation Methods for Recovery of Co and Li from Spent Lithium-Ion Batteries. *ACS Sustainable Chemistry & Engineering*, *6*(9), 12343–12352. https://doi.org/10.1021/acssuschemeng.8b02810

Brierley, C. L. (2008). How will biomining be applied in the future? *Transactions of Nonferrous Metals Society of China*, *18*(6), 1302–1310. https://doi.org/10.1016/S1003-6326(09)60002-9

Burgstaller, W., & Schinner, F. (1993). Leaching of metals with fungi. *Journal of Biotechnology*, *27*(2), 91–116. https://doi.org/10.1016/0168-1656(93)90101-R

Chen, X., Cao, L., Kang, D., Li, J., Zhou, T., & Ma, H. (2018). Recovery of valuable metals from mixed types of spent lithium-ion batteries. Part II: Selective extraction of lithium. *Waste Management*, *80*, 198–210. https://doi.org/10.1016/j.wasman.2018.09.013

Chen, X., Kang, D., Cao, L., Li, J., Zhou, T., & Ma, H. (2019). Separation and recovery of valuable metals from spent lithium-ion batteries: Simultaneous recovery of Li and Co in a single step. *Separation and Purification Technology*, *210*, 690–697. https://doi.org/10.1016/j.seppur.2018.08.072

Donati, E. R., & Sand, W. (Eds.). (2007). *Microbial Processing of Metal Sulfides*. Springer Netherlands. https://doi.org/10.1007/1-4020-5589-7

Dusengemungu, L., Kasali, G., Gwanama, C., & Mubemba, B. (2021). Overview of fungal bioleaching of metals. *Environmental Advances*, *5*, 100083. https://doi.org/10.1016/j.envadv.2021.100083

Ferreira, D. A., Prados, L. M. Z., Majuste, D., & Mansur, M. B. (2009). Hydrometallurgical separation of aluminium, cobalt, copper, and lithium from spent Li-ion batteries. *Journal of Power Sources*, *187*(1), 238–246. https://doi.org/10.1016/j.jpowsour.2008.10.077

Freitas, M. B. J. G., & Garcia, E. M. (2007). Electrochemical recycling of cobalt from cathodes of spent lithium-ion batteries. *Journal of Power Sources*, *171*(2), 953–959. https://doi.org/10.1016/j.jpowsour.2007.07.002

Georgi-Maschler, T., Friedrich, B., Weyhe, R., Heegn, H., & Rutz, M. (2012). Development of a recycling process for Li-ion batteries. *Journal of Power Sources*, *207*, 173–182. https://doi.org/10.1016/j.jpowsour.2012.01.152

Hong, H. (2017). *Biohydrometallurgical Recycling of Metals from Industrial Wastes*. CRC Press. https://doi.org/10.1201/9781315195544

Horeh, N. B., Mousavi, S. M., & Shojaosadati, S. A. (2016). Bioleaching of valuable metals from spent lithium-ion mobile phone batteries using *Aspergillus niger*. *Journal of Power Sources, 320*, 257–266. https://doi.org/10.1016/j.jpowsour.2016.04.104

Houbraken, J., de Vries, R. P., & Samson, R. A. (2014). Modern Taxonomy of Biotechnologically Important *Aspergillus* and *Penicillium* Species. In S. Sariaslani & G. M. Gadd (Eds.), *Advances in Applied Microbiology* (Vol. 86, pp. 199–249). Academic Press. https://doi.org/10.1016/B978-0-12-800262-9.00004-4

Johnson, D. B. (2014). Biomining—Biotechnologies for extracting and recovering metals from ores and waste materials. *Current Opinion in Biotechnology*, *30*, 24–31. https://doi.org/10.1016/j.copbio.2014.04.008

Kang, J., Sohn, J., Chang, H., Senanayake, G., & Shin, S. M. (2010). Preparation of cobalt oxide from concentrated cathode materials of spent lithium-ion batteries using a hydrometallurgical method. *Advanced Powder Technology*, *21*(2), 175–179. https://doi.org/10.1016/j.apt.2009.10.015

Khatri, B. R., Tipre, D. R., & Dave, S. R. (2019). Comparison of Hydro- and Biohydrometallurgical Extraction of Metals from Waste Li-Ion Batteries of Cell Phone. *Journal of Sustainable Metallurgy*, *5*(2), 250–261. https://doi.org/10.1007/s40831-019-00223-z

Kotal, M., Jakhar, S., Roy, S., & Sharma, H. K. (2022). Cathode materials for rechargeable lithium batteries: Recent progress and future prospects. *Journal of Energy Storage*, *47*, 103534. https://doi.org/10.1016/j.est.2021.103534

Lan, Y., Li, X., Zhou, G., Yao, W., Cheng, H.-M., & Tang, Y. (2024). Direct Regenerating Cathode Materials from Spent Lithium-Ion Batteries. *Advanced Science*, *11*(1), 2304425. https://doi.org/10.1002/advs.202304425

Li, J., Shi, P., Wang, Z., Chen, Y., & Chang, C.-C. (2009). A combined recovery process of metals in spent lithium-ion batteries. *Chemosphere*, *77*(8), 1132–1136. https://doi.org/10.1016/j.chemosphere.2009.08.040

Li, L., Ge, J., Wu, F., Chen, R., Chen, S., & Wu, B. (2010). Recovery of cobalt and lithium from spent lithium ion batteries using organic citric acid as leachant. *Journal of Hazardous Materials*, *176*(1), 288–293. https://doi.org/10.1016/j.jhazmat.2009.11.026

Li, L., Lu, J., Ren, Y., Zhang, X. X., Chen, R. J., Wu, F., & Amine, K. (2012). Ascorbic-acid-assisted recovery of cobalt and lithium from spent Li-ion batteries. *Journal of Power Sources*, *218*, 21–27. https://doi.org/10.1016/j.jpowsour.2012.06.068

Li, L., Zeng, G., Luo, S., Deng, X., & Xie, Q. (2013). Influences of solution pH and redox potential on the bioleaching of $LiCoO_2$ from spent lithium-ion batteries. *Journal of the Korean Society for Applied Biological Chemistry*, *56*(2), Article 2. https://doi.org/10.1007/s13765-013-3016-x

Liu, R., Duay, J., & Lee, S. B. (2011). Heterogeneous nanostructured electrode materials for electrochemical energy storage. *Chemical Communications*, *47*(5), 1384–1404. https://doi.org/10.1039/C0CC03158E

Ma, J., Liu, T., Ma, J., Zhang, C., & Yang, J. (2024). Progress, Challenge, and Prospect of LiMnO$_2$: An Adventure toward High-Energy and Low-Cost Li-Ion Batteries. *Advanced Science*, *11*(2), 2304938. https://doi.org/10.1002/advs.202304938

Meshram, P., Pandey, B. D., & Mankhand, T. R. (2015). Hydrometallurgical processing of spent lithium ion batteries (LIBs) in the presence of a reducing agent with emphasis on kinetics of leaching. *Chemical Engineering Journal*, *281*, 418–427. https://doi.org/10.1016/j.cej.2015.06.071

Mishra, D., Kim, D.-J., Ralph, D. E., Ahn, J.-G., & Rhee, Y.-H. (2008). Bioleaching of metals from spent lithium ion secondary batteries using *Acidithiobacillus ferrooxidans*. *Waste Management*, *28*(2), 333–338. https://doi.org/10.1016/j.wasman.2007.01.010

Nayl, A. A., Elkhashab, R. A., Badawy, S. M., & El-Khateeb, M. A. (2017). Acid leaching of mixed spent Li-ion batteries. *Arabian Journal of Chemistry*, *10*, S3632–S3639. https://doi.org/10.1016/j.arabjc.2014.04.001

Nitta, N., Wu, F., Lee, J. T., & Yushin, G. (2015). Li-ion battery materials: Present and future. *Materials Today*, *18*(5), 252–264. https://doi.org/10.1016/j.mattod.2014.10.040

Niu, Z., Zou, Y., Xin, B., Chen, S., Liu, C., & Li, Y. (2014). Process controls for enhancing bioleaching performance of both Li and Co from spent lithium-ion batteries at high pulp density, along with an exploration of their thermodynamics and kinetics. *Chemosphere*, *109*, 92–98. https://doi.org/10.1016/j.chemosphere.2014.02.059

Peng, C., Hamuyuni, J., Wilson, B. P., & Lundström, M. (2018). Selective reductive leaching of cobalt and lithium from industrially crushed waste Li-ion batteries in a sulfuric acid system. *Waste Management*, *76*, 582–590. https://doi.org/10.1016/j.wasman.2018.02.052

Pražanová, A., Plachý, Z., Kočí, J., Fridrich, M., & Knap, V. (2024). Direct Recycling Technology for Spent Lithium-Ion Batteries: Limitations of Current Implementation. *Batteries*, *10*(3), Article 3. https://doi.org/10.3390/batteries10030081

Schippers, A. (2007). Microorganisms Involved in Bioleaching and Nucleic Acid-Based Molecular Methods for Their Identification and Quantification. In E. R. Donati & W. Sand (Eds.), *Microbial Processing of Metal Sulfides* (pp. 3–33). Springer Netherlands. https://doi.org/10.1007/1-4020-5589-7_1

Shi, Y., Chen, G., Liu, F., Yue, X., & Chen, Z. (2018). Resolving the Compositional and Structural Defects of Degraded LiNi$_x$Co$_y$Mn$_z$O$_2$ Particles to Directly Regenerate High-Performance Lithium-Ion Battery Cathodes. *ACS Energy Letters*, *3*(7), 1683–1692. https://doi.org/10.1021/acsenergylett.8b00833

Shin, S. M., Kim, N. H., Sohn, J. S., Yang, D. H., & Kim, Y. H. (2005). Development of a metal recovery process from Li-ion battery wastes. *Hydrometallurgy*, *79*(3), 172–181. https://doi.org/10.1016/j.hydromet.2005.06.004

Sohn, J.-S., Shin, S.-M., Yang, D.-H., Kim, S.-K., & Lee, C.-K. (2006). Comparison of Two Acidic Leaching Processes for Selecting the Effective Recycling Process of Spent Lithium-Ion Battery. *Geosystem Engineering*, *9*(1), 1–6. https://doi.org/10.1080/12269328.2006.10541246

Tarascon, J.-M., & Armand, M. (2001). Issues and challenges facing rechargeable lithium batteries. *Nature*, *414*(6861), 359–367. https://doi.org/10.1038/35104644

Tsang, C.-C., Tang, J. Y. M., Lau, S. K. P., & Woo, P. C. Y. (2018). Taxonomy and evolution of *Aspergillus*, *Penicillium* and *Talaromyces* in the omics era – Past, present and future. *Computational and Structural Biotechnology Journal*, *16*, 197–210. https://doi.org/10.1016/j.csbj.2018.05.003

Wang, G., Wang, G., Fei, L., Zhao, L., & Zhang, H. (2024). Structural Engineering of Anode Materials for Low-Temperature Lithium-Ion Batteries: Mechanisms, Strategies, and Prospects. *Nano-Micro Letters*, *16*(1), 150. https://doi.org/10.1007/s40820-024-01363-y

Wang, J., Chen, M., Chen, H., Luo, T., & Xu, Z. (2012). Leaching Study of Spent Li-ion Batteries. *Procedia Environmental Sciences*, *16*, 443–450. https://doi.org/10.1016/j.proenv.2012.10.061

Xin, B., Zhang, D., Zhang, X., Xia, Y., Wu, F., Chen, S., & Li, L. (2009). Bioleaching mechanism of Co and Li from spent lithium-ion battery by the mixed culture of acidophilic sulfur-oxidizing and iron-oxidizing bacteria. *Bioresource Technology*, *100*(24), 6163–6169. https://doi.org/10.1016/j.biortech.2009.06.086

Xin, Y., Guo, X., Chen, S., Wang, J., Wu, F., & Xin, B. (2016). Bioleaching of valuable metals Li, Co, Ni and Mn from spent electric vehicle Li-ion batteries for the purpose of recovery. *Journal of Cleaner Production*, *116*, 249–258. https://doi.org/10.1016/j.jclepro.2016.01.001

Xu, B., Qian, D., Wang, Z., & Meng, Y. S. (2012). Recent progress in cathode materials research for advanced lithium ion batteries. *Materials Science and Engineering: R: Reports*, *73*(5), 51–65. https://doi.org/10.1016/j.mser.2012.05.003

Xu, P., Tan, D. H. S., Jiao, B., Gao, H., Yu, X., & Chen, Z. (2023). A Materials Perspective on Direct Recycling of Lithium-Ion Batteries: Principles, Challenges and Opportunities. *Advanced Functional Materials*, *33*(14), 2213168. https://doi.org/10.1002/adfm.202213168

Yao, Y., Zhu, M., Zhao, Z., Tong, B., Fan, Y., & Hua, Z. (2018). Hydrometallurgical Processes for Recycling Spent Lithium-Ion Batteries: A Critical Review. *ACS Sustainable Chemistry & Engineering*, *6*(11), 13611–13627. https://doi.org/10.1021/acssuschemeng.8b03545

Zeng, G., Deng, X., Luo, S., Luo, X., & Zou, J. (2012). A copper-catalyzed bioleaching process for enhancement of cobalt dissolution from spent lithium-ion batteries. *Journal of Hazardous Materials*, *199–200*, 164–169. https://doi.org/10.1016/j.jhazmat.2011.10.063

Zeng, G., Luo, S., Deng, X., Li, L., & Au, C. (2013). Influence of silver ions on bioleaching of cobalt from spent lithium batteries. *Minerals Engineering*, *49*, 40–44. https://doi.org/10.1016/j.mineng.2013.04.021

Zhao, S., He, W., & Li, G. (2019). Recycling Technology and Principle of Spent Lithium-Ion Battery. In L. An (Ed.), *Recycling of Spent Lithium-Ion Batteries: Processing Methods and Environmental Impacts* (pp. 1–26). Springer International Publishing. https://doi.org/10.1007/978-3-030-31834-5_1

CHAPTER III

MICROBIAL SCREENING AND DNA SEQUENCING

3.1 Abstract

To identify the most effective fungal strain for bioleaching LCO cathodes, soil and wastewater samples from metal industries in Thailand were collected to isolate and screen various cultures. Potato Dextrose Agar (PDA) supplemented with lithium and cobalt at concentrations ranging from 0% to 1% w/v was used as the screening medium. *Aspergillus* sp. JMET 15 and *Penicillium* sp. JMET 24 were identified as the two strains exhibiting outstanding characteristics, such as very high growth rates (no lag phase) even at lithium and cobalt concentrations as high as 1%, and beneficial by-products, during the screening process.

3.2 Introduction

Recently, numerous fungal strains have been discovered and utilized in various applications, including medical treatments and the food industry. However, many fungal strains remain unidentified. To ensure the potential of these strains is not overlooked, particularly for bioleaching processes, it is crucial to isolate new fungal strains. Different strains exhibit varying capabilities in tolerating and bioleaching heavy metals. Identifying strains with superior bioleaching properties can significantly enhance the efficiency and effectiveness of this process. This study aims to discover and characterize fungal strains capable of bioleaching lithium cobalt oxide (LCO) cathodes, a common component in rechargeable batteries.

3.3   Research objective

This research aims to screen, identify, and select fungal species and strains that are suitable for use as key agents in bioleaching processes under conditions of high concentrations of lithium and cobalt in the environment, while also demonstrating robust growth.

3.4   Screening of suitable microorganisms for bioleaching LCO

Soil and wastewater samples were collected from various metal industry yards in Thailand. Each soil sample (1 g) was mixed with 10 mL of sterile distilled water, followed by serial dilution to dilute a strain concentration of up to 10^{-3} times. Aliquots of 0.1 mL were spread on 3.9% (w/v) potato dextrose agar (PDA) + 0.3 wt.% cathode powder plates. The microbial strains that grew on the PDA plates containing 0.3 wt.% cathode powder were collected (Figure 3.1).
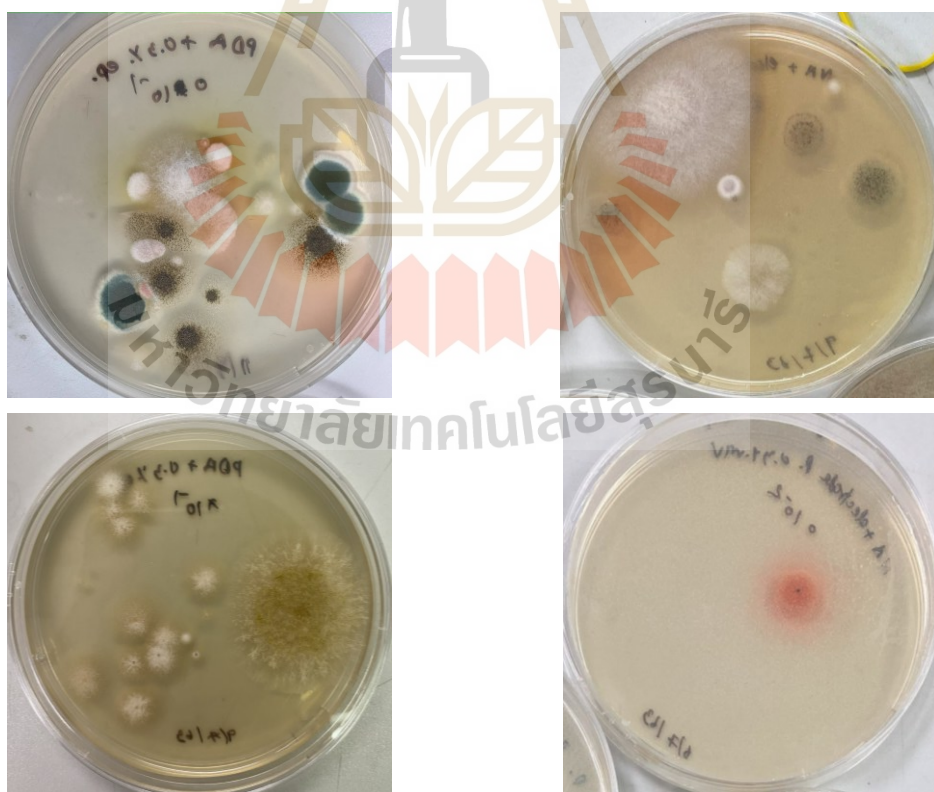
Figure 3.1   Example of fungal colonies that grow on PDA + 0.3 wt.% cathode powder plate (5 days incubation).

Fungal colonies were then isolated into pure cultures on PDA plates containing 0.6 wt.% and 1 wt.% cathode powder, as shown in Figure 3.2. As the concentration of cathode powder increased, many isolates did not survive or exhibited prolonged lag phases due to the toxicity of the cathode powder, which can inhibit fungal growth. Some strains were grown only on old agar in a vertical direction, with mycelium expanding into the air and covering the plate, and did not penetrate 1 wt.% cathode powder agar. Two strains continuously grew on PDA plates containing 1 wt.% cathode powder. Strain e grew the fastest, while strain d was slower but exhibited some interesting behavior. After approximately two weeks, the precipitation of cobalt phosphate was observed, as shown in Figure 3.3.
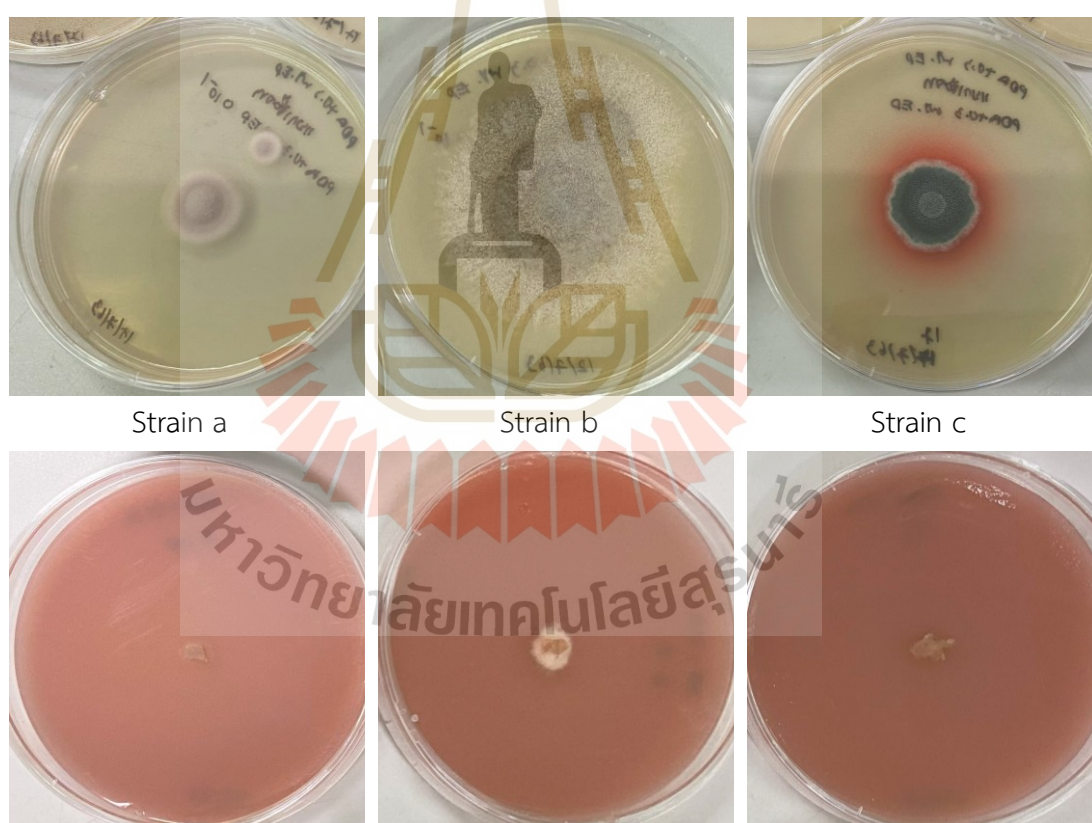
Strain a   Strain b   Strain c

Figure 3.2   Isolated fungal colonies on PDA + 0.6 wt.% cathode powder plates (upper roll), and the same strain on PDA + 1 wt.% cathode powder plates (lower roll) at 7 days incubation.

Strain d   Strain e
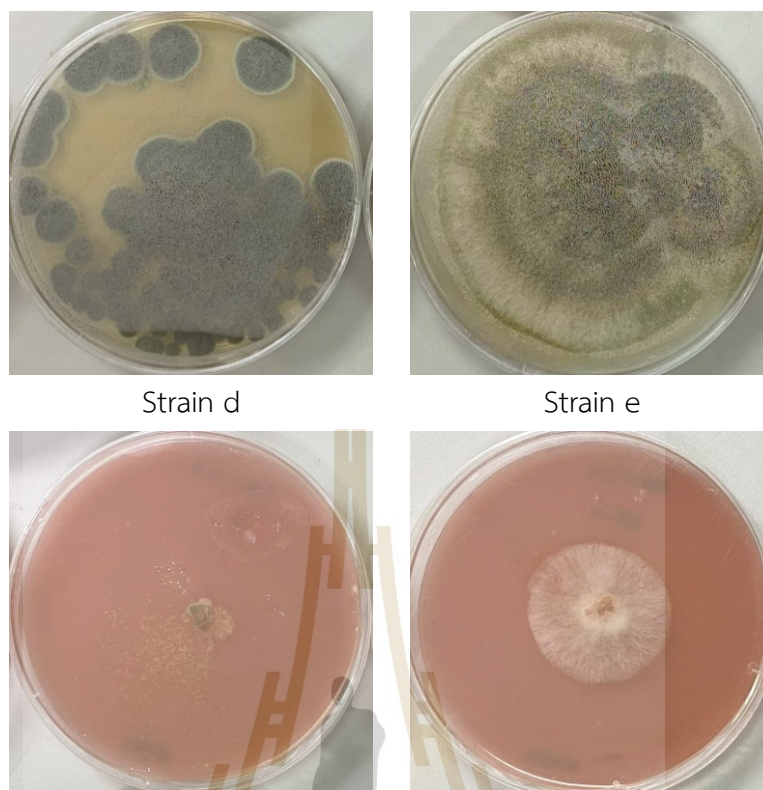
Figure 3.2   Isolated fungal colonies on PDA + 0.6 wt.% cathode powder plates (upper
roll), and the same strain on PDA + 1 wt.% cathode powder plates (lower
roll) at 7 days incubation (continued).
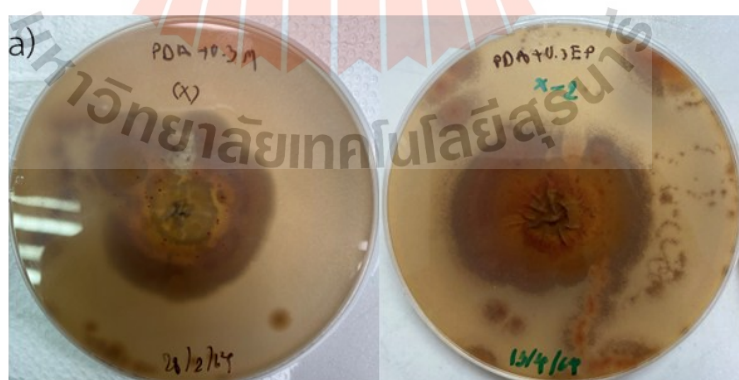
Figure 3.3   Precipitation of cobalt phosphate as pink to red particles from strain d in
PDA + 0.3wt.% cathode powder (a), enlarging scale (b), SEM micrograph of
flower-like structured cobalt phosphate (c), and its X-ray diffraction
pattern (d).
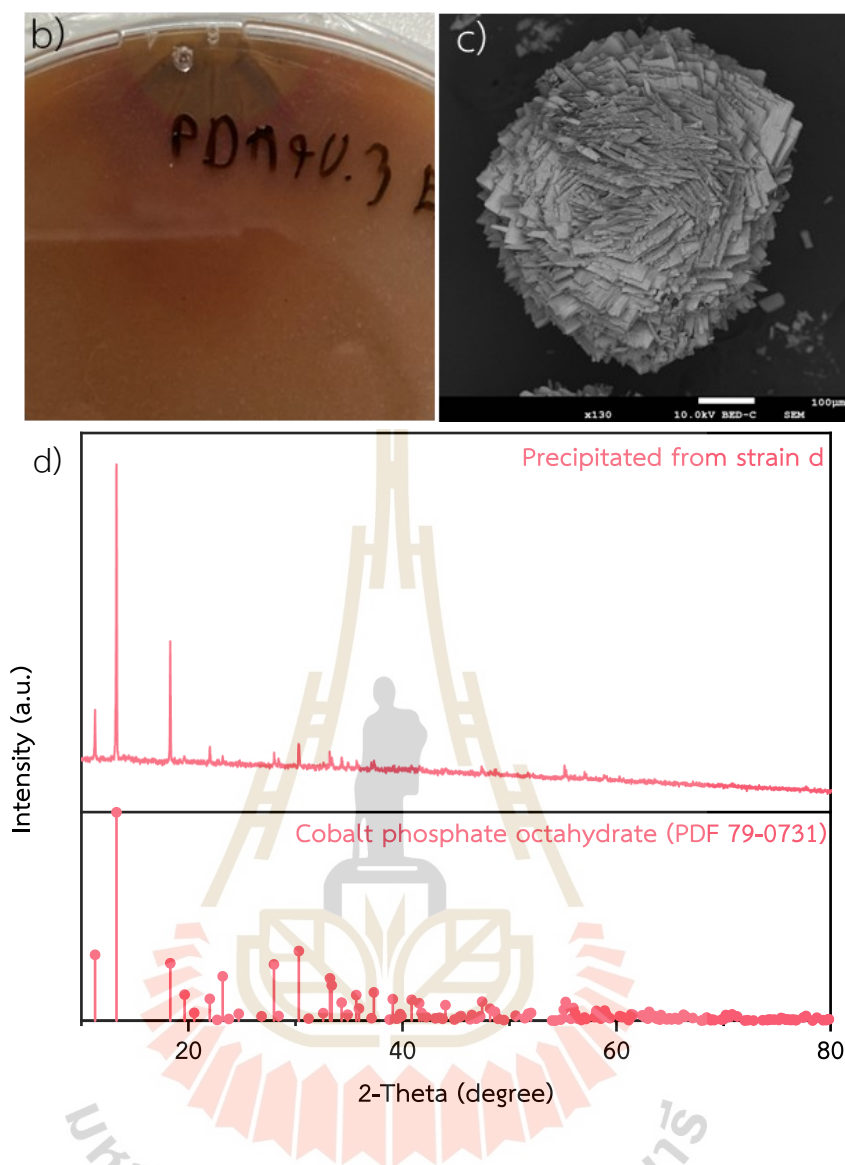
Figure 3.3 Precipitated of cobalt phosphate as pink to red particles from strain d in PDA + 0.3wt.% cathode powder (a), enlarge scale (b), SEM micrograph of flower-like structured cobalt phosphate (c), and its X-ray diffraction pattern (d) (continued).

Due to the interesting characteristics of strain d and the outstanding growth rate of strain e, as discussed above, these two strains were selected for further investigation in the bioleaching part.

3.5 Genomic DNA extraction and Microorganism identification

Two selected fungi from the previous part were re-cultured for species identification through genomic deoxyribonucleic acid (DNA) sequencing in a 250 mL Erlenmeyer flask containing 100 mL potato dextrose broth (PDB) for 3 days. Fungal genomic DNA was directly extracted following this procedure (Cenis, 1992).

3.5.1 Chemicals/reagents for genomic deoxyribonucleic acid (DNA) extraction

1.) Lysis buffer (200 mM Tris-HCl (pH 8.5), 0.5% w/v sodium dodecyl sulfate (SDS), 250 mM NaCl, 25 mM ethylenediaminetetraacetic acid (EDTA))

2.) TE buffer (10 mM Tris (tris(hydroxymethyl)aminomethane), 1 mM EDTA)

3.) 3M sodium acetate (pH 5.2)

4.) Phenol

5.) Chloroform

6.) Isoamyl alcohol

7.) Absolute ethanol

8.) 70% ethanol

3.5.2 Genomic DNA extraction protocol

1.) Several spherical pellets were transferred from a 250 mL Erlenmeyer flask into 1.5-mL microcentrifuge tubes, followed by the addition of 500 µL TE buffer to wash the retained PDB. The tube was then centrifuged for 5 minutes at 13,000 rpm, after which the TE buffer was discarded.

2.) For cell lysis, 300 µL of lysis buffer was added, and the mycelium pellets were crushed using a conical grinder.

3.) DNA purification commenced with the addition of 150 µL of 3M sodium acetate, followed by incubation at -20°C for 10 minutes and subsequent centrifugation for 5 minutes at 10,000xg.

4.) The supernatant was pipetted into a new 1.5 mL microcentrifuge tube.

5.) The 500 µL of phenol : chloroform : isoamyl alcohol (25:24:1) was added into the tube containing supernatant, vortexed for 10 seconds, and incubated at room temperature for 2 minutes.

6.) The mixture was then centrifuged for 10 minutes at 6,000xg, and the supernatant was transferred to a new 1.5 mL microcentrifuge tube.

7.) An equal volume of chloroform : isoamyl alcohol (24:1) was added to the supernatant from step (7).

8.) The mixture was inverted for 5 minutes, incubated at room temperature for 2 minutes, and then centrifuged for 10 minutes at 6,000xg. The supernatant was transferred to a new 1.5 mL microcentrifuge tube.

9.) DNA precipitation was initiated by adding an equal volume of absolute ethanol to the supernatant from step (9), gently mixed by inversion, and incubated at -20°C for 10 minutes.

10.) The mixture was centrifuged for 2 minutes at 3,000xg, and the liquid phase was discarded.

11.) One milliliter of 70% ethanol was added, gently mixed by inversion, and centrifuged for 2 minutes at 3,000xg.

12.) The ethanol was discarded, and the pellet was dried in a laminar flow chamber.

13.) Finally, 50 µL of TE buffer was added, and the sample was stored at 4°C.

To analyze the genomic DNA extracted using the protocol as mentioned above, gel electrophoresis was conducted with 1% w/v agarose in 1X TAE (Tris-acetate-EDTA) buffer. The extracted genomic DNA was more than 10,000 base pairs (bp) and exhibited a broad band of RNA shorter than 500 bp, as illustrated in Figure 3.4 (a). To remove RNA, RNase A was employed according to the protocol described in Section 3.5.3.
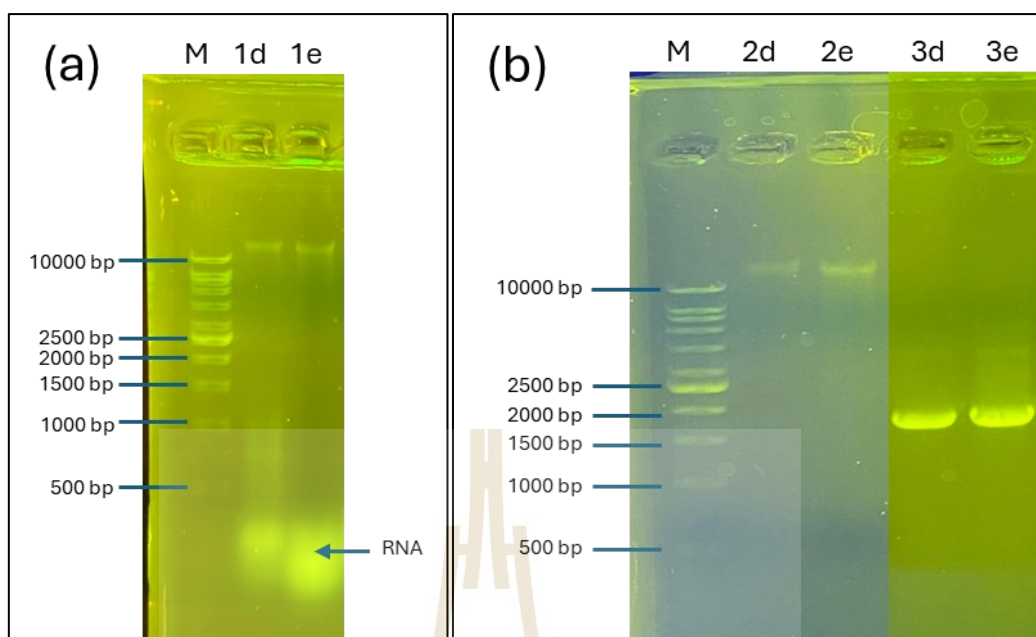
Figure 3.4   Agarose gel electrophoresis (1% Agarose) analysis of extracted genomic
             DNA from strain d and strain e.
             Lane: M, DNA molecular weight markers (1kb DNA ladder, Vivantis); 1d,
             genomic DNA extracted from strain d; 1e, genomic DNA extracted from
             strain e; 2d, RNase-treated genomic DNA from strain d; 2e, RNase-treated
             genomic DNA from strain e; 3d, PCR product from 18s rDNA amplification
             using NS1/NS8 primers for strain d; 3e, PCR product from 18s rDNA
             amplification using NS1/NS8 primers for strain e.

3.5.3   Elimination of RNA protocol

To prevent RNA contamination, which can lead to errors in PCR, RNA should be eliminated by following the protocols.

1.)   10 μL of 2 mg/mL RNase A was added into a 1.5 mL microcentrifuge tube containing genomic DNA from the previous section, and then incubated at 37°C for 30 min.

2.)   Added TE until the final volume was 100 μL.

3.)   Gently mixed by inversion, 250 μL of phenol : chloroform : isoamyl alcohol (25:24:1) was added, vortexed for 10 seconds, the mixture was then

centrifuged for 10 minutes at 13,000 rpm, and the supernatant was transferred to a new 1.5 mL microcentrifuge tube.

4.) Added an equal volume of absolute ethanol to the supernatant, gently mixed by inversion, and incubated at -20°C for 10 minutes. The mixture was centrifuged for 2 minutes at 3,000xg, and the liquid phase was discarded.

5.) One milliliter of 70% ethanol was added, gently mixed by inversion, and centrifuged for 2 minutes at 3,000xg.

6.) The ethanol was discarded, and the pellet was dried in a laminar flow chamber.

7.) Finally, 20 μL of TE buffer was added, and the sample was stored at 4°C.

RNA removed from the above protocol was analyzed on a 1 wt.% agarose gel as illustrated in Figure 3.4 (b).

3.5.4 Amplification of 18S rDNA by polymerase chain reaction (PCR)

The 18S rRNA small-subunit was amplified using the polymerase chain reaction (PCR) using primers NS1 (5′-GTAGTCATATGCTTGTCTC-3′) and NS8 (5′-TCCGCAGGTTCACCTACGGA-3′) (White et al., 1990). Each PCR mixture contained 1-μL 10 × buffer, 0.2 μL of 10-mM dNTPs, 0.2 μL of 10- μM primer, 0.05-μL Taq DNA polymerase (DreamTaq, Thermo Scientific™), 1- μL DNA template solution, and ultrapure sterile water to make a total volume of 10 μL. The PCR was performed under the mentioned conditions: 94 °C for 4 min,30 cycles at 94 °C for 1 min,55 °C for 2 min,72 °C for 1.5 min, and a final extension at 72 °C for 10 min (Uemura et al., 2008). The PCR products from 18S rDNA amplification using NS1/NS8 primers were analyzed on a 1 wt.% agarose gel as illustrated in Figure 3.4 (b), lanes 3d and 3e. The products were approximately 1,800 bp in size.

The PCR products were subjected to sequencing using the barcode-tagged sequencing method (BTSeq™). The sequences were analyzed via the Basic Local Alignment Search Tool from the National Center for Biotechnology Information (NCBI) website. 18s rRNA sequences have been submitted to NCBI GenBank under

accession nos. MZ892606 and MZ892608 for *Aspergillus* sp. JMET 15 and *Penicillium* sp. JMET 24, respectively.

3.6   Conclusion

This study successfully identified two fungal strains, *Aspergillus* sp. JMET 15 and *Penicillium* sp. JMET 24, as highly effective agents for bioleaching lithium cobalt oxide (LCO) cathodes. These strains were isolated from soil and wastewater samples collected from metal industries in Thailand and demonstrated exceptional growth rates and tolerance to high concentrations of lithium and cobalt. The findings highlight the potential of these fungal strains to enhance the efficiency and effectiveness of bioleaching processes, contributing to more sustainable and environmentally friendly methods for recycling rechargeable batteries. Further research and development could optimize the application of these strains in industrial bioleaching operations.

3.7   References

Cenis, J. L. (1992). Rapid extraction of fungal DNA for PCR amplification. *Nucleic Acids Research*, *20*(9), 2380.

Uemura, N., Makimura, K., Onozaki, M., Otsuka, Y., Shibuya, Y., Yazaki, H., Kikuchi, Y., Abe, S., & Kudoh, S. (2008). Development of a loop-mediated isothermal amplification method for diagnosing Pneumocystis pneumonia. *Journal of Medical Microbiology*, *57*(1), 50–57. https://doi.org/10.1099/jmm.0.47216-0

White, T. J., Bruns, T., Lee, S., & Taylor, J. (1990). 38—AMPLIFICATION AND DIRECT SEQUENCING OF FUNGAL RIBOSOMAL RNA GENES FOR PHYLOGENETICS. In M. A. Innis, D. H. Gelfand, J. J. Sninsky, & T. J. White (Eds.), *PCR Protocols* (pp. 315–322). Academic Press. https://doi.org/10.1016/B978-0-12-372180-8.50042-1

CHAPTER IV

BIOLEACHING OF CATHODE POWDER BY *ASPERGILLUS* SP. STRAIN JMET 15 AND *PENICILLIUM* SP. STRAIN JMET 24 IN SUCROSE MEDIUM AND POTATO DEXTROSE BROTH

4.1 Abstract

This study employed bioleaching, a process utilizing microbial activity, to investigate the leaching efficiency of cobalt and lithium from battery waste. Two fungal strains, *Aspergillus* sp. strain JMET 15 and *Penicillium* sp. strain JMET 24, were utilized with different organic carbon sources (sucrose medium and potato dextrose broth) at 1% pulp density. The sucrose medium produced a higher quantity of acid and leached greater concentrations of cobalt and lithium compared to the potato dextrose broth. The leaching efficiency of JMET 24 surpassed that of JMET 15, with cobalt (32.57% and 27.19%) and lithium (65.07% and 40.58%) bioleached by JMET 24 and JMET 15, respectively, after 30 days of cultivation in the sucrose medium. Cobalt was transformed from lithium cobalt oxide to cobalt phosphate-oxalate by JMET 24 in the sucrose medium.

4.2 Introduction

In the study of screening suitable fungi for the bioleaching of lithium-ion battery cathode powder (LCO), as discussed in Chapter 3, it was found that two fungal strains, *Aspergillus* sp. strain JMET 15 and *Penicillium* sp. strain JMET 24, thrived in environments with high concentrations of lithium and cobalt, up to 1%. These two strains were subsequently used in preliminary bioleaching experiments to investigate the mechanisms of leaching and the secretion of fungal metabolites, such as various organic acids, during growth. The efficiency of these metabolites in leaching lithium and cobalt was assessed.

In this phase, two types of media were selected for cultivation and bioleaching: potato dextrose broth (PDB) and sucrose medium (SM). According to related research, the primary energy source for fungal growth is sugar, which serves as a crucial carbon source for bioleaching. Specifically, sugars act as precursors for the production of organic acids, which are essential for metal dissolution from raw materials (Amaro et al., 2022; Angumeenal & Venkappayya, 2013). The PDB contains glucose as the primary carbon source, whereas the sucrose medium contains sucrose.

The rationale for selecting these two media for the bioleaching study of battery powder is that PDB is a complete medium, providing essential nutrients for fungal growth, thereby significantly enhancing fungal proliferation compared to other media. On the other hand, sucrose medium is commonly used for the commercial production of organic acids, such as citric acid and oxalic acid (Angumeenal & Venkappayya, 2013; Shankar & Sivakumar, 2016). When applied to bioleaching, it is hypothesized that this medium will stimulate the two fungal strains to produce a substantial number of organic acids, thereby enhancing the efficiency of lithium and cobalt leaching from degraded LCO battery powder.

4.3   Research objective

The objective of this study was to investigate the mechanism and efficiency of *Aspergillus* sp. strain JMET 15 and *Penicillium* sp. strain JMET 24 for leaching Co and Li from spent LIB waste using media containing different carbon sources [potato dextrose broth (PDB) and sucrose medium (SM)].

4.4   Materials and Methods

4.4.1   Cathode powder raw materials preparation and characterization

The battery waste used in this study consisted of LCO cathode-based smartphone batteries (iPhone, Apple), collected from mobile repair shops in Thailand. The batteries were discharged by immersing them in a 5% w/v sodium chloride (NaCl) solution for 24 hours (Zhang et al., 2013). The deteriorated smartphone batteries were manually dismantled, and the amount of cathode powder was calculated to be an average of 40.41 wt.% of the total battery weight. The percentage amounts (by

weight) of other components are shown in the Figure. 4.1. The cathode powder containing deteriorated LCO adhered to Al foil (as the cathode) with polyvinylidene fluoride (PVDF). The thermal analysis of the cathode electrode, as depicted in Figure 4.2, revealed degradation of PVDF above 500 °C, which is within the same range as other studies (de Jesus Silva et al., 2020; Fu et al., 2021; Thomas et al., 2010). Hence, the electrode was heated to 525 °C in a muffle furnace for 1 hour to destroy the PVDF interlayers before collecting the cathode powder. The scraped cathode powder, analyzed via XRD (Cu-Kα, Bruker, D8-Advanced), was identified as LCO (Figure 4.3), consistent with the chemical composition analysis via ICP-OES, which revealed Co and Li compositions of 58.8% and 6.9% by weight, respectively. Other elements in battery electrodes, such as Ni, Mn, and Fe, were not detected. The average particle sizes, d10, d50, and d90, of the cathode powder were 15.25, 8.55, 13.78, and 22.9 μm, as shown in Figure 4.4, analyzed using a laser diffraction particle size analyzer (Horiba, LA-950V2). The chemical composition of the raw material was analyzed via inductively coupled plasma optical emission spectrometry (ICP-OES) (PerkinElmer, Optima 8000), and phase identification was conducted via X-ray diffraction (XRD) (Bruker, D2 Phaser).
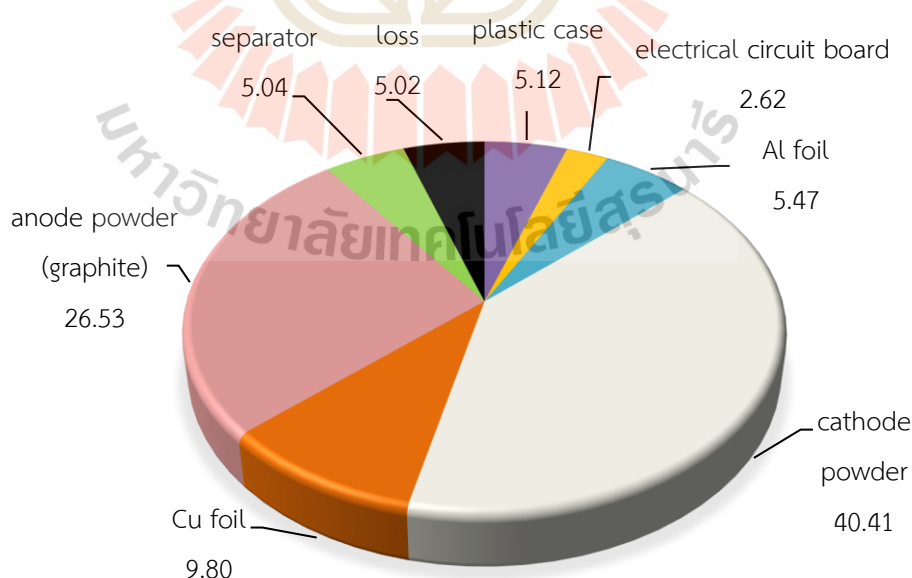
Figure 4.1   Average weight compositions of smartphone battery (iPhone, Apple) waste (wt.%).
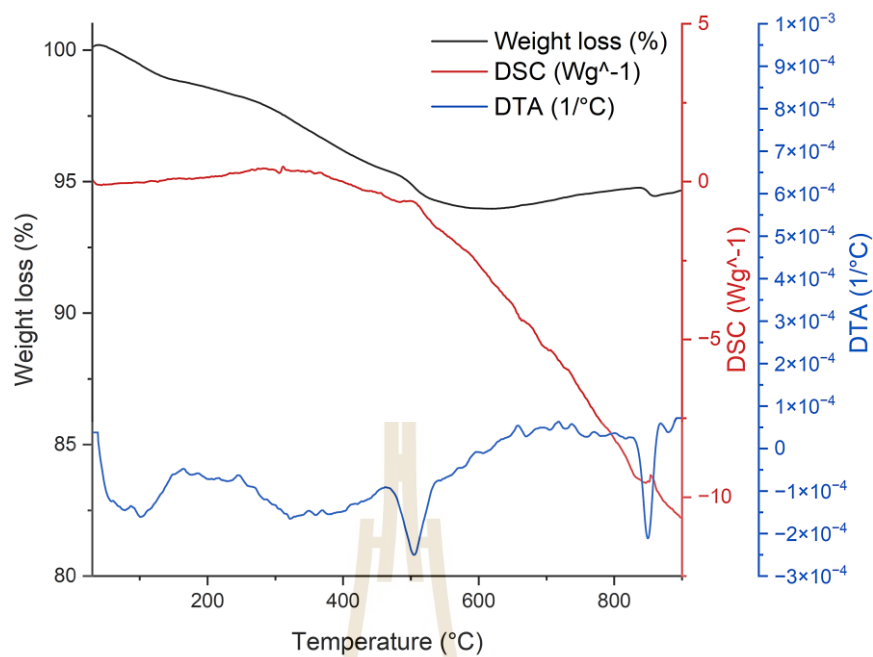
Figure 4.2   Thermal analysis of cathode electrode (containing aluminium foil, LCO
powder, PVDF, and electrolyte)
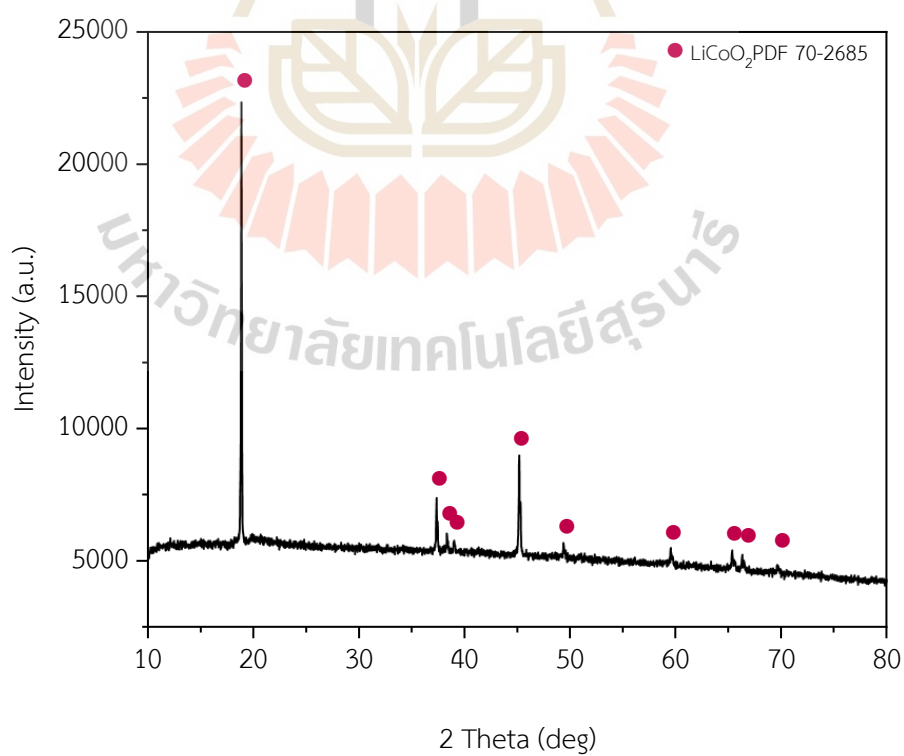
Figure 4.3   X-ray diffraction pattern of raw materials (LiCoO$_2$) in the cathode powder.
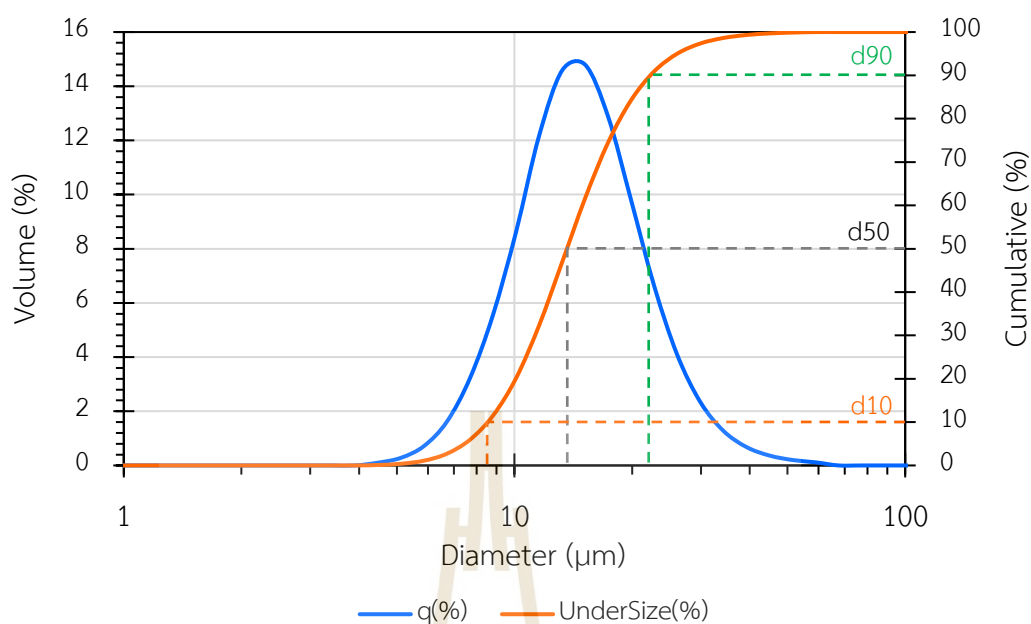
Figure 4.4 Size distribution of LCO powder raw materials analyzed by laser diffraction technique.

4.4.2 Bioleaching experiment

The spores of JMET 15 and JMET 24 were obtained by culturing them on PDA plates for 7 days at 30 °C, followed by washing the plate surfaces with sterile deionized water to collect the spores. The concentration of the spores was adjusted to ~10^6 spore/mL and verified using a light microscope and Neubauer counting chamber. The bioleaching experiments were conducted in 250-mL Erlenmeyer flasks containing 100-mL PDB (HiMedia) or SM. The SM comprised 100-g/L sucrose, 1.5-g/L NaNO$_3$, 0.5-g/L KH$_2$PO$_4$, 0.025-g/L MgSO$_4$.7H$_2$O, 0.025-g/L KCl, and 1.6-g/L yeast extract, and the pH was adjusted to 5.5. The media were sterilized in an autoclave at 121 °C for 15 min. Either a 1-mL fungal spore suspension or 1 g sterile cathode powder (1 % pulp density) was added to the respective defined conditions. The bioleaching experiments were conducted for 30 days at 150 rpm and 25 °C in an orbital shaking incubator, with samples taken on days 0, 3, 5, 7, 9, 11, 15, 20, 25, and 30. The experiments were performed in triplicate.

Samples were named based on their contents and experimental conditions as mentioned: (i) test sample (T) conditions comprising the cathode powder and fungal spore suspension, (ii) cathode sterile (CS) was a negative control where the cathode powder was present exclusively without any fungal spore suspension, and (iii) non-cathode (CN) powder as a positive fungal growth control where the spore suspension was present exclusively without any cathode powder.

4.4.3 Analytical techniques for LCO bioleaching mechanism

The content of each flask was filtered through the Whatman 42 filter paper at intervals of 0, 3, 5, 7, 9, 11, 15, 20, 25, and 30 days. The solid residue comprising residual material and fungal cells on the filter paper was dried at 80°C using a hot air oven for 24 hr., followed by incineration at 500°C in a muffle furnace for 4 hr. The difference in weights between the residue before and after incineration was determined as biomass. The raw materials and residues were analyzed using an XRD instrument equipped with Cu–Kα radiation (Bruker, D8 Advance). The pH value was measured using a pH meter (Metler Toledo, Seven Compact S220-KIT). The filtrate was passed through a 0.45-µm syringe filter for further analysis. Li and Co concentrations in the leached solution were analyzed via ICP-OES.

The amounts of sugar and organic acid were analyzed using high-performance liquid chromatography (HPLC) (Agilent Technologies, 1260) equipped with a refractive index detector and a ZORBAX NH2 column (4.6 mm × 250 mm, 5 µm). Sucrose, glucose, and fructose were analyzed at 35°C. A 10-µL injection was used with a mobile phase consisting of an isocratic solvent system of 75:25 (v/v) acetonitrile and HPLC water, at a flow rate of 1 mL/min. Organic acids (oxalic acid, acetic acid, and citric acid) were identified via HPLC equipped with an ultraviolet–visible (UV–vis) diode array detector at 210 nm and a ZORBAX SB-C18 column (4.6 mm × 250 mm, 3.5 µm). The operation was performed at 30 °C using a 20-µL injection and a 5-mM sulfuric acid isocratic mobile phase at a flow rate of 0.5 mL/min.

The chemical structures of the cathode powder and leaching product were elucidated via X-ray absorption spectroscopy (XAS). Co K-edge spectra were recorded at the SUT-NANOTEC-SLRIXAS beamline (BL5.2) at the Synchrotron Light

Research Institute (SLRI), Thailand. Energy calibration in a transmission mode was conducted utilizing Co-foil. The energy was scanned using a Ge (220) double-crystal monochromator over a range of 20–80 eV, relative to E0, set at 7709 eV, with a photon energy increment of 0.2 eV. The extended X-ray absorption fine structure (EXAFS) measurements were performed by scanning photon energy from 150, to 20, and 30 k to 13 k of E_0 at 7709 eV, using photon energy increments of 5, 0.3, and 0.05 keV, and temporal steps of 1, 2, and 3 s, respectively. Samples were measured for up to 3 scans in fluorescence mode using a 4-element Si-drift detector. The collected data were preprocessed, normalized, and EXAFS fitted using the IFEFFIT program, which integrates Athena and Artemis (Ravel & Newville, 2005).

4.5   Results and Discussion

4.5.1   Effect of sucrose medium on fungal growth in LCO environment

Fungi primarily rely on organic carbon sources for growth as chemoorganoheterotrophs. Sucrose (100 g/L) was used as the primary organic carbon source in the SM, and the initial sucrose concentration in the SM, quantified via HPLC, was 100,000 ppm. Sucrose levels drastically decrease after 3 days of incubation with the JMET 15 and JMET 24 strains, continuing to decrease below the detection limit after 11 days of incubation (<100 ppm). In contrast, fructose and glucose levels increase as a result of sucrose decomposition. The concentration of glucose decreases between days 3 and 5, while the concentration of fructose remains relatively constant from the middle to the later stages of incubation (Figure 4.5a and b).

The sugar consumption results are consistent with those of biomass and pH. Biomass increases on day 3 of incubation under the non-cathode powder condition (CN), while the pH decreases due to the secretion of organic acids by the fungus. The growth rate of JMET 15 in the T condition increases slightly during the initial stage (7 days) and continues to grow steadily by Day 9 (Figure 4.5c). However, JMET 24 shows no lag phase (Figure 4.5, d). The biomass of both strains in the T condition is lower than in the CN condition, as the metals in the cathode powder suppress the growth rate of the fungus.

Figure 4.5   Sugar consumption, pH change, and biomass in 30 days by the two fungi
in the SM and PDB: sugar consumption by (a) *Aspergillus* sp. JMET 15 and
(b) *Penicillium* sp. JMET 24 in the SM. pH change and the biomass of (c)
Aspergillus sp. JMET 15 and (d) *Penicillium* sp. JMET 24 in the SM. Sugar
consumption by (e) *Aspergillus* sp. JMET 15 and (f) *Penicillium* sp. JMET 24
in the PDB. pH change and biomass of (g) *Aspergillus* sp. JMET 15 and (h)
Penicillium sp. JMET 24 in the PDB.

(c)

(d)

Figure 4.5   Sugar consumption, pH change, and biomass in 30 days by the two fungi
             in the SM and PDB: sugar consumption by (a) *Aspergillus* sp. JMET 15 and
             (b) *Penicillium* sp. JMET 24 in the SM. pH change and the biomass of (c)
             Aspergillus sp. JMET 15 and (d) *Penicillium* sp. JMET 24 in the SM. Sugar
             consumption by (e) *Aspergillus* sp. JMET 15 and (f) *Penicillium* sp. JMET 24
             in the PDB. pH change and biomass of (g) *Aspergillus* sp. JMET 15 and (h)
             Penicillium sp. JMET 24 in the PDB (continued).

Figure 4.5   Sugar consumption, pH change, and biomass in 30 days by the two fungi
in the SM and PDB: sugar consumption by (a) *Aspergillus* sp. JMET 15 and
(b) *Penicillium* sp. JMET 24 in the SM. pH change and the biomass of (c)
Aspergillus sp. JMET 15 and (d) *Penicillium* sp. JMET 24 in the SM. Sugar
consumption by (e) *Aspergillus* sp. JMET 15 and (f) *Penicillium* sp. JMET 24
in the PDB. pH change and biomass of (g) *Aspergillus* sp. JMET 15 and (h)
Penicillium sp. JMET 24 in the PDB (continued).

(g)

(h)

Figure 4.5   Sugar consumption, pH change, and biomass in 30 days by the two fungi
in the SM and PDB: sugar consumption by (a) *Aspergillus* sp. JMET 15 and
(b) *Penicillium* sp. JMET 24 in the SM. pH change and the biomass of (c)
Aspergillus sp. JMET 15 and (d) *Penicillium* sp. JMET 24 in the SM. Sugar
consumption by (e) *Aspergillus* sp. JMET 15 and (f) *Penicillium* sp. JMET 24
in the PDB. pH change and biomass of (g) *Aspergillus* sp. JMET 15 and (h)
Penicillium sp. JMET 24 in the PDB (continued).

The acidity of the medium changes with pH increasing from 5.5 to >7 in the sterile condition (CS), as LCO is an alkali oxide. The flasks containing JMET 15 and JMET 24 strains have a low pH. The pH of the medium in the T condition is intermediate between CS and CN, influenced by the alkali oxide at the cathode and the secretion of organic acids by the fungus. Oxalic acid (6,594 ppm) and citric acid (3,484 ppm) were detected with JMET 15, while oxalic acid (5,917 ppm) and citric acid (1,918 ppm) with JMET 24 were detected in the T condition and are shown in Figure 4.6. These organic acids contribute to the observed reduction in pH and play a key role in facilitating metal leaching from the cathode powder by lowering the medium pH and enhancing metal solubility.
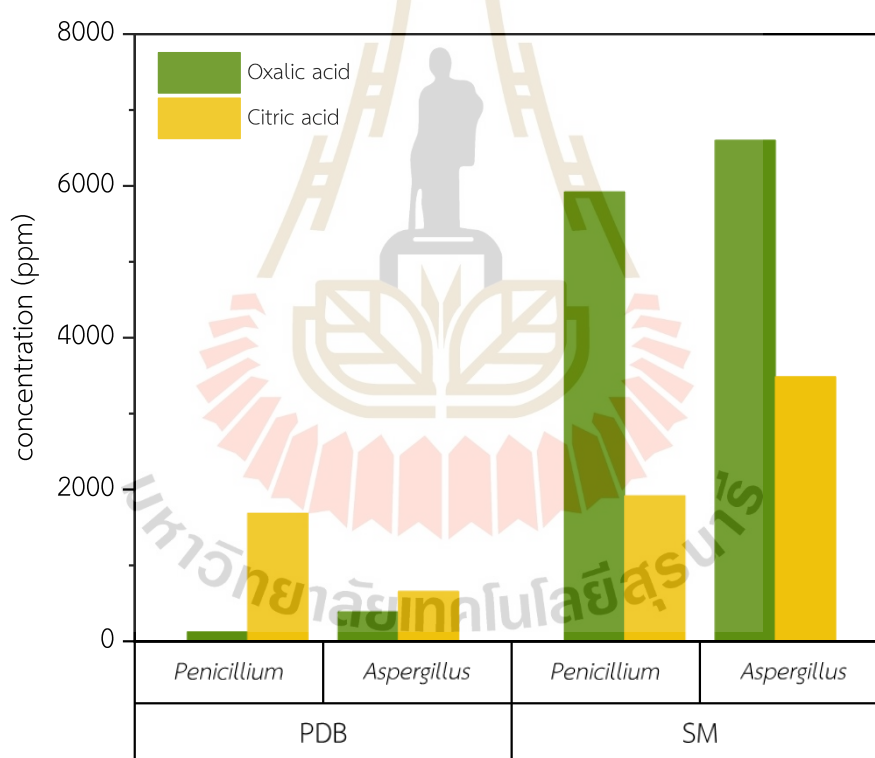
Figure 4.6   Oxalic and citric acid secretion (ppm) by *Aspergillus* sp. JMET 15 and *Penicillium* sp. JMET 24 in the SM or PDB with 1% w/v cathode powder after 30 days of incubation.

4.5.2 Effect of potato dextrose broth on fungal growth in LCO environment

For PDB, glucose is the primary organic carbon source, with concentrations exceeding 10,000 ppm, while ~3,000 ppm sucrose and ~1,000 ppm fructose were detected in the initial broth. Sugar was rapidly consumed within 7–9 days of incubation in T and CN conditions, whereas the sugar level remained constant in the CS condition (Figure 4.5e and f). The growth of the biomass of JMET 15 and JMET 24 strains proceeds similarly under T and CN conditions, indicating that PDB contains other nutrients that promote fungal growth, despite the toxicity of the cathode powder to fungal cells (Figure 4.5g and h).

The pH in the CN condition is initially acidic (4.6–5.4) for the first 5 days before becoming basic (~8). Fungi do not continuously secrete organic acid owing to a lack of sugar resources. Similarly, the pH is higher in the T condition owing to the essential nature of the alkali oxide in the cathode powder. The maximum concentration of oxalic acid (392 ppm) and citric acid (661 ppm) with JMET 15, while the same of oxalic acid (130 ppm) and citric acid (1,688 ppm) with JMET 24, were detected in the T condition and are presented in Figure 4.6.

4.5.3 Efficiency of *Aspergillus* sp. strain JMET 15 and *Penicillium* sp. strain JMET 24 on bioleaching of lithium and cobalt

The concentrations of Co and Li in leached solutions were analyzed via ICP-OES under T and CS conditions (Figure 4.7-4.10). The SM was more effective than the PDB for the growth of both fungal strains, due to the higher initial organic carbon source concentration in the SM (100 g/L sucrose, compared to ~10 g/L glucose and less than 4 g/L sucrose and fructose in the PDB, as analyzed by HPLC). Sugar, an organic carbon source, is the primary factor influencing fungal growth rates. It is the raw material for producing organic acids by the fungus through the tricarboxylic acid cycle metabolic pathway (Dusengemungu et al., 2021; Srichandan et al., 2019). Organic acids were used as leaching agents to leach Co and Li from the cathode powder. Moreover, several organic acids (oxalic acid in this study) reduce Co^{3+} to Co^{2+} (Equations (4.1) and (4.2)) (Verma et al., 2020), which can increase the

leaching efficiency since Co^{3+} is more difficult to dissolve than Co^{2+} (Lee & Rhee, 2003; Sun & Qiu, 2012). Additionally, JMET 24 dissolves more Co from the cathode powder than JMET 15.

Cobalt reduction: $Co^{3+} + e^- \leftrightarrow Co^{2+}$ $\hspace{3cm}$ $E_0 = 1.92$ V $\hspace{2cm}$ (4.1)

Oxalate oxidation: $C_2O_4^{2-} \leftrightarrow 2CO_2 + 2e^-$ $\hspace{3cm}$ $E_0 = 0.49$ V $\hspace{2cm}$ (4.2)

JMET 15 in PDB (T condition) leaches 186 and 181 ppm of Co and Li, respectively, after 30 days, while 132 and 136 ppm of Co and Li are leached, respectively, in the CS condition. JMET 24 in PDB leaches 250 and 143 ppm of Co and Li, respectively, while 106 and 98 ppm of Co and Li are leached, respectively, in the CS condition.
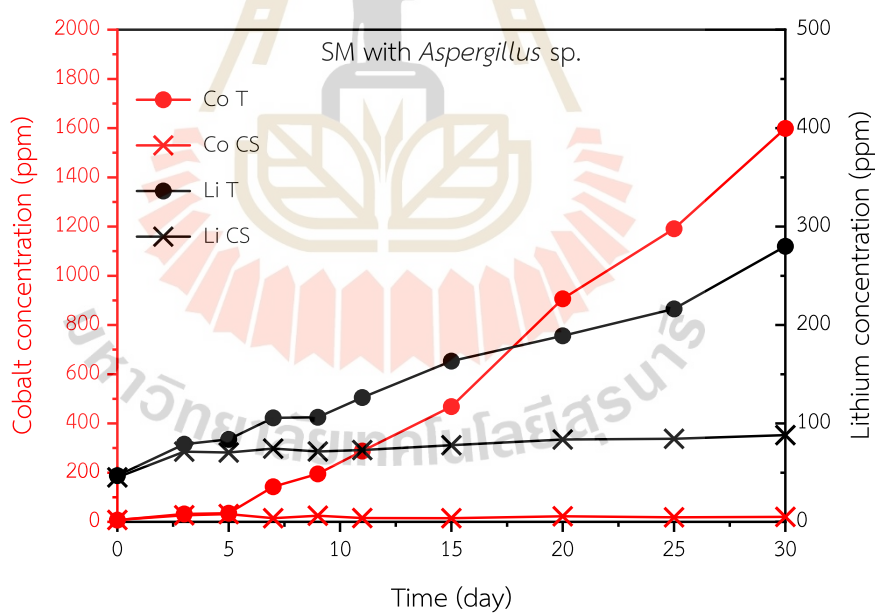
Figure 4.7   Cobalt and lithium concentrations in the SM leached by *Aspergillus* sp. JMET 15
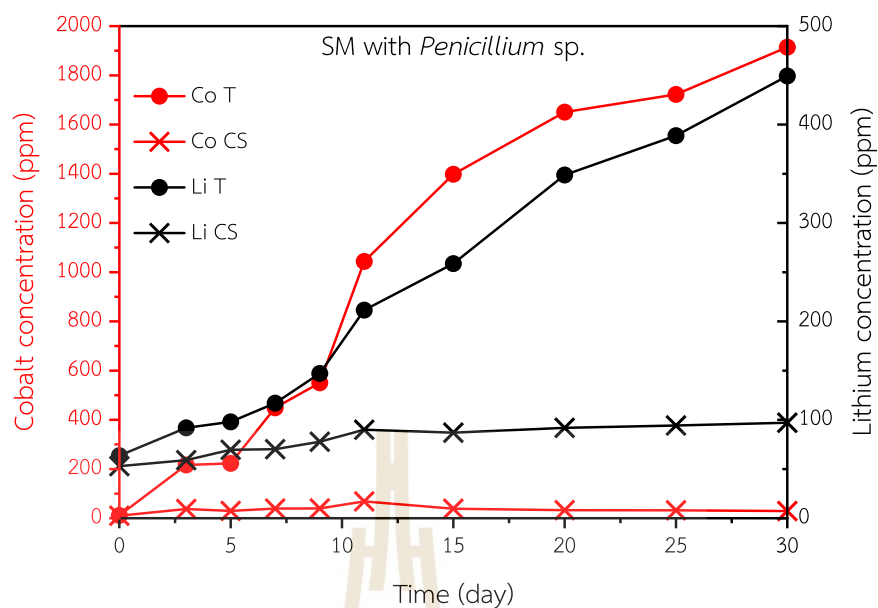
Figure 4.8 Cobalt and lithium concentrations in the SM leached by *Penicillium* sp.
          JMET 24
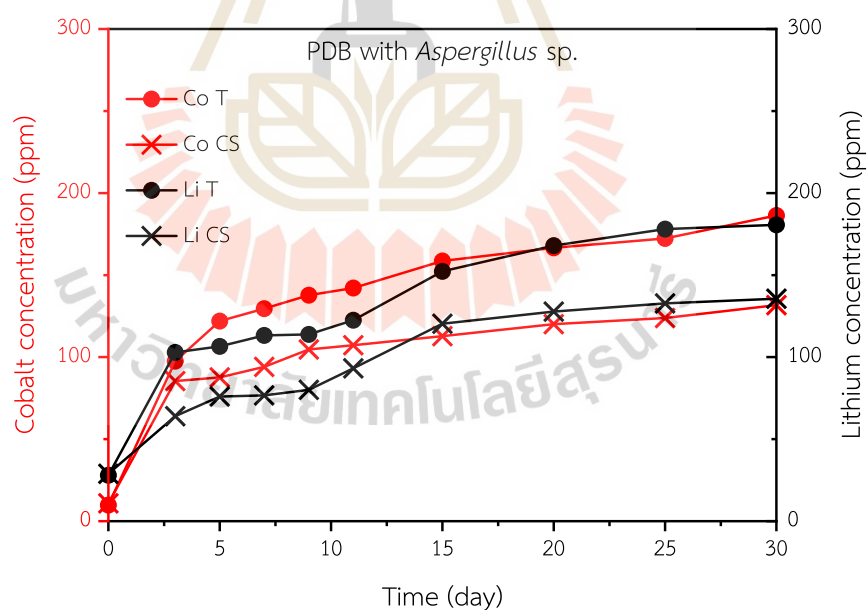
Figure 4.9 Cobalt and lithium concentrations in the PDB leached by *Aspergillus* sp.
          JMET 15
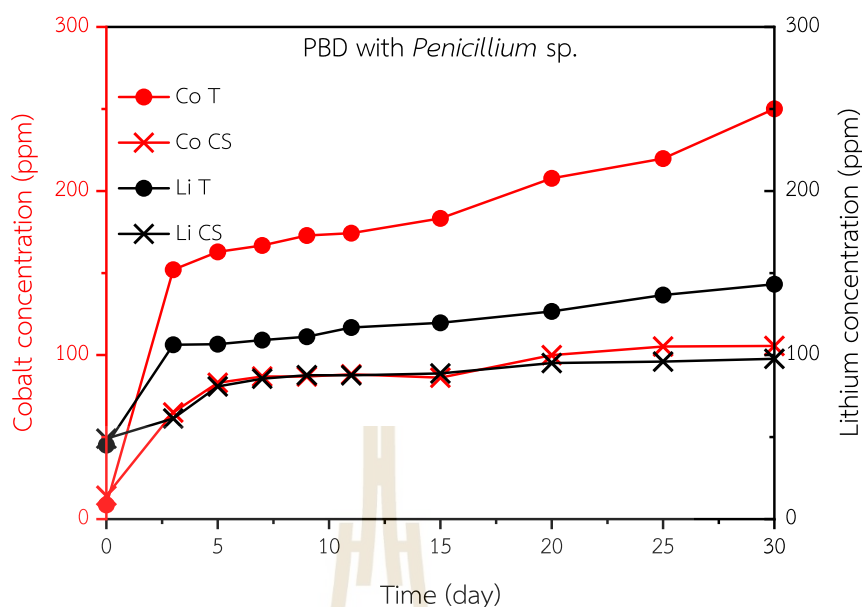
Figure 4.10 Cobalt and lithium concentrations in the PDB leached by *Penicillium* sp. JMET 24

The filtered solution with JMET 15 of the SM contains 1,599 ppm and 280 ppm of Co and Li, respectively, while the filtrate under the CS condition contains 20 ppm and 88 ppm of Co and Li, respectively. JMET 24 leached 1,915-ppm Co and 449-ppm Li, while 29-ppm Co and 97-ppm Li were leached in the CS condition (Figure 4.11). The metals dissolve more in the T condition than in the CS condition. A higher amount of Co dissolves in the PDB than in the SM in sterilized flasks owing to the effect of glucose and fructose (reducing sugars) in the PDB, which reduce Co^{3+} to Co^{2+}.

The maximum Co and Li leaching efficiencies of JMET 24 are 32.57% and 65.07%, respectively, in the SM, whereas those of JMET 15 are 27.19% and 40.58%, respectively, which are lower than the reported values. However, it is moderately high, considering the pulp density of 1% w/v of the cathode powder. Biswal et al. (2018) reported that $LiCoO_2$ bioleaching with a pulp density of 0.5%w/v showed no growth of *A. niger* strains MM1 and SG1 (Biswal et al., 2018). The leaching efficiency reported by Bahaloo-Horeh et al. (2018) was 38 % and 100 % for Co and Li, respectively, for $LiNi_{0.5}Mn_{1.1}Ti_{0.4}O_4$ and $LiCoO_2$ raw materials (Bahaloo-Horeh et al.,

2018). In comparison to bioleaching using bacteria, mixed cultures of sulfur-oxidizing and iron-oxidizing bacteria achieve leaching efficiencies of 90 % for Co and 80 % for Li at a pulp density of 1 % (Xin et al., 2009). In contrast, inorganic autotrophic bacteria such as *Acidithiobacillus ferrooxidans* demonstrate efficiencies of 82 % for Co and 89 % for Li at a pulp density of 10 % (Jegan Roy et al., 2021). This suggests that bacterial leaching of Co is indeed more efficient than fungal methods, as bacterial activity produces sulfuric acid, which enhances the solubility of Co. The amount of Co leached in our study is low because the activity of Co^{2+} and oxalic acid secreted from the fungus induces the crystallization of cobalt oxalate.
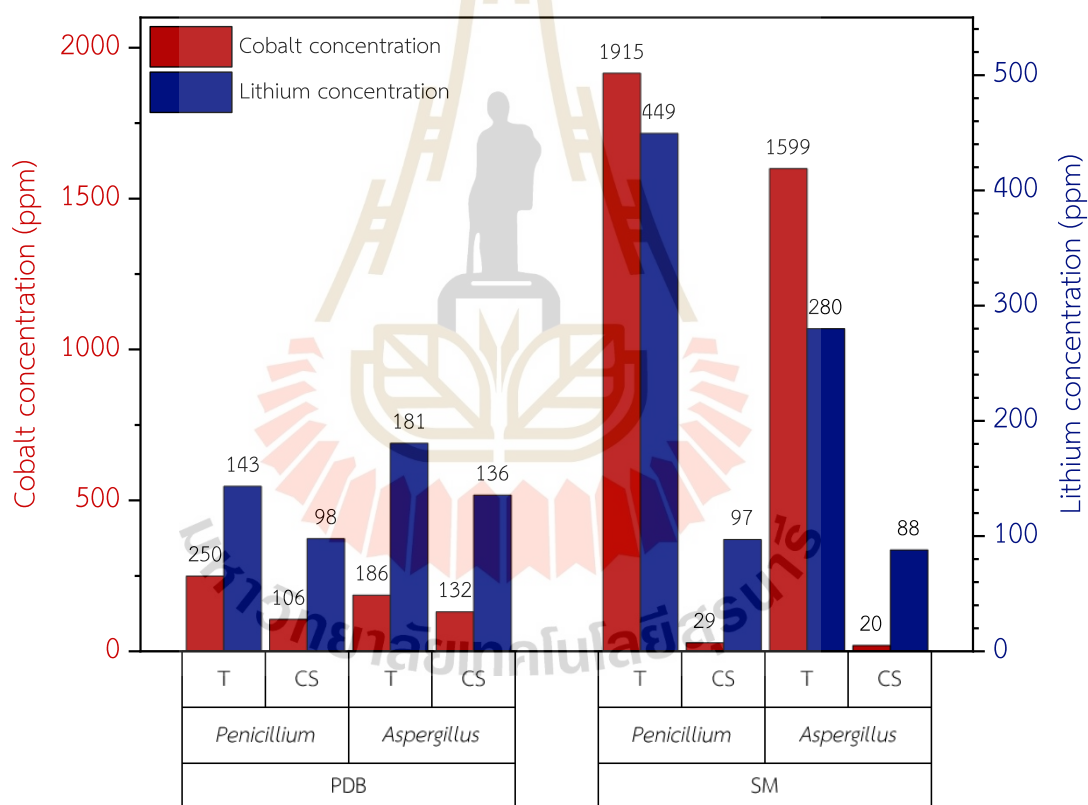
Figure 4.11 Cobalt and lithium concentrations in leaching conditions after 30 days.

4.5.4 Characterization of cathode powder before and after bioleaching

The samples leached by JMET 24 were analyzed via XAS owing to the higher leaching efficiency of JMET 24 to investigate the transformation of Co during bioleaching. The comparison of the chemical structure of leached Co was conducted between the cultured media of JMET 24 (T condition) and the cathode powder via Co K-edge X-ray absorption near edge structure (XANES) and EXAFS analysis. The Co K-edge XANES spectra of Co-foil (Co^0), CoO (Co^{2+}), Co_3O_4 ($Co^{2+,3+}$), cathode powder, media, and precipitate under T and CS conditions are shown in Figure 4.12 (a).

The position of the absorption edge for leached Co in the media of the T condition indicates that Co is in the Co $^{2+}$ form. The spectra of the Fourier-transformed (FT) k^3-weighted EXAFS profile at the Co edge for precipitated Co in CS and T conditions are like the cathode powder spectrum (Figure 4.12, b). However, the spectrum of the T medium exhibited a peak shift to the left compared to the other spectra.

To identify the transformed compound, Co K-edge EXAFS fitting was performed. The FT-EXAFS fit of the cathode powder matches perfectly with LCO, yielding an R-factor of 0.011. The fitted structure reveals six neighboring oxygen atoms (Co–O) at 2.03 Å and six neighboring Co atoms (Co–Co) at 2.598 Å around the Co atom. By contrast, the leached Co in the culture media under the T condition can be fitted with cobalt phosphate-oxalate $[(C_4N_2H_{12})_{0.5}(Co_2(HPO_4)(C_2O_4)_{1.5}$ COD No. 1519108] with an R-factor of 0.0125. Five Co–O bonds were identified, corresponding to neighboring oxygen atoms (1.89–2.18 Å). Moreover, four neighboring carbon atoms are present at 2.81 –2.88 Å. The wavelet transform (WT) analysis of Co K-edge EXAFS was conducted to illustrate further the atomic dispersion of Co (Figure 4.12c). The wavelet transforms of the contour plots of the cathode powder and precipitate (T condition) reveal a high-intensity maximum at 4 Å^{-1}, corresponding to Co–O coordination, and a low-intensity maximum at 6 Å^{-1}, assigned to Co–Co bonding. However, only a high-intensity maximum is observed at 4 Å^{-1} under the T condition, with no intensity, attributed to Co–Co coordination. Thus, the transformation of Co can occur in acidic conditions by culturing *Penicillium* sp. strain JMET 24.
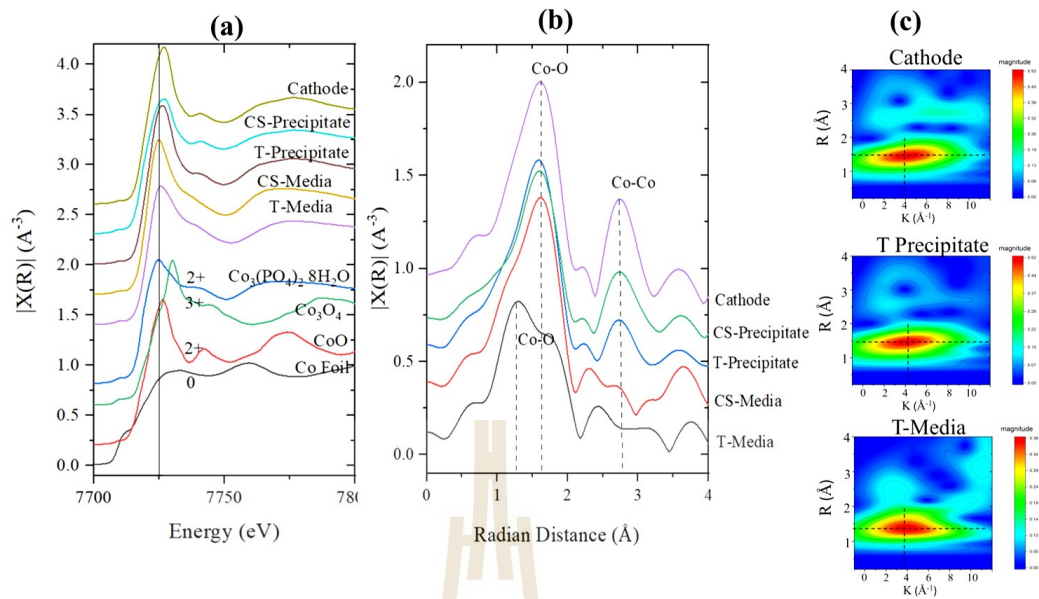
Figure 4.12 (a) Co K-edge XANES spectra of Co reference material and Co leaching
samples, (b) FT-EXAFS spectrum in the R space of Co leaching samples.
(c) WT for the k^3-weight EXAFS signals of leached Co samples.

Fungal cells and the residual cathode powder were collected on a
membrane filter paper after 30 days. The sample was dried and incinerated at 500 °C
to eliminate the biomass. LCO was the primary component of the residual powder,
as analyzed via XRD, consistent with the raw material (Figure 4.13) under the three
conditions. However, a pattern of Co_3O_4 mixed with LCO appears in the 30-day test
with both fungal strains (D30 T). Co_3O_4 is formed by the decomposition of cobalt
oxalate ($CoC_2O_4 \cdot 2H_2O$), which is the product of the reaction between Co ions in the
leach solution and oxalic acid secreted by fungi (Equation (4.3)). $CoC_2O_4.2H_2O$ is
insoluble (Verma et al., 2019) in water and easily precipitated into a solid powder.
Sun and Qiu (2012) analyzed the thermal properties of $CoC_2O_4 \cdot 2H_2O$ in the air. It
decomposes into Co_3O_4 at 290 °C-320 °C (Equations (4.4) and (4.5)) (Sun & Qiu, 2012).

$$Co^{2+} + 2H_2C_2O_4 + 2O \leftrightarrow CoC_2O_4 \cdot 2H_2O(s) \tag{4.3}$$

$$\text{At 150 °C-210 °C, } CoC_2O_4 \cdot 2H_2O = CoC_2O_4 + 2H_2O \tag{4.4}$$
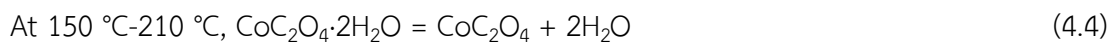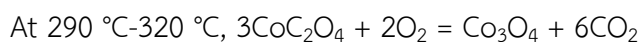
At 290 °C-320 °C, $3CoC_2O_4 + 2O_2 = Co_3O_4 + 6CO_2$ (4.5)
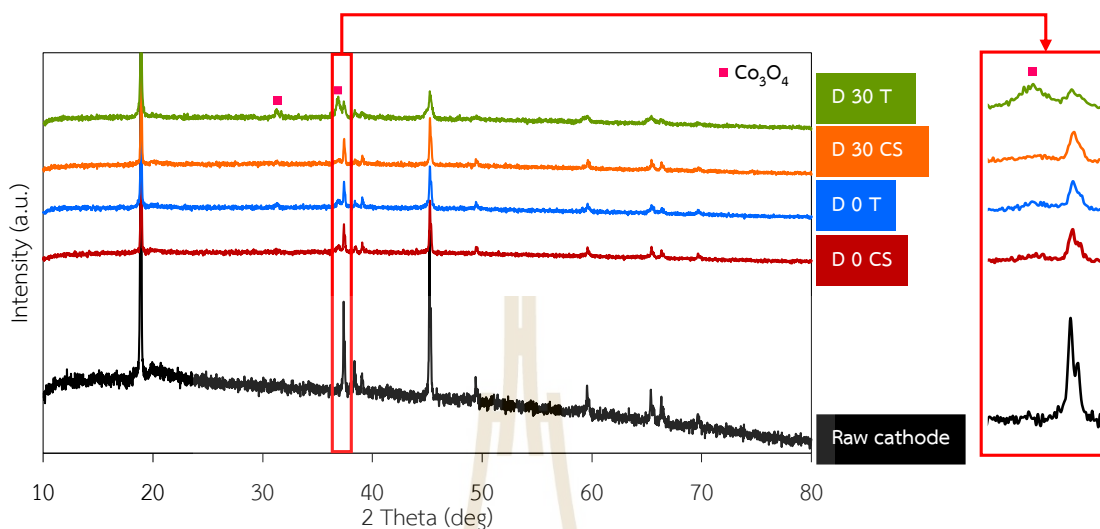
Figure 4.13 XRD patterns of raw materials compared to the residual powder after 0 and 30 days of bioleaching.

4.6   Conclusion

Two potential fungal strains, JMET 24 and JMET 15, were grown in Co and Li environments in the PDB and SM with 1% w/v cathode powder. JMET 24 showed continuous growth while JMET 15 exhibited slow growth in the initial 7 days in the SM. Although no lag phase was observed in the PDB, the leaching efficiency of Co and Li was lower in the PDB than in the SM, due to the lower amount of sugar serving as an organic carbon source in the PDB. The detected sugars were rapidly consumed during the initial stage of the fungal growth (5–9 days). The growth of the fungus and the secretion of organic acids facilitated the leaching of metals from the cathode powder. Both fungal strains increased the leaching of Co and Li from the cathode powder compared to the sterile condition. The highest concentrations of Co and Li in the leached solution were 1,915 ppm and 449 ppm, respectively, in the SM with JMET 24. The EXAFS spectrum fitting revealed the transformation of cobalt into cobalt phosphate-oxalate during the bioleaching process of the cobalt compound in the cultured media under the T condition with JMET 24. The burning of the sample

at 500 °C resulted in the formation of Co_3O_4 as the product, mixed with the retained LCO powder.

4.7   References

Amaro, J. K. C., Xavier, L. V., Ribeiro, M. M. A. de C., Vieira, B. S., & Mendes, G. de O. (2022). Optimization of oxalic acid production by fungi for biotechnological solubilization of rock phosphate. *Scientia Agricola*, *80*, e20210076. https://doi.org/10.1590/1678-992X-2021-0076

Angumeenal, A. R., & Venkappayya, D. (2013). An overview of citric acid production. *LWT - Food Science and Technology*, *50*(2), 367–370. https://doi.org/10.1016/j.lwt.2012.05.016

Bahaloo-Horeh, N., Mousavi, S. M., & Baniasadi, M. (2018). Use of adapted metal tolerant *Aspergillus niger* to enhance bioleaching efficiency of valuable metals from spent lithium-ion mobile phone batteries. *Journal of Cleaner Production*, *197*, 1546–1557. https://doi.org/10.1016/j.jclepro.2018.06.299

de Jesus Silva, A. J., Contreras, M. M., Nascimento, C. R., & da Costa, M. F. (2020). Kinetics of thermal degradation and lifetime study of poly(vinylidene fluoride) (PVDF) subjected to accelerated aging with bioethanol fuel. *Heliyon*, *6*(7), e04573. https://doi.org/10.1016/j.heliyon.2020.e04573

Dusengemungu, L., Kasali, G., Gwanama, C., & Mubemba, B. (2021). Overview of fungal bioleaching of metals. *Environmental Advances*, *5*, 100083. https://doi.org/10.1016/j.envadv.2021.100083

Fu, Y., Schuster, J., Petranikova, M., & Ebin, B. (2021). Innovative recycling of organic binders from electric vehicle lithium-ion batteries by supercritical carbon dioxide extraction. *Resources, Conservation and Recycling*, *172*, 105666. https://doi.org/10.1016/j.resconrec.2021.105666

Jegan Roy, J., Srinivasan, M., & Cao, B. (2021). Bioleaching as an Eco-Friendly Approach for Metal Recovery from Spent NMC-Based Lithium-Ion Batteries at a High Pulp Density. *ACS Sustainable Chemistry & Engineering*, *9*(8), 3060–3069. https://doi.org/10.1021/acssuschemeng.0c06573

Lee, C. K., & Rhee, K.-I. (2003). Reductive leaching of cathodic active materials from lithium-ion battery wastes. *Hydrometallurgy*, *68*(1), 5–10. https://doi.org/10.1016/S0304-386X(02)00167-6

Ravel, B., & Newville, M. (2005). ATHENA, ARTEMIS, HEPHAESTUS: Data analysis for X-ray absorption spectroscopy using IFEFFIT. *Journal of Synchrotron Radiation*, *12*(4), 537–541. https://doi.org/10.1107/S0909049505012719

Shankar, T., & Sivakumar, T. (2016). Optimization of Citric Acid Production Using *Aspergillus niger* Isolated from the Leaf Litter Soil of Sathuragiri Hills. *Universal Journal of Microbiology Research*, *4*(4), 79–87. https://doi.org/10.13189/ujmr.2016.040401

Srichandan, H., Mohapatra, R. K., Parhi, P. K., & Mishra, S. (2019). Bioleaching approach for extraction of metal values from secondary solid wastes: A critical review. *Hydrometallurgy*, *189*, 105122. https://doi.org/10.1016/j.hydromet.2019.105122

Sun, L., & Qiu, K. (2012). Organic oxalate as leachant and precipitant for the recovery of valuable metals from spent lithium-ion batteries. *Waste Management*, *32*(8), 1575–1582. https://doi.org/10.1016/j.wasman.2012.03.027

Swain, B. (2017). Recovery and recycling of lithium: A review. *Separation and Purification Technology*, *172*, 388–403. https://doi.org/10.1016/j.seppur.2016.08.031

Thomas, P., Varughese, K. T., Dwarakanath, K., & Varma, K. B. R. (2010). Dielectric properties of Poly(vinylidene fluoride)/$CaCu_3Ti_4O_{12}$ composites. *Composites Science and Technology*, *70*(3), 539–545. https://doi.org/10.1016/j.compscitech.2009.12.014

Verma, A., Johnson, G. H., Corbin, D. R., & Shiflett, M. B. (2020). Separation of Lithium and Cobalt from $LiCoO_2$: A Unique Critical Metals Recovery Process Utilizing Oxalate Chemistry. *ACS Sustainable Chemistry & Engineering*, *8*(15), 6100–6108. https://doi.org/10.1021/acssuschemeng.0c01128

Verma, A., Kore, R., Corbin, D. R., & Shiflett, M. B. (2019). Metal Recovery Using Oxalate Chemistry: A Technical Review. *Industrial & Engineering Chemistry Research*, *58*(34), 15381–15393. https://doi.org/10.1021/acs.iecr.9b02598

Xin, B., Zhang, D., Zhang, X., Xia, Y., Wu, F., Chen, S., & Li, L. (2009). Bioleaching
mechanism of Co and Li from spent lithium-ion battery by the mixed culture
of acidophilic sulfur-oxidizing and iron-oxidizing bacteria. *Bioresource
Technology*, *100*(24), 6163–6169.
https://doi.org/10.1016/j.biortech.2009.06.086

Zhang, T., He, Y., Ge, L., Fu, R., Zhang, X., & Huang, Y. (2013). Characteristics of wet
and dry crushing methods in the recycling process of spent lithium-ion
batteries. *Journal of Power Sources*, *240*, 766–771.
https://doi.org/10.1016/j.jpowsour.2013.05.009

CHAPTER V
OPTIMIZATION OF BIOLEACHING CATHODE POWDER USING
PENICILLIUM SP. STRAIN JMET 24

5.1   Abstract

In this study, the bioleaching of cobalt and lithium from deteriorated lithium cobalt oxide (LCO) powder was investigated using *Penicillium* sp. strain JMET 24. Our previous findings indicated that *Penicillium* sp. strain JMET 24 achieved leaching efficiencies of 32.57% for cobalt and 65.07% for lithium at a pulp density of 1%. To enhance these efficiencies, we examined the effects of initial pH, chemical composition of the medium, and pulp density. Our results demonstrated that an initial pH of 3 and a newly developed composite medium significantly improved leaching efficiencies, achieving 70.75% for cobalt and 100% for lithium. Additionally, increasing the pulp density to 5% further enhanced the concentrations of leached metals, although the efficiency decreased due to higher initial metal content. These findings suggest that optimizing medium composition and operational parameters can substantially improve the bioleaching process for cobalt and lithium recovery from LCO powder.

5.2   Introduction

In the previous chapter, the bioleaching of cobalt and lithium from deteriorated lithium cobalt oxide (LCO) powder at a 1% pulp density was investigated using two fungal strains: *Aspergillus* sp. strain JMET 15 and *Penicillium* sp. strain JMET 24 in two different media: potato dextrose broth (PDB) and sucrose medium (SM). The results revealed that *Penicillium* sp. strain JMET 24, when grown in sucrose medium, achieved the highest concentrations of cobalt and lithium, at 1,915 ppm and 449 ppm, respectively, corresponding to leaching efficiencies of 32.57% and

65.07%. However, when compared to other recycling processes, these leaching efficiencies were relatively low.

To enhance leaching efficiency, the concentration and type of acid secreted by fungi are essential factors. Other parameters, such as initial pH, the chemical composition of the sucrose medium, and pulp density, should be investigated due to their effects on fungal metabolism. Walaszczyk et al. (2018) reported that the pH of the medium is a key parameter influencing the chemical selectivity of organic acid secretion by fungi (*Aspergillus niger*). The variation in initial pH is responsible for the decomposition of oxaloacetate to oxalate and acetate within the fungal cells. Oxalic acid was most abundantly secreted at a pH of 6, whereas citric acid was most concentrated at a pH of 3 (Walaszczyk et al., 2018). The type and concentration of each component in the nutrient broth also significantly affect organic acid secretion. Numerous studies have reported that glucose is a carbon source that induces higher concentrations of oxalic acid secretion by fungi compared to other sources (Amaro et al., 2022; Bahaloo-Horeh & Mousavi, 2024). In industrial applications, sucrose has been identified as the most suitable carbon source for organic acid biosynthesis (Angumeenal & Venkappayya, 2013; Walaszczyk et al., 2018).

Therefore, in this chapter, additional variables, such as initial pH, the chemical composition of the medium, and pulp density were examined in order to enhance the leaching efficiency of cobalt and lithium using *Penicillium* sp. strain JMET 24 in a sucrose medium.

5.3   Research objective

The objective of this research is to enhance the leaching efficiency of cobalt and lithium from deteriorated lithium cobalt oxide (LCO) powder using *Penicillium* sp. strain JMET 24. This will be achieved by investigating the effects of various parameters, including initial pH, the chemical composition of the medium, and pulp density.

5.4   Materials and Methods

The raw deteriorated LCO cathode powder used in this study originated from the same batch as described in Chapter 4. The chemical composition was determined to be 58.8% cobalt (Co) and 6.9% lithium (Li) by weight, as analyzed by ICP-OES.

For the bioleaching process, 1 mL of *Penicillium* sp. strain JMET 24 spore suspension, at a concentration of approximately 10^6 spores/mL, was inoculated into a 250-mL Erlenmeyer flask containing 100 mL of sterilized sucrose medium. The media were sterilized in an autoclave at 121 °C for 15 minutes. Specific details regarding pH, pulp density, and the chemical composition of the sucrose medium are provided in the sections below. Each condition was maintained for 30 days at 150 rpm in an orbital shaking incubator. The abbreviations T, CS, and CN refer to the test conditions (bioleaching), cathode sterilized (non-fungi), and non-cathode (fungi growth in regular broth), respectively. All experiments were performed in triplicate.

5.4.1   Study of initial pH on leaching efficiency

The sucrose medium (SM) used in this section consisted of the following components per liter: 100 g of sucrose, 1.5 g of $NaNO_3$, 0.5 g of KH_2PO_4, 0.025 g of $MgSO_4 \cdot 7H_2O$, 0.025 g of KCl, and 1.6 g of yeast extract. The pH was adjusted to 2, 3, 4, and 5 by adding 1 N HCl. After sterilizing the medium, the spore suspension was inoculated concurrently with 1 g of sterilized deteriorated LCO cathode powder. Sampling was conducted on days 0, 3, 5, 7, 9, 11, 15, 20, 25, and 30 to determine the concentrations of cobalt and lithium in the leached solution.

5.4.2   Study of the developed medium on leaching efficiency

To compare the influence of the chemical composition of nutrient broth on leaching efficiency, three types of broth were used in this section: PDB, SM, and a new composite medium. The PDB and SM broths had the same chemical composition as described in Chapter 4.

The new composite medium used in this section consisted of the following components per liter: 100 g of sucrose, 1 g of $NaNO_3$, 2 g of KH_2PO_4, 0.025 g of $MgSO_4 \cdot 7H_2O$, 0.025 g of KCl, 3 g of yeast extract, and 24 g of PDB. The pH was not

adjusted, with the initial pH of the medium being 5.5. After sterilization, 1 g of deteriorated LCO cathode powder was added to the flask, resulting in a pulp density of 1%. The flask was then incubated in an orbital shaker at 150 rpm for 30 days. The leaching efficiency was calculated as the ratio of cobalt and lithium in the leached solution to the amount in the raw cathode powder, multiplied by 100.

5.4.3   Study of pulp density on leaching efficiency

The optimum pH and medium, which resulted in the highest concentrations of leached cobalt and lithium in the previous section, were selected. The pulp density was varied at 1%, 5%, and 10% w/v. All other parameters were maintained as in the previous sections.

5.5   Results and Discussion

5.5.1   Effect of initial pH on leaching efficiency

The concentrations of cobalt (Co) and lithium (Li) in bioleaching solutions increased over time at pH levels of 3, 4, and 5 under T conditions, as illustrated in Figure 5.1. Co and Li exhibited the fastest solubilization at an initial pH of 5 within the first 10 days. Subsequently, lower initial pH levels (4 and 3) showed delayed increases in concentrations of Co and Li. After 30 days of incubation, the highest concentrations of Co and Li were observed at an initial pH of 3, while the lowest concentrations were found at an initial pH of 2.

In contrast, under CS conditions, the lowest initial pH resulted in the highest concentrations of Co and Li due to the medium's acidity within the first 3 days of incubation. The concentrations of Co and Li remained constant after this period. The leaching efficiency calculations indicated that pH levels of 3, 4, and 5 had nearly similar efficiencies over 30 days, as presented in Figure 5.2, with the highest efficiency observed at pH 3 (38.65% for Co and 67.1% for Li).

When comparing the leaching efficiency with the final pH and biomass, it reflects the growth of fungi under different conditions as described in Figure 5.3. The growth of JMET 24 was directly influenced by the initial pH of the substrate medium (SM). The highest biomass was observed at an initial pH of 3 under both CN

and T conditions. At an initial pH of 2, no fungal growth (biomass was zero) was detected under CN conditions. However, under T conditions, a slight growth of fungi was observed at an initial pH of 2, regardless of the presence of Co and Li. The basic oxide nature of LCO increased the pH of the media to approximately six across all initial pH conditions, as shown in Figure 5.3(a). The final pH of the CS conditions was lowest at an initial pH of 2 and increased continuously to 7.54 at an initial pH of 5. It was concluded that JMET 24 exhibited efficient growth at an initial pH of 3 and leached Co and Li at the highest concentrations as described above.
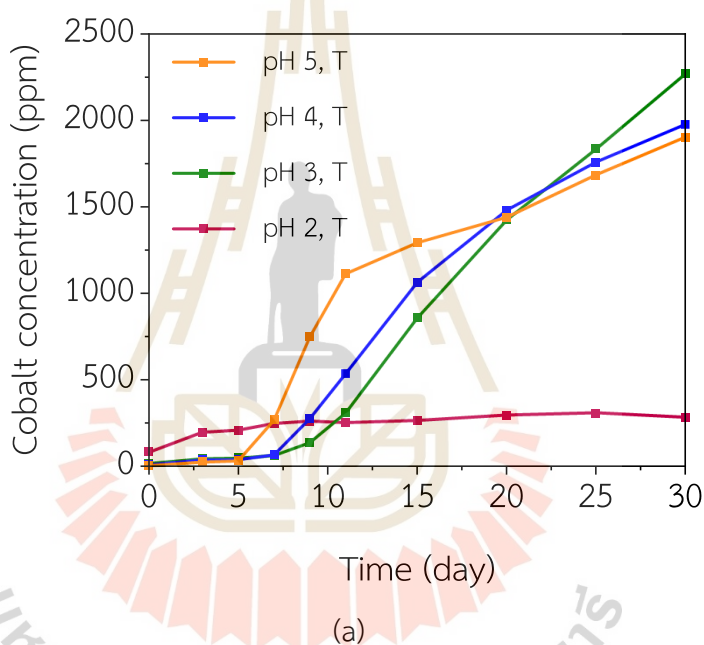
(a)

Figure 5.1   The concentration of metals in various initial pH bioleaching solutions over 0-30 days: (a) cobalt under bioleaching conditions, (b) lithium under bioleaching conditions, (c) cobalt under sterile conditions, and (d) lithium under sterile conditions.
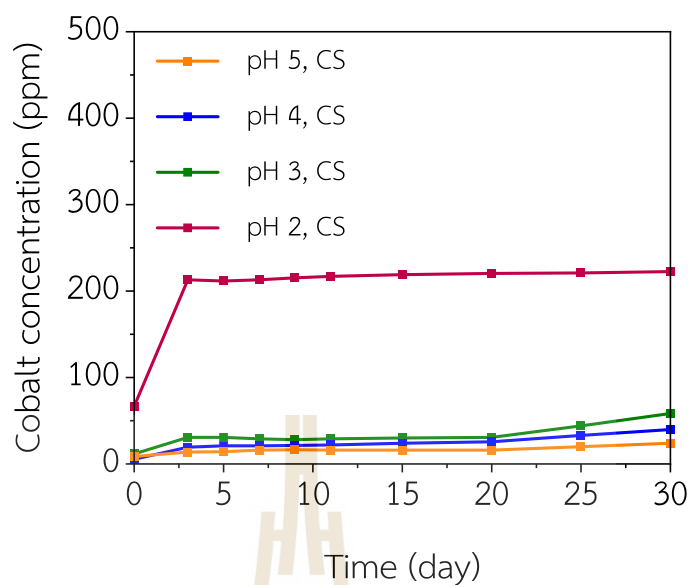
(b)
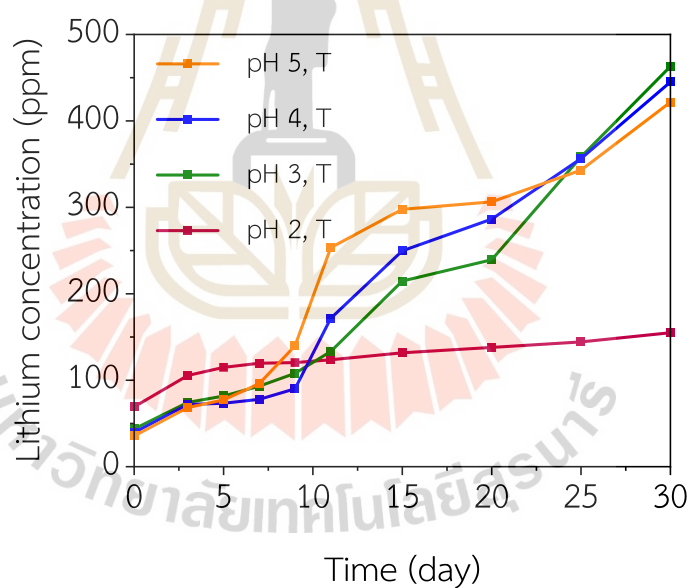
(c)

Figure 5.1   The concentration of metals in various initial pH bioleaching solutions over 0-30 days: (a) cobalt under bioleaching conditions, (b) lithium under bioleaching conditions, (c) cobalt under sterile conditions, and (d) lithium under sterile conditions (continued).

(d)
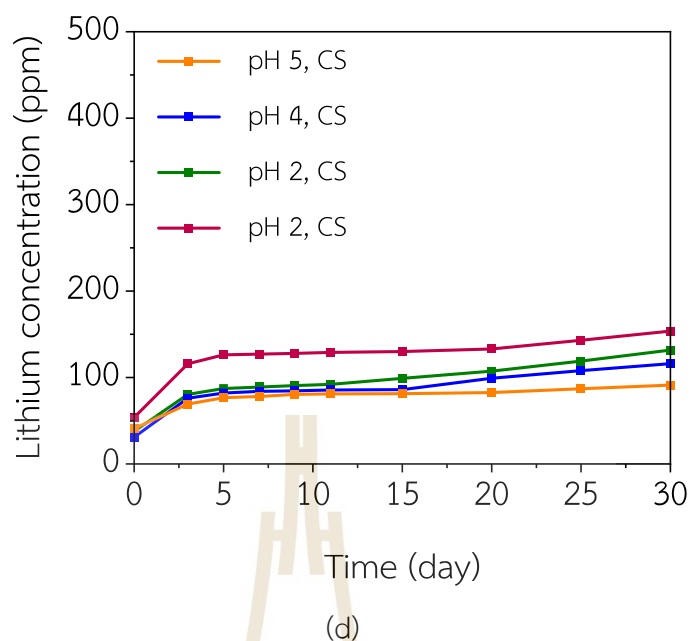
Figure 5.1   The concentration of metals in various initial pH bioleaching solutions over 0-30 days: (a) cobalt under bioleaching conditions, (b) lithium under bioleaching conditions, (c) cobalt under sterile conditions, and (d) lithium under sterile conditions (continued).
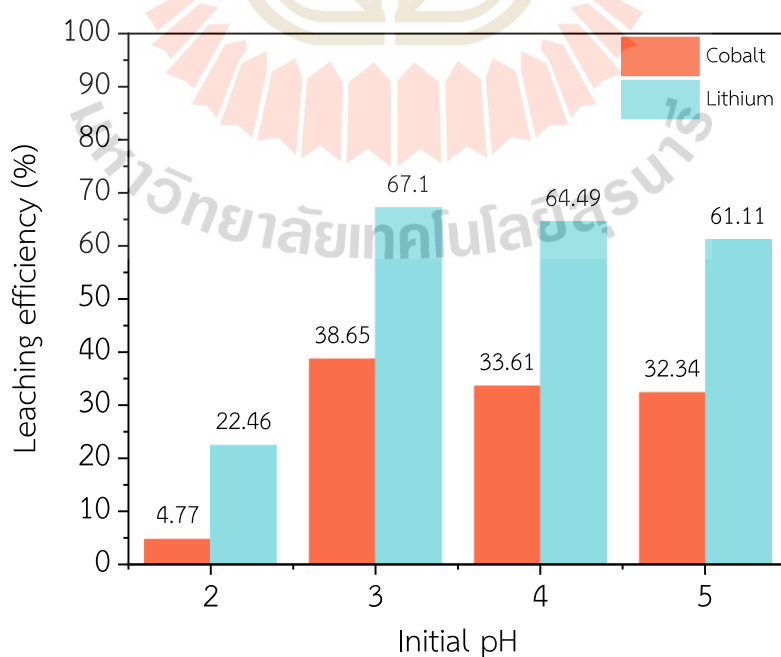
Figure 5.2   Leaching efficiency of cobalt and lithium at various initial pH levels.
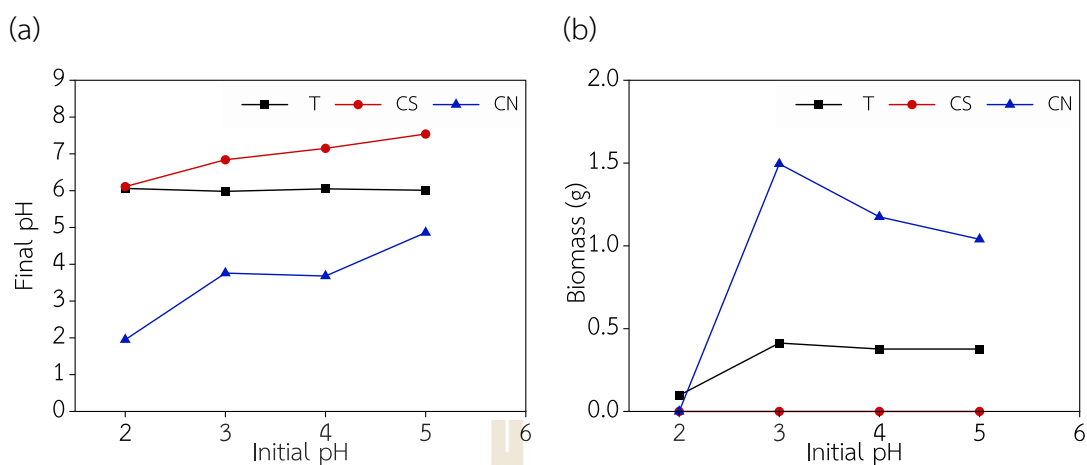
Figure 5.3 The final pH (a) and biomass (b) measured after a 30-day incubation period.

5.5.2 Effect of the developed medium on leaching efficiency

According to the study by Amaro et al. (2022), increased amounts of sugar, KH_2PO_4, and yeast extract can significantly enhance the production of organic acids, particularly oxalic acid (Amaro et al., 2022). Furthermore, previous research has indicated that using PDB for bioleaching LCO powder at a pulp density of 1%, the fungus JMET 24 exhibited robust initial growth. Specifically, during the first three days of the experiment, no lag phase was observed, and the fungus grew similarly in environments with and without Co and Li (Chandakhiaw et al., 2024). The researcher then applied this data to develop an improved culture medium formula, as shown in Table 5.1.

After 30 days of bioleaching, the solution was analyzed for Co and Li concentrations by ICP-OES. It was found that using a new composite medium (CM) resulted in a more than twofold increase in cobalt concentration from 1,915 ppm to 4,160 ppm compared to the sucrose medium (SM). The leaching efficiency also increased from 32.56% to 70.75%, as illustrated in Figure 5.4. Similarly, CM was able to dissolve lithium more effectively than SM, increasing from 449 ppm to 690 ppm, with a corresponding rise in leaching efficiency from 65.12% to 100%, as shown in Figure 5.5.

Table 5.1 Composition of sucrose medium (SM) and new composite medium (CM) per liter.

Ingredients	SM	CM
Sucrose	100 g	100 g
NaNO$_3$	1.5 g	1 g
KH$_2$PO$_4$	0.5 g	2 g
MgSO$_4\cdot$7H$_2$O	0.025 g	0.025 g
KCl	0.025 g	0.025 g
yeast extract	1.6 g	3 g
PDB	-	24 g
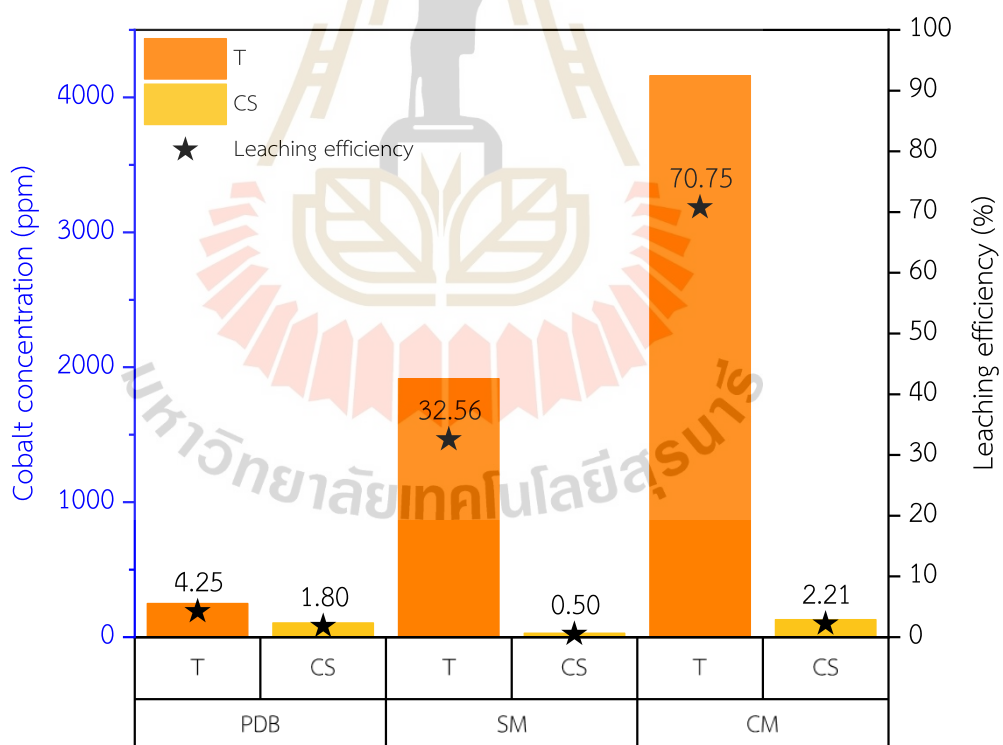
Figure 5.4 Cobalt concentration and leaching efficiency from PDB, SM, and CM bioleaching processes.
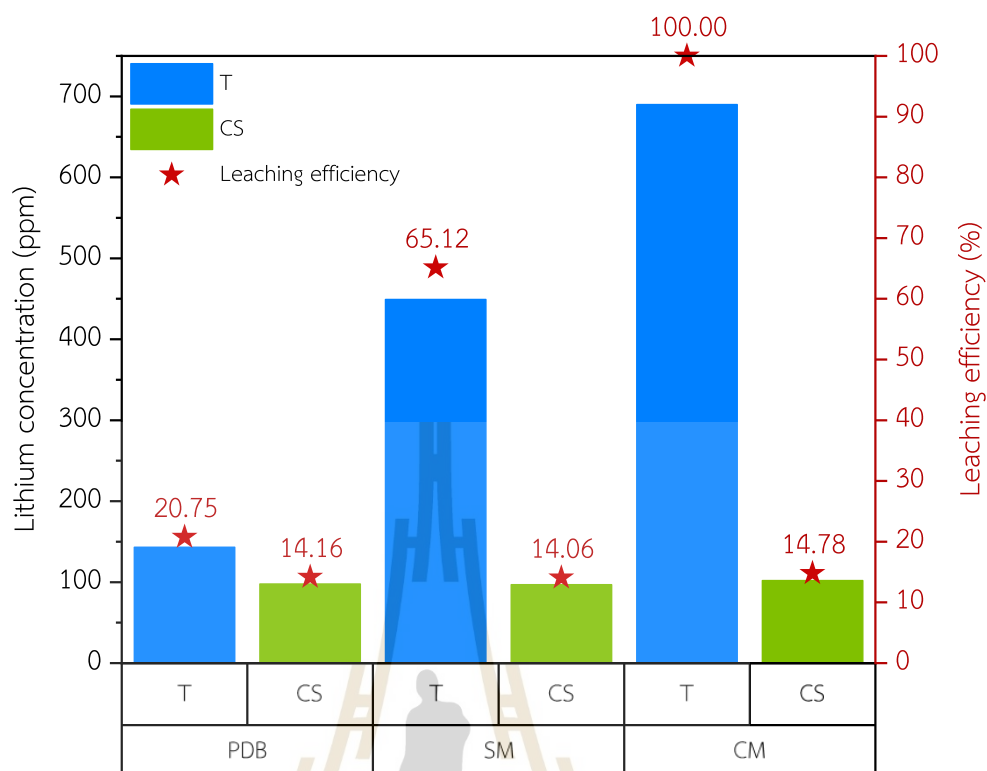
Figure 5.5 Lithium concentration and leaching efficiency from PDB, SM, and CM bioleaching processes.

When the residue from the leaching process was calcined at 500°C in a muffle furnace for 4 hours and analyzed using XRD techniques, it was found that the residue from using CM consisted solely of cobalt oxide (Co_3O_4). This indicates that $LiCoO_2$ in LCO was completely leached, with lithium being fully dissolved during the leaching process. Cobalt, on the other hand, was partially precipitated and partially dissolved, depending on the organic acids produced by the JMET 24 strain. Oxalic acid can bind with cobalt to form water-insoluble cobalt oxalate, which, when calcined at 500°C, transforms into Co_3O_4, as shown in Figure 5.6. In contrast, when using SM and PDB, Co_3O_4 mixed with $LiCoO_2$ was still observed, indicating that the LCO material was not wholly leached.
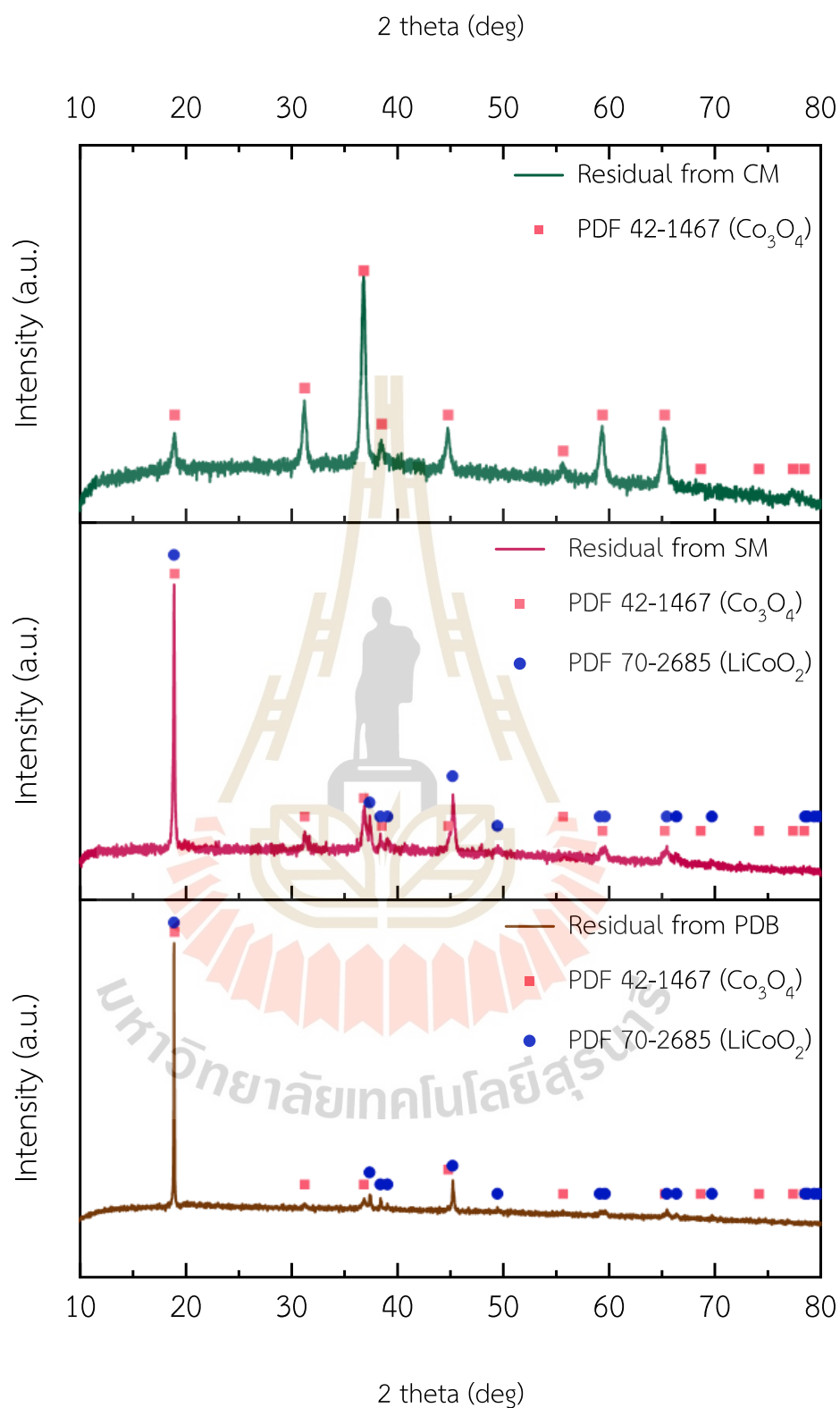
Figure 5.6   XRD patterns of residuals after 30-day bioleaching in PBD, SM, and CM media.

5.5.3   Effect of pulp density on leaching efficiency

From sections 5.5.1 and 5.5.2, it was found that at an initial solution pH of 3, the CM medium could leach cobalt and lithium most effectively. Therefore, experiments were conducted to increase the solid-to-liquid ratio, or pulp density, from 1% to 5% and 10% (to compare and improve the efficiency of bioleaching compared to traditional methods that use corrosive and toxic chemicals but achieve high efficiency, capable of leaching more than 10% w/v of spent battery cathode powder). After a 30-day experiment, it was found that increasing the pulp density to 5% resulted in higher concentrations of cobalt and lithium, reaching 6,510 ppm and 2,070 ppm, respectively. Although the concentrations of both metals increased, the leaching efficiency (%leaching efficiency) decreased to 22.14% and 60%, respectively, due to the higher initial metal content. At a pulp density of 10% w/v, the concentrations of both metals decreased to 4,320 ppm Co and 1,480 ppm Li, with leaching efficiencies of only 7.35% and 21.45%, respectively (Figure 5.7). This decrease is attributed to the reduced fungal growth when a higher amount of cathode powder (10% w/v) was used, as shown in Figure 5.8.
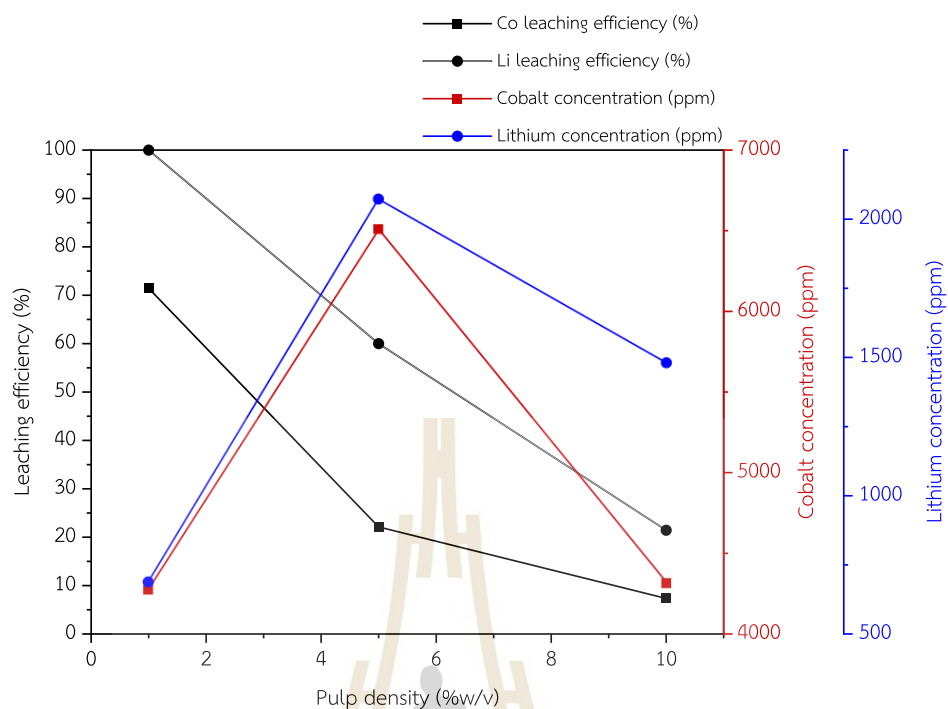
Figure 5.7   Leaching efficiency (%) and concentration of cobalt and lithium in bioleached solution at 1%, 5%, and 10%w/v pulp density.
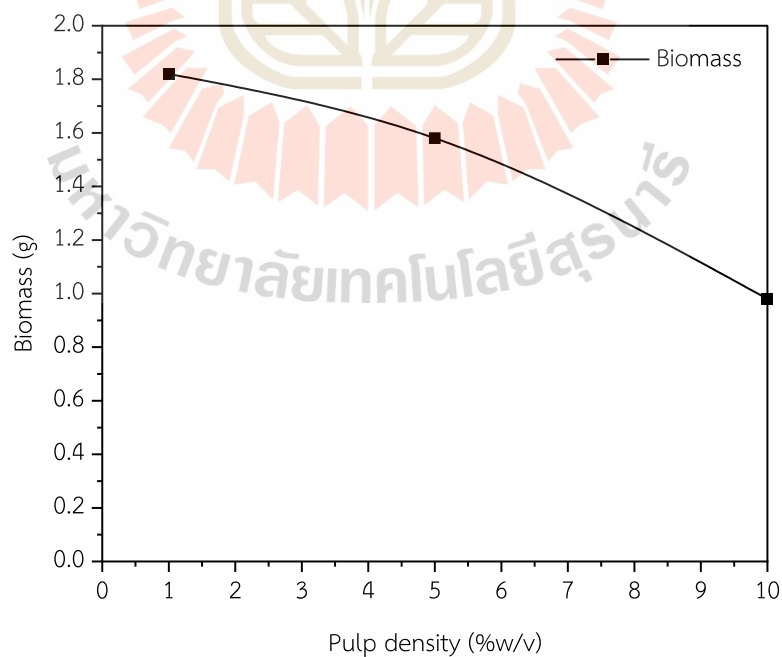
Figure 5.8   Biomass after a 30-day incubation at 1%, 5%, and 10%w/v pulp density.

5.6 Conclusion

This research highlights the potential of *Penicillium* sp. strain JMET 24 in bioleaching cobalt and lithium from deteriorated LCO powder. Our study found that the initial pH of the medium, chemical composition, and pulp density are critical factors influencing leaching efficiency. The optimized conditions, including an initial pH of 3 and a composite medium, yielded significantly higher leaching efficiencies compared to those in the previous section. Increasing the pulp density to 5% further improved metal concentrations, although efficiency decreased. These results underscore the importance of medium optimization and parameter control in enhancing bioleaching processes. Future work should focus on scaling up these findings and exploring the economic feasibility of industrial applications.

5.7 References

Amaro, J. K. C., Xavier, L. V., Ribeiro, M. M. A. de C., Vieira, B. S., & Mendes, G. de O. (2022). Optimization of oxalic acid production by fungi for biotechnological solubilization of rock phosphate. *Scientia Agricola*, *80*, e20210076. https://doi.org/10.1590/1678-992X-2021-0076

Angumeenal, A. R., & Venkappayya, D. (2013). An overview of citric acid production. *LWT - Food Science and Technology*, *50*(2), 367–370. https://doi.org/10.1016/j.lwt.2012.05.016

Bahaloo-Horeh, N., & Mousavi, S. M. (2024). Analyzing the Effects of Culture Media Additives on Oxalic Acid Bioproduction for Use in Metal Bioleaching. *Waste and Biomass Valorization*, *15*(5), 2687–2703. https://doi.org/10.1007/s12649-023-02381-4

Chandakhiaw, T., Teaumroong, N., Piromyou, P., Songwattana, P., Tanthanuch, W., Tancharakorn, S., & Khumkoa, S. (2024). Efficiency of *Penicillium* sp. And *Aspergillus* sp. For bioleaching lithium cobalt oxide from battery wastes in potato dextrose broth and sucrose medium. *Results in Engineering*, *24*, 103170. https://doi.org/10.1016/j.rineng.2024.103170

Walaszczyk, E., Podgórski, W., Janczar-Smuga, M., & Dymarska, E. (2018). Effect of
medium pH on chemical selectivity of oxalic acid biosynthesis by *Aspergillus
niger* W78C in submerged batch cultures with sucrose as a carbon source.
Chemical Papers, 72(5), 1089–1093. https://doi.org/10.1007/s11696-017-0354-x

CHAPTER VI

RECOVERY OF COBALT AND LITHIUM FROM BIOLEACHING

SOLUTION

6.1   Abstract

This study investigates the recovery of cobalt (Co) and lithium (Li) from bioleaching solutions derived from degraded $LiCoO_2$ raw materials, a process crucial for recycling spent lithium-ion batteries (LIBs). The research focuses on the precipitation of cobalt as cobalt oxalate and the recovery of lithium as lithium phosphate. Bioleaching was conducted with a 5% w/v pulp density in CM at an initial pH of 3 over a 30-day incubation period. The bioleached solution contained 6,510 ppm of cobalt and 2,070 ppm of lithium. Cobalt was precipitated as cobalt oxalate by adding oxalic acid at varying stoichiometric ratios and subsequently calcined at 450°C to form cobalt oxide (Co_3O_4). Lithium was recovered as lithium phosphate by adjusting the solution pH to 12.7 and adding disodium hydrogen phosphate. The results demonstrated a 98.68% recovery of cobalt and effective precipitation of lithium phosphate (recovery of 95%). The purities of both compounds were >99.95%, highlighting the potential for efficient and sustainable metal recovery from bioleaching solutions.

6.2   Introduction

Bioleaching is a promising technique that can transform cobalt (Co) and lithium (Li) from degraded $LiCoO_2$ raw materials into ionic forms in solution. This process is particularly valuable for recycling spent lithium-ion batteries (LIBs), as it enables the recovery of these critical metals for reuse in various applications or for the synthesis of new batteries. However, to utilize the recovered metals effectively, additional processing steps are required.

Once the metals are solubilized in the bioleaching solution, various precipitation techniques are employed to recover them. For cobalt, one common method is the precipitation of cobalt hydroxide or cobalt oxalate. Cobalt hydroxide can be precipitated by adjusting the pH of the solution, while cobalt oxalate is formed by adding oxalic acid. These compounds are selected due to their low solubility in water, which enables efficient separation and recovery. Lithium recovery often involves precipitation as lithium phosphate (Li_3PO_4). This is achieved by adding a phosphate source to the bioleaching solution, resulting in the formation of insoluble Li_3PO_4. The choice of lithium phosphate is advantageous due to its stability and ease of handling.

This chapter presents a preliminary study on the recovery of Co and Li from bioleaching solutions. Specifically, it focuses on the precipitation of cobalt as cobalt oxalate and the recovery of lithium as lithium phosphate. These compounds are chosen due to their insolubility in water, which facilitates their separation and recovery in significant quantities. The findings of this study contribute to the development of efficient and sustainable methods for metal recovery from bioleaching solutions, supporting the circular economy and reducing the environmental impact of LIB disposal.

6.3   Research objective

The objective of this study is to investigate the recovery of cobalt (Co) and lithium (Li) from bioleaching solutions derived from degraded $LiCoO_2$ raw materials. Specifically, the study aims to:

1. Precipitate cobalt as cobalt oxalate from the bioleaching solution.
2. Recover lithium as lithium phosphate from the bioleaching solution.

6.4   Materials and methods

The bioleached solution containing cobalt and lithium was filtered from the previous section, which involved a 5% w/v pulp density in CM, an initial pH of 3, and a 30-day incubation period, to separate residuals and fungal cells. The chemical

composition of the bioleached solution was analyzed for cobalt (Co) and lithium (Li) using ICP-OES, yielding concentrations of 6,510 ppm and 2,070 ppm, respectively.

6.4.1 Cobalt recovery

To recover cobalt, the initial step involved precipitating cobalt as cobalt oxalate by adding oxalic acid ($C_2H_2O_4 \cdot 2H_2O$, AR grade, KEMAUS) at 1, 1.2, 1.5, and 2 times the stoichiometric amount. The reaction was maintained at 80°C for 1 hour, compared to room temperature. The resulting precipitate was filtered, dried at 95°C, and subsequently calcined at 450°C for 1 hour. The phase structure of the powder, both before and after calcination, was identified using X-ray diffraction (XRD), and its morphology was examined using field-emission scanning electron microscopy (FESEM). The purity of cobalt oxide was analyzed by inductively coupled plasma optical emission spectrometry (ICP-OES).

6.4.2 Lithium recovery

Following the precipitation of cobalt oxalate, the solution was prepared for lithium precipitation under optimal conditions. The pH of the solution was adjusted to 12.7 by adding a 2M sodium hydroxide solution. Disodium hydrogen phosphate anhydrous (Na_2HPO_4, AR grade, RCI Labscan) was used as the phosphate source. The precipitation process was conducted at ambient temperature. After the precipitation of lithium phosphate (Li_3PO_4), the product was characterized using X-ray diffraction (XRD) to determine the crystal structure, inductively coupled plasma optical emission spectrometry (ICP-OES) to assess purity, and field-emission scanning electron microscopy (FESEM) to examine morphology.

6.5 Results and Discussion

6.5.1 Cobalt recovery as Co_3O_4

When the solution obtained from bioleaching was precipitated to separate cobalt by adding oxalic acid powder in amounts of 1, 1.2, 1.5, and 2 times the stoichiometric ratio calculated from reaction 6.2 (Li et al., 2017), and maintaining the temperature at 80°C with stirring at 500 rpm, a light pink precipitate was observed

after 1 hour. The precipitate was filtered and analyzed using XRD, revealing that it was cobalt oxalate dihydrate, as shown in Figure 6.1. Analysis of the remaining solution after precipitation indicated that the cobalt concentration was reduced to 85.8 ppm, corresponding to a 98.68% recovery under the condition of adding oxalic acid at a 1:1 stoichiometric ratio. The cobalt concentrations remaining in the solution for 1.2, 1.5, and 2 times the stoichiometric ratio are described in Table 6.1. The percentage recovery of cobalt was calculated using the following formula:

$$\text{Percentage Recovery} = \left(\frac{C_{initial} - C_{final}}{C_{initial}}\right) \times 100 \qquad (6.1)$$

The concentration of lithium increased for all conditions due to the overall volume of the system decreasing as a result of water evaporation under 90°C conditions.

$$Co^{2+} + H_2C_2O_4 + 2H_2O \longrightarrow CoC_2O_4 \cdot 2H_2O \downarrow + 2H^+ \qquad (6.2)$$

Table 6.1 Concentrations of cobalt and lithium remain in the solution and the percentage recovery of cobalt.

Oxalic adding (times)	Co (ppm)	Li (ppm)	Recovery of Co (%)
Initial solution	6,510	2,070	-
1	85.8	2,420	98.68
1.2	66	2,390	98.99
1.5	59.5	2,480	99.09
2	19.4	2,500	99.70
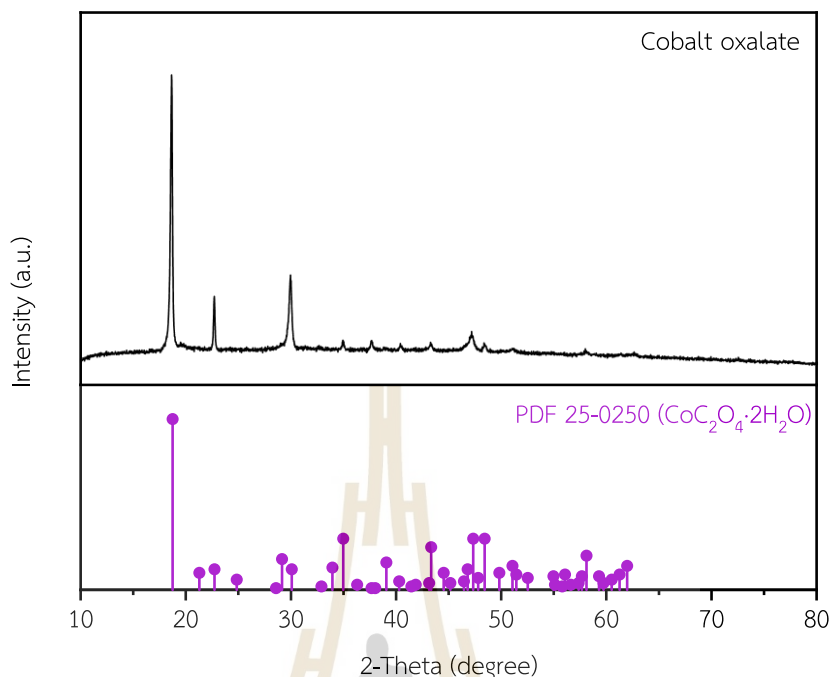
Figure 6.1   The X-ray diffraction pattern of cobalt oxalate dihydrate obtained from oxalate precipitation.

After calcining lithium oxalate at 450°C, which is a temperature that can convert cobalt oxalate to cobalt oxide under normal atmospheric conditions, it was found that, according to the research by Sun and Qiu (2012) the optimal temperature for converting cobalt oxalate to oxide using TGA techniques is up to 320°C (Sun & Qiu, 2012). This transformation occurs in steps as described by equations 6.3 and 6.4, and the reaction is complete at 320°C. This finding aligns with the research by Jin et al. (2015), which states that cobalt oxide forms after calcination at temperatures above 300°C (Jin et al., 2015). Therefore, the temperature at 450°C was chosen to ensure the complete conversion of cobalt oxalate to cobalt oxide. After calcining for 1 hour, XRD analysis revealed that the crystal structure was Co_3O_4, as shown in Figure 6.2.

At 150 °C-210 °C, $CoC_2O_4 \cdot 2H_2O = CoC_2O_4 + 2H_2O$ (6.3)
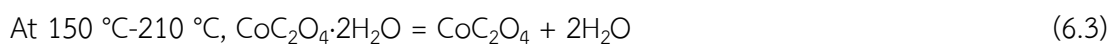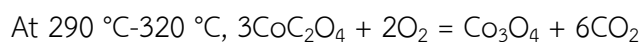
At 290 °C-320 °C, $3CoC_2O_4 + 2O_2 = Co_3O_4 + 6CO_2$ (6.4)
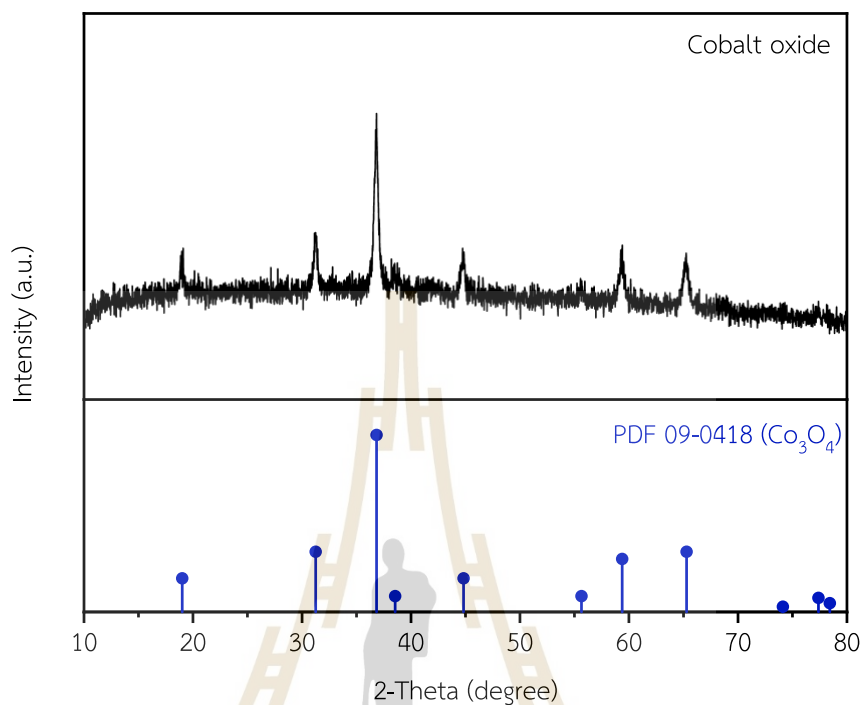
Figure 6.2   The X-ray diffraction pattern of cobalt oxide obtained through oxalate precipitation and subsequent calcination.

When the synthesized cobalt oxalate and cobalt oxide were examined for their morphological characteristics, it was found that the cobalt oxalate had a rod-like structure with a cross-sectional size of less than 100 nanometers. Compared to other research, this morphology is classified as cobalt oxalate nanorods, as shown in Figure 6.3 (Hou et al., 2020; Jin et al., 2015; Li et al., 2017).
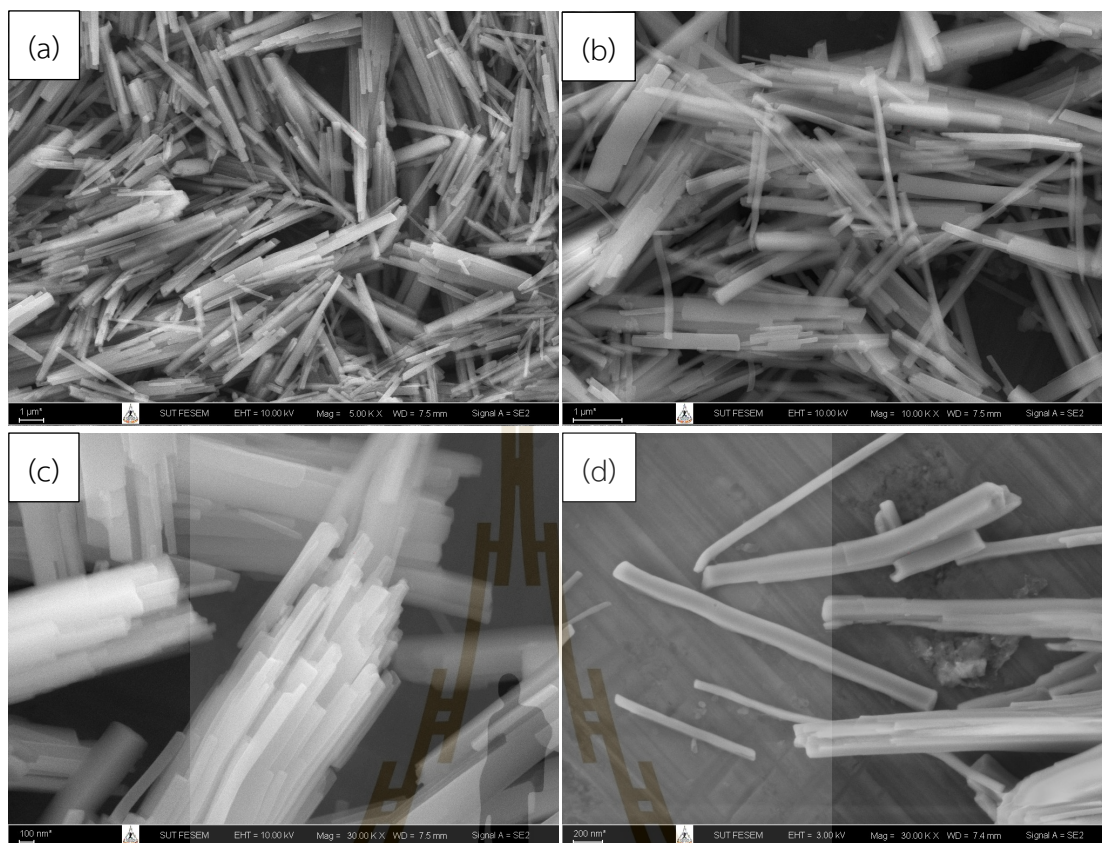
Figure 6.3   Morphology of cobalt oxalate dihydrate observed using FESEM at magnifications of 5,000x (a), 10,000x (b), and 30,000x (c, d).

Additional experiments on the precipitation of cobalt oxalate were conducted by reducing the synthesis temperature from 80°C to room temperature. Using an oxalic acid ratio of 1:1 with the same reaction time of 1 hour, it was found that precipitation at room temperature resulted in cobalt oxalate nanorods with shorter lengths, as shown in Figure 6.4.
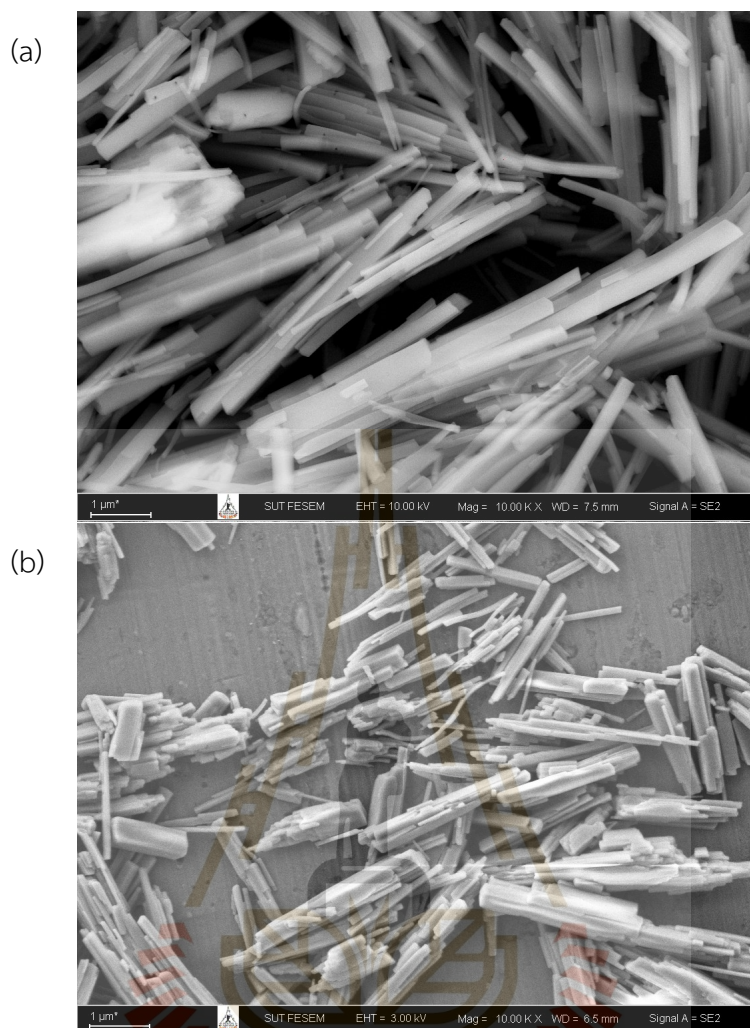
Figure 6.4 Comparison of cobalt oxalate dihydrate precipitated at 80°C (a) and at
room temperature (b), observed under FESEM at a magnification of
10,000x.

FESEM images of cobalt oxide (Co_3O_4) obtained from calcining cobalt oxalate nanorods at 450°C show rods formed by the alignment of cobalt oxide grains. These grains exhibit a porous structure due to decomposition and the release of carbon dioxide gas, as described in equation 6.3. This morphological structure, shown in Figure 6.5, is referred to as a mesoporous nanorod structure. The measured particle size of cobalt oxide ranges from 15 to 50 nanometers. Such characteristics make it suitable for applications in lithium-ion batteries, supercapacitors, electrochemical

sensors, and energy storage devices (Hou et al., 2020; Jin et al., 2015; Li et al., 2017). ICP-OES analyzed the purity of more than 99.95% for the Co_3O_4 product.
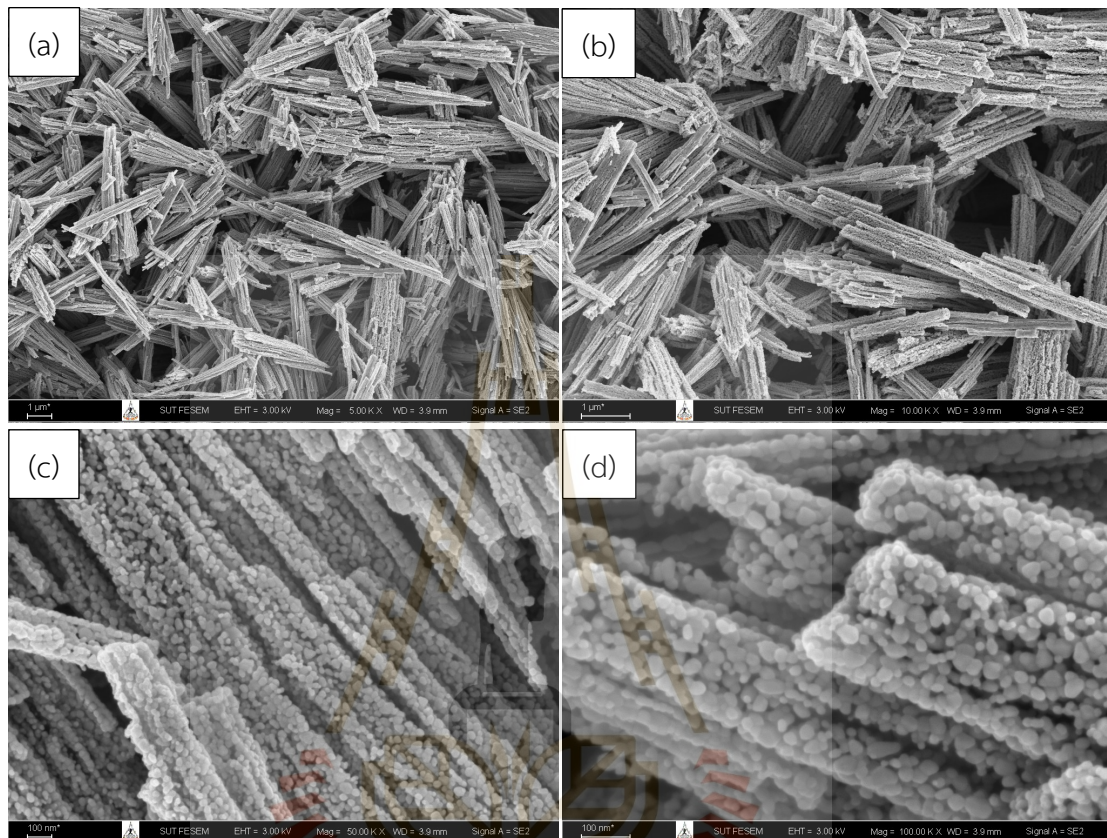
Figure 6.5   Morphology of cobalt oxide observed using FESEM at magnifications of 5,000x (a), 10,000x (b), 50,000x (c), and 100,000x (d).

6.5.2 Lithium recovery as Li_3PO_4

The solution obtained after the precipitation of cobalt contains only lithium, which can be recovered by adjusting the pH to the range of 6-14 in a Li-P-H_2O system, causing lithium to precipitate as lithium phosphate (Zhao et al., 2020). However, according to the research by Xiao and Zeng (2018), controlling the solution to a pH of 12.7 and a phosphorus concentration of 0.1 M results in the minimum solubility of lithium in the solution (remaining at only 0.001 M)(Xiao & Zeng, 2018). Therefore, the researcher chose these conditions for the precipitation of lithium phosphate. The precipitating agent was added after adjusting the solution pH to 12.7. After the precipitation of lithium phosphate, the precipitate was analyzed using XRD, as shown in Figure 6.6, to confirm the compound type. FESEM examination revealed that the lithium phosphate had a double pyramid prism structure with a hollow characteristic, as shown in Figure 6.7. The purity of more than 99.95% was analyzed using ICP-OES.
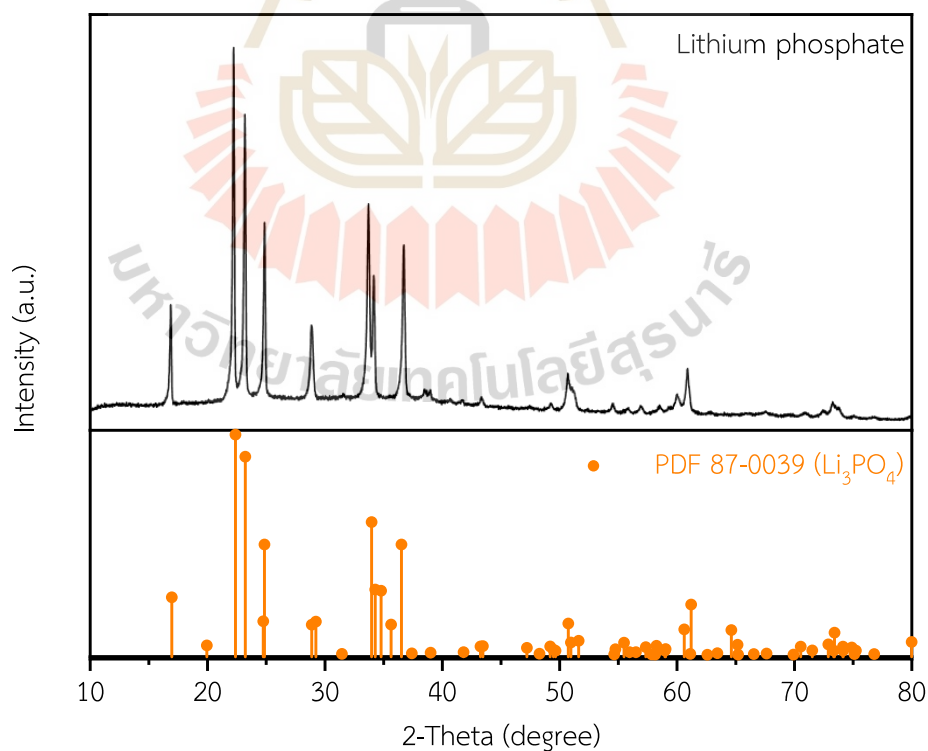
Figure 6.6   The X-ray diffraction pattern of lithium phosphate product.
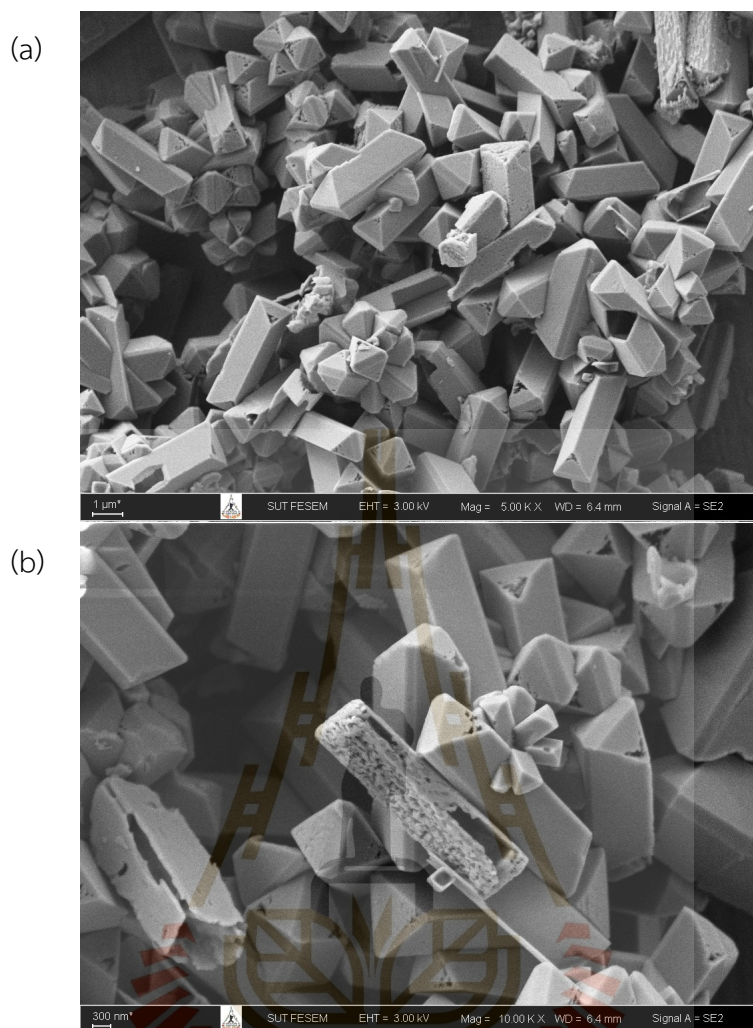
Figure 6.7   Morphology of lithium phosphate observed using FESEM at magnifications
of 5,000x (a) and 10,000x (b).

6.6   Conclusion

This study successfully demonstrated the recovery of cobalt and lithium from bioleaching solutions of degraded $LiCoO_2$ raw materials. The precipitation of cobalt as cobalt oxalate and its subsequent calcination to cobalt oxide, along with the recovery of lithium as lithium phosphate, were achieved with high efficiency. The findings suggest that bioleaching, followed by appropriate precipitation techniques, can be an appropriate method for recycling critical metals from spent lithium-ion batteries (LIBs). This approach supports the circular economy by enabling the reuse of valuable

metals and reducing the environmental impact of LIB disposal. Future research should focus on optimizing the bioleaching and precipitation processes to enhance recovery efficiencies further and explore the scalability of these methods for industrial applications.

6.7   References

Hou, C., Wang, B., Murugadoss, V., Vupputuri, S., Chao, Y., Guo, Z., Wang, C., & Du, W. (2020). Recent Advances in Co_3O_4 as Anode Materials for High-Performance Lithium-Ion Batteries. *Engineered Science*, *Volume 11 (September 2020)*(5), 19–30.

Jin, L.-N., Wang, J.-G., Qian, X.-Y., Xia, D., & Dong, M.-D. (2015). Catalytic Activity of Co3O4 Nanomaterials with Different Morphologies for the Thermal Decomposition of Ammonium Perchlorate. *Journal of Nanomaterials*, *2015*(1), 854310. https://doi.org/10.1155/2015/854310

Li, Y., Wu, H., Wu, Y., & Li, Q. (2017). Facile synthesis of mesoporous Co_3O_4 nanowires for application in supercapacitors. *Journal of Materials Science: Materials in Electronics*, *28*(22), 16826–16835. https://doi.org/10.1007/s10854-017-7598-7

Sun, L., & Qiu, K. (2012). Organic oxalate as leachant and precipitant for the recovery of valuable metals from spent lithium-ion batteries. *Waste Management*, *32*(8), 1575–1582. https://doi.org/10.1016/j.wasman.2012.03.027

Swain, B. (2017). Recovery and recycling of lithium: A review. *Separation and Purification Technology*, *172*, 388–403. https://doi.org/10.1016/j.seppur.2016.08.031

Xiao, C., & Zeng, L. (2018). Thermodynamic study on the recovery of lithium using the phosphate precipitation method. *Hydrometallurgy*, *178*, 283–286. https://doi.org/10.1016/j.hydromet.2018.05.001

Zhao, C., He, M., Cao, H., Zheng, X., Gao, W., Sun, Y., Zhao, H., Liu, D., Zhang, Y., & Sun, Z. (2020). Investigation of solution chemistry to enable efficient lithium recovery from low-concentration lithium-containing wastewater. *Frontiers of Chemical Science and Engineering, 14*(4), 639–650. https://doi.org/10.1007/s11705-019-1806-3

CHAPTER VII

CONCLUSION AND RECOMMENDATIONS

7.1 Conclusion

This dissertation successfully developed a novel bio-hydrometallurgical process for recycling lithium and cobalt from spent lithium-ion batteries using fungal bioleaching. The research identified two effective fungal strains, *Aspergillus* sp. JMET 15 and *Penicillium* sp. JMET 24, which demonstrated exceptional growth and tolerance in high lithium and cobalt environments. These strains significantly enhanced the bioleaching efficiency of lithium-cobalt-oxide (LCO) cathodes, highlighting their potential for sustainable and environmentally friendly battery recycling.

The preliminary studies revealed that *Penicillium* sp. JMET 24 exhibited superior leaching performance in sucrose medium, achieving the highest concentrations of cobalt and lithium in the leached solution. The optimization of the bioleaching process further improved metal recovery, with an initial pH of 3 and a composite medium yielding the best results. Increasing the pulp density to 5% enhanced metal concentrations, although with a slight decrease in efficiency, underscores the importance of medium optimization and parameter control.

The recovery of cobalt and lithium from the bioleached solution was achieved with high efficiency through selective precipitation techniques. Cobalt was recovered as cobalt oxide (Co_3O_4) mesoporous nanoparticles, while lithium was precipitated as lithium phosphate (Li_3PO_4). These findings demonstrate the viability of bioleaching followed by precipitation as a method for recycling critical metals from spent lithium-ion batteries, supporting the circular economy by enabling the reuse of valuable metals and reducing the environmental impact of battery disposal.

7.2   Recommendations

Future research should focus on scaling up these findings and exploring the economic feasibility of industrial applications. Furthermore, optimizing the bioleaching and precipitation processes could further enhance recovery efficiencies, making this approach a competitive alternative to conventional recycling methods. The recommendations for process development and future research are as follows:

1.   **Optimization of Fungal Strains**: Further research should focus on optimizing the growth conditions and genetic modification of *Aspergillus* sp. JMET 15 and *Penicillium* sp. JMET 24 to enhance their bioleaching efficiency. Investigating the metabolic pathways and enzyme production involved in metal leaching could provide insights into improving their performance.

2.   **Medium Composition and Pulp Density**: The composition of the nutrient broth and pulp density are critical factors influencing bioleaching efficiency. Future studies should explore alternative carbon sources and nutrient compositions to maximize fungal growth and metal recovery. Additionally, experiments with varying pulp densities could identify the optimal conditions for industrial-scale applications.

3.   **Precipitation Techniques**: The recovery of cobalt and lithium through precipitation techniques showed promising results. Future research should aim to refine these methods to increase the purity and yield of the recovered metals. Exploring different precipitants and optimizing the precipitation conditions could further enhance the efficiency of metal recovery.

4.   **Scale-Up and Economic Feasibility**: To transition from laboratory-scale experiments to industrial applications, it is essential to conduct pilot-scale studies to evaluate the scalability and economic feasibility of the bio-hydrometallurgical process. Cost-benefit analyses and life cycle assessments could provide valuable information for commercializing the technology.

5.   **Environmental Impact Assessment**: Assessing the environmental impact of the bioleaching process is crucial for ensuring its sustainability. Future research should focus on evaluating the ecological footprint, energy consumption, and waste generation associated with the process. Implementing measures to minimize environmental impact and enhance sustainability should be a priority.

6.   **Integration with Existing Recycling Methods**: Investigating the integration of bioleaching with conventional recycling methods, such as pyro- and hydrometallurgical processes, could offer a hybrid approach that leverages the strengths of both techniques. This could lead to more efficient and comprehensive recycling solutions for lithium-ion batteries.

7.   **Exploration of Other Metal Recovery**: While this research focused on lithium and cobalt, future studies could explore the recovery of other valuable metals from spent lithium-ion batteries, such as nickel and manganese. Expanding the scope of bioleaching to include multiple metals could increase the overall efficiency and economic viability of the process.

8.   **Long-Term Stability and Reusability of Fungal Strains**: Investigating the long-term stability and reusability of the fungal strains in bioleaching processes could provide insights into their practical application in continuous industrial operations. Studies on the regeneration and reuse of fungal biomass could enhance the sustainability and cost-effectiveness of the process.

APPENDIX

LIST OF PUBLICATIONS
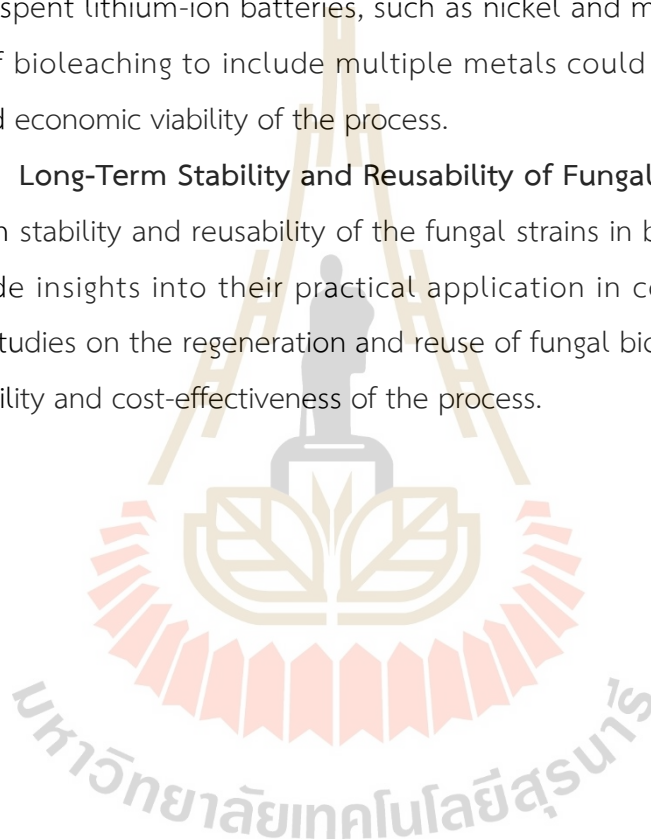
LIST OF PUBLICATIONS

1. International Publications

Chandakhiaw, T., Teaumroong, N., Piromyou, P., Songwattana, P., Tanthanuch, W., Tancharakorn, S., & Khumkoa, S. (2024). Efficiency of *Penicillium* sp. And *Aspergillus* sp. For bioleaching lithium cobalt oxide from battery wastes in potato dextrose broth and sucrose medium. *Results in Engineering*, *24*, 103170. https://doi.org/10.1016/j.rineng.2024.103170

2. Conference paper

Chandakhiaw, T., Longbutsri, C., Wongnaree, N., Somla, S., Mahiwan, N., Patcharawit, T., & Khumkoa, S. (2023). The Production of Hematite Powder from Spent Pickling Hydrochloric Acid. *Materials Science Forum*, *1099*, 181–187. https://doi.org/10.4028/p-sjK581

Wongnaree, N., Sriklang, L., Kansomket, C., **Chandakhiaw, T.**, Patcharawit, T., & Khumkoa, S. (2023). Precipitation of Lithium Phosphate from Cathode Materials of Spent Lithium-Ion Battery by Hydrometallurgy Process. *Materials Science Forum*, *1099*, 175–180. https://doi.org/10.4028/p-arh30R

Kansomket, C., **Chandakhiaw, T.**, Ma-ud, N., Yingnakorn, T., Patcharawit, T., & Khumkoa, S. (2020). Study on Leaching of Molybdenum from a Spent HDS Catalyst. Materials Science Forum, 1009, 143–148. International Conference on Materials Design and Applications / 4th International Conference on Material Engineering and Manufacturing. https://doi.org/10.4028/www.scientific.net/MSF.1009.143

Laungsakulthai, K., **Chandakhiaw, T.**, Wongnaree, N., Thampiriyanon, J., Kritsarikun, W., & Khumkoa, S. (2020). Smelting Reduction of Spent Catalyst Containing Nickel: A Preliminary Study. *Materials Science Forum*, *1009*, 162–167. International Conference on Materials Design and Applications / 4th

International Conference on Material Engineering and Manufacturing.
https://doi.org/10.4028/www.scientific.net/MSF.1009.162

3. Conference Abstract

Longbutsri, C., **Chandakhiaw, T.**, Kansomket, K., Srilang, L., Patcharawit, T., and
Khumkoa, K. (2024). Feasibility Study on Hematite and Strontium Compound
Extraction from Grinding Sludge Generated from Strontium Ferrite Magnet
Manufacturing Factory. 2024 ASEAN Iron and Steel Forum: Sustainable Steel
and Green Construction, Bangkok, 18-21 November 2024

Chandakhiaw, T., Longbutsri, C., Ma-Ud, N., Somla, S., Patcharawit, T., Khumkoa, S.
(2023). A Feasibility Study on Applying *Penicillium* Sp. for Leaching of Lithium
and Cobalt from Lithium-Cobalt Oxide Powder of deteriorated Smartphone
Battery. The 14th Thailand Metallurgy Conference. Chonburi, Thailand.

Chandakhiaw, T., Ma-Ud, N., Laokhen, P., Kansomket, C., Khamseetha, P., Hathong,
P., Khumkoa, S. (2019). Recovery of metals from dry shot blast waste
generated in the stainless-steel production process. The 2nd Global Summit
on Recycling and Waste Management. Tokyo, Japan.

4. Award

The winner of the oral presentation in the Metal Processing session at the 14th Thailand Metallurgy Conference at Chonburi, Thailand, in the topic of "A Feasibility Study on Applying *Penicillium* Sp. for Leaching of Lithium and Cobalt from Lithium-Cobalt Oxide Powder of deteriorated Smartphone Battery".

The most popular SEM image in the 39th International Conference of the Microscopy Society of Thailand (MST39[th]), Thailand, Picture title "Phosphate Flower"

Efficiency of *Penicillium* sp. and *Aspergillus* sp. for bioleaching lithium cobalt oxide from battery wastes in potato dextrose broth and sucrose medium

Thanapon Chandakhiaw [a], Neung Teaumroong [b], Pongdet Piromyou [b], Pongpan Songwattana [b], Waraporn Tanthanuch [c], Somchai Tancharakorn [c], Sakhob Khumkoa [a,*]

[a] School of Metallurgical Engineering, Institute of Engineering, Suranaree University of Technology, Nakhon Ratchasima, 30000, Thailand
[b] School of Biotechnology, Institute of Agricultural Technology, Suranaree University of Technology, Nakhon Ratchasima, 30000, Thailand
[c] Synchrotron Light Research Institute (Public Organization), Muang, Nakhon Ratchasima, 30000, Thailand

ARTICLE INFO

ABSTRACT

Lithium-ion batteries, a primary power source, generate electronic hazardous waste at the end of their lifespan, which is a richer source of highly concentrated metals such as cobalt and lithium than those in natural resources. The waste is a potential renewable resource for the extraction of metals. Bioleaching, a process utilizing microbial activity, was used in this study to investigate the cobalt and lithium leaching efficiency from battery wastes. Two fungal strains, *Aspergillus* sp. strain JMET 15 and *Penicillium* sp. strain JMET 24 were used with different organic carbon sources (sucrose medium and potato dextrose broth) at 1 % pulp density. The sucrose medium derived a higher acid quantity and leached higher concentration of cobalt and lithium than in potato dextrose broth. Leaching efficiency by JMET 24 was higher than JMET 15. Cobalt (32.57 % and 27.19 %) and lithium (65.07 % and 40.58 %) were bioleached by JMET 24 and JMET 15, respectively, after 30 d cultivation in the sucrose medium. Lower pulp density was conducted to achieved higher leaching efficiency by JMET24, cobalt (77.87 % and 74.5 %) and lithium (99.88 % and 78.4 %) were bioleached at 0.1 % and 0.5 % pulp density, respectively. Cobalt oxide (Co_3O_4) was the product of the one-step recovery (leaching and precipitation) process. Cobalt was transformed from lithium cobalt oxide to cobalt phosphate-oxalate by JMET 24 in the sucrose medium. Thus, the potential of bioleaching as an effective method for recovering valuable metals from lithium-ion battery waste is demonstrated, presenting a promising approach for both waste management and resource recovery.

1. Introduction

Technology is continually progressing to enhance human living standards in the globalization age. Numerous wireless electronic gadgets such as communication devices, tablets, smartwatches, medical equipment, military gear, and electric automobiles have been developed, which are powered using batteries. Lithium-ion batteries (LIBs) have been commercially produced and brought to the market by Sony Energytec since 1991 and are the main power source for present wireless electronic devices owing to their long cycle life, low self-discharge rate, the absence of memory effect, high current density, and stability [1].

The International Energy Agency reported that LIB manufacturing would increase from 1.57 TWh in 2022 to 6.79 TWh in 2030 [2]. The lifecycle of a LIB is in the range of 500–30,000 cycles depending on electrode materials: 500–1500 cycles for a lithium cobalt oxide ($LiCoO_2$, LCO) cathode with graphite (C) anode [3,4] 1000–7000 cycles for a nickel manganese cobalt oxide cathode and C anode, and 30,000 cycles for a LCO cathode with lithium titanate oxide (NTO) anode [5]. Thus, the lifespan of portable devices is ~2–3 y, while the lifespan of electric vehicles is ~10 y, generating waste after completing their lifespan [6–9]. The improper management of battery waste can severely affect the environment and human health, causing the leakage of heavy metals

and organic compounds [10]. Battery waste is classified as a renewable resource as it is enriched with valuable metals that can be recovered. LIBs contain 30.8%–42.9 % cobalt (Co), 13 % copper (Cu), 6.5%–10 % aluminum (Al), and 2.45%–8.88 % lithium (Li) based on the LCO cathode composition [11]. Copper–cobalt oxide ore from the Democratic Republic of Congo, the world's largest cobalt producer, contains 11.58 % Co [12,13] and the high-grade spodumene Li-rich mineral contains 3.72 % Li [14]. Therefore, appropriate management of LIB recycling addresses environmental issues and alleviates concerns regarding insufficient ore resources.

The dominant methods to recover valuable metals from battery waste are pyrometallurgy, hydrometallurgy, biometallurgy, and direct recycling. Recycling technologies use pyrometallurgy and hydrometallurgy on an industrial scale. Pyrometallurgy has high capacity and simple operation, while hydrometallurgy enables the recovery of highly pure products in high yields [3,10,15–18]. However, the pyrometallurgical process consumes high energy and emits toxic gases, while the hydrometallurgical process generates secondary waste such as wastewater and acidic fumes [10].

Biometallurgy, a field combining metallurgy and biotechnology, encompasses the interaction between microorganisms and metals or metal compounds for extracting or reclaiming metals from sources such as ores and waste materials [19,20]. This environmentally friendly process has low operating costs and energy requirements [7,21]. Bioleaching, a process for leaching metals by microorganisms (bacteria and fungi) with the ability to reduce and oxidize the metals, produce and secrete acids or enzymes, is used for the biometallurgical recycling of Li and Co from battery waste [21–25].

Numerous bioleaching bacteria (chemolithoautotrophic acidophilic sulfur and/or iron-oxidizing bacteria or archaea) [26] and fungi (filamentous fungi) have been reported [27,28]. However, fungi have several advantages over bacteria. Filamentous fungi have strong adaptability, grow in an environment with high metal concentrations ranging from acidic to basic conditions, and a short lag phase [28–30]. They can leach alkali substrates such as metal oxide compound waste. *Aspergillus* and *Penicillium* are two important genera of filamentous fungi in biotechnology and medicine [31,32]. Biswal et al. [33] reported that the leaching efficiency *Aspergillus niger (A. niger)* was higher than that of bacteria (*Acidithiobacillus thiooxidans*) and acid leaching.

The fungal bioleaching of LIB waste has focused on the leaching efficiency and recovery of Co and Li from leached solutions with *A. niger* [29,33–35], while *Penicillium* is another frequently used fungus primarily utilized to leach waste such as electronic waste, spent catalysts, contaminated soil, slag, mine tailing, and low-grade ores [23,28,36,37]. The bioleaching of battery waste using *Penicillium* has not been extensively explored. Studies by Biswal and colleagues have reported the recovery of metal compounds from bioleaching solutions via sequential precipitation methods. Cobalt was precipitated as compounds such as cobalt sulfide, cobalt hydroxide, or cobalt oxalate by adding sodium sulfide, sodium hydroxide, or sodium oxalate, respectively, as chemical precipitants [33]. Co and Li recovery after bioleaching process was reported but the one-step recovery of Co and Li in bioleaching process has not been explored. The objective of this study was to investigate the mechanism and efficiency of *Aspergillus* sp. strain JMET 15 and *Penicillium* sp. strain JMET 24 for leaching Co and Li from spent LIB waste using media containing different carbon sources [potato dextrose broth (PDB) and sucrose medium (SM)]. Moreover, Co was leached and recovered as Co_3O_4 in one-step.

2. Material and methods

2.1. Preparation of spent LIB powder

The battery waste used in this study was LCO cathode-based smartphone batteries, which were collected from mobile repair shops in Thailand. The batteries were discharged by immersing in a 5 % w/v

sodium chloride (NaCl) solution for 24 h [38]. LCO was manually dismantled after drying to separate the cathode. The cathode powder containing deteriorated LCO adhered to Al foil (as the cathode) with polyvinylidene fluoride (PVDF). The thermal analysis of PVDF revealed complete degradation above 500 °C [39–41]. Hence, the electrode was heated at 525 °C in a muffle furnace for 1 h to destroy PVDF interlayers before collecting the cathode powder. The average particle size, d_{10}, d_{50}, and d_{90} of the cathode powder were 15.25, 8.55, 13.78 and 22.9 μm, analyzed using a laser diffraction particle size analyzer (Horiba, LA-950V2). The chemical composition of the raw material was analyzed via inductively coupled plasma optical emission spectrometry (ICP-OES) (PerkinElmer, Optima 8000), and phase identification was conducted via X-ray diffraction (XRD) (Bruker, D2 Phaser).

2.2. Fungal isolation, screening, and identification

Soil samples from various metal industry yards in Thailand were collected. Each soil sample (1 g) was mixed with 10-mL distilled water. 0.1 mL of aliquots were spread on a 3.9 % (w/v) potato dextrose agar (PDA) plate. Fungal colonies were isolated into pure cultures on PDA plates. Pure cultures were subcultured every 14 d on PDA plates containing 0.3%–1% (increment step of 0.3 %, 0.6 %, and 1 %) cathode powder solutions in the screening step. Two fungi that grew well on PDA plates containing 1 % cathode powder solution were selected for species identification through genomic deoxyribonucleic acid (DNA) sequencing. Fungal genomic DNA was directly extracted in 1.5-mL Eppendorf tubes following the procedure reported by Cenis [42]. Ten μL of 2-mg mL^{-1} RNase A was added into the DNA solution and incubated for 2 h at 37 °C to remove ribonucleic acid (RNA). The 18s rRNA small subunit was amplified using the polymerase chain reaction (PCR) using primers NS1 (5′-GTAGTCATATGCTTGTCTC-3′) and NS8 (5′-TCCGCAGGTTCACCTACGGA-3′) [43]. Each PCR mixture contained 1-μL 10 × buffer, 0.2 μL of 10-mM dNTPs, 0.2 μL of 10-μM primer, 0.05-μL Taq DNA polymerase (DreamTaq, Thermo Scientific™), 1-μL DNA template solution, and ultrapure sterile water to make a total volume of 10 μL. The PCR was performed under the mentioned conditions: 94 °C for 4 min, 30 cycles at 94 °C for 1 min, 55 °C for 2 min, 72 °C for 1.5 min, and a final extension at 72 °C for 10 min [44]. The PCR products were subjected to sequencing using the barcode-tagged sequencing method (BTSeq™). The sequences were analyzed via the Basic Local Alignment Search Tool from the National Center for Biotechnology Information (NCBI) website. 18s rRNA sequences have been submitted to NCBI GenBank under accession nos. MZ892606 and MZ892608 for *Aspergillus* sp. JMET 15 and *Penicillium* sp. JMET 24, respectively.

2.3. Bioleaching experiment

The spores of JMET 15 and JMET 24 were obtained by culturing them on PDA plates for 7 d at 30 °C followed by washing the plate surfaces with sterile deionized water to collect the spores. The spore concentration was adjusted to ~10⁶ spores mL^{-1} and verified using a light microscope and Neubauer counting chamber.

The bioleaching experiments were conducted in 250-mL Erlenmeyer flasks containing 100-mL PDB (HiMedia) or SM. The SM comprised 100-g L^{-1} sucrose, 1.5-g L^{-1} NaNO₃, 0.5-g L^{-1} KH₂PO₄, 0.025-g L^{-1} MgSO₄.7H₂O, 0.025-g L^{-1} KCl, and 1.6 g L^{-1} yeast extract, and the pH was adjusted to 5.5. The media were sterilized in an autoclave at 121 °C for 15 min. Either 1-mL fungal spore suspension or 1-g sterile cathode powder (1 % pulp density) was added to the respective defined conditions. The bioleaching experiments were performed for 30 d at 150 rpm and 25 °C in an orbital shaking incubator with sampling conducted on 0, 3, 5, 7, 9, 11, 15, 20, 25, and 30 d. The experiments were performed thrice.

Samples were named based on their contents and experimental conditions as mentioned: (i) test sample (T) conditions comprising the

cathode powder and fungal spore suspension, (ii) cathode sterile (CS) was a negative control where the cathode powder was present exclusively without any fungal spore suspension, and (iii) non-cathode (CN) powder as a positive fungal growth control where the spore suspension was present exclusively without any cathode powder.

2.4. Varying of pulp density bioleaching

The best bioleaching condition (fungus strain, and media) from the previous part was selected to refine the pulp density to recover pure Co_3O_4. Pulp densities were decreased to 0.1 %, and 0.5 % if the leaching efficiency at 1 % pulp density was incompleted. The other experimental details were controlled in the same way as the previous experiment.

2.5. Analytical techniques

The content of each flask was filtered through the Whatman 42 filter paper at intervals of 0, 3, 5, 7, 9, 11, 15, 20, 25, and 30 d. The solid residue comprising residual material and fungal cells on the filter paper was dried at 80 °C using a hot air oven for 24 h, followed by incineration at 500 °C in a muffle furnace for 4 h. The difference in weights between the residue before and after incineration was determined as biomass. The raw materials and residue were analyzed via XRD equipped with Cu–Kα radiation (Bruker, D2 Phaser). The pH value was measured using a pH meter (Metler Toledo, Seven Compact S220-KIT). The filtrate was passed through a 0.45-μm syringe filter for further analysis. Li and Co concentrations in the leached solution were analyzed via ICP-OES.

The amount of sugar and organic acid were analyzed via high-performance liquid chromatography (HPLC) (Agilent Technologies, 1260) equipped with a refractive index detector and a ZORBAX NH_2 column (4.6 mm × 250 mm, 5 μm). Sucrose, glucose, and fructose were analyzed at 35 °C. A 10-μL injection was used with a mobile phase comprising a 75:25 v/v acetonitrile and HPLC water isocratic solvent system at a flow rate of 1 mL min^{-1}. Organic acids (oxalic acid, acetic acid, and citric acid) were identified via HPLC equipped with an ultra-violet–visible (UV–vis) diode array detector at 210 nm and a ZORBAX SB-C18 column (4.6 mm × 250 mm, 3.5 μm). The operation was performed at 30 °C using a 20-μL injection and a 5-mM sulfuric acid isocratic mobile phase at a flow rate of 0.5 mL min^{-1}.

The chemical structures of the cathode powder and leaching product were elucidated via X-ray absorption spectroscopy (XAS). Co K-edge spectra were recorded at the SUT-NANOTEC-SLRI XAS beamline (BL5.2) at the Synchrotron Light Research Institute (SLRI), Thailand. Energy calibration in a transmission mode was conducted utilizing Co-foil. The energy was scanned using a Ge (220) double crystal monochromator over a range of -20–80 eV relative to E_0 set at 7709 eV with a photon energy increment of 0.2 eV. The extended X-ray absorption fine structure (EXAFS) measurements were performed by scanning photon energy from 150, to 20, and 30 k to 13 k of E_0 at 7709 eV, using photon energy increments of 5, 0.3, and 0.05 keV, and temporal steps of 1, 2, and 3 s, respectively. Samples were measured for up to 3 scans in a fluorescent mode using a 4-element Si-drift detector. The collected data were preprocessed, normalized, and EXAFS fitted using the IFEFFIT program, which integrates Athena and Artemis [45].

3. Results and discussion

3.1. Raw material characterization

The deteriorated smartphone batteries were manually dismantled, and the amount of cathode powder was calculated to be an average of 40.41 wt% of the total battery weight. The percentage amounts (by weight) of other components are shown in Fig. 1. The scraped cathode powder analyzed via XRD was identified as LCO (Fig. 2), consistent with the chemical composition analysis via ICP-OES with Co and Li compositions of 58.8 % and 6.9 % by weight, respectively. Other elements in
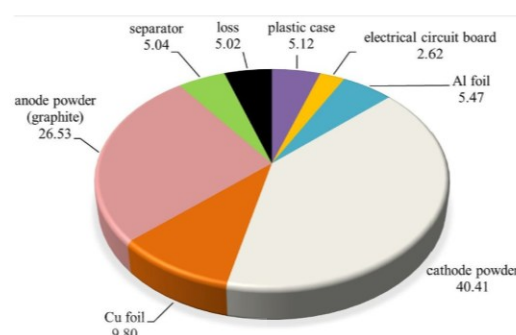
Fig. 1. Average weight compositions of smartphone battery waste (wt.%).
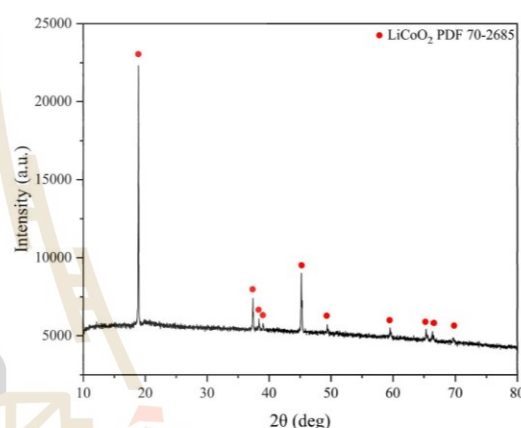
Fig. 2. X-ray diffraction pattern of raw materials ($LiCoO_2$) in the cathode powder.

battery electrodes such as Ni, Mn, and Fe were not detected.

3.2. Fungal growth in sucrose medium

Fungi primarily rely on organic carbon sources for growth as chemoorganoheterotrophs. Sucrose (100 g L^{-1}) was used as the main organic carbon source in the SM, and the initial sucrose concentration in the SM quantified via HPLC was 100,000 ppm. Sucrose levels drastically decrease after 3-d incubation with JMET 15 and JMET 24 strains, which continues to decrease below the detection limit after 11-d incubation (<100 ppm), while fructose and glucose levels increase owing to sucrose decomposition. The concentration of glucose decreases between days 3 and 5, while the concentration of fructose remains relatively constant from the middle to the later stages of incubation (Fig. 3a and b).

The sugar consumption results are consistent with the biomass and pH results. Biomass increases on day 3 of the incubation under the non-cathode powder condition (CN) while the pH decreases owing to organic acid secretion by the fungus. The growth rate of JMET 15 in the T condition slightly increases during the initial stage (7 d) and grows continuously on Day 9 (Fig. 3, c). However, JMET 24 shows no lag phase (Fig. 3, d). The biomass of both strains in the T condition is lower than in the CN condition as the metals in the cathode powder suppress the growth rate of the fungus.
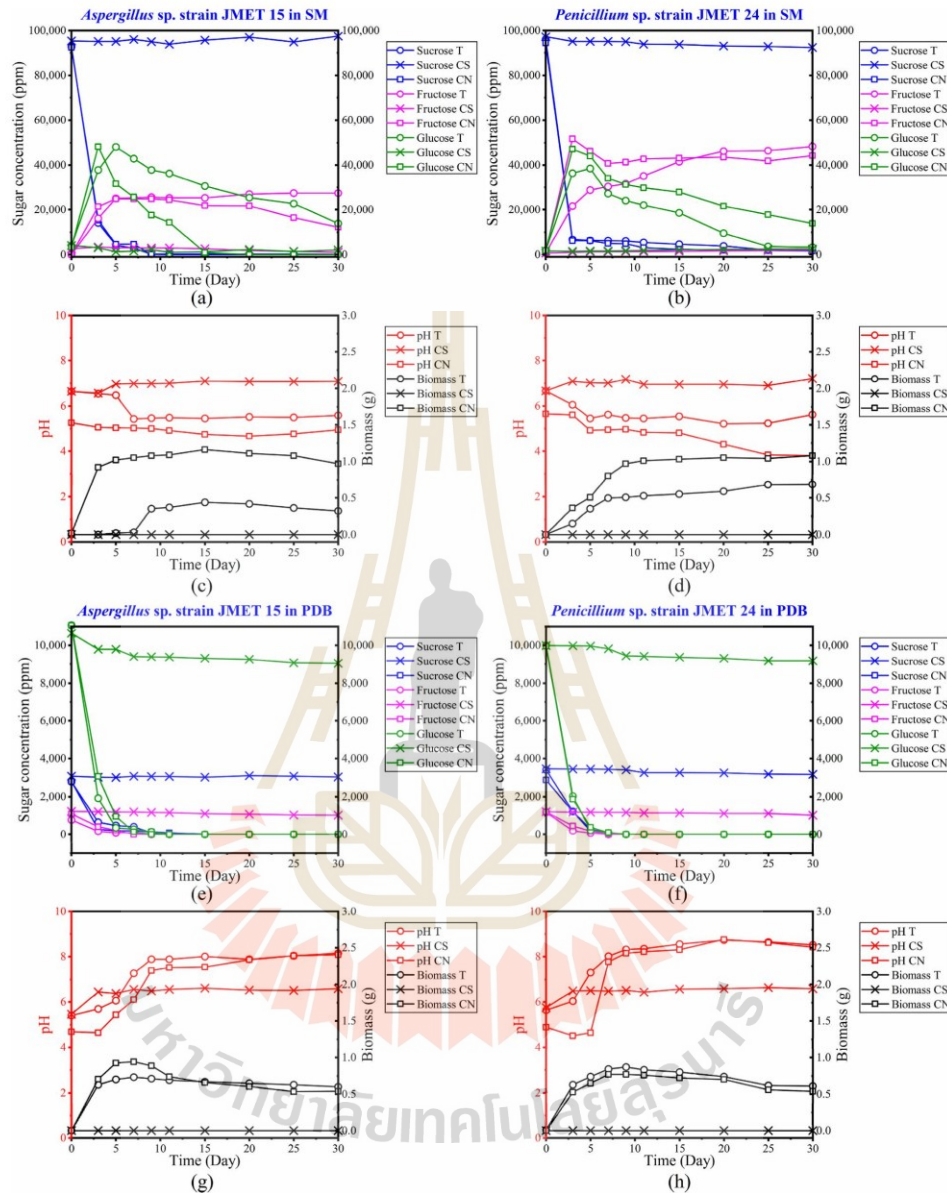
Fig. 3. Sugar consumption, pH change, and biomass in 30 d by the two fungi in the SM and PDB: sugar consumption by (a) *Aspergillus* sp. JMET 15 and (b) *Penicillium* sp. JMET 24 in the SM. pH change and the biomass of (c) *Aspergillus* sp. JMET 15 and (d) *Penicillium* sp. JMET 24 in the SM. Sugar consumption by (e) *Aspergillus* sp. JMET 15 and (f) *Penicillium* sp. JMET 24 in the PDB. pH change and biomass of (g) *Aspergillus* sp. JMET 15 and (h) *Penicillium* sp. JMET 24 in the PDB.

The acidity of the medium changes with pH increasing from 5.5 to >7 in the sterile condition (CS), as LCO is an alkali oxide. The flasks containing JMET 15 and JMET 24 strains have a low pH. The pH of the medium in the T condition is intermediate between CS and CN, which is affected by alkali oxide in the cathode and organic acid secretion from the fungus. Oxalic acid (6594 ppm) and citric acid (3484 ppm) were detected with JMET 15 while oxalic acid (5917 ppm) and citric acid (1918 ppm) with JMET 24 detected in the T condition are shown in Fig. 4. These organic acids contribute to the observed reduction in pH and play a key role in facilitating metal leaching from the cathode powder by lowering the medium pH and enhancing metal solubility.
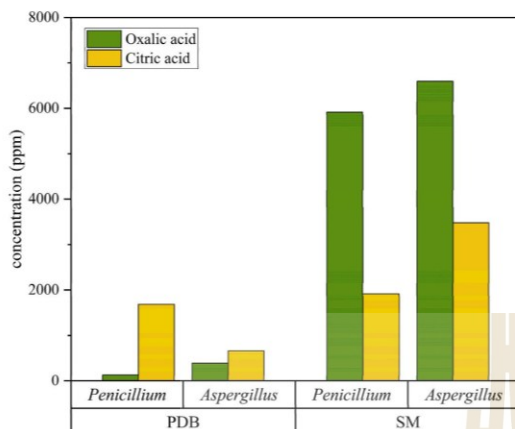
Fig. 4. Oxalic and citric acid secretion (ppm) by *Aspergillus* sp. JMET 15 and *Penicillium* sp. JMET 24 in the SM or PDB with 1 % w/v cathode powder after 30 d incubated.

3.3. Fungal growth in potato dextrose broth

Glucose is the primary organic carbon source for the PDB with concentrations >10,000 ppm, while ~3000-ppm sucrose and ~1000-ppm fructose were detected in the initial broth. Sugar was rapidly consumed within 7–9 d of incubation in T and CN conditions, whereas the sugar level remained constant in the CS condition (Fig. 3e and f). The growth of the biomass of JMET 15 and JMET 24 strains proceed

similarly under T and CN conditions, indicating that PDB contains other nutrients that promote fungal growth, despite the toxicity of the cathode powder to fungal cells (Fig. 3g and h).

The pH in the CN condition is acidic (4.6–5.4) for the initial 5 d before turning basic (~8). Fungi do not continuously secrete organic acid owing to a lack of sugar resources. Similarly, the pH is higher in the T condition owing to the basic nature of the alkali oxide in the cathode powder. The maximum concentration of oxalic acid (392 ppm) and citric acid (661 ppm) with JMET 15 while the same of oxalic acid (130 ppm) and citric acid (1688 ppm) with JMET 24 detected in the T condition are presented in Fig. 4.

3.4. Cobalt and lithium bioleaching

The concentration of Co and Li in leached solutions was analyzed via ICP-OES under T, and CS conditions (Fig. 5). The SM was better than the PDB for the growth of both fungal strains owing to the higher amount of the initial organic carbon source in the SM (100-g L^{-1} sucrose in the SM, and ~10-g L^{-1} glucose and <4-g L^{-1} sucrose and fructose in PDB, as analyzed via HPLC). Sugar, an organic carbon source, is the main factor affecting the fungal growth rate. It is the raw material for producing organic acids by the fungus through the tricarboxylic acid cycle metabolic pathway [28,46]. Organic acids were used as leaching agents to leach Co and Li from the cathode powder. Moreover, several organic acids (oxalic acid in this study) reduce Co^{3+} to Co^{2+} (Equations (1) and (2)) [47], which can increase the leaching efficiency since Co^{3+} is more difficult to dissolve than Co^{2+} [48,49]. Additionally, JMET 24 dissolves more Co from the cathode powder than JMET 15.

$$\text{Cobalt reduction} : Co^{3+} + e^- \leftrightarrow Co^{2+} \quad E^0 = 1.92 \text{ V} \quad (1)$$

$$\text{Oxalate oxidation} : C_2O_4^{2-} \leftrightarrow 2CO_2 + 2e^- \quad E^0 = 0.49 \text{ V} \quad (2)$$
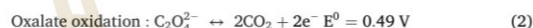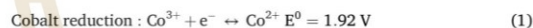
JMET 15 in PDB (T condition) leaches 186 and 181 ppm of Co and Li,
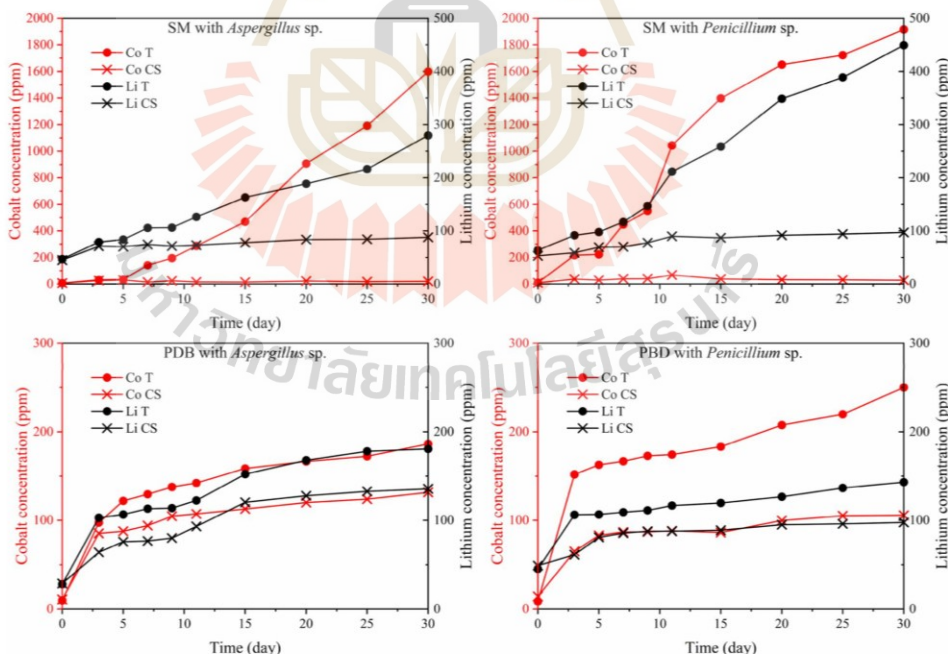
Fig. 5. Cobalt and lithium concentrations in the SM (top) and PDB (bottom) leached by *Aspergillus* sp. JMET 15 (left) and *Penicillium* sp. JMET 24 (right).

respectively, after 30 d, while 132 and 136 ppm of Co and Li are leached, respectively, in the CS condition. JMET 24 in PDB leaches 250 and 143 ppm of Co and Li, respectively, while 106 and 98 ppm of Co and Li are leached, respectively, in the CS condition.

The filtered solution with JMET 15 of the SM contains 1599 and 280 ppm of Co and Li, respectively, while 20 and 88 ppm of Co and Li, respectively, are present in the filtrate under the CS condition. JMET 24 leached 1915-ppm Co and 449-ppm Li, while 29-ppm Co and 97-ppm Li were leached in the CS condition (Fig. 6). The metals dissolve more in the T condition than in the CS condition. A higher amount of Co dissolves in the PDB than in the SM in sterilized flasks owing to the effect of glucose and fructose (reducing sugars) in the PDB, which reduce Co^{3+} to Co^{2+}.

The maximum Co and Li leaching efficiencies of JMET 24 are 32.57 % and 65.07 %, respectively, in the SM, while the same by JMET 15 are 27.19 % and 40.58 %, respectively, which are lower than the reported values. However, it is moderately high considering the pulp density of 1 % w/v of the cathode powder. Biswal et al. [33] reported that $LiCoO_2$ bioleaching with a pulp density of 0.5%w/v showed no growth of A. niger strains MM1 and SG1. The leaching efficiency reported by Bahaloo-Horeh et al. [34] was 38 % and 100 % for Co and Li, respectively for $LiNi_{0.5}Mn_{1.1}Ti_{0.4}O_4$ and $LiCoO_2$ raw materials. In comparison to bioleaching using bacteria, mixed cultures of sulfur-oxidizing and iron-oxidizing bacteria achieve leaching efficiencies of 90 % for Co and 80 % for Li at a pulp density of 1 % [50]. In contrast, inorganic autotrophic bacteria such as Acidithiobacillus ferrooxidans demonstrates efficiencies of 82 % for Co and 89 % for Li at a pulp density of 10 % [51]. This suggests that bacterial leaching of Co is indeed more efficient than fungal methods, as bacterial activity produces sulfuric acid, which enhances Co solubilization. The amount of Co leached in our study is low because the activity of Co^{2+} and oxalic acid secreted from the fungus induces the crystallization of cobalt oxalate.

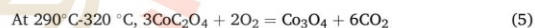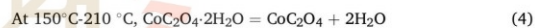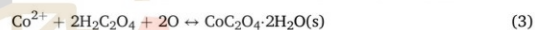### 3.5. Characterization of cathode powder before and after bioleaching

The samples leached by JMET 24 were analyzed via XAS owing to the higher leaching efficiency of JMET 24 to investigate the transformation of Co during bioleaching. The comparison of the chemical structure of leached Co was conducted between the cultured media of JMET 24 (T condition) and the cathode powder via Co K-edge X-ray absorption near-edge structure (XANES) and EXAFS analysis. The Co K-edge XANES spectra of Co-foil (Co^0), CoO (Co^{2+}), Co_3O_4 ($Co^{2+,3+}$), cathode powder, media, and precipitate under T and CS conditions are shown in Fig. 7 (a).

The position of the absorption edge for leached Co in the media of the

T condition indicates that Co is in the Co^{2+} form. The spectra of the Fourier-transformed (FT) k^3-weighted EXAFS profile at the Co edge for precipitated Co in CS and T conditions are similar to the cathode powder spectrum (Fig. 7, b). However, the spectrum of the T medium exhibited a peak shift to the left compared to the other spectra.

To identify the transformed compound, Co K-edge EXAFS fitting was performed. The FT-EXAFS fit of the cathode powder perfectly matches with LCO with an R-factor of 0.011. The fitted structure reveals six neighboring oxygen atoms (Co–O) at 2.03 Å and six neighboring Co atoms (Co–Co) at 2.598 Å around the Co atom. By contrast, the leached Co in the culture media under the T condition can be fitted with cobalt phosphate-oxalate [$(C_4N_2H_{12})0.5(Co_2(HPO_4)(C_2O_4)1.5$ COD No. 1519108] with an R-factor of 0.0125. Five Co–O bonds were identified, corresponding to neighboring oxygen atoms (1.89–2.18 Å). Moreover, four neighboring carbon atoms are presented at 2.81–2.88 Å. The wavelet transform analysis of CoK-edge EXAFS was conducted to further illustrate the atomic dispersion of Co (Fig. 7, c). The wavelet transforms contour plots of the cathode powder and precipitate (T condition) reveal a high-intensity maximum at 4 Å^{-1} corresponding to Co–O coordination and a low intensity of 6 Å^{-1} is assigned to Co–Co bonding. However, only a high-intensity maximum is observed at 4 Å^{-1} under the T condition with no intensity, attributed to Co–Co coordination. Thus, the transformation of Co can occur in acidic conditions by culturing Penicillium sp.

Fungal cells and the residual cathode powder were collected on a membrane filter paper after 30 d. The sample was dried and incinerated at 500 °C to eliminate the biomass. LCO was the main composition of the residual powder as analyzed via XRD, consistent with the raw material (Fig. 8) in the three conditions. However, a pattern of Co_3O_4 mixed with LCO appears in the 30-d test with both fungal strains (D30 T). Co_3O_4 is formed by the decomposition of cobalt oxalate ($CoC_2O_4.2H_2O$), which is the product of the reaction between Co ions in the leach solution and oxalic acid secreted by fungi (Equation (3)). $CoC_2O_4.2H_2O$ is insoluble [52] in water and easily precipitated into solid powder. Sun and Qiu analyzed the thermal properties of $CoC_2O_4.2H_2O$ in the air. It decomposes into Co_3O_4 at 290°C-320 °C (Equations (4) and (5)) [49].

$$Co^{2+} + 2H_2C_2O_4 + 2O \leftrightarrow CoC_2O_4 \cdot 2H_2O(s) \quad (3)$$

At 150°C-210 °C, $CoC_2O_4 \cdot 2H_2O = CoC_2O_4 + 2H_2O$ (4)

At 290°C-320 °C, $3CoC_2O_4 + 2O_2 = Co_3O_4 + 6CO_2$ (5)

3.6. Pure Co_3O_4 recovery at lower pulp density

After 30 days, fungal cells and sediment were filtered out. The leaching solution from each pulp density was analyzed and calculated the leaching efficiency by ICP-OES as depicted in Fig. 9(a) and (b). The fungal cells were eliminated at 500 °C for 4 h in a muffle furnace. Co compound in sediment was decomposed as Equations (4) and (5). The purity of the Co_3O_4 powder can be increased by reducing the pulp density as illustrated in Fig. 10. The X-ray diffraction pattern shows Co_3O_4 mixed with $LiCoO_2$ powder in 0.5–1% pulp density, while only Co_3O_4 was detected in 0.1 % pulp density. The Co_3O_4 powder can be used as a raw material in supercapacitors [53] and electrodes in LIBs [54]. Co and Li ions can be recovered from the leached solution and converted to various cobalt (cobalt oxalate, cobalt sulfide, and cobalt hydroxide) and lithium (lithium carbonate and lithium phosphate) compounds [33,55]. From an industrial perspective, a 0.1 % pulp density is insufficient to meet demand. Therefore, further development of the bioleaching process using fungi at higher pulp densities is essential. Supplementation of oxygen and sugar resources will increase organic acid production activity, allowing for the recovery of high-purity Co_3O_4 at these higher pulp densities. Moreover, research in engineered microbes can enhance the efficiency of recycling processes, not only for LIB
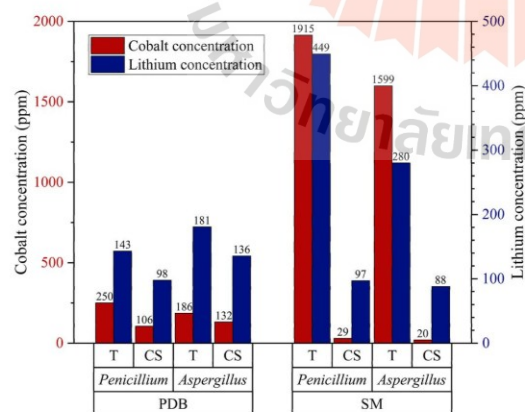
Fig. 6. Cobalt and lithium concentrations in leaching conditions after 30 d.
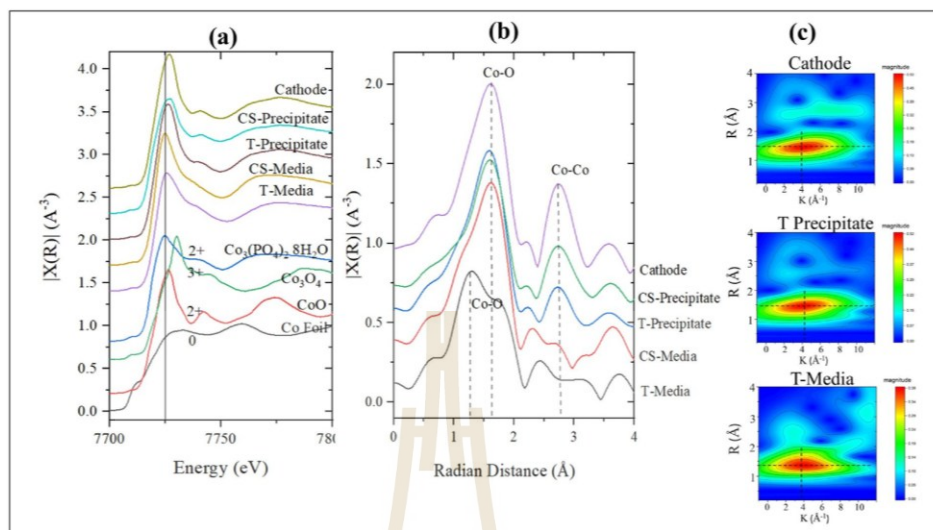
Fig. 7. (a) Co K-edge XANES spectra of Co reference material and Co leaching samples (b) FT-EXAFS spectrum in the R space of Co leaching samples. (c) WT for the k^3-weighted EXAFS signals of leached Co samples.
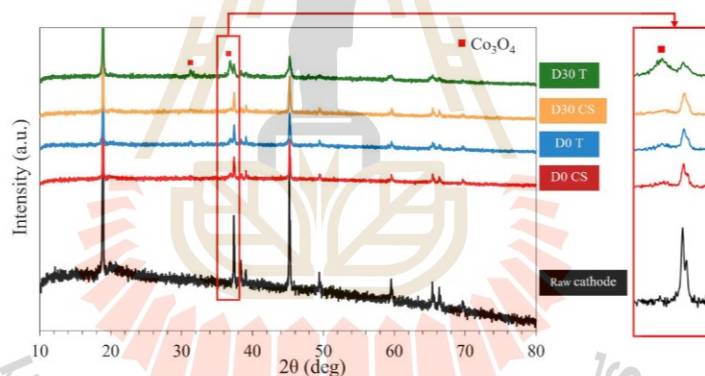
Fig. 8. XRD patterns of raw materials compared to the residual powder after 0 and 30 d of bioleaching.

but also for all electronic wastes and other metal resources [7].

4. Conclusions

Two potential fungal strains JMET 24 and JMET 15 were grown in Co and Li environments in the PDB and SM with 1 % w/v cathode powder. JMET 24 showed continuous growth while JMET 15 exhibited slow growth in the initial 7 d in the SM. Although no lag phase was observed in PDB, the leaching efficiency of Co and Li was lower in the PDB than in the SM owing to the lower amount of sugar as an organic carbon source in the PDB. The detected sugars were rapidly consumed during the initial stage of the fungal growth (5–9 d). The growth of the fungus and the secretion of organic acids facilitated the leaching of metals from the cathode powder. Both fungal strains increased the leaching of Co and Li from the cathode powder compared to the sterile condition. The highest concentrations of Co and Li in the leached solution were 2190 ppm (0.5

% pulp density) and 449 ppm (1 % pulp density), respectively, in the SM with JMET 24. At 0.1 % pulp density gives the highest leaching efficiency of Co (77.87 %) and Li (99.88 %) in SM and *Penicillium* sp. strain JMET 24. The EXAFS spectrum fitting revealed the transformation of cobalt into cobalt phosphate-oxalate during the bioleaching process of the cobalt compound in the cultured media under the T condition with JMET 24. The burning of the sample at 500 °C formed Co_3O_4 as the product via one-step recovery. The highest purity of Co_3O_4 can be recovered at 0.1 % pulp density.

CRediT authorship contribution statement

Thanapon Chandakhiaw: Writing – review & editing, Writing – original draft, Methodology, Investigation, Conceptualization. **Neung Teaumroong:** Writing – review & editing, Validation, Supervision, Resources, Methodology, Conceptualization. **Pongdet Piromyou:**
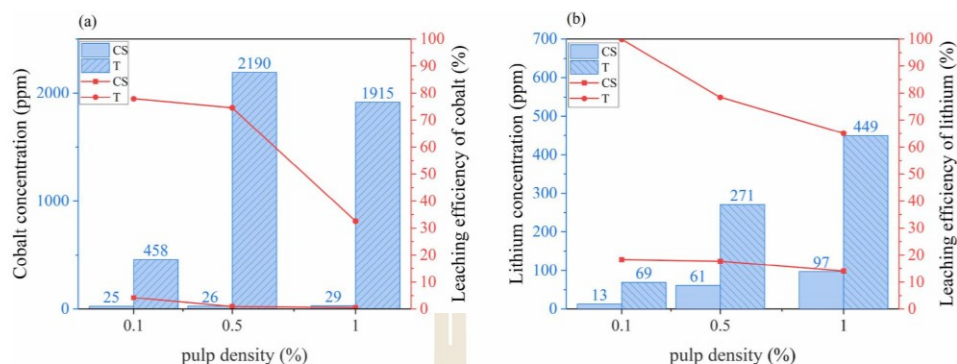
Fig. 9. Concentrations and leaching efficiency of (a) cobalt and (b) lithium at 0.1, 0.5, and 1 % pulp density by *Penicillium* sp. JMET 24.
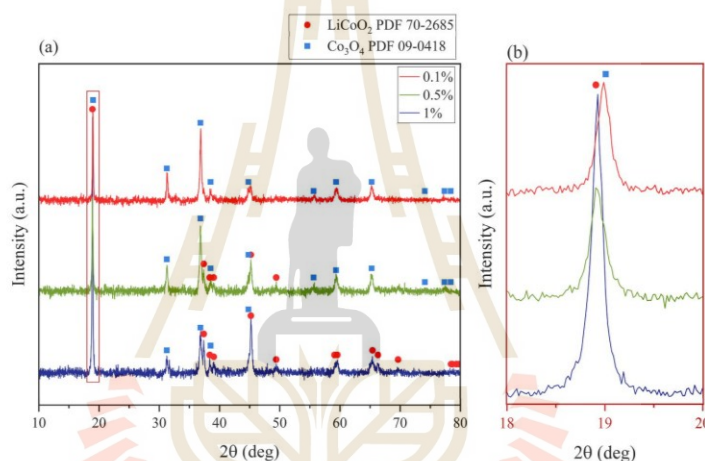
Fig. 10. XRD patterns of the residual powder after 30 d of bioleaching by *Penicillium* sp. at 0.1, 0.5, and 1 % pulp density (a), and enlarged XRD pattern at 18–20 deg (b).

Validation, Supervision, Investigation. **Pongpan Songwattana:** Validation, Supervision, Investigation. **Waraporn Tanthanuch:** Writing – review & editing, Writing – original draft, Visualization, Resources, Formal analysis, Data curation. **Somchai Tancharakorn:** Writing – review & editing, Software, Resources, Data curation. **Sakhob Khumkoa:** Writing – review & editing, Supervision, Resources, Methodology, Funding acquisition, Conceptualization.

Declaration of competing interest

The authors declare that they have no known competing financial interests or personal relationships that could have appeared to influence the work reported in this paper.

Data availability

No data was used for the research described in the article.

References

[1] R.P. Sheth, N.S. Ranawat, A. Chakraborty, R.P. Mishra, M. Khandelwal, The lithium-ion battery recycling process from a circular economy perspective—a review and future directions, Energies 16 (2023) 3228, https://doi.org/10.3390/en16073228.

[2] IEA, Lithium-ion Battery Manufacturing Capacity, 2022-2030 – Charts – Data & Statistics, IEA, 2023 [WWW Document], https://www.iea.org/data-and-statistics/charts/lithium-ion-battery-manufacturing-capacity-2022-2030. accessed 12.27.23.

[3] B. Swain, Recovery and recycling of lithium: a review, Sep. Purif. Technol. 172 (2017) 388–403, https://doi.org/10.1016/j.seppur.2016.08.031.

[4] P.K.S. Zhang, Chao-Yang Wang, San Ping Jiang, Xueliang Sun, Jiujun, Electrochemical Energy: Advanced Materials and Technologies, CRC Press, Boca Raton, 2017, https://doi.org/10.1201/9781351228756.

[5] F. Arshad, J. Lin, N. Manurkar, E. Fan, A. Ahmad, M.-N. Tariq, F. Wu, R. Chen, L. Li, Life cycle assessment of lithium batteries: a critical review, Resour. Conserv. Recycl. 180 (2022) 106164, https://doi.org/10.1016/j.resconrec.2022.106164.

[6] M. Alipanah, A.K. Saha, E. Vahidi, H. Jin, M. Alipanah, A.K. Saha, E. Vahidi, H. Jin, Value recovery from spent lithium-ion batteries: a review on technologies, environmental impacts, economics, and supply chain, Clean Technol. Recycl. 1 (2021) 152–184, https://doi.org/10.3934/ctr.2021008.

[7] B.K. Biswal, R. Balasubramanian, Recovery of valuable metals from spent lithium-ion batteries using microbial agents for bioleaching: a review, Front. Microbiol. 14 (2023).

[8] X. Chen, L. Cao, D. Kang, J. Li, T. Zhou, H. Ma, Recovery of valuable metals from mixed types of spent lithium ion batteries. Part II: selective extraction of lithium, Waste Manag. 80 (2018) 198–210, https://doi.org/10.1016/j.wasman.2018.09.013.

[9] Y.M. Park, H. Lim, J.-H. Moon, H.-N. Lee, S.H. Son, H. Kim, H.-J. Kim, High-yield one-pot recovery and characterization of nanostructured cobalt oxalate from spent lithium-ion batteries and successive Re-synthesis of LiCoO2, Metals 7 (2017) 303, https://doi.org/10.3390/met7080303.

[10] E. Asadi Dalini, Gh Karimi, S. Zandevakili, M. Goodarzi, A review on environmental, economic and hydrometallurgical processes of recycling spent lithium-ion batteries, Miner. Process. Extr. Metall. Rev. 42 (2021) 451–472, https://doi.org/10.1080/08827508.2020.1781628.

[11] D.P. Mantuano, G. Dorella, R.C.A. Elias, M.B. Mansur, Analysis of a hydrometallurgical route to recover base metals from spent rechargeable batteries by liquid–liquid extraction with Cyanex 272, J. Power Sources 159 (2006) 1510–1518, https://doi.org/10.1016/j.jpowsour.2005.12.056.

[12] F.K. Crundwell, N.B. du Preez, B.D.H. Knights, Production of cobalt from copper-cobalt ores on the African Copperbelt – an overview, Miner. Eng. 156 (2020) 106450, https://doi.org/10.1016/j.mineng.2020.106450.

[13] M. Zhang, G. Zhu, Y. Zhao, X. Feng, A study of recovery of copper and cobalt from copper–cobalt oxide ores by ammonium salt roasting, Hydrometallurgy 129–130 (2012) 140–144, https://doi.org/10.1016/j.hydromet.2012.06.014.

[14] K.S. Moon, D.W. Fuerstenau, Surface crystal chemistry in selective flotation of spodumene (LiAl[SiO3]2) from other aluminosilicates, Int. J. Miner. Process. 72 (2003) 11–24, https://doi.org/10.1016/S0301-7516(03)00084-X. Special Issue To Honor Professor Douglas W. Fuerstenau.

[15] Z.J. Baum, R.E. Bird, X. Yu, J. Ma, Lithium-ion battery Recycling—Overview of techniques and trends, ACS Energy Lett. 7 (2022) 712–719, https://doi.org/10.1021/acsenergylett.1c02602.

[16] M. Chen, X. Ma, B. Chen, R. Arsenault, P. Karlson, N. Simon, Y. Wang, Recycling end-of-life electric vehicle lithium-ion batteries, Joule 3 (2019) 2622–2646, https://doi.org/10.1016/j.joule.2019.09.014.

[17] Y. Choi, S.-W. Rhee, Current status and perspectives on recycling of end-of-life battery of electric vehicle in Korea (Republic of), Waste Manag. 106 (2020) 261–270, https://doi.org/10.1016/j.wasman.2020.03.015.

[18] T. Tawonezvi, M. Nomnqa, L. Petrik, B.J. Bladergroen, Recovery and recycling of valuable metals from spent lithium-ion batteries: a comprehensive review and analysis, Energies 16 (2023) 1365, https://doi.org/10.3390/en16031365.

[19] T. Hennebel, N. Boon, S. Maes, M. Lenz, Biotechnologies for critical raw material recovery from primary and secondary sources: R&D priorities and future perspectives, N. Biotech. 32 (2015) 121–127, https://doi.org/10.1016/j.nbt.2013.08.004.

[20] W.-Q. Zhuang, J.P. Fitts, C.M. Ajo-Franklin, S. Maes, L. Alvarez-Cohen, T. Hennebel, Recovery of critical metals using biometallurgy, Curr. Opin. Biotechnol., Environmental biotechnology ● Energy biotechnology 33 (2015) 327–335, https://doi.org/10.1016/j.copbio.2015.03.019.

[21] J.J. Roy, B. Cao, S. Madhavi, A review on the recycling of spent lithium-ion batteries (LIBs) by the bioleaching approach, Chemosphere 282 (2021) 130944, https://doi.org/10.1016/j.chemosphere.2021.130944.

[22] A.I. Adetunji, P.J. Oberholster, M. Erasmus, Bioleaching of metals from E-waste using microorganisms: a review, Minerals 13 (2023) 828, https://doi.org/10.3390/min13060828.

[23] X. Deng, L. Chai, Z. Yang, C. Tang, Y. Wang, Y. Shi, Bioleaching mechanism of heavy metals in the mixture of contaminated soil and slag by using indigenous Penicillium chrysogenum strain F1, J. Hazard Mater. 248–249 (2013) 107–114, https://doi.org/10.1016/j.jhazmat.2012.12.051.

[24] J. Li, H. Zhang, H. Wang, B. Zhang, Research progress on bioleaching recovery technology of spent lithium-ion batteries, Environ. Res. 238 (2023) 117145, https://doi.org/10.1016/j.envres.2023.117145.

[25] H. Watling, Microbiological advances in biohydrometallurgy, Minerals 6 (2016) 49, https://doi.org/10.3390/min6020049.

[26] A. Schippers, Microorganisms involved in bioleaching and nucleic acid-based molecular methods for their identification and quantification, in: E.R. Donati, W. Sand (Eds.), Microbial Processing of Metal Sulfides, Springer, Netherlands, Dordrecht, 2007, pp. 3–33, https://doi.org/10.1007/1-4020-5589-7_1.

[27] W. Burgstaller, F. Schinner, Leaching of metals with fungi, J. Biotechnol. 27 (1993) 91–116, https://doi.org/10.1016/0168-1656(93)90101-R.

[28] L. Dusengemungu, G. Kasali, C. Gwanama, B. Mubemba, Overview of fungal bioleaching of metals, Environ. Adv. 5 (2021) 100083, https://doi.org/10.1016/j.envadv.2021.100083.

[29] N.B. Horeh, S.M. Mousavi, S.A. Shojaosadati, Bioleaching of valuable metals from spent lithium-ion mobile phone batteries using Aspergillus Niger, J. Power Sources 320 (2016) 257–266, https://doi.org/10.1016/j.jpowsour.2016.04.104.

[30] Y. Yao, M. Zhu, Z. Zhao, B. Tong, Y. Fan, Z. Hua, Hydrometallurgical processes for recycling spent lithium-ion batteries: a critical review, ACS Sustain. Chem. Eng. 6 (2018) 13611–13627, https://doi.org/10.1021/acssuschemeng.8b03545.

[31] J. Houbraken, R.P. de Vries, R.A. Samson, Modern taxonomy of biotechnologically important Aspergillus and Penicillium species, in: S. Sariaslani, G.M. Gadd (Eds.), Advances in Applied Microbiology, Academic Press, 2014, pp. 199–249, https://doi.org/10.1016/B978-0-12-800262-9.00004-4.

[32] C.-C. Tsang, J.Y.M. Tang, S.K.P. Lau, P.C.Y. Woo, Taxonomy and evolution of Aspergillus, Penicillium and Talaromyces in the omics era – past, present and future, Comput. Struct. Biotechnol. J. 16 (2018) 197–210, https://doi.org/10.1016/j.csbj.2018.05.003.

[33] B.K. Biswal, U.U. Jadhav, M. Madhaiyan, L. Ji, E.-H. Yang, B. Cao, Biological leaching and chemical precipitation methods for recovery of Co and Li from spent lithium-ion batteries, ACS Sustain. Chem. Eng. 6 (2018) 12343–12352, https://doi.org/10.1021/acssuschemeng.8b02810.

[34] N. Bahaloo-Horeh, S.M. Mousavi, M. Baniasadi, Use of adapted metal tolerant Aspergillus Niger to enhance bioleaching efficiency of valuable metals from spent lithium-ion mobile phone batteries, J. Clean. Prod. 197 (2018) 1546–1557, https://doi.org/10.1016/j.jclepro.2018.06.299.

[35] N. Bahaloo-Horeh, S.M. Mousavi, Enhanced recovery of valuable metals from spent lithium-ion batteries through optimization of organic acids produced by Aspergillus Niger, Waste Manag. 60 (2017) 666–679, https://doi.org/10.1016/j.wasman.2016.10.034.

[36] I. Rezza, E. Salinas, M. Elorza, M. Sanz de Tosetti, E. Donati, Mechanisms involved in bioleaching of an aluminosilicate by heterotrophic microorganisms, Process Biochem. 36 (2001) 495–500, https://doi.org/10.1016/S0032-9592(00)00164-3.

[37] I. Rezza, E. Salinas, V. Calvente, D. Benuzzi, M.I.S. de Tosetti, Extraction of lithium from spodumene by bioleaching, Lett. Appl. Microbiol. 25 (1997) 172–176, https://doi.org/10.1046/j.1472-765X.1997.00199.x.

[38] T. Zhang, Y. He, L. Ge, R. Fu, X. Zhang, Y. Huang, Characteristics of wet and dry crushing methods in the recycling process of spent lithium-ion batteries, J. Power Sources 240 (2013) 766–771, https://doi.org/10.1016/j.jpowsour.2013.05.009.

[39] A.J. de Jesus Silva, M.M. Contreras, C.R. Nascimento, M.F. da Costa, Kinetics of thermal degradation and lifetime study of poly(vinylidene fluoride) (PVDF) subjected to bioethanol fuel accelerated aging, Heliyon 6 (2020) e04573, https://doi.org/10.1016/j.heliyon.2020.e04573.

[40] Y. Fu, J. Schuster, M. Petranikova, B. Ebin, Innovative recycling of organic binders from electric vehicle lithium-ion batteries by supercritical carbon dioxide extraction, Resour. Conserv. Recycl. 172 (2021) 105666, https://doi.org/10.1016/j.resconrec.2021.105666.

[41] P. Thomas, K.T. Varughese, K. Dwarakanath, K.B.R. Varma, Dielectric properties of Poly(vinylidene fluoride)/CaCu3Ti4O12 composites, Compos. Sci. Technol. 70 (2010) 539–545, https://doi.org/10.1016/j.compscitech.2009.12.014.

[42] J.L. Cenis, Rapid extraction of fungal DNA for PCR amplification, Nucleic Acids Res. 20 (1992) 2380.

[43] T.J. White, T. Bruns, S. Lee, J. Taylor, 38 - amplification and direct sequencing of fungal ribosomal rna genes for phylogenetics, in: M.A. Innis, D.H. Gelfand, J. J. Sninsky, Thomas J. White (Eds.), PCR Protocols, Academic Press, San Diego, 1990, pp. 315–322, https://doi.org/10.1016/B978-0-12-372180-8.50042-1.

[44] N. Uemura, K. Makimura, M. Onozaki, Y. Otsuka, Y. Shibuya, H. Yazaki, Y. Kikuchi, S. Abe, S. Kudoh, Development of a loop-mediated isothermal amplification method for diagnosing Pneumocystis pneumonia, J. Med. Microbiol. 57 (2008) 50–57, https://doi.org/10.1099/jmm.0.47216-0.

[45] B. Ravel, M. Newville, ATHENA, artemis, hephaestus: data analysis for X-ray absorption spectroscopy using IFEFFIT, J. Synchrotron Radiat. 12 (2005) 537–541, https://doi.org/10.1107/S0909049505012719.

[46] H. Srichandan, R.K. Mohapatra, P.K. Parhi, S. Mishra, Bioleaching approach for extraction of metal values from secondary solid wastes: a critical review, Hydrometallurgy 189 (2019) 105122, https://doi.org/10.1016/j.hydromet.2019.105122.

[47] A. Verma, G.H. Johnson, D.R. Corbin, M.B. Shiflett, Separation of lithium and cobalt from LiCoO2: a unique critical metals recovery process utilizing oxalate chemistry, ACS Sustain. Chem. Eng. 8 (2020) 6100–6108, https://doi.org/10.1021/acssuschemeng.0c01128.

[48] C.K. Lee, K.-I. Rhee, Reductive leaching of cathodic active materials from lithium ion battery wastes, Hydrometallurgy 68 (2003) 5–10, https://doi.org/10.1016/S0304-386X(02)00167-6.

[49] L. Sun, K. Qiu, Organic oxalate as leachant and precipitant for the recovery of valuable metals from spent lithium-ion batteries, Waste Manag. 32 (2012) 1575–1582, https://doi.org/10.1016/j.wasman.2012.03.027.

[50] B. Xin, D. Zhang, X. Zhang, Y. Xia, F. Wu, S. Chen, L. Li, Bioleaching mechanism of Co and Li from spent lithium-ion battery by the mixed culture of acidophilic sulfur-oxidizing and iron-oxidizing bacteria, Bioresour. Technol. 100 (2009) 6163–6169, https://doi.org/10.1016/j.biortech.2009.06.086.

[51] J. Jegan Roy, M. Srinivasan, B. Cao, Bioleaching as an eco-friendly approach for metal recovery from spent NMC-based lithium-ion batteries at a high pulp density, ACS Sustain. Chem. Eng. 9 (2021) 3060–3069, https://doi.org/10.1021/acssuschemeng.0c06573.

[52] A. Verma, R. Kore, D.R. Corbin, M.B. Shiflett, Metal recovery using oxalate chemistry: a technical review, Ind. Eng. Chem. Res. 58 (2019) 15381–15393, https://doi.org/10.1021/acs.iecr.9b02598.

[53] X. Hu, L. Wei, R. Chen, Q. Wu, J. Li, Reviews and prospectives of Co3O4-based nanomaterials for supercapacitor application, ChemistrySelect 5 (2020) 5268–5288, https://doi.org/10.1002/slct.201904485.

[54] Z.H. Mahmood, M. Jarosova, H.H. Kzar, P. Machek, M. Zaidi, A. Dehno Khalaji, I. H. Khlewee, U.S. Altimari, Y.F. Mustafa, M.M. Kadhim, Synthesis and characterization of Co3O4 nanoparticles: application as performing anode in Li-ion

batteries, J. Chin. Chem. Soc. 69 (2022) 657–662, https://doi.org/10.1002/jccs.202100525.

[55] N. Wongnaree, L. Sriklang, C. Kansomket, T. Chandakhiaw, T. Patcharawit, S. Khumkoa, Precipitation of lithium phosphate from cathode materials of spent lithium-ion battery by hydrometallurgy process, Mater. Sci. Forum 1099 (2023) 175–180, https://doi.org/10.4028/p-arh30R.

The Production of Hematite Powder from Spent Pickling Hydrochloric Acid

Thanapon Chandakhiaw[1,a], Chaiyasit Longbutsri[1,b], Natcha Wongnaree[1,c], Sirunya Somla[1,d], Napat Mahiwan[1,e], Tapany Patcharawit[1,f], and Sakhob Khumkoa[1,g,*]

[1]School of Metallurgical Engineering, Institute of Engineering, Suranaree University of Technology, Nakhon Ratchasima, Thailand
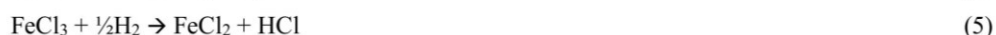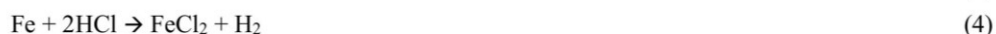
[a]thanapon2459@gmail.com, [b]chaiyasitlong095@gmail.com, [c]natcha.wongnaree@outlook.com, [d]sirunya.b6114947@gmail.com, [e]napat.b6112097@gmail.com, [f]tapany@sut.ac.th, [g]sakhob@sut.ac.th

Abstract. This research aimed to study the recycling process and the feasibility of recovering iron as hematite or red oxide powder (Fe_2O_3) from spent pickling acid (hydrochloric acid). The spent hydrochloric acid waste from the pickling bath in the sheet rolling steel industry contains approximately 233 g of iron dissolved in one liter of the spent acid. To recover iron, 2 M NaOH was added to the spent acid until reaching pH 7. The iron was precipitated as iron oxide and/or hydroxide. Next, the oxidation of ferrous oxide was carried out by adding H_2O_2 35%v/v to control the shade color. The precipitates were subsequently separated from the acid solution by a filter press. The precipitates were dried at 110°C for 24 h and calcined at 700°C for 2 h to synthesize and modify the crystallinity of ferric oxide. Ferric oxide was subject to water washing, where contaminating sodium chloride could be dissolved and filtered out. After drying at 110°C for 24 h, high-purity hematite was achieved. Hematite recovered from the spent pickling acid via this process provided more than 97% purity at 94.4% recovery.

Introduction

In the sheet hot-rolling steel industry, the oxide scale has occurred on the steel surface. The scale must be removed from hot-rolled steel before cold-rolling process to produce high-quality cold-rolled steel. These oxide scales can be removed by the pickling process, in which hydrochloric acid and sulfuric acid were commonly selected in the industry. Advantages of hydrochloric acid are viable for operating at ambient temperature, high corrosiveness, low diffusion of hydrogen in the steel, and less attachment of salt to the steel surface. However, hydrochloric acid can be vaporized, and the recovery system of acid was expensive. Though sulfuric acid was easier to recover than hydrochloric acid, but it has a rather high corrosion rate, hydrogen diffusion, and must be heated. In Thailand, hydrochloric acid was preferred to use in the steel industry. Chemical reactions between hydrochloric acid and oxide scale are given in Eq. (1)-(5) [1-4].

$$Fe_2O_3 + Fe + 6HCl \rightarrow 3FeCl_2 + 3H_2O \tag{1}$$

$$Fe_3O_4 + 8HCl \rightarrow FeCl_2 + 2FeCl_3 + 4H_2O \tag{2}$$

$$FeO + 2HCl \rightarrow FeCl_2 + H_2O \tag{3}$$

$$Fe + 2HCl \rightarrow FeCl_2 + H_2 \tag{4}$$

$$FeCl_3 + \tfrac{1}{2}H_2 \rightarrow FeCl_2 + HCl \tag{5}$$

Normally, there was 180-200 g/L of HCl concentration in the pickling process (or 18 wt.% of HCl) and the operating temperature would be around 80-90°C [4]. The reaction rate decreased when the acid was repeatedly used, and the ferrous ions will be accumulated in the pickling bath. If the pickling efficiency of the acid was not sufficient, it would be considered a waste. Chemical compositions of

the spent hydrochloric acid contained overall metal of 150-250 kg/m^3, or 13 wt.% of iron dissolved in 1-2% of HCl. Iron can be found either in form of ferrous or ferric ions [4-6].

There were various recycling processes of spent pickling hydrochloric acid, e. g., evaporation and crystallization [6], solvent extraction [7], membrane separation [5, 8], chemical precipitation [9], pyrohydrolysis [10], and ion exchange [11]. Each process had different advantages and disadvantages for different objectives. However, all processes had the same principle to first separate iron ions out of the acid, and later the acid and/or iron will be reused or recycled in different ways. Nevertheless, the chemical precipitation process of iron and iron oxide (hematite) production was the most suitable on cost effective, less complexity, simple chemical used, and for the appreciable demand for hematite products in the pigment industry in Thailand.

Materials and Methods

Raw Materials. Spent pickling acid (hydrochloric acid) in this research was obtained from the sheet hot-rolling steel industry in Thailand. The chemical compositions were analyzed by ICP-OES as shown in Table 1. The initial pH of 0.33 was measured by a pH meter.

Table 1. Chemical composition of spent pickling acid (ICP-OES).

Element	Fe	Ca	Al	Cr	Ni	Zn	Mg	Si	Sn	Pb
Conc. [mg/L]	232,967	636	127	126	79	40	24	<50	<50	<50

Analytical Methods. The chemical compositions of raw materials and solutions were analyzed by ICP-OES technique (PerkinElmer® Optima™ 8000). The chemical compositions of solid compounds along the process were analyzed by WD-XRF technique (PANanalytical AXIOS^{mAX}, 30 mm. beam size, and scan time 18 min.). X-ray diffractometer was used to determine phases and compounds, using Bruker model D8 ADVANCE Cu Kα at condition 40 kV, 40 mA. The solution's pH was measured using a pH meter (METTLER TOLEDO Five Easy F20). Field emission scanning electron microscope (FE-SEM, Zeiss AURIGA FE-SEM/FIB/EDX) and laser diffraction particle size analyzer (HORIBA/LA-950V2) were used to characterize the morphology and size of the hematite powder.

Hematite Powder Production. The spent hydrochloric acid was through various processes, starting from precipitation, oxidation, filtration, calcination, washing, and drying. The flow chart of hematite powder production is illustrated in Fig. 1.
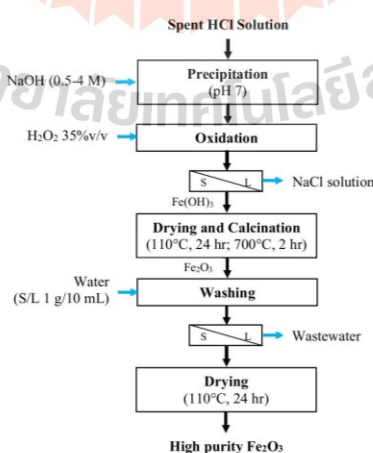

Fig. 1. Flow chart of hematite powder production.

In the precipitation processes, sodium hydroxide solution at 0.5, 1, 2, and 4 M concentrations was gently added to the spent hydrochloric acid. The solution's pH was monitored by pH meter while sampling of the solution at each pH was carried out to analyze the amount of iron by ICP-OES. Subsequently, 35%v/v of hydrogen peroxide was added to the system to oxidize ferrous to ferric iron. The powder was separated from the solution by a filter press machine. The powder sludge was dried in the hot air oven at 110°C for 24 h before synthesizing the hematite powder in the calcination process by using the muffle furnace at 700°C for 2 h. Hematite powder from the calcination process was washed with water to eliminate the sodium chloride salt. Hematite powder without salt was filtered and dried in the hot air oven again to achieve standard quality hematite powder.

Results and Discussion

When sodium hydroxide solution (0.5, 1, 2, and 4 M) was added to the spent hydrochloric acid, the pH increased. The concentration of iron in the solution decreased due to iron precipitated from the solution as iron oxide and/or oxyhydroxide. The iron concentration at varied pH in the precipitation process, due to sodium hydroxide addition is shown in Fig. 2. Complete iron precipitation was obtained when the solution reached pH 8. However, it should be noted that excessive amount of sodium hydroxide solution was used to change from pH 7 to 8. Further, in wastewater management, a high volume of the chemical solution should be avoided. Thus, precipitation at pH 7 was considered to be more suitable than at pH 8 for wastewater management and iron recovery. The lower iron concentration, as shown in Fig. 2, when using low concentrations of sodium hydroxide (1 and 2 M) is due to the dilution effect.
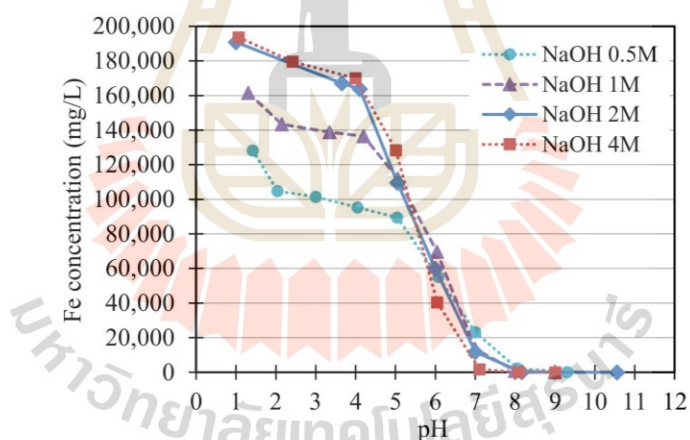
Fig. 2. Concentration of iron in the solution at each pH and NaOH solution concentration.

To meet a required shade of hematite powder, 35%v/v of hydrogen peroxide was added to the system to oxidize ferrous to ferric iron. Hydrogen peroxide can react as a reducing and oxidizing agent. To optimize the volume of hydrogen peroxide, 35%v/v hydrogen peroxide varied at amounts of 0, 40, 50, 60, 70, 80, 90, and 100 mL were added to 600 mL solution at pH 7. The precipitates obtained after oxidation were filtered and dried for the XRD analysis. The diffraction patterns of precipitate when adding various amounts of hydrogen peroxide are shown in Fig. 3. Ferrous iron was found in the form of $FeCl_2 \cdot 2H_2O$ compound when hydrogen peroxide addition was lower than 70 mL. When hydrogen peroxide addition was higher than 80 mL the compounds were found as hematite and sodium chloride. The precipitated from all conditions in the oxidation process were filtered, dried, and calcined at 700°C for 2 h to examine the appearance color. The apparent color from each condition is shown in Fig. 4. The apparent color when adding 80 mL of hydrogen peroxide was closest to the commercial red iron oxide pigment.
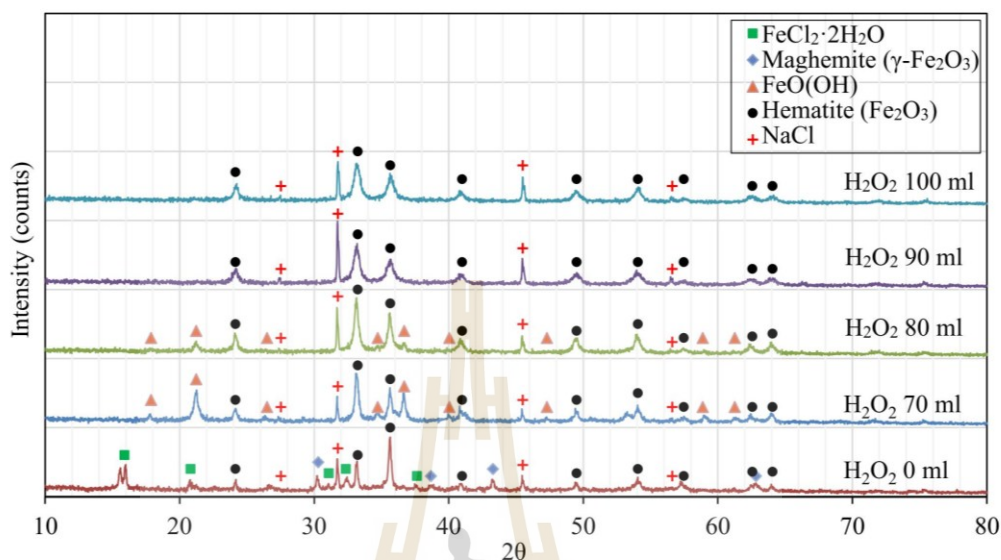
Fig. 3. Diffraction patterns of the precipitates from various amounts of hydrogen peroxide addition.
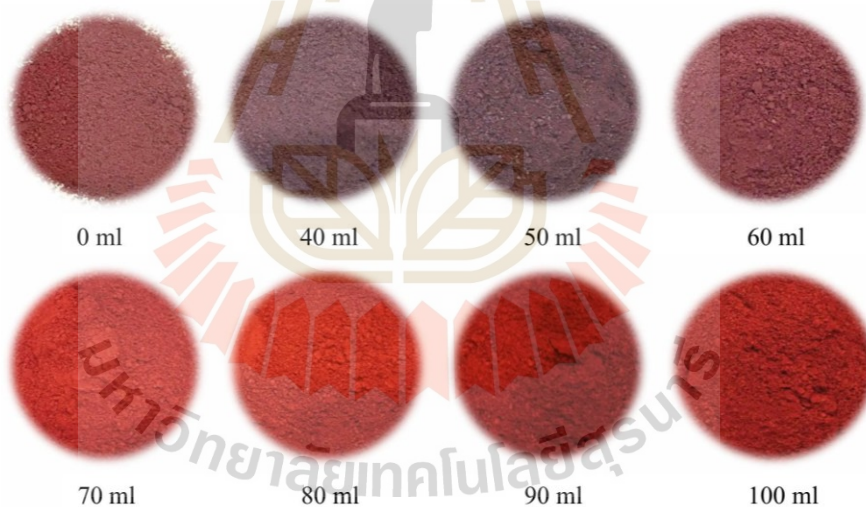
Fig. 4. Apparent colors of hematite when adding hydrogen peroxide from 0 to 100 mL, then drying and calcining at 700°C for 2 h.

The precipitate at pH 7 using 80 ml of 35%v/vH$_2$O$_2$ was filtered and then dried in the hot air oven at 110°C for 24 h before calcination in a muffle furnace at 700°C for 2 h to completely synthesis the hematite crystal. The main impurity of hematite powder was sodium chloride which can be removed by washing with water due to the solubility of sodium chloride in water being much higher than hematite. The precipitate was dried in the hot air oven at 110°C for 24 h again after washing. The diffraction patterns of hematite after calcining and washing are shown in Fig. 5. (a) and (b) respectively. Disappearance of NaCl peaks was evident after washing.
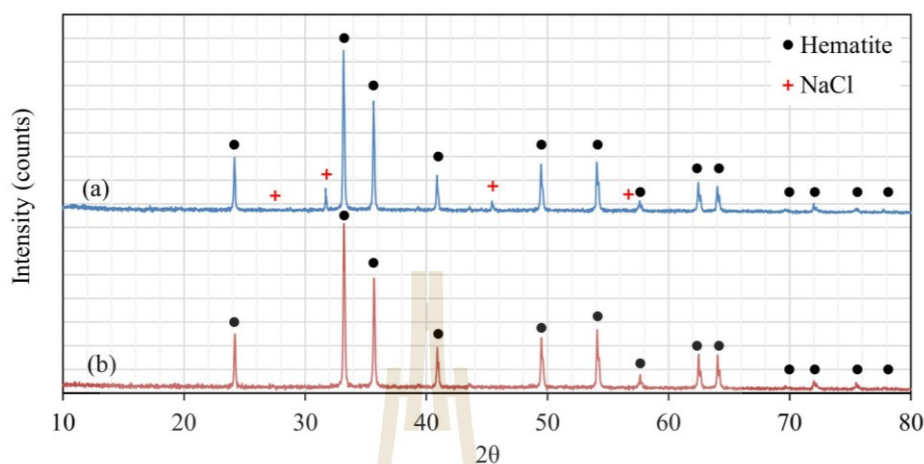
Fig. 5. Diffraction patterns of hematite after calcining (a) and after washing (b).

The final hematite powder was analyzed for the chemical composition by WD-XRF as shown in Table 2. The purity of 97.6% was calculated from the WD-XRF result after powder washing. The recovery of iron was 94.4% based on the weight of iron in hematite powder ($W_{\text{Fe in hematite powder}}$) divided by the weight of the total iron in spent hydrochloric acid ($W_{\text{Fe in spent acid}}$), as expressed in Eq. (6). The morphology of hematite powder analyzed by FE-SEM exhibited very fine polygonal shape as shown in Fig. 6. Laser diffraction particle size analyzer as shown in Fig. 7 reported the mean size of hematite powder of 2.52 μm with standard deviation of 2.58 μm. Other parameters such as D_{10}, D_{50}, D_{90} and S_w are inserted in the graph.

$$\text{Iron Recovery (\%)} = \frac{W_{\text{Fe in hematite powder}}}{W_{\text{Fe in spent acid}}} \times 100 \tag{6}$$

Table 2. Chemical composition of hematite powder after calcination and washing.

Element	Fe	O	Na	Al	Cl	Cr	Mn	Bal.
After calcination, (wt.%)	53.93	33.98	3.367	0.09	8.22	0.16	0.10	0.16
After washing (wt.%)	68.265	30.366	0.61	0.089	0.23	0.16	0.13	0.15

Fig. 6. SEM image of final hematite powder.

D_{av}	D_{10}	D_{50}	D_{90}	S_w	Unit
2.52	0.55	1.53	5.90	2.48	µm

Fig. 7. Particle size distribution of final hematite powder.

Summary

The spent hydrochloric acid from the hot-rolling steel industry can be used as a raw material to produce hematite powder for pigment industry. To achieve the hematite pigme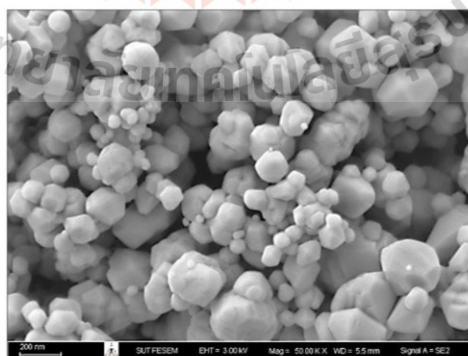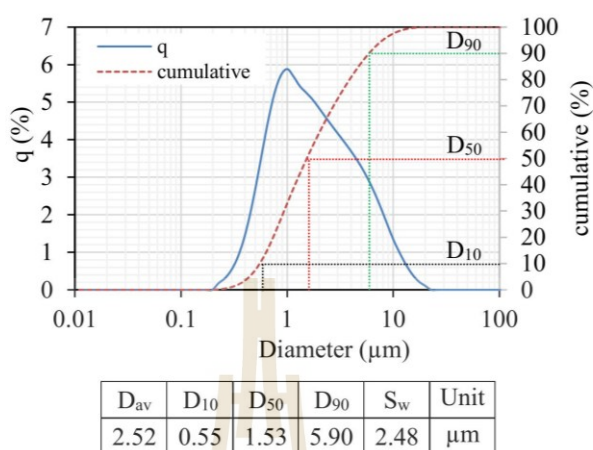nt powder standard, the spent acid was passed through the precipitation process using 2 M NaOH solution at pH 7 to separate the iron from the solution. Next, 80 ml of 35%H_2O_2 was added to the system per 600 ml of solution at pH 7 to control the shade appearance. The precipitate was filtered and dried in the hot air oven at 110°C for 24 h. Subsequently the calcination process in a muffle furnace at 700°C for 2 h was applied to form Fe_2O_3. The water washing process was carried out to remove sodium chloride impurity. Finally, the powder was dried to obtain the required hematite powder product.

References

[1] L. Alcaraz, B. Sotillo, J. F. Marco, F. J. Alguacil, P. Fernández and F. A. López: Obtention and characterization of ferrous chloride FeCl$_2$·4H$_2$O from water pickling liquors, Material, Vol 14, 4840, 2021.

[2] A. Devi, A. Singhal and R. Gupta: Treatment of spent pickling liquor, International Journal of Advance Research in Science Engineering, Vol. 5, No. 3, pp. 259-263, 2016.

[3] A. Agrawal and K. K. Sahu: An overview of the recovery of acid from spent acidic solutions from steel and electroplating industries, Journal of Hazardous Materials, Vol. 171, pp. 61-75, 2009.

[4] W. F. Kladnig: A review of steel pickling and acid regeneration-an environmental contribution, International of Material & Product Technology, Vol. 19, No. 6, pp.550-560, 2003.

[5] G. Leonzio: Recovery of metal sulphates and hydrochloric acid from spent pickling liquors, Journal of Cleaner Production, Vol. 129, pp. 417-426, 2016.

[6]   R. Gueccia, S. Randazzo, D. C. Martino, A. Cipollina and G. Micale: Experimental investigation and modeling of diffusion dialysis for HCl recovery from waste pickling solution, Journal of Environmental Management, Vol. 235, pp. 202-212, 2019.

[7]   R. M. Machado, M. L. F. Gameiro, J. M. A. Rodrigues, M. R. Ismael, M. T. A. Reis and J. M. R. Carvalho: Recovery of hydrochloric acid from galvanizing industrial effluents, Separation Science Technology, Vol. 52, No. 8, pp. 1333–1340, 2017.

[8]   J. Xu, S. Lu, D. Fu: Recovery of hydrochloric acid from the waste acid solution by diffusion dialysis" Journal of Hazardous Materials, Vol. 165, No. 1, pp. 832–837, 2009.

[9]   Y. Chang, X. Zhai, B. Li and Y. Fu: Removal of iron from acidic leach liquor of lateritic nickel ore by goethite precipitate, Hydrometallurgy, Vol. 101, No. 1, pp. 84–87, 2010.

[10]   Y. Gao, T. Yue, W. Sun, D. He, C. Lu and X. Fu: Acid recovering and iron recycling from pickling waste acid by extraction and spray pyrolysis techniques", Journal of Cleaner Production, Vol. 312, 127747, 2021.

[11]   E. Marañón, F. Suárez, F. Alonso, Y. Fernández and H. Sastre: Preliminary study of iron removal from hydrochloric pickling liquor by Ion exchange, Industrial & Engineering Chemistry Research, Vol. 38, pp. 2782–2786, 1999.

Precipitation of Lithium Phosphate from Cathode Materials of Spent Lithium-Ion Battery by Hydrometallurgy Process

Natcha Wongnaree[1,a], Loeslakkhana Sriklang[1,b], Chatisa Kansomket[1,c]
Thanapon Chandakhiaw[1,d] Tapany Patcharawit[1,e] and Sakhob Khumkoa[1,f,*]

[1]School of Metallurgical Engineering, Institute of Engineering, Suranaree University of Technology, Nakhon Ratchasima, Thailand

[a]natcha.wongnaree@outlook.com, [b]loeslakkhana.sk@hotmail.com, [c]k.chatisa@gmail.com, [d]thanapon2459@gmail.com, [e]tapany@sut.ac.th, [f]sakhob@sut.ac.th

Keywords: Recycling, Hydrometallurgy, Lithium-ion battery, Lithium phosphate

Abstract. Spent lithium-ion batteries (LIBs) have significantly increased due to the high consumption of LIBs for automobile applications; therefore, the recovery of valuable materials to use as the second resource can bring economic benefits and reduce an environmental impact. This study investigated the production of lithium phosphate (Li_3PO_4), which can be used as a starting material for the synthesis of LIBs, from spent $LiNi_xMn_yCo_zO_2$ (NMC) cathodes. The experimental procedure started with discharging, dismantling the battery, and removing the aluminum foil, followed by the leaching of cathode material before precipitating the lithium phosphate from the solution. In the leaching stage, the parameters to optimize the process were studied. The results showed that the lithium leaching efficiency could be achieved at 96.10% using 2 M H_2SO_4, 8 vol.% H_2O_2, 40 g/L pulp density, and 4 hrs at 70°C. The final precipitate product of 98.98% purity of Li_3PO_4 was recovered from the solution using Na_2HPO_4 under the experimental condition.

Introduction

The pursuit of high-performance energy-stored sources with a reusable, sustainable, and friendly environment leads to a significantly increased consumption of lithium-ion batteries. Especially for the lithium-ion battery, which is predicted to use over 100% of lithium-ion batteries in electric vehicle industries in 2083-2087 [1]. On the contrary, spent lithium-ions are generated after approximately 10-12 years of use [2-4]. Moreover, spent lithium-ion batteries consist of valuable metals such as lithium, cobalt, nickel, manganese, copper, and aluminum, which require urgent of technology improvement for extraction of those metals to be used as secondary resources materials instead of mining [5].

The critical recycling path of lithium-ion batteries is the cathode electrode, which can be divided by chemical compositions of active materials that coat on an aluminum foil surface. This is for examples $LiNi_{0.33}Mn_{0.33}Co_{0.33}O_2$ (NMC111), $LiNi_{0.5}Mn_{0.3}Co_{0.2}O_2$ (NMC532) and $LiNi_{0.83}Mn_{0.05}Co_{0.12}O_2$ (NMC811) [6], which costs about 65-70% of the materials in a cell [7]. Recently, the hydrometallurgical and direct recycling methods have attracted the attention of researchers because of the advantages of low energy consumption, less carbon dioxide emission, and can provide high purity of the final products [8-13].

Lithium compounds such as Li_2CO_3, Li_3PO_4, $LiNO_3$, and $LiOH$, which are used as a lithium source to synthesize the active materials in lithium-ion batteries, have a dramatic demand and limited supply, leading to an increased cost of lithium compounds. Consequently, the strategies for recycling Li are economic benefits and attract people's attention. However, the Li-recovery technologies still need to be further improved [14]. Therefore, this study proposes the recovery of lithium from the spent NMC cathode by producing a Li_3PO_4 compound that can be used as a precursor to regenerate lithium iron phosphate (LFP) active material and can be applied to produce LiOH, which is used to synthesize the active material for Ni-rich cathode. In addition, removing Al foil from the cathode to separate the active material is operated, followed by studying leaching conditions with different H_2SO_4 concentrations and temperatures. Moreover, the Li_3PO_4 precipitation process and its purifying by washing with hot water are studied [15, 16].

Experimental

Material Preparation. The experiment started from discharging of a battery module in a 10 wt.% NaCl solution for 2 days, followed by physical and mechanical separation of the battery to wire, casing, metal, polymer, anode, and cathode. Then, the manually separated cathode was cut into a small size of 5×5 mm^2, as shown in Fig. 1, which was used as the raw material of this experiment.

(a)   (b)

Fig. 1. Cathode material a) cathode b) reduced size of the cathode.

Methodology. The overall route of the experimental procedure in this study is shown in Fig. 2, which consisted of discharging the battery, mechanical/physical dismantling of the lithium-ion battery, removing the aluminum foil, and followed by hydrometallurgical processes to recover lithium. Firstly, aluminum foil of the cathode by dissolving in 2 M NaOH at a solid-liquid ratio of 50 g/L at 50°C for 30 min to separate the active materials that coated on the aluminum foil surface. Additionally, the stirring on the hot plate with a magnetic bar was applied in order to accelerate the leaching reactions. Then, the cathode material was leached at varied concentrations of H$_2$SO$_4$ from 1 M to 4 M, which a concentration of H$_2$O$_2$, temperature, time, S/L ratio, and stirring speed were fixed at 8 vol.%, 70°C, 4 hrs, 50g/L, and 250 rpm., respectively. The leaching efficiency of lithium was calculated by Equation (1). In the lithium recovery step, the prepared solution of 300 g of NaOH in 1 L of deionized water was used to precipitate Co-Ni-Mn ions from the solution to form metal hydroxide compounds reaching pH 10. After that, the filtered solution was heated up to about 95°C before adding Na$_2$HPO$_4$ into the riches lithium solution with a 0.2:1 molar ratio of Na$_2$HPO$_4$ and lithium ion to precipitate Li$_3$PO$_4$ white powder. Finally, the precipitated Li$_3$PO$_4$ was washed in 95°C hot water to remove contamination Na.
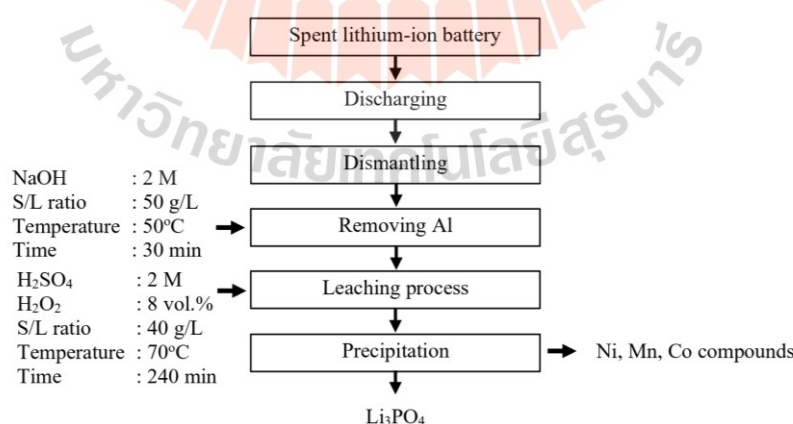

Fig. 2. Experimental flow chart.

$$\text{Leaching efficiency of Lithium (\%)} = \frac{\text{Amount of lithium in solution}}{\text{The initial amount of lithium in the active material}} \times 100 \qquad (1)$$

Characterization. Crystal structures of the initial cathode material and precipitated Li_3PO_4 were examined by X-ray diffractometer (XRD) (Bruker D2 PHASER) using Cu Kα radiation. The concentration of metal ions in the solution was analyzed by the inductively coupled plasma-optical emission spectrometry (ICP-OES) (Optima 8000, Perkin Elmer). Comparison of Na content in Li_3PO_4 powder before and after washing with 90ºC hot water was measured by wavelength dispersive X-ray fluorescence spectroscopy (WDXRF) (PANalytical AXIOS).

Results and Discussion

Raw Material Characterization. Fig. 3 exhibits the X-ray diffraction pattern of the active material in the initial cathode, which can be matched with the standard pattern of $Li(Mn_{0.333}Co_{0.333}Ni_{0.333})O_2$, and also has the same appearance as NMC111 commercial grade XRD pattern [18]. Additionally, the carbon peak is detected in the XRD examination, which generally came from the carbon black mixed in the slurry before coating onto the aluminum foil step in the battery-producing process.
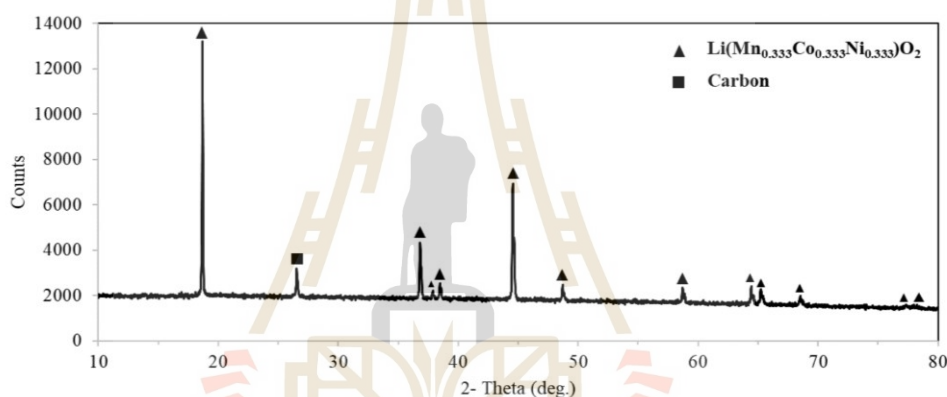

Fig. 3. X-ray pattern of the initial cathode material.

Removal of Aluminum

The cathode material that covered two sides of aluminum foil surfaces is separated by selectively dissolving an aluminum layer with 2 M NaOH solution. In this process, Li, Ni, Co, and Mn are not generally leached into the solution except the Al, which strongly reacts with the alkaline solution. The changing of chemical composition before and after the aluminum removal is shown in Table 1. It is apparently shown that the aluminum foil is completely removed from the cathode material.

Table 1. Chemical composition of initial cathode and after aluminum foil removing analyzed by ICP-OES.

Sample	Chemical composition (wt.%)					
	Li	Ni	Co	Mn	Al	Other
Initial cathode material	4.75	13.59	12.79	11.98	12.61	balanced
Cathode material after removing the aluminum foil	6.00	18.14	17.1	15.87	-	balanced

Leaching of Lithium. The leaching step is aimed at dissolving lithium into an H_2SO_4 solution, and H_2O_2 is used as an oxidant to accelerate chemical reactions. The lithium leaching efficiency is studied by varying the concentration of H_2SO_4 under constant condition control of temperature and time. According to the data as presented in Table 2, it can be seen that the lithium leaching efficiency with different concentrations of H_2SO_4 does not exhibit a significant difference at ambient

temperature, which the result shows about 67-72%. However, the effect of the leaching efficiency of metals is dramatically increased to approximately 96.10% at 70ºC, as shown in Table 3. The lithium-ion concentration in the solution is 2.4 g/L, which will be further precipitated to recover the lithium metal in the form of lithium compound in the next stage.

Table 2. Leaching efficiency of lithium in different concentrations solution of H_2SO_4 at ambient temperature and 8 vol.% H_2O_2 for 240 min. and 40 g/L of solid and liquid ratio.

The concentration of H_2SO_4 (M)	Leaching efficiency of lithium (%)
1	67.33
2	68.74
3	71.09
4	71.94

Table 3. Leaching efficiency of dissolved metals in 2 M of H_2SO_4 at 70ºC with 8 vol.% H_2O_2 for 4 hrs and 40 g/L of solid and liquid ratio.

Metal	Li	Ni	Co	Mn
Leaching efficiency (%)	96.10	100.00	100.00	96.48

Precipitation of Li_3PO_4. There are two stages in the precipitation of metals from the solution: impurity metals removal and Li_3PO_4 precipitation. In the first stage, impurities metals that are cobalt, nickel, and manganese were removed by selective precipitation to be complex compounds with NaOH to pH 10. Then, the remained lithium solution is increased temperature and recovered by adding sodium hydrogen phosphate to obtain Li_3PO_4 powder, and the chemical reaction of Li_3PO_4 precipitation is expressed in Equation (2). At this stage, precipitated Li_3PO_4 still remains a high amount of Na (4.74 wt.%), which was contaminated by flocculants and needs to be removed by washing with hot water. The result before and after Na cleaning is shown in Table 4. It can be seen that single washing with hot water can significantly remove Na content (remaining 1.25 wt.%) in precipitated powder. Additionally, the Li_3PO_4 can be further purified to obtain the requirement of battery-grade materials by increasing the water washing time. It may result greater amount of wastewater, which indeed requires treatment. In this study, 98.69% purity of Li_3PO_4 powder is achieved according to the ICP-OES result, as shown in Table 5. Moreover, Fig. 4 represents the picture of a cleaned Li_3PO_4 particle and its XRD pattern, which can be perfectly matched with the Li_3PO_4 standard pattern and shows the same pattern as in other research papers [17, 18]. Therefore, it can be confirmed that the obtained powder is in the Li_3PO_4 form.

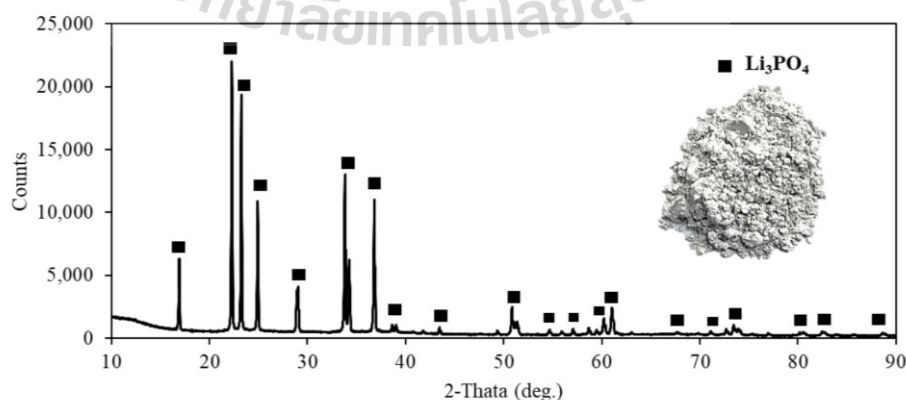$$3LiSO_4 + 2Na_2HPO_4 = 3Na_2SO_4 + 2Li_3PO_4 \tag{2}$$

Fig. 4. XRD spectrum of precipitated Li_3PO_4 powder.

Table 4. Chemical composition of precipitated Li_3PO_4 powder before and after washing with water, which was analyzed with the XRF technique.

Element	Precipitate (wt.%)	washed precipitate (wt.%)
O	50.39	56.98
P	43.25	40.06
Na	4.74	1.35
Co	0.05	0.05
Mg	0.17	0.17
Al	0.03	0.03
Si	0.20	0.21
S	0.86	0.80
Cl	0.24	0.11
Ca	0.07	0.07

Table 5. Chemical composition of Li_3PO_4*.

Element	Al	Si	Mg	Ca	Na
wt.%	0.170	0.105	0.102	0.055	0.880

* Calculated by 100 wt.% of impurity metals

Summary

This work aims to investigate the lithium recovery process from the spent lithium-ion battery, which the experiment started from dismantling NMC111 cathode, followed by removing the aluminum foil, leaching, and Li_3PO_4 precipitating steps. It can be noticed that cathode material could be entirely separated by selectively leaching aluminum foil under the condition of 50 g/L of S/L ratio, 2 M NaOH, and 30 min. at 50°C. Under the appropriate condition of the leaching process, lithium could be leached with a high leaching efficiency of 96.10% using 2 M of H_2SO_4, 8 vol.% H_2O_2, 40 g/L pulp density, and 4 hrs at 70°C. Finally, the purity of 98.69% Li_3PO_4 could be precipitated from the solution by selectively precipitation of undesired metals at pH 10, followed by Li_3PO_4 precipitation with Na_2HPO_4 at 95°C.

Acknowledgment

References

[1] B. E. Murdock, K. E. Toghill and N. Tapia-Ruiz: A Perspective on the Sustainability of Cathode Materials used in Lithium-Ion Batteries, Advanced Energy Materials, Vol. 1, No. 39, 2102028, 2021.

[2] D. Chung, E. Elgqvist, and S. Santhanagopalan: Automotive Lithium-ion Cell Manufacturing: Regional Cost Structures and Supply Chain Considerations, Clean Energy Manufacturing Analysis Center (CEMAC), 2016.

[3] M. Malik, K. H. Chan, and G. Azimi: Review on the synthesis of $LiNixMnyCo1-x-yO_2$ (NMC) cathodes for lithium-ion batteries, Materials Today Energy, Vol. 28, 101066, 2022.

[4] Thailand Automotive Institute: Spent Battery Management Business Report, 2018.

[5] M. Chen, X. Ma, B. Chen, R. Arsenault, P. Karlson, N. Simon, and Y. Wang: Recycling End-of-Life Electric Vehicle Lithium-Ion Batteries, Joule, Vol. 3, No. 11, 2019, pp. 2622–2646.

[6] P. Liu, L. Xiao, Y. Tang, Y. Chen, L. Ye and Y. Zhu: Study on the reduction roasting of spent $LiNixCoyMnzO_2$ lithium-ion battery cathode materials, Thermal Analysis and Calorimetry, Vol. 147, No. 24, 2018, pp. 1323-1332.

[7] D. L. Thompson, J. M. Hartley, S. M. Lambert, M. Shiref, G. D. J. Harper, E. Kendrick, P. Anderson, K. S. Ryder, L. Gaines and A. P. Abbott: The importance of design in lithium ion battery recycling - a critical review, Green Chemistry, Vol. 22, pp. 7585-7603, 2020.

[8] D. A. Ferreira, L. M. Zimmer Prados, D. B. Majuste and M. B. Mansur: Hydrometallurgical separation of aluminium, cobalt, copper and lithium from spent Li-ion batteries, Power Sources, Vol. 187, No. 1, 2009 pp. 238-246.

[9] N. Vieceli, R. Casasola, G. Lombardo, B. Ebin, and M. Petranikova: Hydrometallurgical recycling of EV lithium-ion batteries: Effects of incineration on the leaching efficiency of metals using sulfuric acid, Waste Management, Vol. 125, 2021, pp. 192-203.

[10] C. Peng, F. Liu, Z. Wang, B. P. Wilson and M. Lundström: Selective extraction of lithium (Li) and preparation of battery grade lithium, Power Sources, Vol. 415, 2019, pp. 179-188.

[11] X. Chen, Y. Chen, T. Zhou, D. Liu, H. Hu and S. Fan: Hydrometallurgical recovery of metal values from sulfuric acid leaching liquor of spent lithium-ion batteries, Waste Management, Vol. 38, 2015, pp. 349-356.

[12] W. S. Chen and H. J. Ho: Recovery of Valuable Metals from Lithium-Ion Batteries NMC Cathode Waste Materials by Hydrometallurgical Methods, Metals, Vol. 8, No. 5, 321, 2018.

[13] Q. Li, K. Yip Fung, and K. M. Ng: Separation of Ni, Co, and Mn from spent $LiNi_{0.5}Mn_{0.3}Co_{0.2}O_2$ Cathode Materials by Ammonia Dissolution, ACS Sustainable Chemistry&Engineering, Vol. 7, No. 15, 2019, pp. 12718-12725,

[14] J. Kumar, X. Shen, B. Li, H. Liu, and J. Zhao: Selective recovery of Li and $FePO_4$ from spent LiFePO4 cathode scraps, Waste Management, Vol. 113, 2020, pp. 32-40.

[15] J. Li and Z.-Feng Ma: Past and Present of LiFePO4: From Fundamental Research to Industrial Applications, Chem, Vol. 5, No. 1, 2019, pp. 3-6.

[16] D. J. Shin, S. H. Joo, D. Lee and S. M. Shin: Precipitation of lithium phosphate from lithium solution by using sodium phosphate, The Canadian Journal of Chemical Engineering, Vol. 100, No. 12, 2021, pp. 1-8.

[17] M. P. Do, J. J. Roy, B. Cao and M. Srinivasan: Green closed-loop cathode regeneration from spent NMC-based lithium-ion batteries through bioleaching, ACS Sustainable Chem. Eng., Vol. 10, No. 8, 2022, pp. 2634-2644.

[18] S. Tao, J. Li, L. Wang, L. Hu and H. Zhou: A method for recovering Li_3PO_4 from spent lithium iron phosphate, Ionics, Vol. 25, 2019, pp. 5643-5653.

Study on Leaching of Molybdenum from a Spent HDS Catalyst

Chatisa Kansomket[1,a], Thanapon Chandakhiaw[1,b], Natthicha Ma-ud[1,c],
Tanongsak Yingnakorn[1,d], Tapany Patcharawit[1,e] and Sakhob Khumkoa[1,f]

[1]School of Metallurgical Engineering, Institute of Engineering, Suranaree University of Technology,
Nakhon Ratchasima, Thailand

[a]k.chatisa@gmail.com, [b]thanapon2459@gmail.com, [c]natthicha.12@gmail.com
[d]Tanongsak@sut.ac.th, [e]tapany@sut.ac.th, [f]sakhob@sut.ac.th

Abstract. The aim of this study is to investigate the extraction of molybdenum from the spent HDS catalyst. The experiment was performed by using the pyro-hydrometallurgical process; calcination and leaching. The spent catalyst was calcined at different temperatures in order to investigate the effect of calcination temperature on the recovery of molybdenum in the subsequent process. Leaching of the calcined samples was subsequently performed by using the different concentrations of leaching reagent. The leaching was conducted by varying the concentration of $NaCO_3$ of 20 g/L, 30 g/L and 40 g/L with a fixed leaching temperature of 90°C, a S/L ratio (weight of calcined sample/volume of leaching reagent) of 100 g/L and leaching time of 1 hrs. under the stirring condition at a speed of 250 rpm. It was found that carbon and sulfur contained in the spent HDS catalyst could be reduced by the calcination process and resulting in enhanced extraction efficiency of molybdenum. The extraction efficiency of molybdenum increased with increasing concentration of leaching reagent. At a certain concentration of leaching reagent, the extraction efficiency of the sample calcined at lower temperatures was higher than the sample which was subjected to calcination at a higher temperature.

Introduction

Hydrodesulfurization (HDS) catalyst is widely used in petroleum refinery plant in order to increase process efficiency. Typical HDS catalyst are Ni, Mo and Co on the alumina support [1]. During Hydrodesulfurization reaction the activity of the catalyst gradually decreases, and the catalyst becomes inactive. When the catalyst is completely deactivated, it become the spent HDS catalyst and causes a large scale of solid waste problem in petroleum refineries. The spent HDS catalyst is classified as one of hazardous waste because it contains various hazardous components, such as Al, V, Mo, Co, Ni, As, P and Fe as well as nonmetallic elements, such as S, C, and oils that are hazardous to the environment [2, 3]. The spent HDS catalyst is prohibited for landfill since the heavy metals can be leached out. This type of waste is increasing significantly depending on the demand of the catalyst in the petroleum refinery industry. The amount of spent HDS catalyst is estimated to be approximately 150,000-170,000 tons/year [4]. Due to the spent HDS catalyst contains high valuable metal such as 19-30 wt.% Mo, 1-12 wt.% V, 1-6 wt.% Ni, 1-6 wt.% Co, therefore, it can be recycled by using them as raw materials for recovery of available metals [5,6]. The recovery of metals from spent HDS catalyst can be carried out by hydrometallurgy and pyrometallurgy processes. Advantages of hydrometallurgical process may be more environmentally friendly, and lower temperature required. However, some reagents are expensive, the reaction rates are quite slow and the process requires large amount of concentrate solution.

Hydrometallurgical process involves leaching with alkaline or acidic solution. In traditional methods, the spent HDS catalyst is initially calcined in order to remove carbon and to convert metal sulfide to metal oxide or sulfate and subsequently leached by using suitable reagent [7-11]. Many investigation have focus on leaching parameters concerning extraction of metals from waste. Nonetheless, effect of calcination temperature of the spent HDS catalyst on extraction ability of metals in leaching process has not been clarified. Therefore the objective of this work is to investigate

the extraction of metals from a spent HDS catalyst which was calcined at different temperatures. The extraction of Mo from spent HDS catalyst was taken into consideration.

Experimental

The experiment was carried out according to the diagram as illustrated as in Fig.1. The experimental sequence is composed of material preparation, calcination, leaching and analyzing.
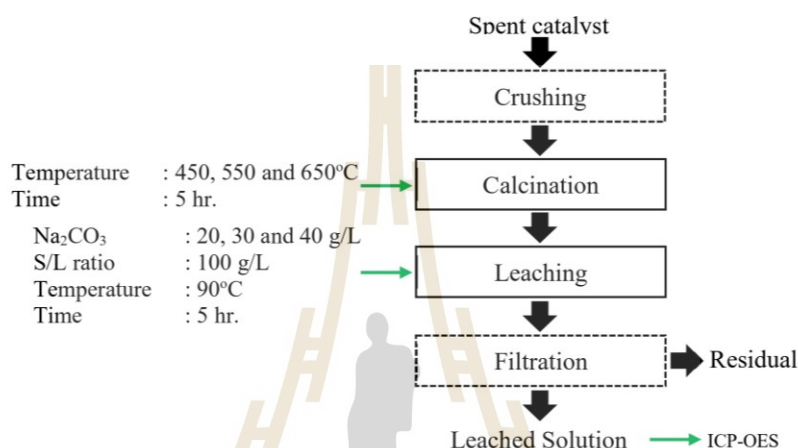

Fig. 1. Experimental flow chart.

Material. A spent HDS catalyst, the so-called Ni-Mo spent catalyst, used in this research was obtained from a petroleum industry in Thailand. The chemical composition of the raw material was analyzed by using WD-XRF Model: Rigaku, ZSXPrimusIV and is shown in Table 1. The as-received spent catalyst of was cylindrical shaped, which was subsequently crushed and ground to fine powder, as shown in Fig. 2.

Table 1. Chemical composition of Ni-Mo spent catalyst.

Element	Mo	Ni	Al	P	C	O	S	Fe	Ca	Na	Other
mass %	11.40	2.55	28.2	2.21	6.81	40.55	7.18	0.12	0.06	0.29	balance

(a)   (b)

Fig. 2. Ni-Mo spent catalyst (a) as received, (b) crushed sample.

Calcination. The spent catalyst was calcined in a muffle furnace at different temperatures ranging from 450°C to 650°C at a holding time of 5 hrs. As holding time is reached, then the calcined sample was furnace cooled to room temperature.

152

Leaching. The calcined sample was subsequently leached with alkali reagent. The leaching were conducted by varying the concentration of $NaCO_3$ of 20 g/L, 30 g/L and 40 g/L with a fixed leaching temperature of 90°C, a S/L ratio (wieght of calcined sample/volume of leachant) of 100 g/L and leaching time of 1 hrs. under stirring at speed of 250 rpm. The chemical composition of the leached solution was then analyzed by ICP-OES model: Perkin Elmer/Optima8000)

Results and Discussion

Effect of Calcination Temperature. The spent HDS catalyst were calcined in a muffle furnace at different temperatures ranging from 450°C to 650°C. The chemical composition of calcined samples at 450°C, 550°C and 650°C are shown in Table 2. It was found that carbon and sulfur were reduced significantly resulting in increasing concentration of other components. By calcination, molybdenum sulfide would be changed to molybdenum oxide by chemical reaction (1). The surface morphology of samples were characterized by SEM-EDX analysis. According to the results in Fig. 3, it was observed that high calcining temperature caused an increase in surface area of the fine particles.

$$2MoS_2 + 7O_2 = 2MoO_3 + 4SO_2 \tag{1}$$

Table 2. Chemical composition of calcined samples.

Calcination temperature [°C]	Chemical composition [mass%]										
	Mo	Ni	Al	P	C	O	S	Fe	Ca	Na	others
Non calcination	11.40	2.55	28.2	2.21	6.81	40.55	7.18	0.12	0.06	0.29	balance
450	12.60	2.74	30.19	2.35	4.08	45.94	1.10	0.18	0.08	0.35	balance
550	12.25	2.72	30.26	2.34	4.06	46.13	1.13	0.21	0.09	0.45	balance
650	12.51	2.77	32.18	2.47	3.36	45.53	0.25	0.19	0.08	0.28	balance

Effect of Sodium Carbonate Concentration. Chemical compositions of leached solution of each test condition are shown in Table 3 and represented in Fig. 4. Based on this experiment, the efficiency of extraction of molybdenum is taken into consideration. It was found that the extraction efficiency of molybdenum from the calcined sample was higher than from non-calcined one.

At a certain concentration of leaching reagent, lower calcination temperature seemed to give higher extraction efficiency of molybdenum. It was found from Fig. 4 that leaching of sample calcined at 450°C at 20 g/L Na_2CO_3 gave Mo extraction efficiency of 93%, while Mo extraction efficiency 89% was reached for the sample subjected to calcination at 650°C. With increasing of calcination temperature, Mo may transform into a complex compound which is difficult to leach.

The significant increasing tendency of Mo extraction efficiency was observed when the concentration of leaching reagent is increased. According to Fig. 4, for the sample calcined at 450°C, the extraction efficiency is of 93% at 20 g/L Na_2CO_3, whereas the extraction efficiency is raised up to approximately 97% when using 40 g/L Na_2CO_3.

(a) as received sample

(b) calcination at 450°C

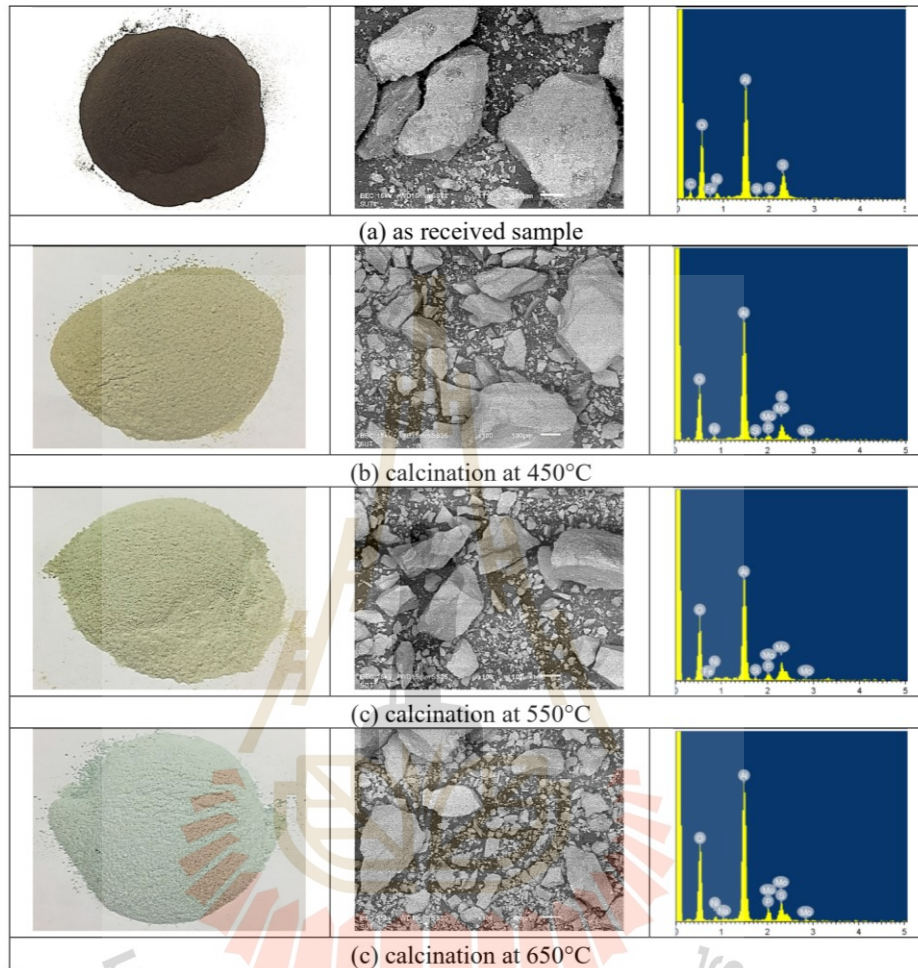(c) calcination at 550°C

(c) calcination at 650°C

Fig. 3. SEM images of as-received and calcined sample at different temperature.

Table 3. Chemical composition of leached solution of different test conditions.

| Calcination condition	Na$_2$CO$_3$ concentration (g/L)	Chemical composition of leach solution [mg/L]					
		Mo	Ni	Na	P	Fe	Al
Non-calcined	20	0.3295	n/a	0.5669	0.0296	n/a	0.0135
	30	0.3209	n/a	0.9657	0.0407	n/a	0.0184
	40	0.3379	n/a	1.4255	0.0370	n/a	0.0097
Calcination at 450°C	20	1.1775	n/a	0.3158	0.0082	n/a	0.0143
	30	1.2114	n/a	0.5400	0.0158	n/a	0.0178
	40	1.2202	n/a	0.8026	0.0252	n/a	0.0199
Calcination at 550°C	20	1.1000	n/a	0.3070	0.0182	n/a	0.0203
	30	1.1474	n/a	0.5920	0.0316	n/a	0.0244
	40	1.1572	n/a	0.9505	0.0426	n/a	0.0269
Calcination at 650°C	20	1.1229	n/a	0.3553	0.0299	n/a	0.0226
	30	1.1492	n/a	0.4828	0.0428	n/a	0.0203
	40	1.1745	n/a	0.7247	0.0562	n/a	0.0213
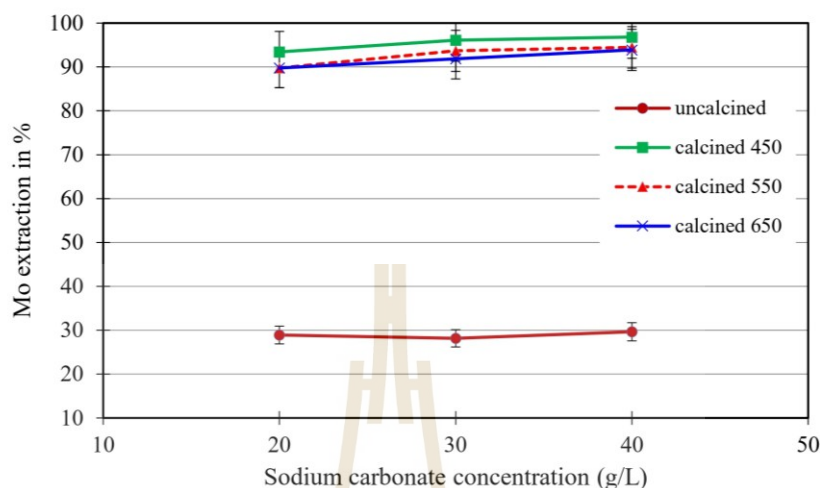
Fig. 4. Effect of Na_2CO_3 concentration on Mo extraction (leaching temperature: 90°C, leaching time: 1 hr., stirring speed: 250 rpm).

Conclusions

In present study, the recovery of molybdenum from spent HDS catalyst was investigated. The experiment was performed by using pyro-hydrometallurgical process. Effect of calcination temperature of sample together with the effect of concentration of leaching reagent on efficiency of extraction of molybdenum was clarified. It was found that carbon and sulfur contained in spent HDS catalyst could be reduced by calcination process and resulting in enhancing of extraction efficiency of molybdenum. Efficiency of extraction of molybdenum is increased with increasing concentration of leaching reagent. At a certain concentration of leaching reagent, the extraction efficiency of the sample calcined at lower temperature was higher than the sample which was subjected to calcination at higher temperature.

Acknowledgement

References

[1] W. MULAK, A. SZYMEZYCHA, A. LESNIEWICZ, W. ZYNICKI, Preliminary results of metals leaching from a spent hydrodesulfurization (HDS) catalyst, Physical Problems of Mineral Processing, 40 (2006), 69-76.

[2] US EPA (United States Environmental Protection Agency), Hazardous waste management system, Federal Register, 68(202) (2003), 59935-59940.

[3] H.AL. SHEEHA, M. MARAFI, V. RAGHAVAN, M.S. RANA, Recycling and recovery route for spent hydro-processing catalyst waste, Industrial & Engineering Chemistry Research, 52 (2013), 12794-12801.

[4] A. YARAŞ, H. ARSLANOĞLU, Extraction of selected metals from spent hydrodesulfurization catalyst using alkali leaching agent, Separation Science and Technology, (2019), 1-12.

[5] I.S.S. PINTO, H.M.V.M. SOARES, Recovery of molybdates from an alkaline leachate of spent hydrodesulphurization catalyst - proposal of a nearly - closed process, Journal of Cleaner Production, 52(2013), 481-487.

[6] W.T. MOHAMMED, N.S. ABMEDZEKI, M.F. ABDUNABI, Extraction of valuable metals from spent hydrodesulfirization catalyst by two stage leaching method, Iraqi Journal of Chemical Petroleum Engineering, 12(4) (2011), 21-35.

[7] J. LIU, Z. QIU, J. YANG, L. CAO, W. ZHANG, Recovery of Mo and Ni from spent acrylonitrile catalysts using an oxidation leaching-chemical precipitation technique, Hydrometallurgy, 164 (2016), 64-70.

[8] M. MARAFI, M.S. RANA, Refining waste spent hydroprocessing catalyst and their metal recovery, world academy of science, Engineering and Technology International Journal of Energy and Environmental Engineering, 11(10) (2017), 979-983.

[9] S. NAGIB, R.S.A. HAMEED, Recovery of vanadium from hydrodesulfurization wated catalyst using calix[4] resorcinarenes, Green Chemistry Letter and Review, 10(4) (2017), 210-215

[10] K.H. PARK, D. MOHAPATRA, C. NAM, Two stage leaching of activated spent HDS catalyst and solvent extraction of aluminium using organo-phosphinic extractant, Cyanex 272, Hazardous Materials, 148 (2007), 287-295.

[11] K.H. PARK, H.I. KIM, P.K. PARHI, D. MISHRA, C.W. NAM, J.T. PARK, D.J. KIM, Extraction of metals from Mo–Ni/Al$_2$O$_3$ spent catalyst using H$_2$SO$_4$ baking-leaching-solvent extraction technique, Journal of Industrial and Engineering Chemistry, 18 (2012), 2036–2045.

Smelting Reduction of Spent Catalyst Containing Nickel: A Preliminary Study

Kitti Laungsakulthai[1,a], Thanapon Chandakhiaw[1,b], Natcha Wongnaree[1,c], Jirapracha Thampiriyanon[1,d], Woranittha Kritsarikun[1,e] and Sakhob Khumkoa[1,f]

[1]School of Metallurgical Engineering, Institute of Engineering, Suranaree University of Technology, Nakhon Ratchasima, Thailand

[a]leo8055@hotmail.com, [b]thanapon2459@gmail.com, [c]D6200299@g.sut.ac.th, [d]jirapracha@gmail.com, [e]woranittha1997@gmail.com, [f]sakhob@sut.ac.th

Abstract. The aim of this research was to study the recycling process and the feasibility to smelt the spent nickel catalyst for the production of nickel alloy or ferronickel. The smelting process was carried out in a laboratory induction furnace. The effects of SiO_2/CaO for slag forming on metal recovery and smelting time were investigated. Petroleum coke was used as reductant. Mill scale was used as an iron resource for ferro-alloy production, while CaO was used as slag forming agent. The raw materials were mixed together and put into a graphite crucible, which was then placed in the induction furnace. After the melt was completed, the melt was poured into a mold to solidify. The chemical composition of the product was analyzed by XRF and XRD. It was found that the smelting time was decreased with increasing SiO_2/CaO from 1.0 to 2.3. For nickel alloy production, increasing of SiO_2/CaO increased the weight of metal product. For the ferronickel production, however, the weight of metal product was found not to vary with different ratio of SiO_2/CaO.

Introduction

Nickel is commercially important as being mainly used as high performance alloys, key alloying element for stainless steel production and electroplating to improve tribological properties and decoration on many types of material surfaces. While nickel consumption is still in high demand, extraction of nickel from ore called 'laterite' however finds some drawback. The ore is classified to 'limonite' containing 0.8-1.5 wt.% Ni and 'saprolite' containing 1.8-3.0 wt.% Ni [1,2]. With such low content of nickel, the extraction requires high amount of ores and fluxing materials. Therefore, nickel recycling from industrial wastes offers alternative solutions for engineering applications and environmental issues.

One type of commercial catalysts used in sweeteners industry is nickel containing catalyst with its good performance for addition and removal of hydrogen in the hydrogenolysis to synthesis aspartame. After deteriorated in service by the formation of coke, which leads to deactivation [3], the deactivated nickel catalyst has to be eliminated as industrial waste. The spent catalyst contains significantly high amount of nickel of almost 30 wt% and some contains up to 40 wt.% of aluminium and some has 10 wt.% of silicon [4, 5]. Due to high nickel content in the spent catalyst, it is therefore suitable for recycling as the renewal resources with value-added, and can reduce disposal by incineration as hazardous waste and landfill. As a result, this study initiated recycling process to recover nickel from spent catalyst as nickel metal or ferronickel.

From the literature survey, extraction of nickel from spent nickel catalysts could be performed via hydrometallurgical and pyrometallurgical processes. The hydrometallurgy process involves acid leaching to obtain nickel in the solution prior to extraction by using different techniques, giving mostly nickel compounds [6-9]. Pyrometallurgical process involves smelting of the spent catalyst from the petroleum refinery resembling that of nickel smelting from ores in submerged arc reaction furnace in the iron ore smelting. The attained product is nickel in the form of ferroalloy [10]. In this work spent nickel catalysts waste from aspartame production were used in the smelting reduction

process via induction furnace to produce nickel alloy and ferronickel. In order to produce a ferronickel, mill scale waste from the hot rolling process of steel which mainly contains iron oxides was the source of iron.

Materials and methods

Raw materials. Spent nickel catalysts waste generated from aspartame Production Company in Thailand was used as one of the raw materials for smelting in this study. The chemical composition is shown in Table 1.

Table 1. Chemical composition of spent nickel catalyst.

Element	Ni	C	O	Si	Al	Fe	Mo	P	S	Other
mass%	22.3	22.1	40.2	11.3	1.8	0.32	0.33	0.4	0.06	balance

Calcium oxide was used as fluxing material. The addition of CaO is required depending on the content of SiO_2 contained in spent catalyst. However, the ratio of SiO_2/CaO of 1, 1.6 and 2.3 was adjusted. Petroleum coke with the chemical composition as shown in Table 2 was used as reductant. Petroleum coke is used at equivalent to amount required by stoichiometry. Petroleum coke is not required when the carbon content in the waste is sufficient high. In order to produce ferronickel, mill scale waste from the hot rolling process of steel was used as the resource of iron. Mill scale is added according to stoichiometry for the production of ferronickel of various commercial grades. In this study, ferronickel grade FeNi40 was taken into consideration. The chemical composition of mill scale composed of 80 wt.% of Fe_2O_3 and 20% of Fe_3O_4 is shown in Table 3.

Table 2. Properties of petroleum coke.

Type of reductant	Fixed carbon [%]	Moisture [%]	Volatile matter [%]	Ash [%]
Petroleum coke	98.72	0.08	0.43	0.85

Table 3 Chemical composition of mill scale.

Element	Fe	O	Si	Mn	Ca	Al	Other
[mass%]	70.43	27.45	0.41	0.32	0.29	0.14	balance

Analytical Methods. The chemical compositions of the raw materials and products were analyzed by WD-XRF technique (Rigaku model ZSX Primus IV, 10 mm. beam size, and scan time 18 min.). X-ray diffractometer was used to determine phases and compounds (Using Bruker model D8 ADVANCE Cu Kα at condition 40 kV, 40mA).

Smelting Reduction Process. The smelting reduction of spent catalyst was carried out in laboratory induction furnace. All of the raw materials were crushed and ground with a jaw crusher machine to obtain particle size of 2-3 mm. Spent catalyst of 1 kg was used for each of smelting condition. The raw materials were mixed together according to the stoichiometry calculation (based on 1 kg of spent catalyst) and SiO_2/CaO ratios were specified for each condition before putting into a graphite crucible. Then, the graphite crucible was placed in induction furnace. The smelting reduction of raw materials took place during heating up the furnace. Smelting was completed in about 50-58 min. and the melt attained at temperatures of about 1500-1550°C. The melt was later poured into the steel mold. The solidified metal and slag were collected, weighed and analyzed. The experimental procedure flow chart is illustrated in Fig. 1.

Results and Discussion

SiO_2 and CaO are the common slag's components. These components determine the properties of slag, e.g. melting point and viscosity, which correspond to refining of the melt. High ratio of SiO_2/CaO results in lower melting temperature of slag. For this preliminary study, the ratio of SiO_2/CaO of 1, 1.6 and 2.3 was selected. Based on this study, the effect of SiO_2/CaO on the recovery of metal and smelting time were investigated. The chemical composition of metal product and slag would be discussed.
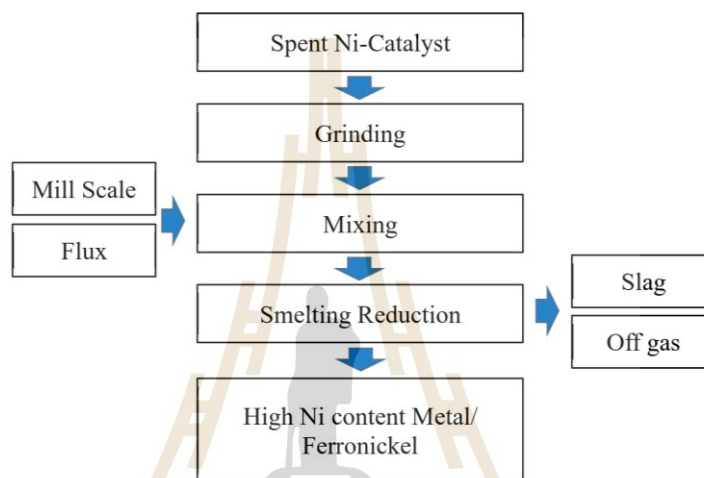

Fig. 1. Experimental flow chart of smelting reduction of spent nickel catalyst.

Effect of SiO_2/CaO on Metal Yield. The effect of SiO_2/CaO on weight of metal product is shown in Fig.2. It was found that the weight of ferronickel production grade FeNi40 was not effected by SiO_2/CaO ratio. For nickel alloy grade, increasing of SiO_2/CaO increased the weight of the metal product. However, the weight of metal product was not significantly different for SiO_2/CaO ratio at 1.6 and 2.3.
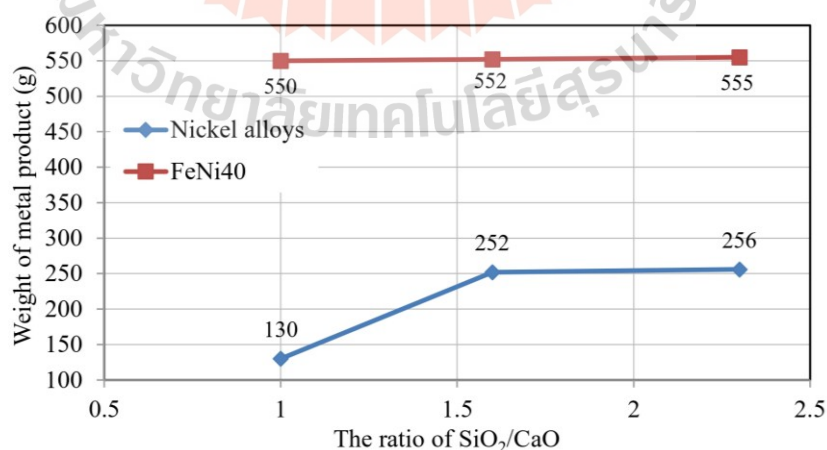

Fig. 2. Effect of SiO_2/CaO on weight of metal production.

Effect of SiO₂/CaO on Smelting Time. The effect of SiO$_2$/CaO on smelting time is shown in Fig.3. For both nickel alloy and ferronickel production, the smelting time decreased with increasing SiO$_2$/CaO. It may be therefore interpreted that high fraction of SiO$_2$ might influence the decreasing of slag melting point. That means, the smelting time of raw materials containing slag component with high SiO$_2$/CaO decreased. For nickel alloy production, the smelting temperature of 1480-1500°C was reached with the smelting time of 50 min. For ferronickel production the smelting temperature of 1500-1550°C was reached with the smelting time of 52 min.
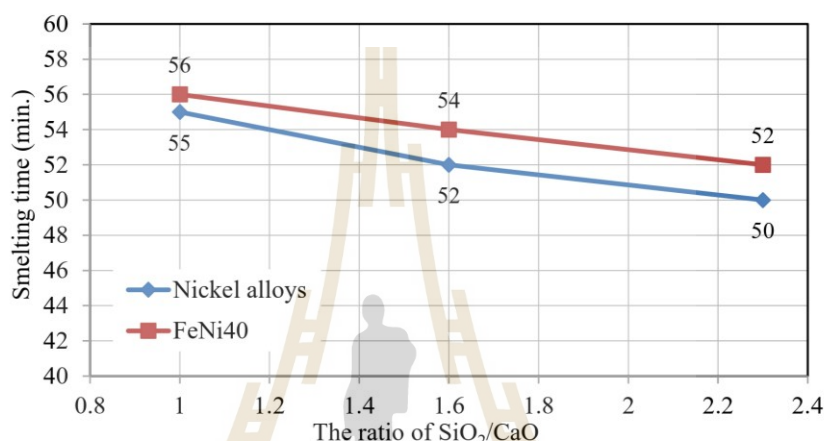

Fig. 3. Effect of SiO$_2$/CaO on smelting time.

Effect of SiO₂/CaO on refining of metal and slag. The chemical compositions of the metal product and slag were analyzed by the WD-XRF and shown in Table 4 and 5, respectively. For nickel alloy production as specified in, trial conditions 1-3, the high content of nickel of up to 89 wt.% was achieved. High nickel recovery increased with increasing SiO$_2$/CaO. For ferronickel grade FeNi40 production, as stated in trial conditions 4-6, the content of nickel contained in ferronickel alloy was approximately 40 wt.%, which is in good agreement with ferronickel grade FeNi40. Moreover, the recovery of nickel of more than 98% has received.

Table 4. Chemical compositions of the metal product of each smelting condition.

Conditions	Targets	Elements [mass %]									%recovery	
		Ni	Fe	C	Si	Al	Mo	P	S	Others	Ni	Fe
1	Ni	86.00	1.12	2.00	3.60	0.09	1.36	1.20	0.06	4.57	97.8	89.6
2	Ni	87.40	1.13	1.90	2.80	0.08	1.33	1.10	0.08	4.18	98.8	89.0
3	Ni	89.00	1.55	1.40	3.10	0.15	1.24	1.30	0.07	2.19	55.2	63.0
4	FeNi40	39.50	56.00	1.20	0.12	0.09	0.82	0.41	0.21	1.65	99.2	90.0
5	FeNi40	39.70	56.00	1.00	0.14	0.08	0.84	0.39	0.22	1.63	98.8	89.5
6	FeNi40	39.80	55.00	1.00	0.21	0.06	0.86	0.42	0.20	2.45	98.5	87.6

The slag composition of smelting reduction to produce nickel alloy and ferronickel is shown in Table 5. For nickel alloy production, trial conditions 1-3, the main slag system is SiO$_2$-CaO-Al$_2$O$_3$. Typical slag composition contained of approximately 41.6 %SiO$_2$, 42.3 %CaO, 11.0 %Al$_2$O$_3$, by weight with SiO$_2$/CaO = 0.98. Such a slag system has a 1350-1450°C melting range. For ferroalloy production, trial conditions 4-6, the main slag system is SiO$_2$-CaO-Fe$_2$O$_3$-Al$_2$O$_3$. Typical slag composition contained of approximately 38.6 %SiO$_2$, 27.4 %CaO, 18.2 %Fe$_2$O$_3$ and 10.5 %Al$_2$O$_3$, by weight with SiO$_2$/CaO = 1.41. The slag has a 1400-1450°C melting range.

Table 5. Chemical compositions of slag of each smelting condition.

Conditions	Elements [mass %]											
	Ni	Fe	Si	Ca	O	Al	Mg	Na	Mn	P	S	Others.
1	0.12	0.08	23.0	25.79	44.98	3.7	0.64	1.08	n/d	0.01	0.12	0.48
2	0.16	0.06	21.0	28.32	44.71	3.3	0.62	1.07	n/d	0.09	0.08	0.59
3	0.18	0.2	17.0	33.3	44.32	2.6	0.66	0.69	n/d	0.3	0.06	0.69
4	0.18	7.1	21.8	22.0	43.0	2.7	0.51	1.25	0.29	0.32	0.02	0.83
5	0.14	6.2	18.8	26.0	43.2	2.3	0.51	1.3	0.6	0.31	0.02	0.62
6	0.11	5.8	15.2	30.58	43.0	1.8	0.52	1.3	0.8	0.24	0.06	0.59

Morphologies of metal product and slag are shown in Fig. 4. The weight and amount of metal of nickel alloy were lesser than that of ferronickel due to the addition of iron concerted mill scale. The characteristic of slag was shiny black, dense, and brittle.
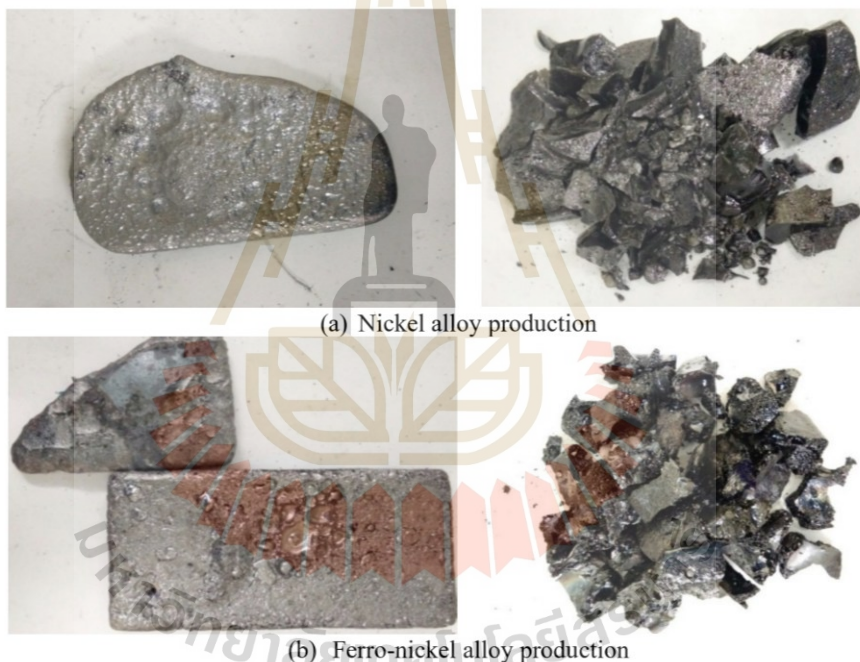

(a) Nickel alloy production

(b) Ferro-nickel alloy production

Fig. 4. Recycling product (a) nickel alloy production, (b) ferro-nickel production.

Conclusions

The experiment on smelting reduction of spent nickel catalyst to produce nickel alloy and ferronickel was carried out in laboratory induction furnace. Effect of SiO_2/CaO contained in raw materials on metal recovery and smelting time were investigated. It was found that increasing of the SiO_2/CaO ratio increased the weight and %recovery of the metal. In addition, smelting time decreased with increasing SiO_2/CaO. Based on this experiment, it was feasible to smelt nickel from spent nickel catalyst in the induction furnace to produce nickel alloy. Ferronickel can be produced when smelting spent nickel catalyst together with mill scale in the induction furnace.

References

[1] D.R. SWINBOURNE, Understanding ferronickel smelting from laterites through computational thermodynamics modelling, Mineral Processing and Extractive Metallurgy, 123(3) (2014), 127-140.

[2] Z. WANG, M. CHU, Z. LIU, H. WANG, W. ZHAO, H. GAO, Preparing ferro-nickel alloy from low-grade laterite nickel ore based on metallized reduction - magnetic separation, Metals, 7(8) (2017), 313-327.

[3] D.L. TRIMM, The formation and removal of coke from nickel catalyst, Catalysis Reviews, 16(1) (1977), 155-189.

[4] F.F. WONG. C.-M. LIN, C.-P. CHANG, J.-R. HUANG, M.-Y. YEH, J.-J. HUANG, Recovery and reduction of spent nickel oxide catalyst via plasma sintering technique, Plasma Chemistry and Plasma Processing, 26(6) (2006), 585-595.

[5] E.A. ABDEL-AAL, M.M. RASHAD, Kinetic study on the leaching of spent nickel oxide catalyst with sulfuric acid, Hydrometallurgy, 74(3-4) (2004), 189-194.

[6] N.M. AL-MANSI, N.M.A. MONEM, Recovery of nickel oxide from spent catalyst, Waste Management, 22 (2002), 85-90.

[7] K.K. SAHU, A. AGARWAL, B.D. PANDEY, Nickel recovery from spent nickel catalyst. Waste Management Research, 23(2) (2005), 148-54.

[8] R.N. OZA, N. SHAH, S. PATEL, Recovery of nickel from spent catalysts using ultrasonication-assisted leaching, Journal of Chemical Technology & Biotechnology, 86(10) (2011), 1276-1281.

[9] K.R. VUYYURU, K.K. PANT, V.V. KRISHNAN, K.D.P. Nigam, Recovery of nickel from spent industrial catalysts using chelating agent, Ind. Eng. Chem. Res., 49 (2010), 2014-2024.

[10] J.-J. PAK, D.-H. KIM, M.-K. PAEK, Y.-D. KIM, Ferroalloy production from spent petroleum catalysts by reductive smelting and selective oxidation processes, REWAS, (2019), 167-175.

การศึกษาความเป็นไปได้ในการใช้เชื้อ *Penicillium sp.* เพื่อชะละลายลิเทียมและโคบอลต์จากผงลิเทียมโคบอลต์ออกไซด์ของแบตเตอรี่โทรศัพท์มือถือที่เสื่อมสภาพ

A Feasibility Study on Applying *Penicillium Sp.* for Leaching of Lithium and Cobalt from Lithium-Cobalt Oxide Powder of deteriorated Smartphone Battery

T. Chandakhiaw[1], C. Longbutsri[1], N. Ma-ud[1], S. Somla[1], T. Patcharawit[1], S. Khumkoa[1*]

[1] School of Metallurgical Engineering, Suranaree University of Technology, Suranaree, Muang, Nakhon Ratchasima, 30000, Thailand

Presenter E-mail address: thanapon2459@gmail.com

*Corresponding Author E-mail address: sakhob@sut.ac.th

บทคัดย่อ

แบตเตอรี่ลิเทียมไอออนได้ถูกนำมาใช้เป็นแหล่งพลังงานของอุปกรณ์เคลื่อนที่หลากหลายชนิด สำหรับแบตเตอรี่ลิเทียมไอออนที่ใช้ในโทรศัพท์มือถือจะมีอายุการใช้งานเฉลี่ย 2-3 ปี เมื่อหมดอายุการใช้งานก็จะเกิดเป็นของเสียที่ต้องมีการจัดการอย่างถูกวิธี แบตเตอรี่ที่ใช้แล้วอุดมไปด้วยโลหะที่มีค่าทางเศรษฐกิจ คือ โคบอลต์ ลิเทียม ทองแดง และอะลูมิเนียม เมื่อไม่นานมานี้มีรายงานเกี่ยวกับเทคโนโลยีการรีไซเคิลเพื่อนำโลหะเหล่านี้กลับมาใช้งานใหม่หลากหลายวิธี แต่วิธีเหล่านี้มีข้อจำกัดด้านผลกระทบต่อสิ่งแวดล้อม อนึ่ง วิธีทางชีวภาพถูกพิจารณานำมาประยุกต์ใช้ในกระบวนการสกัดโลหะ เนื่องจากเป็นวิธีที่ส่งผลต่อสิ่งแวดล้อมน้อยมาก อย่างไรก็ตาม ยังมีรายงานทางด้านเทคนิคและวิธีการที่เกี่ยวข้องน้อย งานวิจัยนี้ได้ศึกษาถึงความเป็นไปได้ที่จะนำวิธีการทางโลหวิทยาชีวภาพมาใช้ในการสกัดโลหะมีค่าจากแบตเตอรี่โทรศัพท์มือถือที่เสื่อมสภาพแล้ว ในการทดลองได้ใช้เชื้อจุลินทรีย์ที่พบได้ในประเทศไทย (เชื้อรากลุ่ม *Penicillium sp.*) เป็นสารที่ใช้ในการสกัดโลหะ จากการศึกษาพบว่าในสารละลายที่เลี้ยงเชื้อราในอาหารเลี้ยงเชื้อ (sucrose media) เวลา 30 วัน ร่วมกับผงแคโทดในแบตเตอรี่มีลิเทียมและโคบอลต์ละลายอยู่ในความเข้มข้นสูงกว่าสารละลายที่มีเพียงอาหารเลี้ยงเชื้อแต่ไม่มีเชื้อรา (กลุ่มควบคุมปลอดเชื้อ) โดยในการทดลองที่มีเชื้อราจะพบลิเทียม และโคบอลต์เข้มข้น 449.3 และ 1,914.7 ppm ตามลำดับ ส่วนการทดลองที่ไม่มีเชื้อราพบลิเทียม และโคบอลต์เพียง 77.0 และ 29.2 ppm ตามลำดับ

Abstract

Lithium-ion batteries (LIBs) were used as the power sources in various smart portable devices. LIBs in smartphones have a lifespan of 2-3 years. Afterwards it is classified as electronic waste, and it will be properly managed. Used-LIBs contain valuable metals such as cobalt, lithium, copper, and aluminum. Recently, there have been many reports about the recycling technology of LIBs for recovery of such valuable metals. Those technologies, however, still have limitations in their impact on the environment. Meanwhile, bio-hydrometallurgy is considered to apply in extraction of metal since it is benign to the environment. However, there are still a few reports on the involved techniques and methods. This research investigated the possibility of applying bio-metallurgy methods to extract such valuable metals from deteriorated smartphone battery. In the experiment, the leaching process was carried out by using fungi (*Penicillium sp.*) in sucrose media as a leachant and leaching period was 30 days. The experimental results showed that the content of lithium and cobalt in the leachate obtained from leaching with fungi in sucrose are higher than in the leached obtained from the leaching without fungi (the control sterile condition). It was found that lithium and cobalt in solution of the first condition is approximately 449 ppm and 1,915 ppm respectively, whereas lithium and cobalt in solution of another one is approximately 77 ppm and 29 ppm respectively.

คำสำคัญ : แบตเตอรี่ลิเทียมไอออน; เทคโนโลยีรีไซเคิลโลหะ; โลหวิทยาชีวภาพ; การชะละลายด้วยเชื้อรา

Keywords: Lithium-ion battery; Recycling; Bio-hydrometallurgy; Fungal leach

TMETC14

14th Thailand Metallurgy Conference

ประกาศนียบัตรฉบับนี้ให้ไว้เพื่อแสดงว่า

T. Chandakhiaw, C. Longbutsri, N. Ma-ud, S. Somla, T. Patcharawit, S. Khumkoa

ได้รับรางวัลชมเชยดีเด่นในการนำเสนอแบบปากเปล่า

METAL PROCESSING

เรื่อง

"A Feasibility Study on Applying *Penicillium* spp. for Leaching of Lithium and Cobalt from Lithium-Cobalt Oxide Powder of Deteriorated Smartphone Battery"

The 14th Thailand Metallurgy Conference

ระหว่างวันที่ 21 – 23 พฤศจิกายน 2566

ณ โรงแรมอมารี พัทยา ประเทศไทย

Assist. Prof. Nayot Kurukitkoson, Ph.D.
Dean of Faculty of Engineering

BUU ENG   MTEC NSTDA   TEPNET

(https://e-sign.buu.ac.th/verify)

2ⁿᵈ Global Summit on

RECYCLING AND WASTE MANAGEMENT

July 22-23, 2019 | Tokyo, Japan

Recovery of metals from dry shot blast waste generated in the stainless-steel production process

Thanapon Chandakhiaw, N Ma-Ud, P Laokhen, C Kansomket, P Khamseetha, P Hathong and S Khumkoa
Suranaree University of Technology, Thailand

Dry shot blast generated during stainless steel production contains high content of valued metals such as iron chromium and nickel. These metals are in the form of oxides and it can be used as a raw material in iron and steel. This work aims to study the feasibility of metals recovery from dry shot blast by smelting reduction process. Smelting reduction of dry shot blast by using coking coal as reductant was conducted in an induction furnace. The effect of metallurgical parameters e.g. stoichiometry ratio of reductant per oxygen containing in dry shot blast, CaO/SiO_2 of slag forming and CaF_2 in slag, on %recovery of metal product was investigated. The results based on this study showed that the weight of metal product increases with increased the amount of coke to about 1.5 of stoichiometric molar ratio. Increasing of coke above this amount leads to decrease %recovery of metal product. Moreover, the weight of metal product is increased when the ratio of CaO/SiO_2 in slag decreased from 2 to 1. The chemical composition of the metal product is in the range of commercial grade and it can be used as raw materials to produce steel and cast iron alloy.

Biography

Thanapon Chandakhiaw has completed his bachelor degree in metallurgical engineering with first class honor from the School of Metal-lurgical Engineering, Suranaree University of Technology, Thailand. Presently, he is pursuing PhD at the same school.
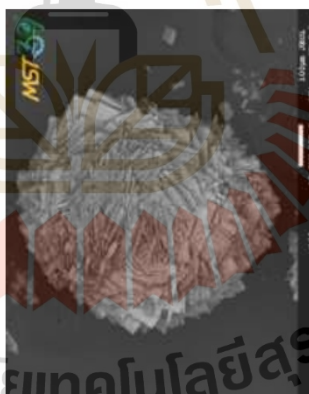
sakhob@sut.ac.th

BIOGRAPHY

Thanapon Chandakhiaw was born on September 23, 1996, in Chaiyaphum, Thailand. After graduating from Darasamutr Sriracha School, Chonburi, Thailand, in 2013, he pursued a Bachelor's degree in Metallurgical Engineering at the Institute of Engineering, Suranaree University of Technology (SUT), graduating with first-class honors (gold medal) in 2017. Following his outstanding academic achievement, he received a full scholarship from SUT to pursue a Doctor of Philosophy (Ph.D.) in Materials Engineering under the supervision of Assistant Professor Dr. Sakhob Khumkoa.

During his academic career, he has served as a teaching assistant for various undergraduate courses, including Mechanical Metallurgy Laboratory, Chemical Metallurgy Laboratory, Thermodynamics of Materials, Metal Injection Moulding, Metal and Materials Technology for Processing, and Introduction to Engineering Profession. Since 2015, he has been an active research staff member at the Innovative Processing and Recycling of Metals Research Center (IPRMRC), where his work focuses on transforming industrial and household metal waste into valuable raw materials.

Thanapon has established himself as an expert in the field, serving as an invited speaker and lecturer at the DPIM Academy, organized by the Department of Primary Industries and Mines, where he has delivered specialized presentations on "Recycling Technology of Used Zinc Carbon Batteries to Produce Ferromanganese" and "Recycling Technology of Used EV Batteries to Recover Lithium and Metal Compounds for Producing New Batteries."